Coordination Chemistry Reviews 462 (2022) 214506

Contents lists available at ScienceDirect

Coordination Chemistry Reviews

journal homepage: www.elsevier.com/locate/ccr

Review

# Revisiting metallodrugs for the treatment of skin cancers

Carlos M. Manzano [a,1], Douglas H. Nakahata [b,1], Raphael E.F. de Paiva [c,d,*,1]

[a] Inorganic Chemistry Department, Institute of Chemistry, University of Campinas – UNICAMP, P.O. Box 6154, 13083-970 Campinas, SP, Brazil
[b] Instituto de Química, Universidade Federal de Goiás – UFG, Campus Samambaia, 74690-900 Goiânia, GO, Brazil
[c] Deparment of Fundamental Chemistry, Institute of Chemistry, University of São Paulo – USP, 05508-000 São Paulo, SP, Brazil
[d] School of Chemical Sciences, Dublin City University, Glasnevin, Dublin 9, Ireland

ARTICLE INFO

*Article history:*
Received 9 December 2021
Accepted 8 March 2022
Available online xxxx

ABSTRACT

Metallodrugs were classically screened against skin cancer (either *in vitro* or *in vivo*) at the peak of the development of platinum anticancer agents. New systematic studies appeared in the past two decades. Herein, we cover the most recent literature concerning metal complexes in the treatment of skin cancers, including *in vitro*, *in vivo* and clinical data. We have compiled the antitumoral potency for each compound in every skin cancer cell line originally tested in a table. This smart table has been deposited in the open access repository Zenodo and it can be accessed at https://zenodo.org/record/5055531. Structure-activity relationships based on a careful analysis of the literature and databases allowed us to discuss possible lead coordination complexes for skin cancer chemotherapy. Additionally, recent advances were made in the understanding of skin composition, photodynamic therapies, immunological responses elicited by metals and the molecular mechanisms of skin cancers. Skin carcinomas represent an excellent prototype for looking into and developing metallodrug-based photodynamic therapy (PDT) strategies and the most recent developments towards that purpose are also covered here. With the substantial advances gained in those areas, we believe this is the perfect moment for revisiting metallodrugs as viable alternatives for the treatment of skin cancers, and how to introduce selectivity. In this context, we explore the major advances made in understanding the unique chemical composition of the outer layers of the skin and alterations observed in keratinocyte carcinomas (KCs) and melanoma as new strategies for designing selective metallodrugs against skin cancers. Signalling pathways unique to either KCs or melanoma are also explored.
© 2022 The Authors. Published by Elsevier B.V. This is an open access article under the CC BY license (http://creativecommons.org/licenses/by/4.0/).

**Contents**

1. Introduction . . . 1
 1.1. Metallodrugs as viable alternative treatments for skin cancers . . . 1
 1.2. The physiology of the outer skin layers . . . 2
 1.3. Skin cancers . . . 3
 1.4. Gold standard interventions and approved targeted chemotherapies . . . 3
2. Scope . . . 5
3. Metal complexes with *in vitro* or pre-clinical data over skin cancer cell lines . . . 6
 3.1. Platinum . . . 6
  3.1.1. The case of cisplatin and its analogues . . . 6
  3.1.2. Other Pt(II) compounds . . . 7
  3.1.3. Pt(IV) compounds . . . 10
 3.2. Palladium . . . 12
  3.2.1. Palladium(II) complexes . . . 12
  3.2.2. Palladium(0) complexes . . . 14
 3.3. Copper . . . 14

* Corresponding author.
*E-mail address:* raphael.enoque@gmail.com (R.E.F. de Paiva).
[1] These authors contributed equally.

https://doi.org/10.1016/j.ccr.2022.214506
0010-8545/© 2022 The Authors. Published by Elsevier B.V.
This is an open access article under the CC BY license (http://creativecommons.org/licenses/by/4.0/).

3.3.1. Copper(I) . . . 14
3.3.2. Copper(II): the case of elesclomol . . . 15
3.3.3. Copper(II) compounds of phenanthroline and related ligands . . . 16
3.3.4. Copper(II) compounds of bi and tripodal ligands . . . 18
3.3.5. Miscellaneous Cu(II) compounds . . . 20
3.4. Gold . . . 22
3.4.1. Auranofin . . . 22
3.4.2. Systematic variation of the structure of auranofin . . . 22
3.4.3. Other Au(I)-phosphane compounds . . . 23
3.4.4. Gold(I) N-heterocyclic carbene compounds . . . 26
3.4.5. Au(III) compounds . . . 28
3.5. Silver . . . 31
3.5.1. The case of silver sulfadiazine . . . 31
3.5.2. Silver(I) compounds . . . 31
3.6. Ruthenium . . . 33
3.6.1. Ruthenium compounds for Photodynamic Therapy (PDT): the case of octahedral compounds with π-expansive ligands . . . 33
3.6.2. Other ruthenium compounds for PDT . . . 35
3.6.3. Other octahedral ruthenium compounds . . . 36
3.6.4. Ruthenium-arene compounds . . . 39
3.7. Iridium . . . 42
3.7.1. Octahedral iridium complexes . . . 42
3.7.2. Iridium-arene compounds . . . 43
3.8. Rhodium . . . 45
3.9. Iron . . . 45
3.9.1. Ferrocene-based compounds . . . 46
3.9.2. Other Fe(II) and Fe(III) compounds . . . 46
3.10. Gallium . . . 47
3.11. Vanadium . . . 48
3.12. Zinc . . . 49
4. Results of clinical trials . . . 49
4.1. Cisplatin and combination therapies containing cisplatin . . . 49
4.2. Elesclomol . . . 50
5. Discussion and perspectives . . . 50
5.1. Identifying lead compounds and their key features for the development of the next generation of active metallodrugs against skin cancer. 50
5.1.1. Pt(II) and Pt(IV) complexes . . . 50
5.1.2. Pd(II) complexes . . . 50
5.1.3. Cu(I) and Cu(II) complexes . . . 51
5.1.4. Au(I) and Au(III) . . . 52
5.1.5. Ag(I) complexes . . . 52
5.1.6. Ru(II) complexes . . . 52
5.2. Photodynamic therapy . . . 53
5.3. New directions and unexplored strategies for skin cancer targeted therapies using metallodrugs . . . 54
5.3.1. The Chemical Structure of the Skin: insights from modern 'omics' and implications for the development of new therapy strategies targeting skin cancers . . . 54
5.3.2. The Hedgehog pathway . . . 55
5.3.3. Wnt/ β-catenin signaling pathway . . . 56
5.3.4. Protein Disulfide Isomerase . . . 56
5.3.5. Bromodomain and extra-terminal domain (BET) proteins . . . 57
5.3.6. Hypoxia-inducible factor and glucose transporters . . . 57
5.3.7. Inflammation and skin cancers . . . 57
5.3.8. Antibody-drug conjugates . . . 58
6. Outlook . . . 58
7. Skin cancer and related cell lines for *in vitro* screening . . . 58
Declaration of Competing Interest . . . 58
Acknowledgements . . . 59
Appendix A. Supplementary data . . . 59
References . . . 59

## 1. Introduction

### *1.1. Metallodrugs as viable alternative treatments for skin cancers*

From the early years of screening the anticancer properties of cisplatin, skin cancer cell lines such as keratocyte carcinomas (KCs) and melanoma, have been among the panels of cell lines evaluated [1]. As part of combination therapies, platinum drugs have found their use in treatment regimens against melanoma [2,3]. However, platinum resistance is a drawback [4,5], along with lack of selectivity and lack of a more targeted approach [3]. In this context, there is much potential for further development of metallodrugs specific for the treatment and management of skin cancer conditions.

Besides platinum drugs, many other metal ions have been explored in the last decades as alternatives for skin cancer treatment, such as Au(I), Ag(I), Ru(II), Pd(II), Cu(II), among others, offering a wide varied of 3D structures with diverse mechanisms of action. New generations of metal chemotherapeutics have offered the prospect of combating the remarkable global problem of cancer

resistance to platinum-based drugs and expanding the range of treatable cancers [6]. Potential new chemotherapeutics explore the unique properties of each transition metal, combining a wide range of 3D motifs [7], fine-tunable ligand exchange kinetics, diverse photochemical and photophysical properties, variable oxidation states and the ability to form specific interactions with biomolecules [6,8-10]. These properties are virtually impossible to be replicated by organic motifs alone.

KCs and local cutaneous melanoma offer a distinct opportunity for the development of topical treatments based on metallodrugs. The cationic nature of many complexes, their tunable polarity and capability to act as pro-drugs or "trojan horse" drugs that change properties as they pass through different skin layers are characteristics that make metallodrugs excellent candidates for topical treatments. Ultimately, metallodrugs can be tailored to modulate their level of penetration through the skin, representing important strategies for the local KCs but also offering an opportunity to reach systemic levels as needed (important, for example, for invasive melanoma).

Skin cancer models provide also excellent prototypes for developing photodynamic therapy (PDT) strategies, given the topical nature of this condition (specially at the cancer early stages, in the absence of metastases). Light-activation of metallodrugs is currently being extensively investigated, including in clinical trials [10].

Many signaling pathways are unique to skin cancers and melanoma, and can be exploited for the development of more selective therapeutical compounds. In addition, in recent years the unique glycome and proteome of the skin affected by skin cancers has been elucidated, opening even further avenues to drug design (see Section "New directions and unexplored strategies for skin cancer targeted therapies with metallodrugs"). This knowledge, combined with the versatility of metallodrugs, represents a strategy with untapped potential for the development of active compounds against skin cancers.

Within this context, we believe this is the perfect moment for revisiting metallodrugs not only as viable but as promising alternatives for the treatment of skin cancers.

This review starts with a brief overview of the physiological characteristics of the outer skin layers, and a description of each type of skin cancer, as well as differences among them. Ultimately, this contribution aims at exploring the lessons we can learn from the skin physiology and the pathologies of skin cancers and how to translate this knowledge to targeted chemotherapeutics based on metallodrugs as new strategies for the treatment of skin cancers.

### 1.2. The physiology of the outer skin layers

The skin is the largest organ in the human body, and it weighs about 4 kg and covers almost 2 $m^2$. Among its many functions, the skin's intricate network serves as a physical barrier, preventing invasion of infectious pathogens and entry of potentially hazardous chemical compounds and it offers protection against, heat, cold, physical impact and stress and sunlight. It also plays a fundamental role in maintaining body homeostasis [11-14]. The skin also possesses endocrine and exocrine functions. The endocrine function includes the metabolism of vitamin D in the keratinocytes with the assistance of UV light from the sun, while the exocrine functions of the skin are mediated by sweat and sebaceous glands [13,15,16].

The skin is formed by three major layers (Fig. 1): the outer one is the epidermis which is supported in the dermis, a layer formed by collagen and elastin and connected by an interfibrillar gel of glycosaminoglycans, water and salts [13,14]. Since the epidermis is avascular, its homeostatic status requires nutrient diffusion from the dermis. Moreover, the dermis is where the neural and lymphatic systems of the skin and epidermal appendages (glands, hair follicles, nails, sensory nerve receptors) are located [18]. The deepest layer of the skin is the hypodermis (or subcutis), which has fat as its major component and it is formed by loose connective tissue [12,13].

The human epidermis is a highly specialized stratified squamous epithelium. Since the dead surface of the epidermis (cornified layer) is constantly being shed, it undergoes constant turnover by stem cells dividing in the only mitotically active basal

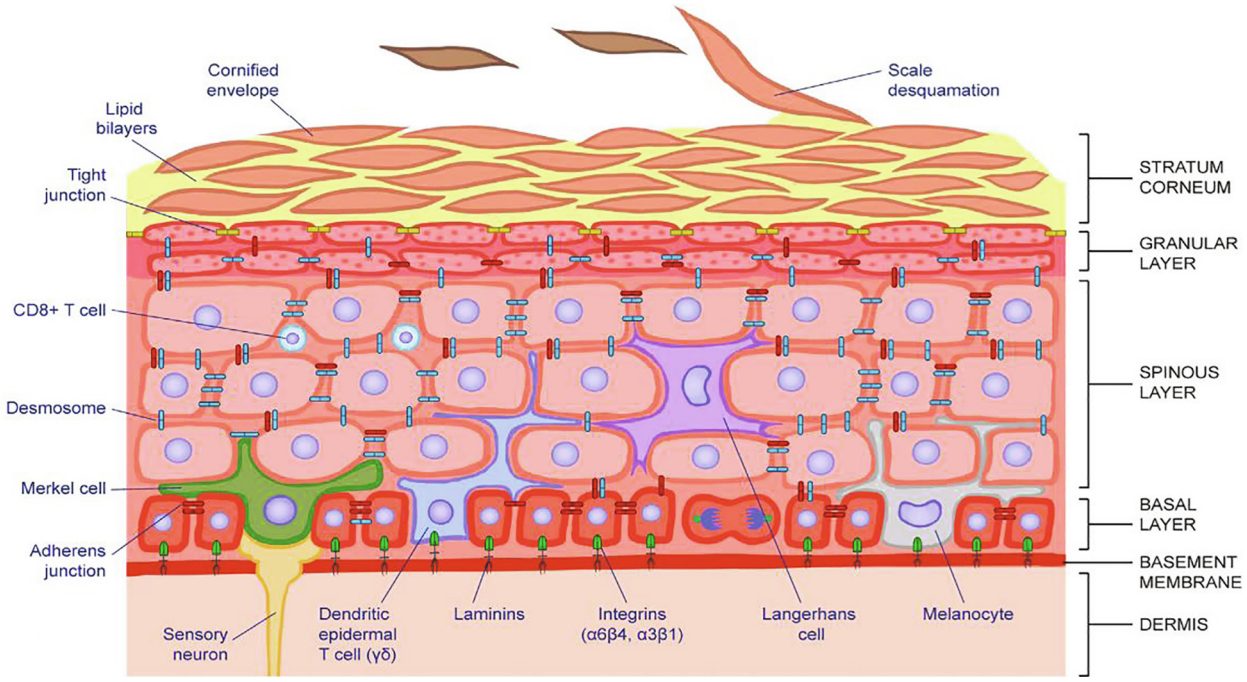


**Fig. 1.** The stratified nature of the epidermis. The basal layer is located above the dermis. Adapted from Gonzales et al [17].

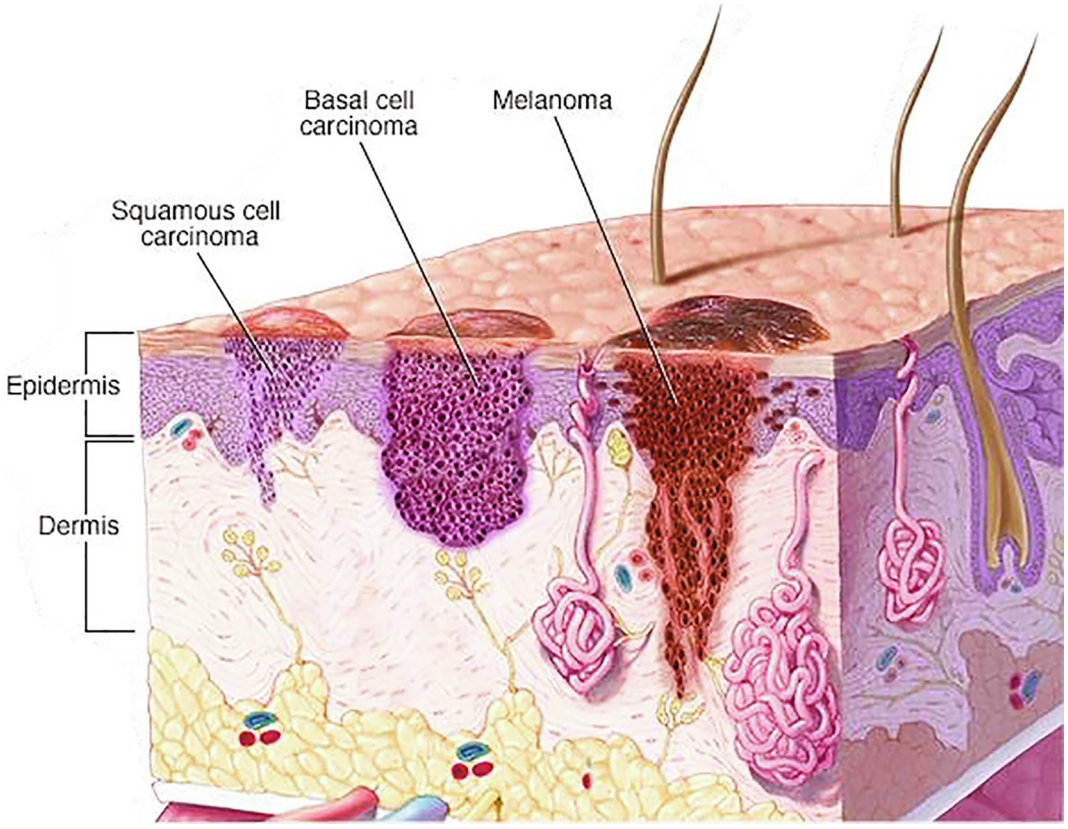


**Fig. 2.** Skin cancer begins in the cells that make up the outer layer (epidermis) of the skin. New skin cells are continuously generated in the basal cell layer. In this layer, basal cell carcinoma (BCC) can appear. As new cells continuously migrate outwards, they continuously undergo differentiation, becoming flattened squamous cells. In this region, squamous cell carcinoma (SCC) can occur. Finally, melanoma arises in the pigment cells (melanocytes) and, depending on the progression, it can go beyond the dermis and reach systemic circulation. Used with permission of Mayo Foundation for Medical Education and Research, all rights reserved.

cell layer (in a process called keratinopoiesis) [17], which is in contact with the dermis through hemidesmosomes and integrin-based adhesions. The squamous (or spinous) cell layer receives this name due to the great number of desmosomes that connect these cells. It is the thickest epidermal layer and it is located above the basal cell one. The granular cell layer follows the squamous one, and it is granular due to the presence of keratohyalin granules, protein structures whose main function is to promote cross-linking of keratin filaments. The granular cell layer gradually loses its organelles and become more compact, until the formation of the *stratum corneum* [13,14]. As mentioned, the intercellular connections are formed by abundant desmosomes (especially in the squamous cell layer) and adherens junctions (structures formed by transmembrane proteins called cadherins) that promote mechanical coupling and provide physical resistance [13,17].

The most abundant cell type in the epidermis are keratinocytes, with a population of approximately $1.4 \times 10^{11}$ cells/$m^2$ [18,19]. Each of the previously mentioned layers of the epidermis is the result of different stages of gradual differentiation as the keratinocytes move upward form the basal cell layer to the surface of the skin. These keratinocytes construct a heavily crosslinked cornified envelope of protein and lipids, which serves as the first line of defense of the skin against physical, chemical and biological menaces [20]. During the differentiation process, which takes approximately one month, keratinocytes profoundly change their morphology and start to produce keratin, cytokines, growth factors, interleukins and complement factors [13,14,18].

Melanocytes are a second population of dendritic cells found in the epidermis and the only ones capable of synthesizing melanin in melanosomes via a tyrosinase-dependent pathway [21]. They are present in the basal layer of the epidermis, in hair follicles and in the mucosa (iris, mesencephalon and cochlea) [22]. In the epidermis, they transfer melanin to keratinocytes via melanosomes. Increased exposure to ultraviolet light results in increased melanogenesis and melanin transfer to keratinocytes (tanning), enhancing the photoprotection potential of the skin and protecting genetic information from radiation damage. The combination of ultraviolet radiation and chemical exposures with genetic traits represent the main factors associated with melanocyte disorders, including melanoma development [21-24].

Merkel cells are a unique population of oval-shaped mechanosensors found in the dermal-epidermal junction. They are abundant in highly sensitive skin, including palms, fingertips and the plantar surface of the toes. Merkel cells have synaptic contacts with sensory nerve endings and play a role in sensory discernment [25-27]. The fourth major cell population found in the epidermis are dendritic Langerhans cells and they reside mostly in the squamous layer of the skin. These cells act as "sentinels" of the skin immune system that survey the epidermis for foreign antigens, activating appropriate responses in accordance to their surrounding microenvironment [28-31].

### 1.3. Skin cancers

Cutaneous melanoma and keratinocyte carcinomas (basal cell carcinoma, BCC; squamous cell carcinoma, SCC) are currently the most common types of cancer in caucasians. According to the Global Cancer Observatory (GCO), the International Agency for Research on Cancer of the World Health Organization, over 2 million cases of keratinocyte carcinomas (KC, also named nonmelanoma skin cancer [32,33]) were registered worldwide in 2020, with a mortality of 6.2%. Concerning mel-

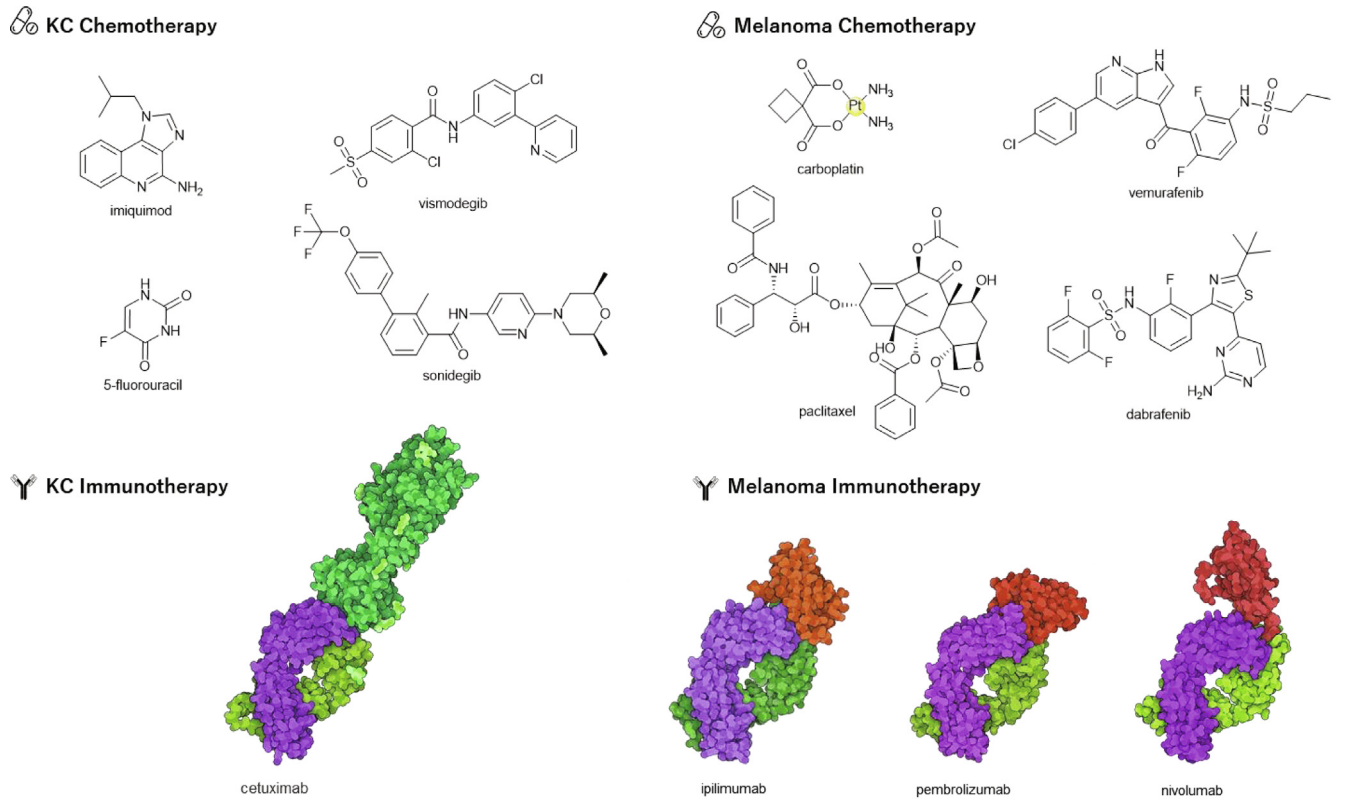


**Fig. 3.** Chemo- and immunotherapeutic interventions used for KCs and Melanoma. KC-specific chemotherapy includes vismodegib and sonidegib, SMO-targeting (hedgehog pathway) chemotherapeutics. Melanoma-specific chemotherapeutics include vemurafenib and dabrafenib, BRAF enzyme inhibitors (part of the BRAF/MEK/ERK pathway). For KC immunotherapy, we show cetuximab as an example. The extracellular domain of the epidermal growth factor receptor (dark green) is shown in complex with the Fab fragment of cetuximab (PDB 1YY9, Li et al. [63]) For melanoma immunotherapy, we show ipilimumab: CTLA-4 (orange) binding to the Fab fragment of ipilimumab (PDB 5TRU, Ramagopal et al. [64]); pembrolizumab: PD-1 (red) in complex with pembrolizumab Fab (PDB 5GGS, Lee et al. [65]); nivolumab: extracellular domain of PD-1 (red) complexed with Fab fragment of nivolumab (PDB 5GGR, Lee et al. [65]). Antibodies figures were prepared with Illustrate [66]. (For interpretation of the references to color in this figure legend, the reader is referred to the web version of this article.)

anoma, the number of cases was 324.635 with a mortality rate of 17.5%. However, incidence and mortality rates of KCs are believed to be underreported or are at least incomplete [34-36] because traditional cancer registries often exclude KC since skin cancer typification is not mandatory in many countries.

UV light exposure is, in general, the overwhelming environmental risk factor for skin cancer development. Over 80% of KCs affect sun-exposed areas such as the head, neck and the back of the hands [34,35]. Immunosuppression is also a very relevant risk factor for squamous cell carcinoma (SCC), as immunosuppressed transplant recipients bear a 100-fold risk for the development of cutaneous SCC. In these cases, the tumors occur earlier in life and are more aggressive, with a metastasis rate of up to 10% [37]. Cutaneous human papillomavirus of the genus beta is a particular risk factor in SCC. Viral DNA has been detected in 18–84 % of SCCs and it is suggested that the correlation comes from viral inhibition of DNA repair and/or apoptosis of UV-damaged cells [38]. Additional risk factors common to both KCs are eye (green/ blue) and hair (blonde/red) colors, age (>70 years), sex (males) and chronic inflammation of the skin [38].

A general representation of these three types of skin cancer is given in Fig. 2.

Squamous cell carcinoma (SCC) develops from the stem cells of the basal cell layer of the epidermis. On the other hand, basal cell carcinoma can develop from the keratinocyte stem cell-rich hair follicle's bulge region or again from stem cells of the basal cell layer of the epidermis [39,40]. The origin of melanoma cells is still under debate. There is evidence that precursor cells may arise from the differentiated melanocytes or from melanocyte progenitor cells in the bulge region of hair follicles or even from neural crest-derived Shwann cell precursors [41].

Skin SCC accounts for approximately 20% of all cases of KCs and its development is related to frequent chronic UV exposure, and is sometimes associated with non-healing wounds or scarring. It is also often associated chronic immuno-inflammatory processes, such as actinic keratosis or Bowen disease (very early, *in situ* form of SCC). On the other hand, cutaneous basal cell carcinoma is usually associated with intermittent, infrequent, intense UV exposure and almost invariably arises *de novo* [42].

Basal cell carcinomas (BCCs) are the most frequently diagnosed human cancer in people of European ancestry, being responsible for 80 % of KCs. Although appearing with high incidence, mortality is extremely low. BCC was considered a "molecular black box" until the late 1990 s and early 2000 s [42]. Most of the cases have sporadic occurrence, but correlation with basal cell nevus syndrome has been identified, with mutations on the patched 1 (PTCH 1) gene [43] and p53 [44] aberrant Hedgehog signaling as the pivotal defect leading to formation of these tumors [42,45]. This discovery has facilitated a remarkable increase in our understanding of BCC carcinogenesis and has highlighted the promising development of Hedgehog inhibitors in halting or reversing the growth of BCCs [46,47].

Melanoma arises from genetic mutations in melanocytes, especially due to UV exposure [48]. Although it accounts for only 1% of all skin malignant tumors, cutaneous malignant melanoma is the most aggressive and the deadliest form of skin cancer therefore, early identification and mutation tests are crucial for a successful treatment [49].

Both cutaneous SCC and melanoma are very likely to metastasize whereas cutaneous BCC very seldom does [42]. It is estimated

**Table 1**
Definition of antitumoral potency parameters used across the studies compiled in this review.

| | |
|---|---|
| $EC_{50}$ | The $EC_{50}$ is the concentration at which half the maximal effect is observed; this is the usual measure for agonist assays [83]. |
| $IC_{50}$ | Concentration of a substance that causes a defined inhibition of a given system: $IC_{50}$ is the median concentration that causes 50% inhibition [84]. |
| $GI_{50}$ | The drug concentration resulting in a 50% reduction in the net protein increase (as measured by SRB staining) in control cells during the drug incubation [85]. |
| TGI | The drug concentration resulting in total growth inhibition. Signifies a cytostatic effect [85]. |
| $LC_{50}$ | The drug concentration resulting in a 50% reduction in the measured protein at the end of the drug treatment as compared to that at the beginning) indicating a net loss of cells following treatment. Signifies a cytotoxic effect [85]. |
| $LD_{50}$ | Lowest amount of a substance which kills 50% of test animals under defined conditions [84]. |

that <0.1 % of the BCC cases metastasize. For SCC, 8% of patients relapse and 5% present metastasis within 5 years. The prognosis of patients with metastatic SCC is 10–20% survival rate over 10 years [18].

Finally, a rarer type of skin cancer, first describe in 2008, is called Merkel cell carcinoma (MCC). Similar to the other types of skin cancers, MCC occurs on sun-exposed areas. Nevertheless, its more distinct trait is that approximately 80% of cases in the northern hemisphere are caused by the Merkel cell polyomavirus (MCV), while UV-induced DNA damage is implicated in MCV-negative cases [50].

### *1.4. Gold standard interventions and approved targeted chemotherapies*

The first line of treatment for cutaneous KCs is the surgery resection of the tumor. Mohs micrographic surgery tends to be favored over standard surgical excision for offering greater surgical precision [51-53], which is especially important for carcinomas in the nose, ears, and mouth for example. Also, the recurrence rate for keratinocyte carcinomas is significantly lower when they are treated with Mohs micrographic surgery than with traditional surgery. Moreover, various forms of physical destruction and topical radiation therapy may be used in cases of low risk tumors [54]. Although KCs have a lower mortality rate than melanoma and the surgical forms of treatment are efficient in many cases, these diseases and their treatment have negative social and emotional impacts due to the possible disfiguring and destruction of skin in exposed areas resulting in anxiety, depression and social isolation [55]. Therefore, new forms of less aggressive therapies, including neoadjuvant chemotherapy, are highly desired in these situations [56].

Nonsurgical topical treatments of KCs are usually recommended only for smaller or superficial tumors and in the absence of metastasis [52,57], as an adjuvant to the Mohs technique. These options are radiation and photodynamic therapies, immunotherapy with intralesional interferon, topical 5% imiquimod and chemotherapy with 5-fluorouracil or retinoids. Oral capecitabine (a prodrug to 5-fluorouracil), paclitaxel (Taxol) or intravenous platinum-based regimens are also described in some cases [52].

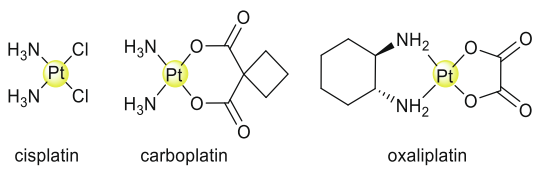


**Fig. 4.** Structures of the Pt(II) drugs cisplatin, carboplatin, and oxaliplatin.

One of the most common topical treatments for cutaneous KC is a 5% formulation of Imiquimod (Fig. 3, KC chemotherapy), a topical immune response modifier that targets the toll-like receptors 7 and 8, which are commonly involved in responses to pathogens [58]. It is capable of enhancing both innate and adaptive immune pathways and up-regulates inflammatory pathways targeting diseased tissue [58]. There is evidence that topical imiquimod activates Langerhans cells inducing migration to local lymph nodes to activate the adaptive immune system in mice [59]. Other cells activated by imiquimod include natural killer cells, macrophages and B-lymphocytes [60]. It is often recommended for patients that are not surgical candidates or refuse to undergo surgery, which in most cases are elderly patients [61]. According to the 2018 Guidelines of care for the management of cutaneous SCC, topical therapies (imiquimod or 5-FU) and PDT are not recommended for the treatment of cSCC on the basis of available data [62]. Radiation therapy is used in situations where surgical treatment is not viable, but this mode of treatment may result in lower cure rates [62].

Cemiplimab-rwlc (Libtayo) was approved by the FDA in the end of 2018 specifically for the therapy of advanced and/or metastatic cutaneous SCC. Cemiplimab is an intravenous human monoclonal antibody directed against programmed cell death-1 receptor (PD-1). It blocks T-cell inactivation and enhances the immune system's anti-tumor response [67,68]. It is interesting to notice that SSC has characteristic high mutation rates and the disease risk is strongly associated with immunosuppression, which made immunotherapy a perfect alternative of treatment [68]. Squamous cell skin cancer cells also often overexpress epidermal growth factor receptors (EGFR) on their surfaces. Cetuximab, an EGFR antagonist (Fig. 3, KC immunotherapy), has been approved by the FDA for the therapy of locally, regionally advanced or metastatic squamous cell carcinoma of the head and neck, either as monotherapy for recurrent progression of the disease after platinum-based therapy, or in combination with radiation therapy or platinum-based therapy with fluorouracil [69].

It is very rare for basal cell cancers to reach an advanced stage, but if they do, these cancers can be hard to treat. As previously discussed, most basal cell cancers have mutations in in the hedgehog signaling pathway. Vismodegib (Erivedge®) and sonidegib (Odomzo®) are examples of organic Hedgehog signaling pathway inhibitors that clinically used to treat some advanced or recurrent basal cell skin cancers [70,71]. However, it was reported that the use of vismodegib against BCCs caused the development of cutaneous SCC at sites distant to the primary BCC. This is unexpected, since hedgehog/Gli1 signaling was thought to be relevant for the regulation of hair follicles [34]. It was also shown that an aberrant hedgehog/Gli1 signal pathway facilitates proliferation, invasion, and migration of cutaneous SCC through regulating vascular endothelial growth factors [72].

Although surgery is also the primary treatment of all stages of melanoma [73], the chemotherapy for advanced melanoma is different than for KC (Fig. 3). The only chemotherapy treatment for advanced melanoma since the 1970′s was often single agent dacarbazine, but now there are potentially multiple lines of treatment that were introduced in the last 10 years. Examples include immunotherapy, targeted treatment options and drug combination therapy, which includes carboplatin plus paclitaxel [74]. Nonetheless, an actual improvement of overall survival of patients using these new treatments is still debatable. There are still challenges and opportunities to the development of novel melanoma chemotherapeutics. Many other drugs have been frequently prescribed off-label, such as temozolomide, paclitaxel, docetaxel and cisplatin, but the revolution in the treatment of melanoma was the introduction of the first immunotherapeutic drugs ipilimumab

[75], pembrolizumab [76] and nivolumab [77], that are checkpoint inhibitors [74].

In cases of unresectable or metastatic melanoma with BRAF gene mutation, which happens in 40% of cutaneous melanoma, first line therapy with dabrafenib plus trametinib is very efficient in short-term (objective response rates of 64–69%) [78,79] and was recently proven to be long-term beneficial in approximately one third of the patients [80]. Vemurafenib is an inhibitor of the B-Raf enzyme developed by fragment-based drug discovery for the treatment of late-stage melanoma. The name "vemurafenib" comes from V600E mutated BRAF inhibition.

## 2. Scope

The scope of this review covers non-melanoma (cutaneous keratinocyte carcinomas) and melanoma skin cancer treatments based on metallopharmaceutical compounds, discussing examples of anticancer agents for which are available quantitative *in vitro* antiproliferative data ($IC_{50}$ or similar) or *in vivo* experiments using animal models, and finally describing case reports of treatment regimens with cisplatin and ongoing clinical trials.

This review is focused on examples of metal complexes from the last 2 decades, but important classical references are also included for contextualization. To enable a structure–activity discussion, the search was also limited to discrete molecular entities, therefore excluding metal nanoparticles and metal-containing therapeutic interventions without defined molecular formula.

We have compiled the antitumoral potency for each compound in every skin cancer cell line originally tested in a table. This table has been deposited in the open access repository Zenodo and it can be accessed at https://zenodo.org/record/5055531 [81]. Compounds are grouped by oxidation state of the metal center and ligand type. Other information listed include molecular weight with and without the counter ion(s), charge, cell lines tested, type of assay, incubation time, whether the data is part of a NCI-60 screening [82] (which consists of nine tumor subtypes and approximately 60 cell lines, including 8 melanoma cell lines), year and citation to the original reference.

A definition of the antitumoral potency parameters mentioned here ($IC_{50}$, $GI_{50}$ and/or TGI) is given in Table 1. A description of the KC and melanoma cell lines assayed for antiproliferative screening *in vitro* in the studies mentioned throughout this review is given at the end of this manuscript.

With this data analysis, we proceeded with the identification of lead compounds and discuss their key features for the development of new strategies to treat skin cancers.

In the final section, we analysed how the advances in modern "omics" are leading to new biological targets that may be of relevance for devising metallodrugs with selectivity for skin tumours.

## 3. Metal complexes with *in vitro* or pre-clinical data over skin cancer cell lines

### 3.1. Platinum

#### 3.1.1. The case of cisplatin and its analogues

Cisplatin and the analogues carboplatin and oxaliplatin (Fig. 4) are ubiquitously used as positive controls in antiproliferative experiments. For that reason, they constitute an excellent body of data to evaluate the consistency of the different antiproliferative protocols discussed in this review, and as a good parameter for comparing the cytotoxic response across many cell lines.

Data on the *in vitro* activity of cisplatin over melanoma and KC cell lines was gathered and ordered from the literature using the $IC_{50}$ value as parameter. Such data is presented in Table S1 and Fig. S1. The first noticeable trend in the data obtained from different sources is that, for identical experimental conditions (same cell line), the incubation time greatly affects the distribution of $IC_{50}$ values of cisplatin. The greater the incubation time, the lower the average and standard deviation of the $IC_{50}$ values reported across different studies. This can be observed, for instance, in MTT assays with cisplatin against the A375 malignant melanoma cell line with 48 h of incubation, we found an average $IC_{50}$ of 14.6 ± 7.1 μM, while for 72 h the average $IC_{50}$ value found across the literature was 3.8 ± 3.5 μM. The influence of the incubation time in MTT assays using cisplatin against 518A2, A375, A431 and B16-F10 cell lines is shown in Fig. S2.

Another important variable is the antiproliferative assay selected to determine $IC_{50}$, as for example MTT or sulforhodamine B (SRB). For A431 cells, the mean $IC_{50}$ values for cisplatin tested by MTT assay are 40.1 μM for 24 h of incubation (n = 1), 10.4 μM for 48 h (n = 2) and 2.5 μM for 72 h (n = 8). However, the general $IC_{50}$ values obtained by SRB assays are lower across all incubation times, 4.45 μM for only 6 h of incubation (n = 2), 4.85 μM for 24 h

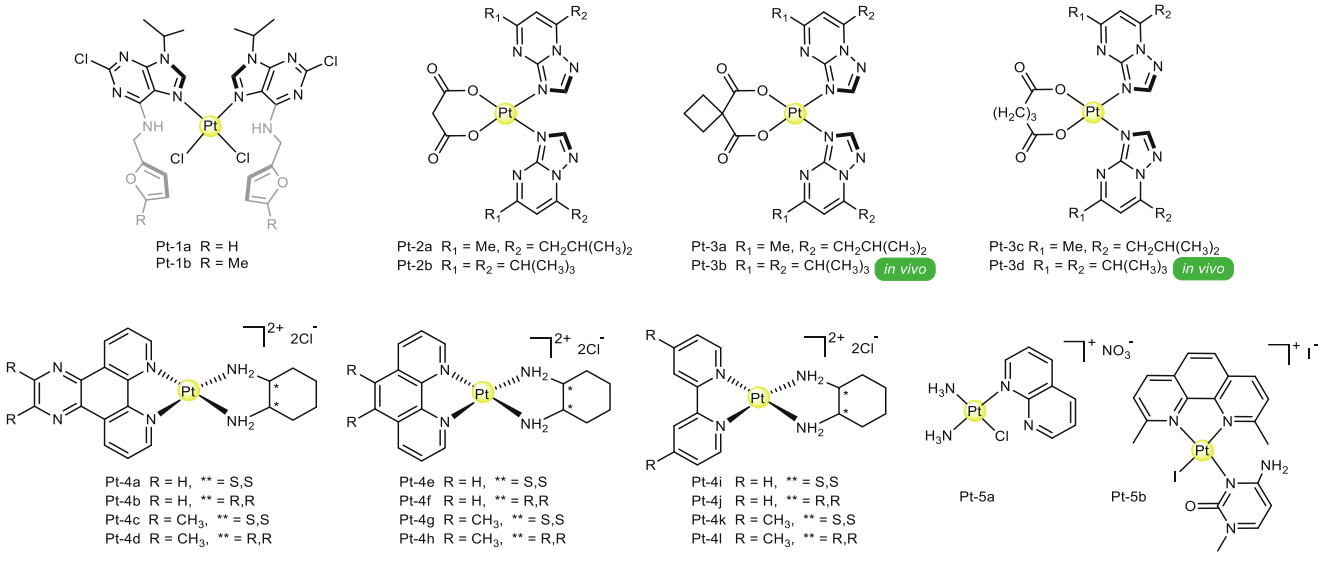


**Fig. 5.** Platinum(II) complexes of N-heterocyclic ligands.

(n = 2) and 0.65 for 96 h (n = 1). Moreover, comparing only SCC cell lines, the A431 cells were the most susceptible to cisplatin at 48 h, 72 h and 96 h of incubation.

It can also be observed that assays performed with the WST-1 kit gave $IC_{50}$ values much higher than in the case of MTT- or MTS-based assays. This trend is observed for A549 and B16-F10 cells, at either 24 or 48 h of incubation.

A summary of antitumoral activity potencies of carboplatin, and oxaliplatin is also given at Table S1. Although less data was found for these complexes, NCI-60 assays were available for all of them. When comparing their $IC_{50}$ values, it is noticeable that cisplatin and oxaliplatin are more potent against the melanoma cell lines in the NCI-60 assays than carboplatin ($IC_{50}$ values range from 43.7 to 190.7 μM, average of 127.1 μM).

The molecular mechanisms of cisplatin and its derivative complexes are associated to the crosslink with the purine bases on the DNA, which interferes with the mechanisms of DNA repair, leading to effective DNA damage and subsequently inducing apoptosis in the cancer cells. However, a very small amount of the platinum drug generally reaches the nucleus of the cancer cell to exert its mechanism, as the rest may interact with other nucleophilic targets in the bloodstream or in the cell membrane, the cytoplasm and organelles, where protein interactions and redox processes may also be involved. Moreover, it has become clearer in the last years that metal drugs can significantly impact the patient's immune system and that the immune factor contributes more than early anticipated to their anticancer activities [86].

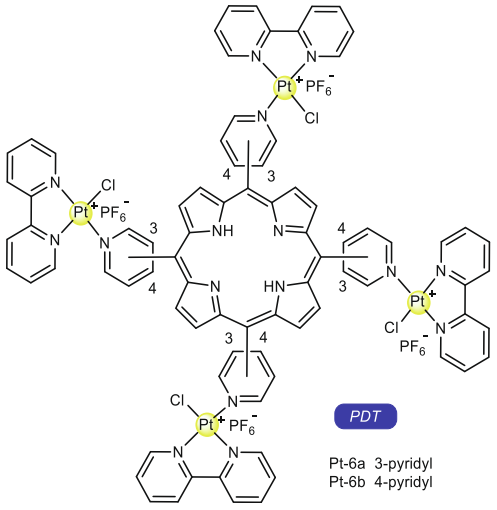


**Fig. 6.** Porphyrin photosensitizer complexes **Pt-6a** and **Pt-6b**.

There is evidence in the literature suggesting that the immune-modulating effects of platinum-based agents, may be very significative in achieving clinical response [87]. One way it may happen is by triggering immunogenic mode of tumor cell death (ICD). In the process of ICD, the cell is exposed to stressors causing alterations in the cell membrane and immune signaling in the tumor microenvironment, including exposure of calreticulin and heat-shock proteins (HSPs) 70/90 to the cell surface and releasing of high-mobility group box 1 protein (HMGB1), type 1 interferon (IFN) and protein CXCL10 [88-90].

In a recent study, it has been shown that cisplatin treatment selectively decreased the amounts of myeloid-derived suppressor cells (MDSC), in a murine B16 melanoma model. It was paralleled by loss of the MDSC marker Gr-1 and gain of the dendritic cells marker CD40 at the cell surface and loss of activity against CTL (cytotoxic T lymphocytes) and CIK (cytokine-induced killer) effector cells [91]. Accordingly, the immune-inhibitory functions of MDSC were distinctly reduced by cisplatin in the A375 human melanoma xenograft nude mouse model, and proliferation of CTL, together with IFN-γ production, were massively enhanced when cocultured with cisplatin-pretreated MDSC [92].

The immunogenic effect of cisplatin and oxaliplatin were evaluated in a preclinical model head and neck squamous cell carcinoma (HNSCC) [89]. In this study, human HNSCC cell lines were treated with cisplatin or oxaliplatin and, in both cases, markers associated with immunogenic cell death (ICD) such as calreticulin, HSP70, MHC class I and PD-L1 were identified in increased levels in the cells surface, but the complexes fail to induce robust secretion of HMGB1 and ATP [89].

Then, in a syngeneic mouse model of oral cancer, immunocompetent mice were inoculated with the HNSCC cells killed *in vitro* by either of the complexes. This inoculation was able to prevent the establishment and growth of subsequently injected live tumor cells in a small proportion of the animals. Therefore, in this case, cisplatin and oxaliplatin chemotherapy were able to induce similar immunogenic responses at clinically relevant doses in the preclinical models of HNSCC [89].

Additive activity is seen when cisplatin or oxaliplatin are combined with anti-PD-1 immunotherapy in this same model, with both complexes inducing similar tumour growth delay. The results suggest that these Pt(II) drugs might be further explored in chemotherapy regiments in combination with PD-1 blockade and perhaps other immunotherapies [89].

### 3.1.2. Other Pt(II) compounds

Trávníček and coworkers reported Pt(II) complexes of derivatives of kinetin, a plant hormone [93]. The cisplatin-like compounds (**Pt-1a** and **Pt-1b**, Fig. 5) showed promising activity over the G-361 melanoma cell line, with $IC_{50}$ values of 3.8 ± 0.1 and 4.0 ± 0.2 μM (MTT, 24 h, cisplatin: 5.8 ± 0.8 μM), respectively and

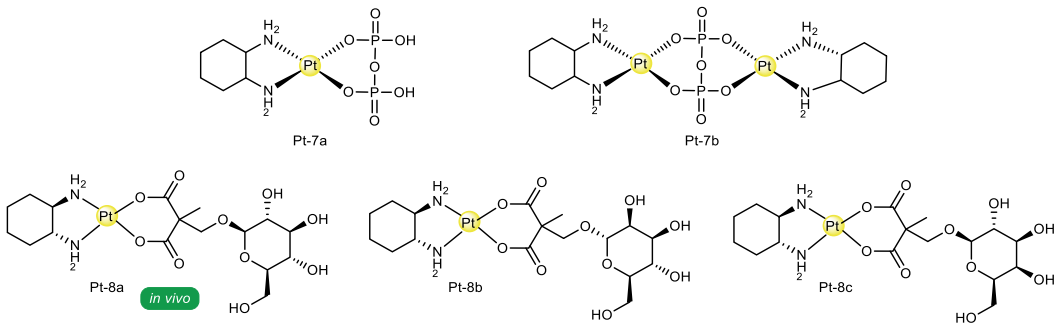


**Fig. 7.** Pt(II) complexes of pyrophosphate and glycoconjugate ligands.

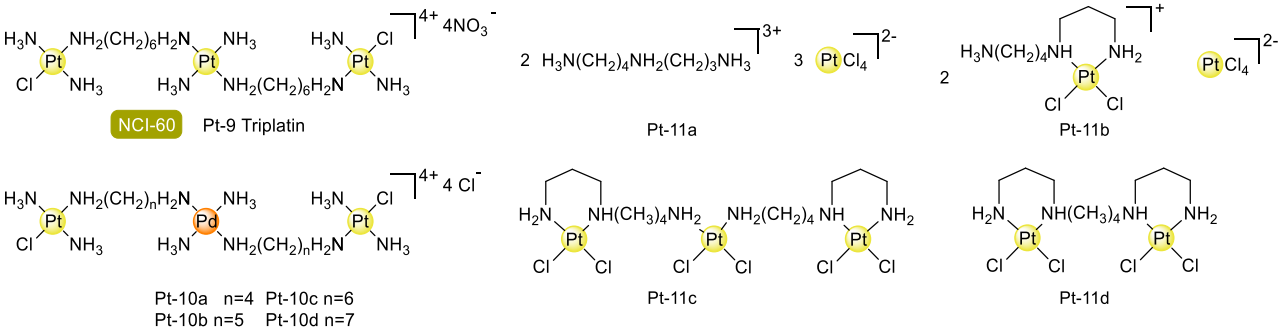


**Fig. 8.** Triplatin and other polynuclear Pt(II) complexes.

these were also able to overcome cisplatin resistance on the A2780R cell line, with an approximate 10-fold increased activity when compared to cisplatin.

The *in vitro* antiproliferative activity of heteroleptic Pt(II) complexes with purine ligands and dicarboxylic acids such as malonate (**Pt-2a** and **Pt-2b**, Fig. 5) [94], glutarate (**Pt-3a** and **Pt-3b**, Fig. 5) [95] and cyclobutane-1,1-dicarboxylato, or CBDC, (**Pt-3c** to **Pt-3d**, Fig. 5) [95] were evaluated by Łakomska et al. against several cancer cell lines, including B16 and FaDu.

From the complexes with malonate ligand, **Pt-2b** yielded the highest antiproliferative results, with $IC_{50}$ = 3.79 ± 0.33 μM for B16, which is 6.9 times lower than $IC_{50}$ for **Pt-2a** and also superior to cisplatin ($IC_{50}$ = 8.30 ± 1.53 μM). As for FaDu cells, **Pt-3b** also showed better results ($IC_{50}$ = 2.86 ± 0.53 μM) than **Pt-3a** ($IC_{50}$ = 1 3.78 ± 5.74 μM) and similar to cisplatin ($IC_{50}$ = 2.83 ± 1.00 μM). The difference in cytotoxicity of **Pt-2a** and **Pt-2b** might be explained by the higher lipophilicity of the latter. Both **Pt-2a** and **Pt-2b** are more selective to cancer cells than cisplatin in comparison to normal mouse fibroblast cells (BALB/3T3).

The complexes with glutarate and CBDC ligands followed a similar trend. Derivatives with the lipophilic pyrimidine ligand (**Pt-3b** and **Pt-3d**, $IC_{50}$ = 1.9 ± 0.4 and 2.5 ± 0.5 μM, respectively) showed much higher antiproliferative activity against FaDu cells than their less lipophilic analogues **Pt-3a** and **Pt-3b**, which were about 10-fold less active *in vitro*. Additionally, **Pt-3b** and **Pt-3d** exhibited better activity and selectivity than cisplatin, carboplatin and oxaliplatin against cancer cells including FaDu.

Moreover, cell cycle arrest was assayed for the **Pt-2a** and **Pt-2b** complexes in A549 cells and for the **Pt-3b** and **Pt-3d** complexes in 4 T1 cells. It was observed that these complexes arrested cell cycle

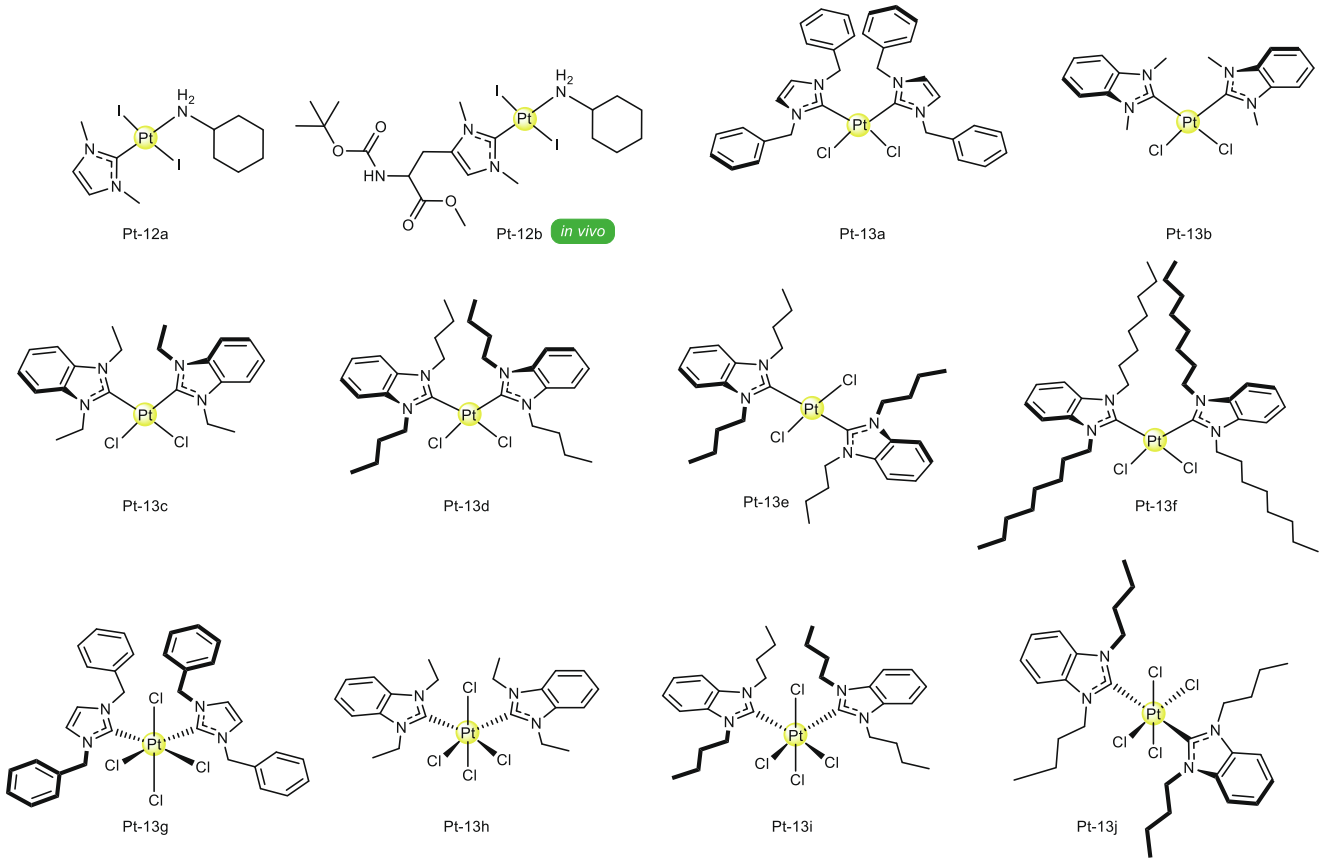


**Fig. 9.** Pt(II) and Pt(IV) complexes with NHC ligands.

in the G0/G1 phase in A549 cells and decreased the number of cells in the S phase, without affecting cells in the G2/M phase.

The toxicity of the complexes **Pt-3b** and **Pt-3d** was tested on healthy BALB/c animal models. They exhibited less toxicity ($LD_{50}$ = 30 mg/kg for **Pt-3b** and $LD_{50}$ > 100 mg/kg for **Pt-3d**) when compared with cisplatin ($LD_{50}$ = 13.6 mg/kg, i.p.) and oxaliplatin ($LD_{50}$ = 19.8 mg/kg, i.p.) in BALB/3C mice. Additionally, **Pt-3d** did not cause myelosuppression or thrombocytopenia in mice at the administered dose of 20 mg/kg. Notably, its accumulation in the liver of the animals was 5-fold lower than for **Pt-3b**.

The series of Pt(II) complexes **Pt-4a** to **Pt-4l** (Fig. 5) was designed for DNA interaction studies and its correlations with cytotoxicity. These molecules have polyaromatic N^N ligands and a diaminocyclohexane ligand with either S,S or R,R configurations [96].

The use of the varying N^N ligands allowed comparing the DNA affinity and aromatic surface area of these complexes. The methylated variants of each ligand were included due to the impact that these groups have in the cytotoxicity and DNA binding properties. It was shown by UV–vis binding assays, linear dichroism spectroscopy and isothermal titration calorimetry, that complexes with S,S ligand configurations were capable of binding to DNA with an affinity of approximately $10^5$–$10^6$ $mol^{-1}$, preferentially to GC base-pairs over AT ones, as suggested by mass spectrometry studies, and with intercalation as the primary binding mode (other potential modes were possible at higher concentrations of complex). Complexes **Pt-4g** and **Pt-4i** were found to be the most and least potent DNA binders, respectively [96].

The S,S isomers were also significantly more cytotoxic to A431 cells than their respective R,R analogues, with the pair **Pt-4g** (S,S) and **Pt-4h** (R,R) showing the lowest $IC_{50}$ values of 0.05 ± 0.02 μM and 0.93 ± 0.03 μM, respectively. For complexes **Pt-4e** to **Pt-4l**, the DNA affinity correlated well with the observed cytotoxicity, suggesting that DNA binding plays a role in the apoptotic activity of these complexes.

Inspired by the promising anticancer activity of pyriplatin and phenanthriplatin, Margiotta and coworkers reported a Pt(II) of 1,8-naphthyridine, **Pt-5a** (Fig. 5) [97]. The cytotoxicity of **Pt-5a** against A375 and A431 cells was compared with the values presented by **Pt-5b**, a compound previously reported by the same group. Despite undergoing ligand replacement in the presence of glutathione, **Pt-5a** showed low micromolar range $IC_{50}$ values over both cell lines, while **Pt-5b** presented submicromolar values. Improved cell uptake of **Pt-5a** and **Pt-5b** and the cellular DNA platination levels were in part associated to cytotoxicity, but a direct correlation with $IC_{50}$ values was not found.

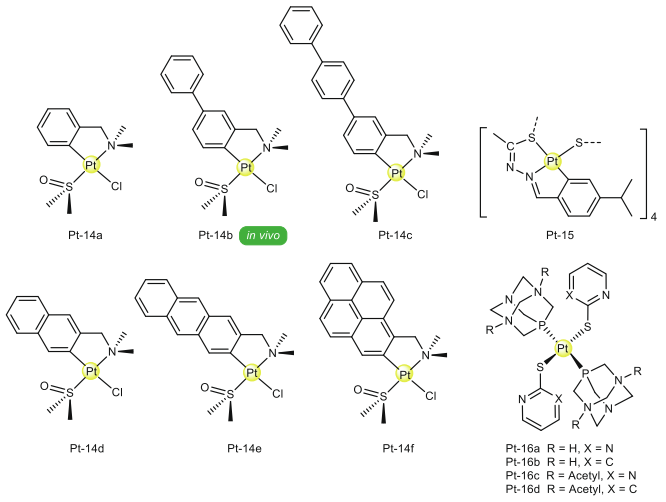


**Fig. 10.** Organometallic Pt(II) complexes (**Pt-14a-f** and **Pt-15**) and Pt(II) complex with phosphadamantane and thiopyridine or thiopyrimidine ligands (**Pt-16a-d**).

The porphyrin complexes **Pt-6a** and **Pt-6b** (Fig. 6) [98] were evaluated as photosensitizers against WM1366 human cutaneous melanoma cells. After 30 min of light exposure (white LED – 400 to 800 nm, 50 $mW/cm^2$) **Pt-6a** and **Pt-6b** inhibited the growth of the melanoma cells with $IC_{50}$ of 4.50 ± 0.58 nM and 3.01 ± 0.27 n M, respectively. In the dark, the complexes were not able to reach $IC_{50}$ in the highest concentration tested (56.25 nM). They were also less toxic to normal CHO hamster ovarian cells, showing some selectivity. These complexes showed affinity to low density lipoproteins (LDL), which can be a target as neoplastic cells have higher uptake of LDL [99]. The complexes induced apoptosis of WM1366 cells via activation of caspases 3 and 9. Reorganization of actin was also observed corroborating with death by apoptosis.

The Margiotta group reported mononuclear (**Pt-7a,** Fig. 7) and binuclear (**Pt-7b**) pyrophosphate Pt(II) complexes that release kiteplatin, [$PtCl_2$(*cis*-1,4-diaminocyclohexane)], upon hydrolysis [100]. Kiteplatin has been tested for antitumor activity in solid tumors before, exhibiting a different and broader spectrum of activity than cisplatin and oxaliplatin. Although its binding mode to DNA is similar to cisplatin, DNA adducts of kiteplatin inhibit DNA polymerase more efficiently, and makes DNA repairing more difficult, which helps to overcome resistance to platinum drugs [101].

The cytotoxicity of **Pt-7a** and **Pt-7b** was assessed over a panel of cancer cell lines, which included A375 melanoma. The $IC_{50}$ values over this cell line after 72 h incubation (MTT assay) were 1.26 ± 0.11 and 0.22 ± 0.03 μM for the mononuclear and binuclear complexes, respectively (control: cisplatin, 2.41 ± 0.62 μM), which indicated that the binuclear species is much more active than the mononuclear one. These results were related to the increased cell uptake of **Pt-7b** and due to its faster rate of hydrolysis in biologically-relevant media, which resulted in the release of the active species kiteplatin.

A series of Pt(II) glycoconjugate complexes of glucose, mannose and galactose, **Pt-8a** to **Pt-8c** (Fig. 7), has been reported [102]. Glycoconjugation is a promising strategy for the development of metallodrugs, since cancer cells usually display a high rate of glycolysis due to overexpression of glucose transporters. Glucose transporter 1 (GLUT1) was shown to be overexpressed in KCs [103] and is related to enhanced metastasis in malignant melanoma [104]. Compounds **Pt-8a** to **Pt-8c** were more water-soluble than oxaliplatin and presented submicromolar activity against A375 melanoma cells (**Pt-8c** was the most active, $IC_{50}$ = 0.37 ± 0.21 μM) and low micromolar ($IC_{50}$ = 9.10 ± 0.40 μM for **Pt-8b**) against A431 cells. Additional experiments confirmed the GLUT-mediated uptake of these compounds. *In vivo* studies in DBA/2 mice models revealed that **Pt-8a** is much more tolerated than cisplatin and oxaliplatin, and the maximum tolerated dose and $LD_{50}$ values were 6- and 10-fold higher than cisplatin, respectively. 100 % of mice bearing L1210 ascitic leukemia treated with **Pt-8a** survived for 52 days after a 3-week treatment protocol, compared with only 20 % for cisplatin-treated mice under the same protocol. This study highlighted that metallodrug-glycoconjugates should be more explored in future studies as a strategy for drug development, especially in skin cancer therapy.

Farrell's group pioneered the development of trinuclear platinum compounds, starting with triplatin (**Pt-9**; previously known as BBR3464, Fig. 8). Triplatin (**Pt-9**) was screened against the NCI-60 panel and showed a cytotoxic profile that differs from that of cisplatin. Looking at the melanoma cell lines, triplatin had nanomolar $GI_{50}$ values against SK-MEL-5, UACC-257 and UACC-62. The highest potency was observed against UACC-62, for which the compound had an $GI_{50}$ of 4.8 nM [105]. The promising results encouraged the authors to further assay **Pt-9** against a panel of four additional melanoma cell lines that are naturally resistant to

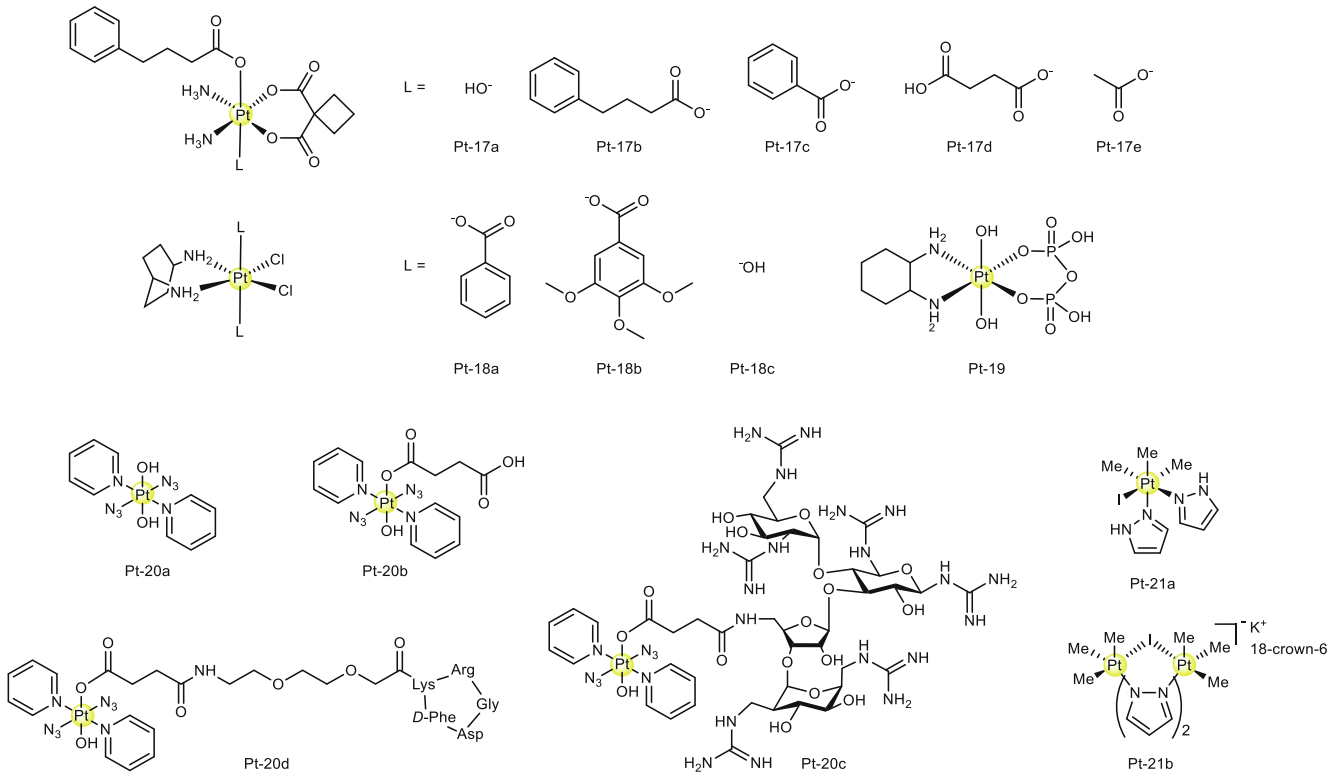


**Figure 11.** Other Pt(IV) complexes (Pt-17 to Pt-21)

**Fig. 11.** Other Pt(IV) complexes (Pt-17 to Pt-21).

cisplatin (Me665/2/21, Me665/2/60, M14 and JR8). Against this focused panel, **Pt-9** was at least 20-fold more potent than cisplatin, with a striking > 800-fold increase in cytotoxicity observed against Me665/2/60 ($IC_{50}$ = 40 ± 16 nM for **Pt-9**, vs. 35.3 ± 6.6 μM for cisplatin).

Inspired by the structure of triplatin (**Pt-9**), Huq and colleagues prepared trinuclear analogues with a central Pd(II) unit and linkers with variable chain lengths (**Pt-10** series, Fig. 8) [106]. The compounds were assayed *in vitro* against Me-10538 melanoma cell lines. **Pt-10c** and **Pt-10d** (with 6 and 7 carbon atoms in the diamine linker, respectively) were more potent than cisplatin, with $IC_{50}$ values of 0.87 ± 0.004 and 2.52 ± 0.8 μM (vs. 4.96 ± 0.7 μM for cisplatin). Cellular uptake was studied in A2780 cells. Intracellular platinum levels followed the increase of lipophilicity upon increasing the size of linker chain (**Pt-10d** > **Pt-10c** ≈ **Pt-10b** > **Pt-10a**). In all cases, the uptake was higher than that observed for cisplatin, although all compounds but **Pt-10c** were less toxic than cisplatin for this particular cell line.

Polynuclear Pt(II) complexes (**Pt-11a** to **Pt-11d**, Fig. 8) were tested against HSC-3 cells [107]. Complex **Pt-11a** was the least active with $IC_{50}$ = 96.0 μM and **Pt-11c** is the most cytotoxic with $IC_{50}$ = 11.0 μM, while **Pt-11b** and **Pt-11d** exhibit $IC_{50}$ = 20.0 μM. Results indicated that the antiproliferative activity increased with the number of Pt(II) ions coordinated to nitrogen atoms in cisplatin-like moieties, which is consistent with more specific covalent binding sites of these complexes with DNA. Moreover, **Pt-11a** to **Pt-11d** showed very low toxicity ($IC_{50}$ > 100 μM) to non-neoplastic L-132 cells (human embryonic fibroblasts from lung tissue) and therefore were potentially selective towards cancer cells [107].

Two platinum-NHC compounds, **Pt-12a** and **Pt-12b** (Fig. 9), had their cytotoxicity tested against 518A2 melanoma cells [108]. The two compounds had low micromolar $IC_{50}$ values (3.7 ± 0.1 and 1. 7 ± 0.1 μM, respectively), and were more active than the corresponding cisplatin and the Ru(II), Ir(III) and Au(I) compounds bearing the same ligand. The cytotoxicity correlated with cell uptake since **Pt-12a** and **Pt-12b** had almost 10-fold increased uptake when compared to cisplatin. DNA interaction studies indicated that **Pt-12b** induced a higher degree of alteration of topology and morphology, which is in agreement with it being more active than **Pt-12a**. Treatment of 518A2 cells resulted in cell cycle arrest in the S-phase and G2/M−phase and a slight reduction of cells in G1-phase, which resembles cisplatin. Antivascular effects of the compounds were evaluated on the extra-embryonic blood vessels in the chorioallantoic membrane of fertilized chicken eggs. Compound **Pt-12a** caused destruction of small blood vessels as well as hemorrhages within the first 8 h after topical application while **Pt-12b** led to the destruction of both small capillaries and big blood vessels within 24 h, correlating with its greater cytotoxicity. This effect is relevant for the development of antimetastatic metallodrugs.

Schobert's group also developed a series of Pt(II) and Pt(IV) compounds with NHC ligands [109]. A total of ten compounds (**Pt-13a** to **Pt-13j**, Fig. 9) were prepared, varying the position of the carbenes to one another (*cis*/*trans*) and changing the nature of substituents on the N-atom of the ligands. Their cytotoxicity was determined over 518A2 melanoma cells and the non-tumorigenic HDFa dermal fibroblasts. The Pt(II) compound **Pt-13d** and the pro-drug Pt(IV) analogue **Pt-13i** were the most active compounds, with remarkably similar cytotoxic profiles. The $IC_{50}$ values found against 518A2 were 1.3 and 1.7 μM for **Pt-13d** and **Pt-13i** after 72 h of incubation. However, the compounds were also highly toxic over the non-tumorigenic HDFa cell line. On the other hand, despite slightly lower potency against the melanoma cell line, compound **Pt-13g** had better selectivity in relation to the fibroblast cell line. The *trans* isomers of **Pt-13e** and **Pt-13j** were not as active over 518A2 cells, but were equally potent as the *cis* isomers on other cell lines (e.g. HT29 colon adenocarcinoma) [109].

A series of six organometallic Pt(II) compounds, **Pt-14a** to **Pt-14f** (Fig. 10), bearing aromatic rings of different sizes had their anticancer properties evaluated over a panel of several cancer cell lines [110]. All six compounds had low micromolar activity against 518A2 melanoma cells, but they displayed the highest activity against A2780 cells, including the cisplatin-resistant one. Overall, compounds **Pt-14b** and **Pt-14d** were the most active ones and this correlated well with their higher cell uptake and greater degree of DNA platination. Flow cytometry experiments indicated high incidence of apoptosis in A2780 cells treated with 1 μM of these two compounds, without increasing necrotic population. Additionally, the compounds did not enhance caspase-3 activity and suppressed ROS generation by the mitochondria, which suggested a caspase-independent mechanism of apoptosis induction. This effect was also correlated with their anti-angiogenic properties. Incubation of EA.hy926 (human umbilical vein endothelial cells) with **Pt-14a** to **Pt-14f** at sub-cytotoxic concentrations resulted in inhibition of the formation of capillary-like structures. Increased lipophilicity resulted in a higher effect when compared to the starting motif of **Pt-14a**. *In vivo* antivascular properties of some of the compounds were evaluated by the chick embryo's chorioallantoic membrane assay. Treatment with 10 nmol of **Pt-14b** resulted in significant vascular-disruptive effects, with degradation of big blood vessels. The antiangiogenic and antivascular properties of the compounds correlated with their ability to inhibit microtubule polymerization. 518A2 melanoma cells treated with 2 μM of **Pt-14b** had an extensive degeneration of the tubulin network, with the cells also appearing rounded. The findings of this study suggest that it is possible to fine-tune the aromaticity/lipophilicity for this class of compounds and achieve desired biological activities.

The distinct tetranuclear Pt(II) complex **Pt-15** (Fig. 10) had its cytotoxicity evaluated against two keratinocyte cell lines PAM and PAM-RAS [111]. While PAM is a normal murine keratinocyte, RAM-RAS is a modified with the H-ras oncogene. The $IC_{50}$ value of cisplatin over PAM and PAM-RAS is 165 μM for both, and **Pt-15** inhibits the same cell lines with $IC_{50}$ = 9 ± 0.6 μM and 30 ± 3 μM, respectively.

Miranda et al [112]. studied water-soluble Pt(II) complexes with *trans* phosphadamantane ligands and thiopyridine or thiopyrimidine ligands (**Pt-16a** to **Pt-16d**, Fig. 10). Complexes **Pt-16a** ($IC_{50}$ = 0.29 μM) and **Pt-16b** ($IC_{50}$ = 0.21 μM) exhibited higher antiproliferative activities than cisplatin, 5-fluorouracil and etopoxide against M19 MEL cells.

### 3.1.3. Pt(IV) compounds

Erxleben in collaboration with Montagner developed a series of Pt(IV) compounds with axial 4-phenylbutyric acid ligands (**Pt-17** series, Fig. 11), a known acid histone deacetylase (HDAC) inhibitor [113]. HDAC inhibitors play an important role in the restriction of the growth and proliferation of melanoma cells especially by inducing cell cycle arrest and apoptosis with different mechanisms [114]. This series was conceptualized to expand on the structure of carboplatin. Compound **Pt-17c** was the most cytotoxic against A431 squamous cell carcinoma ($IC_{50}$ = 5 μM) and A375 melanoma ($IC_{50}$ = 11.1 μM). For comparison, compound **Pt-17c** along with **Pt-17b** were the only two derivatives with positive logP values. **Pt-17c** had the highest intracellular accumulation of all compounds in the series. Finally, HDAC inhibition was followed in A431 cells, with **Pt-17c** identified as the most potent HDAC inhibitor in the series.

Margiotta, Natile and co-authors developed a series of platinum compounds with a fixed 1R,2R-DACH equatorial ligand, and varying axial carboxylate ligands (**Pt-18a** and **Pt-18b**, Fig. 11) [115]. These compounds were designed as Pt(IV) pro-drug analogues of kiteplatin. The parent compound **Pt-18c**, with axial $HO^-$ ligands was also studied in comparison. **Pt-18a** had excellent cytotoxicity against A375 melanoma, with an $IC_{50}$ of 0.06 μM. Uptake experiments were carried out using LoVo cells. **Pt-18a** had the highest

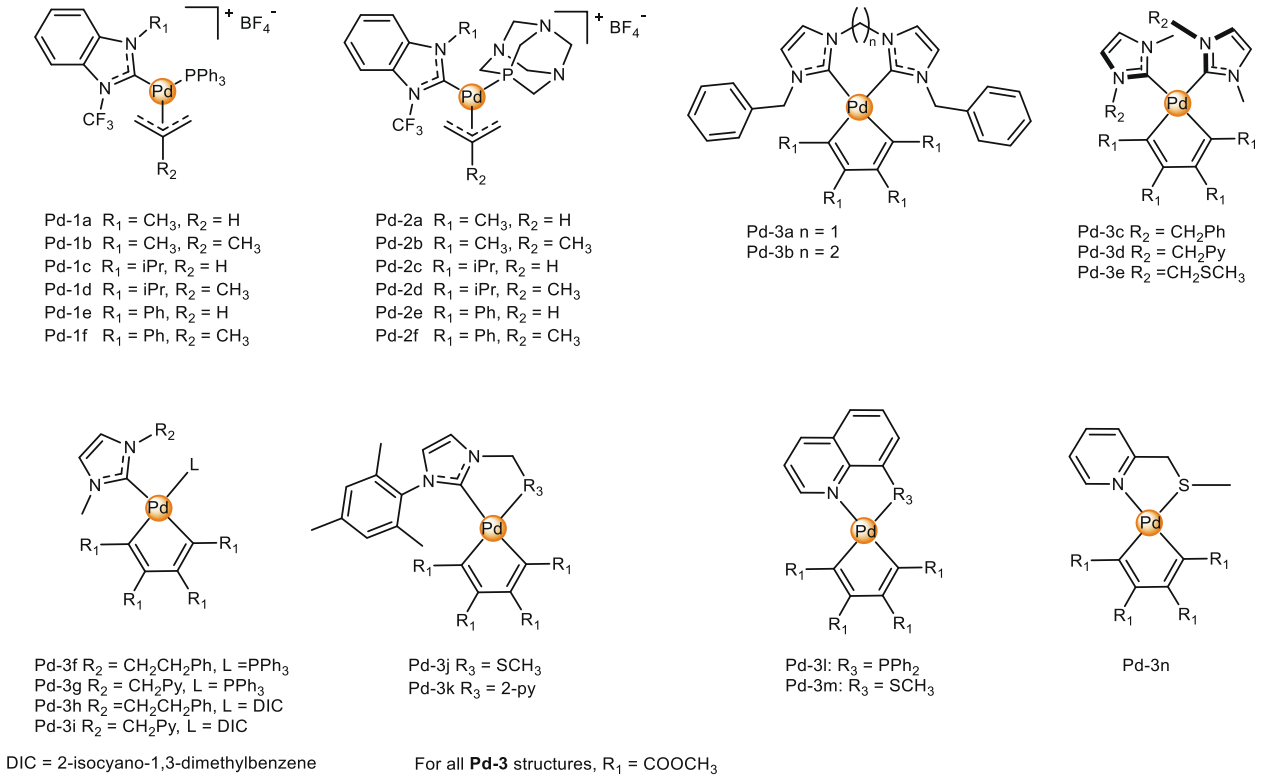


**Fig. 12.** Series of Pd(II) complexes of NHC ligands..

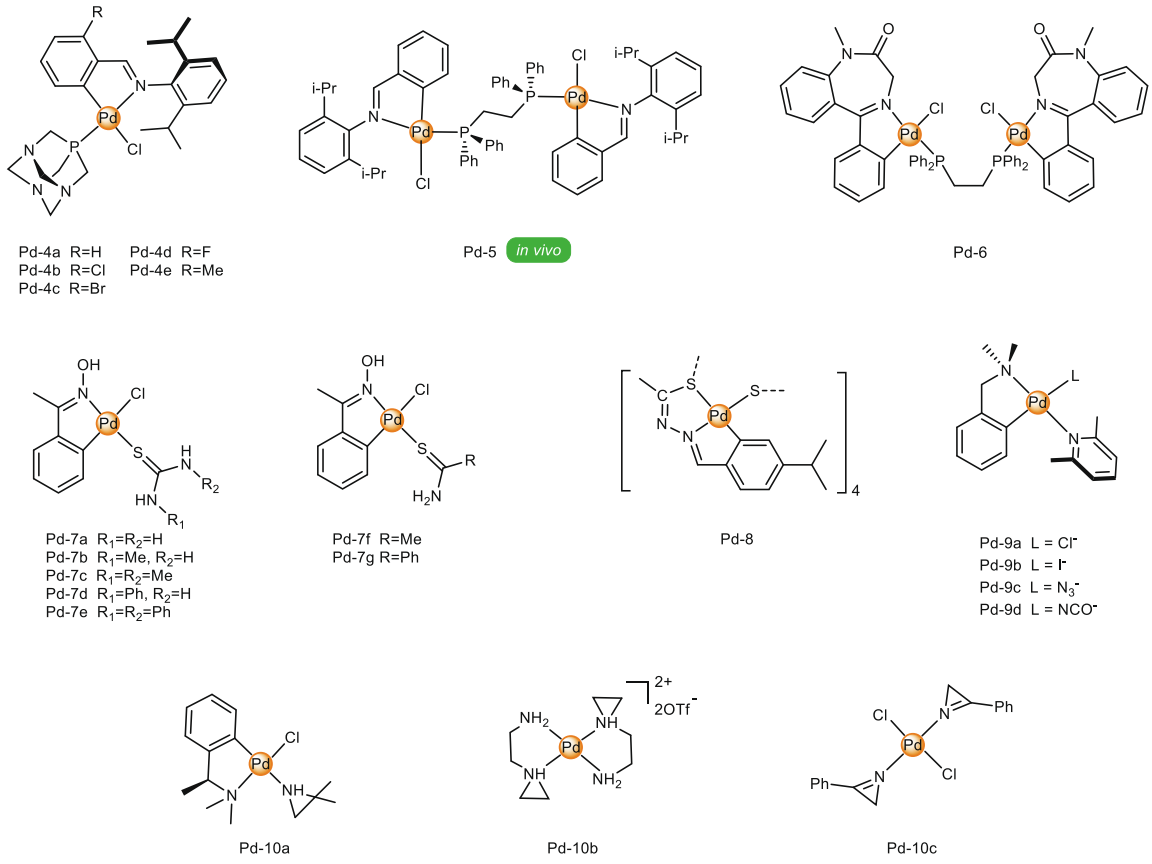


**Fig. 13.** Cyclopalladated compounds.

internalization in the series, but both **Pt-18a** and **Pt-18b** had higher uptakes than kiteplatin. These results correlated with the higher cytotoxicity of compounds **Pt-18a** and **Pt-18b** in relation to kiteplatin, highlighting the effect of the hydrophobic axial carboxylate ligands on the uptake.

The complex **Pt-19** (Fig. 11) is the Pt(IV) analogue of **Pt-7a**, that was designed to mimic the activity of kiteplatin [116]. Complex **Pt-19** is very stable in physiological conditions, and less stable in acidic environment (pH 4.62), undergoing hydrolysis. This lower stability in acidic pH might be an interesting feature as some tumors have acidic microenvironment in their sorroundings. Regarding the activity over A375 cells, **Pt-19** ($IC_{50}$ = 3.05 ± 0.44 μM) was less potent than the Pt(II) analogue **Pt-7a** ($IC_{50}$ = 1.26 ± 0.11 μM). However, this result was expected as many Pt(IV) drugs are less cytotoxic than their Pt(II) analogues due to the reductive activation step necessary to carry out their cytotoxic activity. Moreover, experiments using the HTC-15 colon cancer cells showed that the uptake of the Pt(IV) complex was less than half that of the square planar Pt(II) analogue, which also helped explaining the difference in their antiproliferative activities [117].

Sadler, Marchán and co-workers developed a series of photoactivable Pt(IV) compounds (**Pt-20** series, Fig. 11), including a guanidinoneomycin conjugate [118]. The effect of conjugation on photoactivation, intracellular accumulation and phototoxicity was investigated. The intracellular accumulation of Pt was determined by exposure of SK-MEL-28 to 10 μM doses of the compounds in the dark for 1 h. The guanidinoneomycin conjugate (**Pt-20c**) had a final intracellular concentration of Pt of (276.2 ± 14.3) pmol Pt/$10^6$cells, which is about a four-fold increase in relation to either parent compound, **Pt-20a** and **Pt-20b**. Phototoxicity was studied upon 60 min pre-incubation of SK-MEL-28 cells with the compounds, followed by irradiation with visible light (5 J $cm^{-2}$; $\lambda_{max}$ = 420 nm, λ < 400 nm filtered off, 60–70 min). $IC_{50}$ values were determined by the neutral red dye uptake 24 h after irradiation. Both the conjugate **Pt-20c** and the succinylated precursor **Pt-20b** had the same $IC_{50}$ (15.5 μM), slightly higher than that of **Pt-20a** (10.2 μM). The authors highlighted that the higher intracellular accumulation of **Pt-20c** did not translate into an increased phototoxicity towards SK-MEL-28. The authors hypothesized that an alternative mechanism of action for the **Pt-20c** conjugate must exist, and that guanidinoneomycin modulates the mechanism of action of the drug as a whole, facilitating RNA platination by the photoreleased Pt(II) species.

In another study, Sadler, Marchán and co-workers further explored the **Pt-20b** motif conjugating an integrin-targeting RGD-containing peptide to afford **Pt-20d** [119]. This vector was combined with the photoactivatable Pt(IV) pro-drug for visible light activation within the tumor, conferring a dual control over selectivity. Cytotoxicity was explored towards SK-MEL-28, an $\alpha_V\beta_3$-overexpressing cell line. As negative control, the DU-145 human prostate carcinoma cell line was selected, since the expression of $\alpha_V\beta_3$ integrin was considerably lower, whereas that of $\alpha_V\beta_5$ integrin was similar, as determined by flow cytometry. The phototoxicity of **Pt-20d** was similar to the parent succinylated compound **Pt-20b** against SK-MEL-28 (visible light; $\lambda_{irradiation}$ = 420 nm, 5 J $cm^{-2}$). The conjugated **Pt-20d** was less toxic against DU-145, which has lower levels of expression of $\alpha_V\beta_3$ integrin. Differences were even more pronounced when **Pt-20d** was irradiated with UVA radiation (365 nm, 5 J $cm^{-2}$). The authors highlighted that conjugation to the RGD-containing cyclic peptide

conferred selectivity to **Pt-20d** as further confirmed by cellular uptake experiments. Cells were exposed to a 10 μM dose of compounds **Pt-20a**, **Pt-20b** and **Pt-20d** for 1 h in the dark. **Pt-20d** had an accumulation about 2.8-fold higher in SK-MEL-28 when compared to DU-145.

Complexes **Pt-21a** and **Pt-21b** (Fig. 11) are distinct monomeric and dimeric organometallic Pt(IV) complexes, with methyl, iodide and pyrazole ligands [120]. The difference in antiproliferative activity between the mononuclear and the dinuclear species is clear when the $IC_{50}$ values for the inhibition of A253, A431 and FaDu cells are observed. While the $IC_{50}$ values for **Pt-21a** ranged from 19.3 to 36.4 μM, for **Pt-21b** the numbers were significantly lower, ranging from 0.95 to 2.32 μM. It shows that the *in vitro* antiproliferative activity of **Pt-21b** is comparable to cisplatin, which exhibited $IC_{50}$ > 1.2 μM for the same three cancer cell lines. Although the reason for the higher activity of **Pt-21b** is unclear, it was hypothesized that the presence of two Pt centers in the complex could allow a bridging coordination of DNA nucleobases, improving the cytotoxicity in comparison to the mononuclear **Pt-21a**.

## 3.2. Palladium

### 3.2.1. Palladium(II) complexes

For being isoelectronic and isostructural to Pt(II), antiproliferative Pd(II) complexes have been sought after since the discovery of the antitumoral properties of cisplatin. Pd chemistry still represents an attractive area of research within the bioinorganic and medicinal inorganic chemistry fields [121-125], although a breakthrough development is still to be found. To the best of our knowledge, no clinical trials have been conducted on palladium metallodrugs for the treatment of skin cancers, although several *in vitro* studies have been reported.

*Pd-NHC compounds.*

Palladium(II)-η3-allyl complexes bearing N-trifluoromethyl NHC (**Pd-1a-f** and **Pd-2a-f**, Fig. 12) were synthesized and characterized by Scattolin et. al. [126]. The complexes were very cytotoxic in a panel of cancer cell lines, most notably to the cisplatin-resistant ovarian cancer cell line A2780cis and to A375 malignant melanoma cells. The **Pd-1a-f** complexes of triphenylphosphane were more active ($IC_{50}$ between 0.028 and 0.24 μM) than the **Pd-2a-f** complexes that contain the 1,3,5-triaza-7-phosphaadamantane (PTA) ligand ($IC_{50}$ between 0.21 and 14 μM). However, the change to PTA ligand increased immensely the selectivity of the complexes to cancer cells. The $IC_{50}$ of the complexes **Pd-1a-f** against the non-tumorigenic MRC-5 cells was lower than 1.8 μM. For the **Pd-2a-f** complexes this value was > 100 μM (with the exception of **Pd-2e**, $IC_{50,MCR-5}$ = 4.6 ± 0.2 μM). Also, the introduction of a methyl substituent on the 2-position of allyl fragment led to less cytotoxic compounds.

**Pd-2f** was active against cisplatin-resistant A2780cis cells. It also showed less toxicity than cisplatin against liver organoids. **Pd-2f** was found to damage the mitochondria at first, rather than targeting DNA. It was hypothesized by the authors that part of the mechanism of action of these complexes is related to nucleophilic attack by biomolecules to the allyl fragment present in the ligands. This is favored by the presence of the electron-withdrawing $CF_3$ moiety and unfavored (electronically and sterically) by the methyl substituent on the allyl group [126].

A series of 14 Pd(II) organometallic compounds, **Pd-3a** to **Pd-3n** (Fig. 12) had their cytotoxicity evaluated on a panel of 7 cancer cell lines, including A375 melanoma cells [127]. Compound **Pd-3a** was the most active of the series against A375 cells, with $IC_{50}$ of 0.3 ± 0.1 μM, being almost 16 times more active than cisplatin (4.7 ± 0.4 μM). Meanwhile, compounds, **Pd-3l** to **Pd-3n**, which do not present the NHC ligand, were almost inactive over all cell lines. *In cellulo* studies revealed that **Pd-3a** was able to induce DNA double-strand cleavages, while flow cytometry studies revealed increased subG1 population after treatment with the same compound in a dose and time dependent manner. Compound **Pd-3a** induced A2780 cell death via an apoptotic pathway, as indicated by release cytochrome *C* from mitochondria to the cytoplasm and by the detection of increased caspase 3 and 7 levels when compared to control.

*Cyclopalladated compounds*

Mapolie's group prepared a series of cyclopalladated compounds based on a C^N ligand motif, and PTA as a co-ligand (Fig. 13). Compound **Pd-4b**, bearing the chlorido substituent was the most cytotoxic in the series, with an $IC_{50}$ of 6.03 μM against ME1402 melanoma [128].

The binuclear Pd(II) compound **Pd-5** (Fig. 13) able to inhibit ME1402, WM1158 and 501mel melanoma cells in the low micromolar range ($IC_{50}$ = 0.19, 0.20 and 0.25 μM, respectively). It was also selective to cancer cells, as **Pd-5** killed >90% of melanoma cells at the concentration of 0.4 μM, while in the same concentration of compound approximately 70% of normal fibroblast cells survived [129].

The complex induced apoptosis (sub-G1 peak) in ME1402 and WM1158 cells by both intrinsic and extrinsic pathways, provoked nuclear fragmentation and caused an increase in the levels of poly (ADP-ribose) polymerase (PARP) cleavage. For the same two cell lines, **Pd-5** also simultaneously induced the formation of autophagosomes and led to an increase in the autophagy markers LC3II and Beclin1 as a cell death mechanism. Cells treated with the complex showed high levels of vacuolization, a decrease in healthy intracellular organelles and swollen mitochondria.

The capacity of **Pd-5** to induce DNA double strand breaks (DSBs) was evaluated by the levels of γ-H2AX, a variant form of histone H2A that is directly phosphorylated at Ser139 in response to DSBs. Based on this assay, **Pd-5** was found to cause DNA damage in both ME1402 and WM1158 cells.

It was also found that **Pd-5** anti-tumor function is mediated by the p38 and ERK1/2 signaling pathways. Furthermore, **Pd-5** inhib-

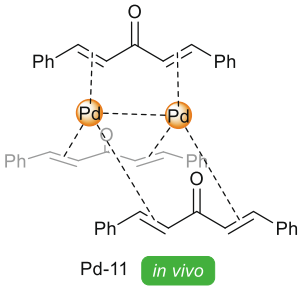


**Fig. 14.** Palladium(0) organocatalyst complex (**Pd-11**).

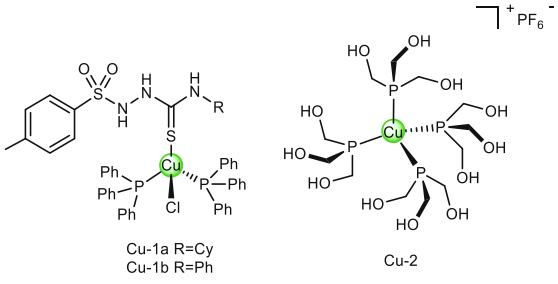


**Fig. 15.** Copper(I) compounds with phosphane ligands.

ited the Akt/mTOR signaling pathway, which is a key negative regulator of autophagy and apoptosis and it has been confirmed to be highly active in several cancers including melanoma [130]. Finally, the effect of **Pd-5** *in vivo* was evaluated in 6-week-old nude mice injected with ME1402 cells. After 15 days of treatment with the complex, 90% of reduction in the tumor size was observed, while treatment with cisplatin only reduced the size by 56.4%. The mice tumors treated with **Pd-5** were later examined *in vitro*, where an increase in levels of cleaved PARP and LC3II, and a high level of vacuolization and double membrane autophagosomes were identified, therefore confirming the effects observed *in vitro* using model of ME1402 and WM1158 cells [129].

Spencer, Hursthouse and co-workers prepared a binuclear cyclopalladated compound based on a functionalized 1,4-benzodiazepine ligand (**Pd-6,** Fig. 13) [131]. This compound had excellent cytotoxicity against B16 cells *in vitro*, with an $IC_{50}$ of 4.2 ± 1.8 nM with an exposure of 72 h (cisplatin: 3.0 ± 0.8 μM). This compound was also tested for cathepsin B inhibition, registering an $IC_{50}$ value of 2.98 μM.

Netto's group synthesized a series of cyclopalladated compounds derived from acetophenone oxime and varying thioamides as co-ligands, **Pd-7a** to **Pd-7g** (Fig. 13) [132]. The compounds were assayed against murine B16F10-Nex2 melanoma and human A2058, SK-MEL-110, SK-MEL-05 melanoma cell lines, in addition to oral squamous cell carcinoma Cal27. $IC_{50}$ values were determined by MTT with 24 h incubation. Against Cal27, **Pd-7c** had an $IC_{50}$ of 29.21 ± 1.2 μM, while against B16-F10-Next2, **Pd-7c** and **Pd-7g** had $IC_{50}$ values of 33.07 ± 3 and 25.92 ± 3 μM. In this last case, **Pd-7g** was equipotent to cisplatin. The other compounds had $IC_{50}$ values above 40 μM for the remaining cell lines.

The tetranuclear Pd(II) complex **Pd-8,** (Fig. 13) is the analogue of **Pt-15** complex. It is interesting to notice that **Pd-8** is more active than **Pt-15** against both keratinocyte cells tested, especially PAM. The $IC_{50}$ for the cyclopalladated complex are 5.0 ± 0.4 μM for PAM-RAS and 8.0 ± 0.3 μM for PAM. Furthermore, the activity of both complexes are greater than the activity of the free ligand [111].

The cyclopalladated complex induced changes on DNA secondary structure conformational which were different from those caused by the **Pt-15** analogue. However, both complexes, **Pd-8** and **Pt-15**, shared a unique capability to form DNA interhelical cross-links, that is a property not observed in cisplatin–DNA interactions, suggesting that part of the mechanism of action of these tetranuclear cyclometalated compounds may be due to DNA interhelical cross-link formation.

Cunha et al. reported the activity of organometallic Pd(II) complexes **Pd-9a** to **Pd-9d,** (Fig. 13) against four different melanoma cell lines: A2058, B16-F10-nex2, SK-MEL-110 and SK-MEL-5 [133]. These Pd(II) complexes exhibited comparable levels of cytotoxic activity against all tumor cell lines assayed, indicating that the nature of the anionic ligand R did not play a significant role in the observed activity. The murine melanoma B16-F10-nex2 cells were the most sensible to the compounds, with $IC_{50}$ values between 0.27 and 0.76 μM, and being 20-fold more potent than cisplatin for the same cell line. In fact, for all the melanoma cells the *in vitro* activities of **Pd-9a** to **Pd-9d** were higher than cisplatin. It is important to notice that the Pd(II) complexes inhibited the SK-MEL-110 cells, which contain p53 mutations and are very resistant to apoptosis induction, with $IC_{50}$ of 4.95–8.84 μM (cisplatin: $IC_{50}$ = 85.00 ± 11.03 μM for SK-MEL-110), and in a time dependent manner (with incubation times of 24, 48 and 72 h). Cell death induction properties by late apoptosis of all compounds studied in SK-MEL-5 cells were also verified. Moreover, biophysical assays showed that **Pd-9a** to **Pd-9d** were able to interact with DNA in a non-intercalative binding mode.

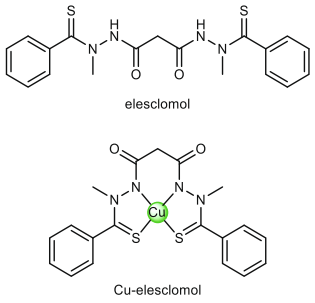


**Fig. 17.** Chemical structure of Elesclomol and its Cu(II) complex.

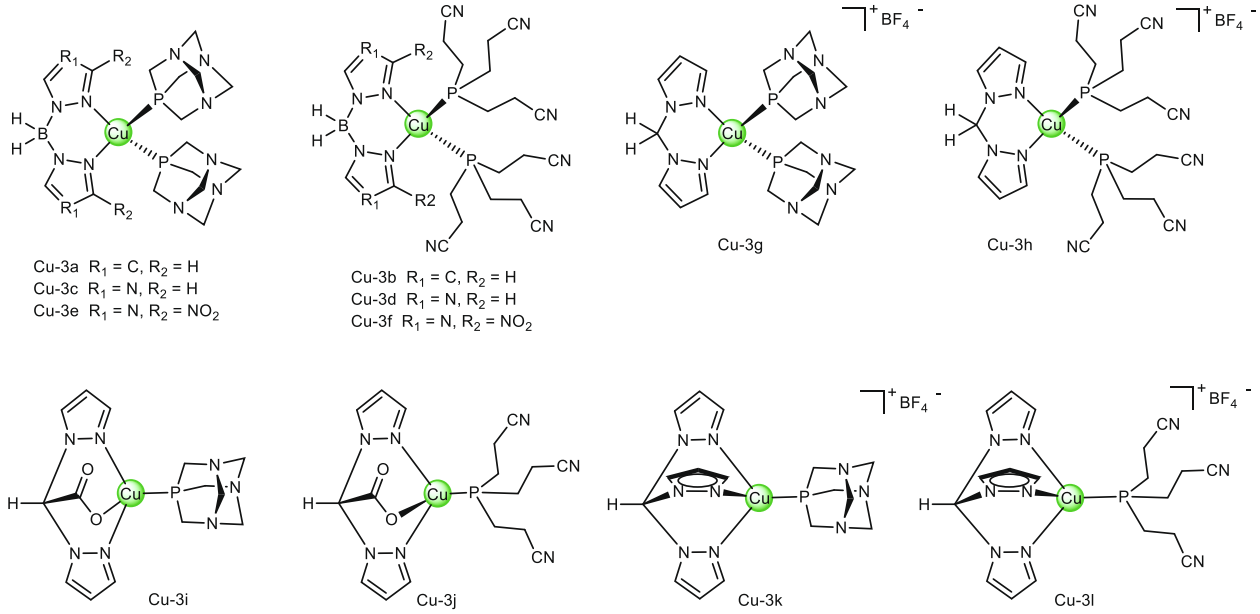


**Fig. 16.** Copper(I) compounds with phosphane and pyrazolyl ligands.

Square planar Pd(II) complexes of the three-membered aziridine ring, **Pd-10a** to **Pd-10c** (Fig. 13), were reported [134]. The compounds presented low activity against WM-115 melanoma cells ($IC_{50}$ > 40 μM after 46 h of incubation). The analogue copper (II) compound (**Cu-23a**, *vide infra*) showed greater cytotoxicity than the Pd ones.

*3.2.2. Palladium(0) complexes*

The organocatalyst **Pd-11** (Fig. 14) is widely used as a $Pd^0$ precursor in many catalytic transformations [135]. Treatment of B16 and A375 melanoma cells with 11 μM of **Pd-11** resulted in > 95 % decrease in viable cells, although no direct $IC_{50}$ value was reported.[136] The compound inhibited phosphorylation of both MAPK and AKT pathways, which are important signaling pathways to target with anticancer drugs, as these pathways confer survival and proliferative advantages to melanoma, such as induction of angiogenic factors (e.g. vascular endothelial growth factor - VEGF) [136].

A gene array study was performed on A375 melanoma cells and revealed that the N-myristoyltransferase-1 (NMT-1) gene was strongly down-regulated by **Pd-11**. This complex was also able to inhibit purified NMT, which catalyzes the attachment of myristate to the N-terminal glycine of several proteins, with an $IC_{50}$ value of 1.0 ± 0.3 μM. Expression levels of vascular endothelial growth factor, VEGF, in both A375 and B16 cells were also highly inhibited after treatment with 11 μM of **Pd-11**. VEGF-mediated signaling contributes to angiogenesis and with melanoma progression and prognosis. Given that **Pd-11** affected key pathways related to melanoma, the authors evaluated its efficacy on mice models injected with A375 and B16 cells. Treatment resulted in 97% decreased tumor volume compared with control on the group bearing B16 tumors, whereas a 65% reduction was observed for the A375 group. Local and systemic toxicity effects were not observed during treatment. Indeed, additional reports demonstrated that it is also efficient in inducing apoptosis in chronic lymphocytic leukemia B-cells [137] and that **Pd-11** is active *in vivo* against pancreatic cancer in mice models [138]. A recent report on **Pd-11** studied its effect in uveal melanoma, which rises from uveal melanocytes and is different from the cutaneous one in several ways [139]. It is clinically more difficult to diagnose and treat uveal melanomas with mutations in the G-proteins GNAQ and GNA11, which are genetically more common in this type of melanoma. The authors verified that **Pd-11** inhibits ARF6 (a GTPase), which may orchestrate GNAQ uveal melanoma oncogenesis. This was one of the few studies where the metal compound was administered orally to mice models bearing 92.1 uveal melanoma tumor xenografts. Results showed 50% reduction in tumor volume when compared to controls and no major body weight loss.

*3.3. Copper*

Copper is an endogenous metal, utilized by Nature for its redox chemistry [140]. Owing to its redox properties, copper can generate ROS and for that reason it is tightly regulated and cellular pools of the free ion in biological media are virtually non-existent [141]. Tumour growth and metastasis have a heightened requirement for copper. Cuproplasia has been defined as the regulated copper-dependent cell proliferation, and it ss linked to a diverse array of cellular processes, including mitochondrial respiration, antioxidant defence, redox signalling, kinase signalling, autophagy and protein quality control [142].

These properties have been exploited for the development of potential therapeutics, and many more translational opportunities are still available. The development of copper compounds as anticancer agents gained a dramatic boost from the works of Sigman [143,144], that rationalized the intercalation- and ROS-dependent mechanism of phosphodiester bond cleavage in nucleic acids induced by copper compounds bearing bidentate aromatic ligands such as phenanthroline. Although DNA remains an important target, targeting cuproplasia-related pathways can lead to much more structurally diverse (metallo)drugs.

*3.3.1. Copper(I)*

Maia and coworkers reported two novel tetrahedral Cu(I) complexes of thiosemicarbazides of composition [$CuCl(PPh_3)_2$(*p*-toluenesulfohydrazide)] (**Cu-1a** and **Cu-1b,** Fig. 15) [145]. The compounds showed increasing activity with longer incubation times over the B16-F10 melanoma cell line. For instance, compound **Cu-1b** had $IC_{50}$ values starting at 32.6 ± 3.1 μM at 12 h incubation time and 18.4 ± 1.7 μM at 48 h. The compounds were at least twice more active than cisplatin (36.7 ± 2.1 μM) when tested in the same conditions (48 h). Moreover, the luminescence properties of these compounds could be further explored to track them inside cells. An additional property of these compounds is their high trypanocidal activity and selectivity towards the amastigote form of *Trypanosoma cruzi*.

The Gandin group investigated the antitumor activity of the tetrahedral Cu(I) complex of tris(hydroxymethyl)phosphane (thp), **Cu-2** (Fig. 15), over a panel of 31 cancer cell lines [146]. Speciation studies revealed that, under dilute regime, the complex undergoes ligand dissociation, forming coordinatively unsaturated $[Cu(thp)_n]^+$ species (*n* = 3 and 2). The cytotoxicity of **Cu-2** varied from < 0.3 μM to 9 μM over the panel, with values of 1.1 ± 0.7 and 4.0 ± 0.1 μM over melanoma MeWo and A375 cell lines, respectively. Cell uptake studies revealed that intracellular copper content increased after treatment with the complex and uptake was concentration-dependent and saturable, suggesting an active-transport mechanism. Binding experiments with copper-recruiting methionine-rich peptides revealed that they may *trans*-chelate copper from **Cu-2**, therefore representing physiological pathways by which this compound is internalized.

Porchia et al. studied the antiproliferative activity of Cu(I) complexes (**Cu-3a** to **Cu-3l,** Fig. 16), taking into account that reduction of Cu(II) to Cu(I) is an important step in the mechanism of copper cell uptake prior to internalization through transmembrane trans porters [147]. The Cu(I) ion is a "soft" cation in Pearson's principle (hard species are weakly polarizable, while soft ones are highly polarizable), therefore justifying the use of soft donor atoms such as phosphorous in tertiary phosphanes and aromatic $sp^2$ hybridized nitrogen of pyrazolyl derivatives. These complexes were tested against a panel of tumor cell lines including A431 and A375. The complexes that were able to inhibit such cell lines in the lower concentrations were **Cu-3a** ($IC_{50}$ = 8.16 and 4.92 μM), **Cu-3b** ($IC_{50}$ = 7.25 and 5.54 μM), **Cu-3i** ($IC_{50}$ = 6.74 and 7.19 μM) and **Cu-3j** ($IC_{50}$ = 1.65 and 3.07 μM). In general, the neutral coordination compounds showed better antiproliferative activity than the ones with a positive charge, suggesting that the internalization of these derivatives does not take place through the hCtr1 channels that is responsible for the uptake of charged Cu(I) species. These neutral complexes would rather be internalized by passive diffusion (with chelate pyrazolyl ligand acting as a strong binding metal ionophore). Compound **Cu-3j** was the most lipophilic of the series, which correlated with its high cytotoxicity activity. This study is an elegant example of how one can tune several features only present in coordination compounds, such as the oxidation state, charge and ligand bond strength, to discover more potent antiproliferative agents.

*3.3.2. Copper(II): the case of elesclomol*

Elesclomol (STA-4783, Fig. 17) is a small molecule developed by Synta with antineoplastic activity against a broad variety of cancers in animal models and it has been tested in clinical trials for

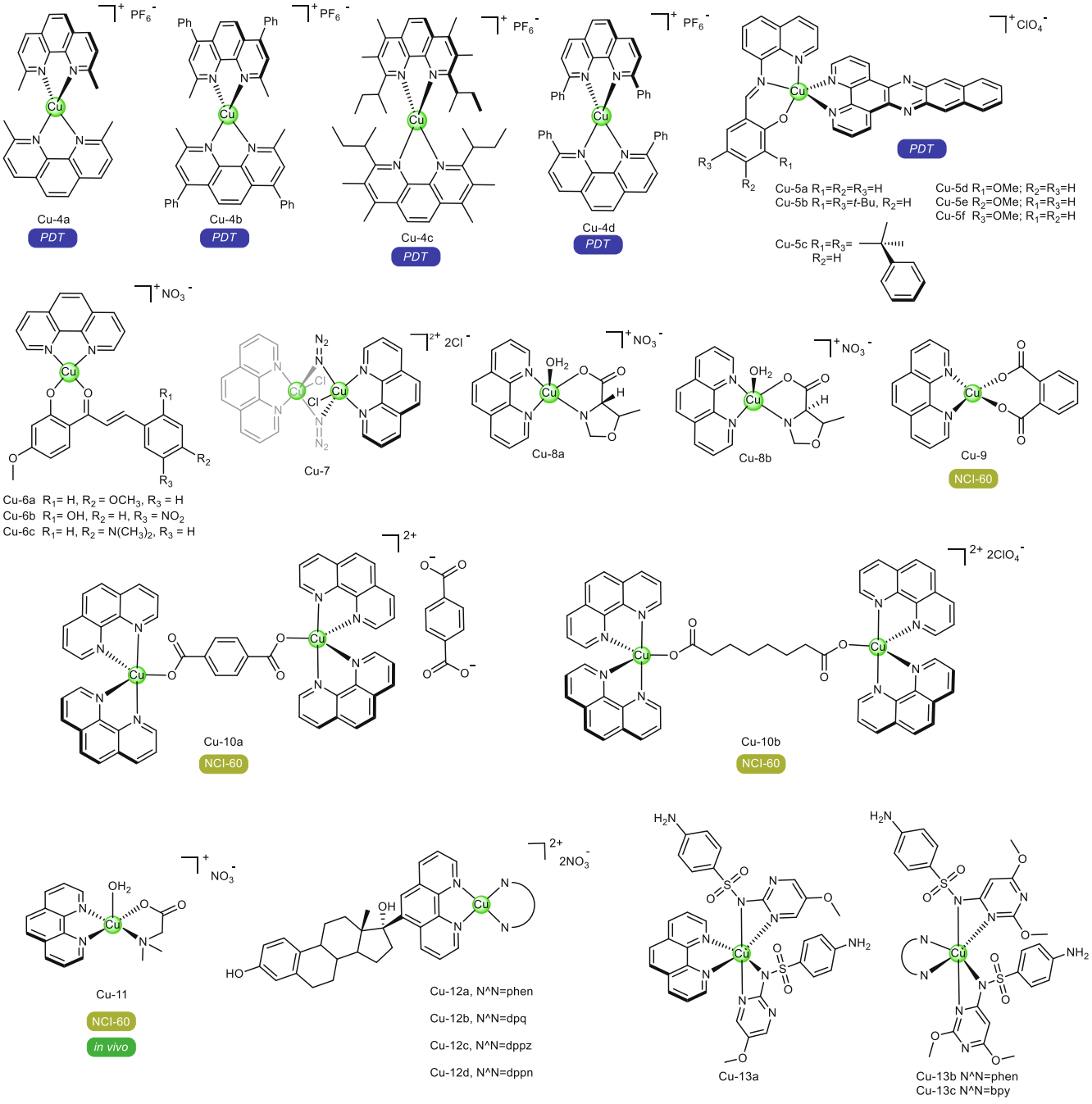


**Fig. 18.** Cu(II) complexes with 1,10-phenanthroline and related ligands.

treatment of metastatic melanoma [148]. The main mechanism by which this compound acts is derived from its ability to strongly bind copper in serum, forming the distorted square compound **Cu-elesclomol** (stability constant of $10^{24.2}$ $M^{-1}$, Fig. 17) [149,150].

Early studies showed that when MDA-MB435 melanoma cells were treated with elesclomol in the absence of copper in the media, no cytotoxicity was observed. The absence of other metal ions, such as iron, manganese and zinc did not have any effects on elesclomol activity. Additionally, it was observed that this compound enters cells as the Cu(II) compound **Cu-elesclomol**, since cell uptake studies revealed high levels of intracellular copper after treatment with elesclomol only. Further experiments showed that after intracellular dissociation of **Cu-elesclomol**, elesclomol exits cells, where it can bind more copper and internalize it again, creating a cyclic process of copper incorporation. The $IC_{50}$ values of both elesclomol and **Cu-elesclomol** against MDA-MB435 cells were remarkably found to be ≤100 nM. On GSH-depleted K562 cells, treatment with elesclomol and **Cu-elesclomol** resulted in $IC_{50}$ as low as 4.7 and 3.2 nM, respectively [151]. An NCI-60 screening experiment (NSC: 766922) of **Cu-elesclomol** revealed that the $GI_{50}$ was < 10 nM in 25 % of the cell lines. For the melanoma cells present in the panel, the $GI_{50}$ were < 60 nM, with the exception of SK-MEL-2, which showed a $GI_{50}$ of 110 nM. A COMPARE (NSC 174939) analysis identified that **Cu-elesclomol** showed best correlations with known copper chelators, such as thiosemicarbazones, carbodithioic acids and neocuproin [152].

Interestingly, the Ni(II) and Pt(II) analogue complexes of elesclomol showed less cytotoxic activity ($IC_{50}$ values of 185 and

5600 nM, respectively) when compared to elesclomol and **Cu-elesclomol** ($IC_{50}$ values of 8.2 and 5.4 nM, respectively) against K562 cells. Such results indicate that the copper-elesclomol motif is necessary for the optimal activity. Nonetheless, the reminiscent activity of the Ni(II) and Pt(II) compounds seems to be due the complexes themselves and not due to elesclomol dissociation, since titration with Cu(II) did not result in displacement of Ni(II) ions from the corresponding complex. This may be explored for further investigations on other metal complexes of elesclomol [150].

In terms of mechanistic aspects, **Cu-elesclomol** selectively binds to mitochondria in cancer cells, where reduction to Cu(I) starts copper redox cycling with the subsequent generation of ROS, especially superoxide and hydrogen peroxide, which interferes in mitochondrial electron transport [149,151,153]. Interestingly, none of these effects were observed for normal peripheral blood mononuclear cells, demonstrating high selectivity of this drug candidate for cancer cells [149]. Cell cycle analysis revealed that elesclomol and **Cu-elesclomol** caused progressive increase in the sub-$G_0/G_1$ phase in CHO cells, which was indicative of apoptosis or necrosis. An annexin V-FITC flow cytometric experiment showed that **Cu-elesclomol** progressively increased the proportion of both apoptotic and apoptotic/necrotic cells, while elesclomol treatment did not result in apoptosis when compared to controls, at least under the tested conditions. Treatment with either compound also seems to lead to DNA double strand breaks, as confirmed by increased expression levels of phosphorylated H2AX (γH2AX), which recognizes this type of DNA damage [152]. Initial *in vivo* studies intriguingly showed that in a single agent treatment of mice bearing a U937 human lymphoma xenograft model (intravenous, 3 times a week) with elesclomol resulted in no efficacy. However, it enhanced the efficacy of Taxol when administered together. Taxol-enhancing effects were also observed for elesclomol in an MDA-MB-435 human melanoma xenograft model in nude mice [148]. To the best of our knowledge, there is no study comparing the differences between *in vivo* administration of elesclomol or **Cu-elesclomol**.

### 3.3.3. Copper(II) compounds of phenanthroline and related ligands

Al Hageh et al. explored Cu(I) bis-phenanthroline complexes (**Cu-4a** to **Cu-4d**, Fig. 18) for their use in photochemotherapy against A375 cells [154]. In the absence of light, complexes **Cu-4a**, **Cu-4c** and **Cu-4d** were able to inhibit the growth of A375 cells in the low micromolar concentration range ($IC_{50}$ between 1.8 and 7.0 μM). However, with light treatment (30 min, blue-LED) complexes **Cu-4c** and **Cu-4d** showed improved activity over the same cell line with PI (phototherapeutic index) = 12.5 and 1.2, respectively. Therefore, **Cu-4c** displayed the highest cytotoxicity when activated by the blue-LED ($IC_{50}^{irr}$ = 0.56 ± 0.01 μM), consistently with its longest excited state lifetime (an important photophysical feature for photodynamic agents) and the highest log P value (log P = 2.64 ± 0.16).

Fluorescence imaging indicated an intracellular uptake and perinuclear localization of **Cu-4c** in A375 cells, with loss of membrane integrity after 6 h, leading to cell death. Moreover, the cytotoxic activity of this complex was attributed to the formation of ROS following light activation.

Lin and co-workers [155] developed a series of photocytotoxic Cu(II) compounds bearing an N,N,O-tridentate Schiff base ligand based on quinolin-8-amine motif and the extended, aromatic dppn (**Cu-5a** to **Cu-5f,** Fig. 18). The compounds were assayed against the SCC15 and BCC cell lines, either in the dark ($IC_{50}^{dark}$) or upon irradiation with blue light (430 nm; $IC_{50}^{irr}$). In either case the cell exposure time was of 24 h. Against SCC15, the most cytotoxic compound in the dark was **Cu-5b** ($IC_{50}^{dark}$ = 3.28 ± 0.57 μM), which also reached the lowest $IC_{50}^{irr}$, of 0.03 ± 0.01 μM. Comparing the PI values, on the other hand, the compounds that most benefited from irradiation were **Cu-5f** and **Cu-5d**, with PI values of 296 and 329 respectively. Finally, against BCC cells in the dark, **Cu-5b** and **Cu-5e** were the most cytotoxic ($IC_{50}^{dark}$ = 7.71 ± 0.55 and 6.79 ± 1.02 respectively), while **Cu-5e** remained the most cytotoxic upon irradiation ($IC_{50}^{irr}$ = 0.05 ± 0.01). **Cu-5d** and **Cu-5f** have PI values of 296 and 293 respectively. Compound **Cu-5d** was shown to induce apoptosis in SCC15 and BCC by activation of caspase-3 when irradiated.

Complexes **Cu-6a** to **Cu-6c** (Fig. 18) were primarily designed against ovarian cancer, showing impressive inhibition of cisplatin resistant A2780R cells, but they also showed activity against G361 melanoma cells with $IC_{50}$ varying from 2.4 to 3.5 μM, displaying greater *in vitro* activity than cisplatin ($IC_{50}$ = 7.5 μM) [156].

Hammud and co-workers [157] prepared a μ-azido dinuclear Cu (II)phenanthroline complex (**Cu-7,** Fig. 18). The compounds were assayed against a panel of cell lines that contained the B16-F10 melanoma one. The compound had an $IC_{50}$ value around 1 μM, irrespective of exposure time (24 or 48 h).

Two enantiomeric ternary Cu(II) complexes **Cu-8a** and **Cu-8b** (Fig. 18) showed better antiproliferative activity than cisplatin against HK-1 (nasopharyngeal SCC) and HSC-2 (oral cavity SCC) cells. The Cu(II) complexes show $IC_{50}$ of approximately 3.0 μM over both cells, while $IC_{50}$ of cisplatin is 11 ± 3.2 μM for HK-1 and 24 ± 8. 0 μM for HSC-2. Additionally, these complexes also show selectivity to the SCC cells as they are less toxic to NP69 cell line, that is normal nasopharyngeal cell line [158]. Although the chirality did not cause any significant change in the antiproliferative profile of the complexes, there was a distinct effect of chirality in the DNA binding recognition, as **Cu-8b** was able to interact with a specific DNA fragment that **Cu-8a** was not. Overall, the DNA binding ability of these complexes was attributed to the presence of the phenanthroline ligand in the structure.

The antiproliferative activity of complex **Cu-9** (Fig. 18), with o-phthalate and 1,10-phenanthroline ligands, was reported on the NCI-60 panel of cancer cells (NSC 767443) [159]. The compound exhibited the lowest lethal dose concentration inducing 50% cell death ($LC_{50}$) of 1 and 5 μM for against SK-MEL-2 and UACC-257 cells. The complex interacted with DNA in an intercalative mode, preferentially to G-C rich regions of DNA, and was also responsible for ROS generation that caused DNA damage, such as double strand breaks. The superoxide anion radical is the main ROS generated by the complex and acts significantly on the decrease of cell viability. The mechanism of action of **Cu-9** was further evaluated in SKOV3 epithelial adenocarcinoma ovarian cells. Apoptosis was induced predominantly by activation of caspase 9 (intrinsic pathway) and of caspase 8 (extrinsic). **Cu-9** also targets mitochondria, as confocal microscopy analysis showed reduced mitochondrial fluorescence due to loss of membrane potential and also evidenced morphological changes that are characteristic of apoptosis.

Copper(II) metallonucleases **Cu-10a** and **Cu-10b** (Fig. 18) were investigated by the Kellet group against the NCI-60 panel of cancer cell lines (NSC: 767,441 and 767442) [160]. **Cu-10a** showed remarkable selectivity towards the SK-MEL-5 melanoma cells, with a $GI_{50}$ value of46 nM. Furthermore, **Cu-10b** also presented low micromolar and nanomolar activity against all 9 tested melanoma cell lines. Experiments indicated the induction of apoptosis by both compounds in SKOV3 cells occurs primarily through the intrinsic caspase 9 pathway. The delocalized cationic charge and lipophilic nature of **Cu-10a** and **Cu-10b** was correlated with their preferential targeting of mitochondria and its membrane depolarization. Since mitochondrial membrane depolarization is usually associated with ROS, the authors carried out a series of experiments and DFT calculations, identifying superoxide and singlet oxygen as the main ROS in cells treated with the two agents. Data revealed that **Cu-10a** and **Cu-10b** were able to induce single and double-stranded DNA breaks. Circular dichroism experiments indicated

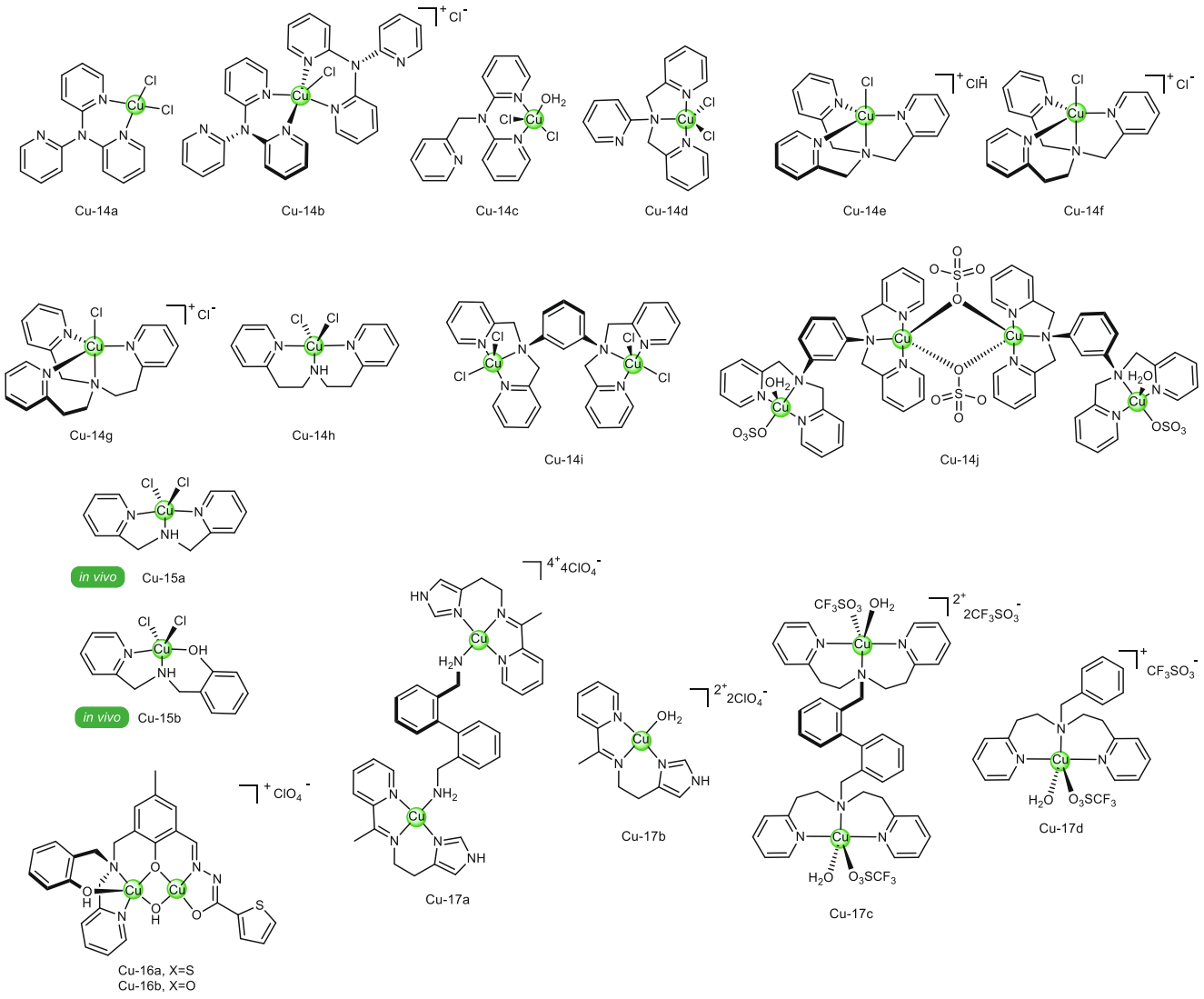


**Fig. 19.** Cu(II) complexes with bi and tripodal ligands.

that **Cu-10b** is a high-affinity intercalator at the TA/TA step, while generating Z-like DNA at the AT/AT step.

A Cu(II) complex of phenanthroline and dimethylglycine ligands, **Cu-11** (Fig. 18), was tested against the NCI-60 cancer cell panel (NSC: 774845) [161]. This compound was active against all 9 melanoma cells, with $GI_{50}$ values between 0.5 and 2 μM. A series of *in vivo* studies were performed to determine the toxicity of this compound. Firstly, a single dose injection with variable concentration of the compound led to a maximum tolerated dose (MTD) of 17.5 mg/kg. Subacute doses of 4 and 6 mg/kg administered for a longer period (14 days) did not induce systemic toxicity as well. Hematological parameters were normal when doses of 4 and 5 mg/kg were administered, with only mild leukocytosis observed in the group treated with the higher dose. Finally, efficacy studies were performed in mice bearing either HK-1 and C666-1 nasopharyngeal squamous carcinoma tumor xenografts. For HK-1, dosages of 4, 6 (daily injections) and 8 (every 2 days injections) mg/kg were used. Treatment at the highest dose resulted in 2 cases of lethality, so the experiment did not proceed. The other dose regimens resulted in almost 5-fold reduction in tumor volume, with no major side effects, as evaluated by maintenance of body weight and histopathological examination of heart, liver, kidney and lungs.

On mice bearing Epstein-Barr virus-positive C666-1 tumor xenografts, the 4 mg/kg dose was inefficient to reduce tumor volume, while 6 mg/kg caused an average 2-fold reduction but even so mortality was observed. This is relevant since Epstein-Barr virus is strongly correlated to nasopharyngeal carcinoma risk. The origin of toxicity in this case was not identified conclusively, since histopathological analysis of heart, liver, kidney and lung did not show any abnormalities [161].

Aiming to target estrogen receptors (ER), the Montagner group conjugated estradiol to the Cu(II)-phenanthroline motif and varied the planar N-heterocyclic co-ligands, resulting in **Cu-12a** to **Cu-12d** (Fig. 18) [162]. DNA binding studies were performed using high throughput ethidium bromide and Hoechst 33,258 fluorescence quenching assays. The compounds were not selective for fluorophore displacement but followed the same trend where **Cu-12c** > **Cu-12b** > **Cu-12a** > **Cu-12d**. These results demonstrated that there is an optimal size of the extended planar ring for ideal DNA intercalation, so that steric hindrance does not play a major role. The same trend was observed in a gel electrophoresis experiment, where **Cu-12c** displayed the highest cleaving effect at 0.5 μM. An alkaline comet assay also revealed DNA damage in cells treated with **Cu-12d** for 3 h. Cytotoxicity assays demonstrated that the

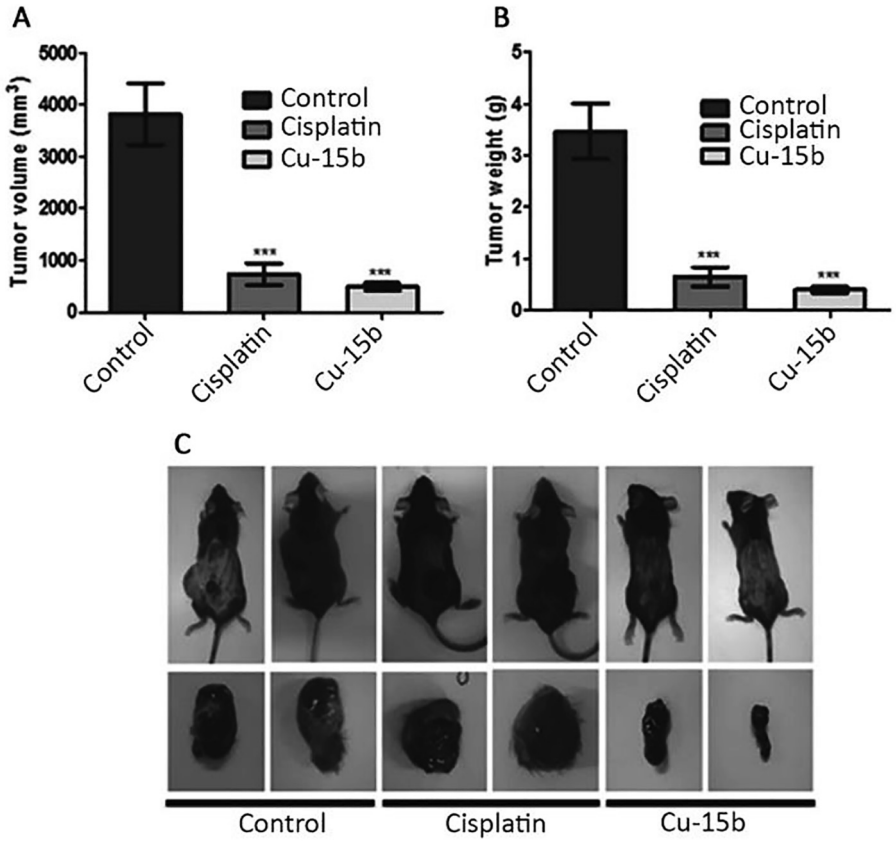


**Fig. 20.** Evaluation of B16-F10 murine melanoma tumor inhibition by compound **Cu-15b** in a C57BL/6 murine model. A. Evaluation of tumor growth inhibition of **Cu-15b** in comparison to cisplatin. B. Comparison of tumor mass weight. C. Representative images of the animals and tumors. Adapted from Borges et. al. [166]. Reprinted with permission from Elsevier.

compounds are highly effective against ER + A431 and ER- HCT-15 cells (low and submicromolar $IC_{50}$ values), therefore no selective targeting due to the estradiol moiety is observed from these experiments. In contrast to the DNA binding experiments, **Cu-12d** was as cytotoxic as the other compounds, which is probably correlated to its lipophilic character and higher cell uptake. Measurement of ROS in A2780 cells with a peroxide-sensitive fluorescent probe revealed high levels of hydrogen peroxide after treatment with **Cu-12d** at 10 μM.

Corbi and colleagues reported on heteroleptic Cu(II)-(N^N)-sulfonamide complexes, **Cu-13a** to **Cu-13c** (Fig. 18), which were shown to be efficient metallonucleases [163]. The compounds were tested over a panel of 9 cancer cell lines using the SRB assay. After 48 h of incubation, the phen-containing compounds **Cu-13a** and **Cu-13b** displayed low micromolar $GI_{50}$ values over the UACC-62 melanoma cell line, which correlated with their pronounced nuclease activity. Compound **Cu-13b** was 7 times more selective to the melanoma cell line when compared to the non-tumorigenic HaCaT immortalized keratinocyte cells. Additional investigation [164] on compound **Cu-13b** showed that it caused cell cycle arrest at sub-G1 phase and its cytotoxicity was not influenced by copper transporter 1 (CTR1) expression levels, indicating another mechanism of cell uptake.

*3.3.4. Copper(II) compounds of bi and tripodal ligands*

Jopp and colleagues [165] evaluated a panel of mononuclear Cu (II) compounds based on tripodal polypyridylamine ligands (**Cu-14a** to **Cu-14g,** Fig. 19). The authors started from tris(2-pyridylmethyl)amine (tmpa), an analogue to bpa (bis-picolylamine; ligand of **Cu-14h**) with one extra methylpyridyl arm (ligand present in **Cu-14e**). From there, the authors evaluated the systematic lengthening of each pyridyl "arms" in tmpa by the insertion of a methylene spacer group (in compounds **Cu-14f** and **Cu-14g**), or shortening of the arms by removal of methylene groups (as observed in compounds **Cu-14a** to **Cu-14c**). Finally, the authors compared the mononuclear compounds to a dinuclear (**Cu-14i**) or tetranuclear analogue (**Cu-14j**), based on ligands containing two "bpa-like" sites. The systematic structural variation was compared to cytotoxic potency of the compounds against the tumoral cell lines A375 and A431. Among the mononuclear compounds, **Cu-14c** and **Cu-14e** to **Cu-14h** were the most active, with single-digit μM $IC_{50}$ values against both cell lines. Overall, the most active complex was the highly cationic (8+) tetranuclear **Cu-14j**. With $IC_{50}$ values in the submicromolar range, this derivative was markedly more cytotoxic than cisplatin against this cell line panel. Finally, the parental ligand bpa was inactive against the panel of the cell lines studied. On the other hand, tmpa (ligand of **Cu-14e**) and pmea (ligand of **Cu-14f**) were cytotoxic against both cell lines. This activity was hypothesized to be linked to the copper sequestration capabilities of the ligand, which might occur in cancer cells as well.

Complexes **Cu-15a** and **Cu-15b** (Fig. 19) [166] are structurally very similar to **Cu-14h**. They were able to inhibit B16-F10 cells with $IC_{50}$ = 88.47 ± 1.10 μM and 21.11 ± 1.12 μM and the higher activity of **Cu-15b** was attributed to the presence of the coordinated phenol group [167]. Therefore, **Cu-15b** was selected for further *in vitro* and *in vivo* tests. Flow cytometry reveled that treatment of B16-F10 cells with **Cu-15b** caused an accumulation in the sub-G1 phase of 77% of the cells, which is 24% more than the arrest caused by cisplatin in the same concentration. The Cu (II) complex did not induce primary necrosis on the cells and induced intrinsic apoptosis, indicated by the release of cytochrome

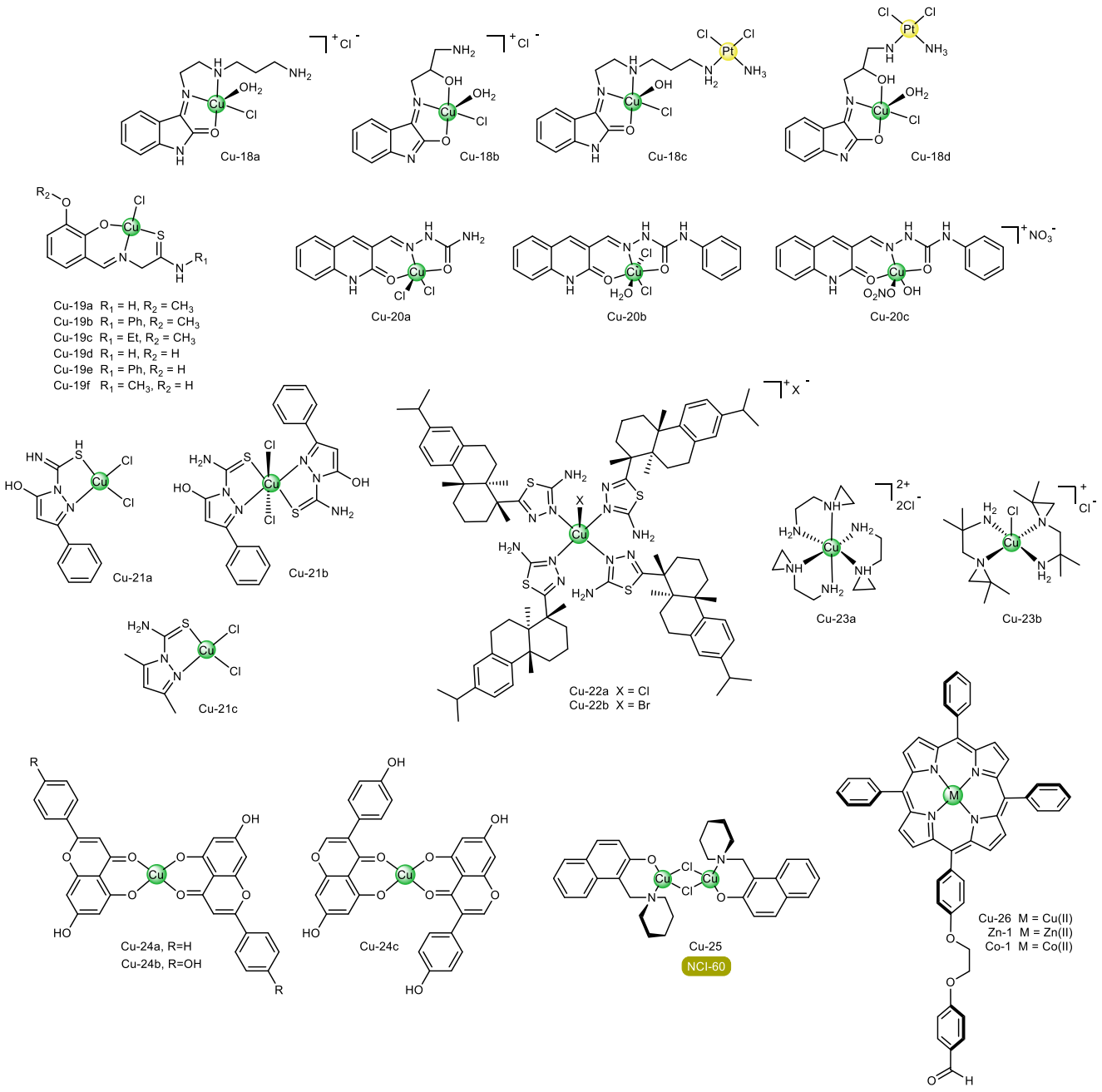


**Fig. 21.** Cu(II) complexes with diverse ligands.

*C* to the cytoplasm and the simultaneous loss of mitochondrial outer membrane potential, with activation of caspases 3, 6, and 9.

*In vivo* assays determined the lethal dose ($LD_{50}$) of **Cu-15b** for BALB/c nude ($LD_{50}$ = 24.61 mg/kg) and C57BL/6 mice ($LD_{50}$ = 179.4 mg/kg). The complex was able to suppress the growth of THP-1 monocytic sarcoma in Balb/c nude mice and also B16-F10 melanoma in C57BL/6 mice. For the melanoma model, mice were treated with 45 mg/kg of **Cu-15b** showing 87% inhibition of tumor growth compared with the untreated control group. On the other end, the group treated with cisplatin exhibited an 80% suppression of tumor growth (Fig. 20). Mice treated with the Cu(II) complex also showed preservation of the skin, epidermis and adnexal, but the deep dermis was compromised by neoplastic masses. Nonetheless, the treatment of the mice with **Cu-15b** or cisplatin did not cause any changes in the visceral organs [166].

With the same strategy of using binuclear Cu(II) complexes, Rey and co-workers[168] prepared two compounds (**Cu-16a** and **Cu-16b,** Fig. 19) bearing hydrazonic ligands, which displayed sub or low-micromolar activity over B16-F10 cell line, with $IC_{50}$ values of 0.32 ± 0.46 and 1.23 ± 0.45 μM. The corresponding ligands were also active on low micromolar range. The authors evaluated the influence of the compounds on plasmid DNA conformation by DLS. The incubation of plasmid pBR3222 with complex concentrations starting at 25 μM were shown to form two populations with average hydrodynamic radii of 130 and 800 nm, which the authors attributed to formation of circular plasmid and aggregation. Such DNA targeting capacity followed by oxidative damage was associated to the high cytotoxicity of the compounds.

Da Costa Ferreira and co-workers evaluated the cytotoxicity of mono and dinuclear copper compounds bearing imine (**Cu-17a**

and **Cu-17b)** and tripodal (**Cu-17c** and **Cu-17d**) ligands (Fig. 19) against B16-F10 and TM1MNG3 cell lines [169]. The mononuclear analogues were less toxic than the corresponding dinuclear compounds. Comparing the two cell lines, the dinuclear species were more toxic against the heavily melanogenic B16F10 cell line (15.4 and 16.0 μM for **Cu-17a** and **Cu-17c**, respectively) than against TM1MNG3, which has no detectable melanin. The *in vitro* tyrosinase-like activity observed for **Cu-17a** and **Cu-17c**, suggested that these complexes may influence the melanogenesis process. The authors concluded that the high melanin levels found on B16-F10 cells make them more susceptible to the dinuclear compounds. Nuclease effects were observed for **Cu-17a** and **Cu-17b**, making DNA a suitable additional molecular target of these compounds.

Further studies [170] by the same group reported the influence of cellular melanin content on the cytotoxicity of complexes **Cu-17a** and **Cu-17b**. The cytotoxicity of **Cu-17a** on three murine cell lines Tm1 (no melanin), Tm5 (tumorigenic, melanogenic) and Ma (non-tumorigenic, melanogenic) highly correlated with the melanin content of the cells. The $IC_{50}$ values of **Cu-17a** were 22.3 ± 1.9 μM, and 20.0 ± 7.0 μM against human melanoma SK-MEL-05 and SK-MEL-147 cells respectively. This compound did not show activity towards the HaCaT keratinocyte cell line, confirming selectivity towards melanocytes. Flow cytometry experiments revealed a ROS-mediated (superoxide) cytotoxic pathway for this complex. Finally, biophysical experiments of melanin binding showed that compound **Cu-17a** is more easily reduced than the mononuclear one in the presence of this biomolecule. Overall, the results indicated that the reactivity of these complexes toward melanoma cells could result from how easily they are reduced by melanin, which leads to *in situ* and selective trigger of the catalytic Cu(II)/Cu(I) oxidative cycle with formation of damaging ROS.

The da Costa Ferreira group also reported a series Cu(II)-oxindolimine compounds, **Cu-18a** and **Cu-18b** (Fig. 21), and their corresponding Cu(II), Pt(II) heterobimetallic complexes, **Cu-18c** and **Cu-18d** (Fig. 21) [171,172]. The compounds were stable in reducing media since no apparent reactions occurred with the presence of 20 M equivalents of GSH. The compounds interacted with DNA trough an interplay of covalent binding and intercalation of the oxindolimine ligand. Agarose gel electrophoresis assays revealed that compound **Cu-18b** induced the highest degree of DNA oxidative cleavage in the presence of $H_2O_2$. Contrastingly, compound **Cu-18c** was the only one that did not show nuclease activity, which was attributed to its binding to DNA by the platinum moiety. This different reactivity of the complexes towards DNA was dictated by the size of the linker between the Cu(II) and Pt(II) metallic centers. All four compounds were able to inhibit the activity of the CDK1/cyclin B kinase protein, while not being able to strongly inhibit alkaline phosphatase protein. Therefore, the compounds were assumed to have a greater influence in phosphorylation steps. While **Cu-18a** and **Cu-18b** were highly cytotoxic against B16-F10 melanoma cells ($IC_{50}$ values of 1.98 ± 0.18 and 2.72 ± 1.06 μM, respectively), introduction of the cisplatin motif resulted in three-fold decrease of activity when comparing **Cu-18a** and **Cu-18c**. For all cases, the cytotoxicity was higher than cisplatin, demonstrating promising potential of copper-oxindolimine complexes against melanoma.

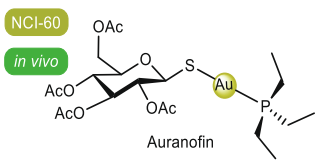


**Fig. 22.** Structure of Auranofin.

### 3.3.5. Miscellaneous Cu(II) compounds

Copper(II) complexes of substituted salicylaldehyde thiosemicarbazone ligands, **Cu-19a** to **Cu-19f** (Fig. 21) have been recently reported [173]. The ligands and metal complexes were highly cytotoxic over a panel of 6 cancer cell lines. Remarkably, they exhibited nanomolar activity over the A375 melanoma cell line. The most active compound was **Cu-19a**, with an $IC_{50}$ value of 3 ± 0.4 nM, which is at least 3 orders of magnitude lower than the value found for cisplatin (3.11 ± 0.98 μM). Additional mechanistic details were investigated with non-skin cancer cell lines. The compounds are preferentially localized in mitochondria and they inhibit Protein Disulfide Isomerase, a biomolecule that is emerging as a new biomolecular target for cancer treatment, including melanoma [174-177]. The authors speculated that compounds **Cu-19a** to **Cu-19f** induce a non-oxidative stress mediated cancer cell death, which is the usual mechanism for many redox-active copper compounds.

Raja and co-workers [178] studied a series of copper compounds with semicarbazones derived from 2-oxo-1,2-dihydroquinoline (**Cu-20a** to **Cu-20c,** Fig. 21). From **Cu-20b** to **Cu-20c**, the only difference is the presence of two chlorido ligands in the former (resulting in a neutral compound, with octahedral geometry around the copper center) and a coordinated nitrate in the latter (cationic species, with square-pyramidal geometry). The charge is probably the factor responsible for the increased cytotoxicity against A431 observed for the cationic **Cu-20c** ($IC_{50}$ = 3.26 ± 0.12 μM) in comparison to the neutral **Cu-20b** ($IC_{50}$ = 12.4 ± 1.4 μM).

Lipophilic Cu(II) complexes of pyrazole derivatives **Cu-21a** to **Cu-21c** (Fig. 21) were shown to have DNA alkylating properties and to slightly alter the secondary structure of DNA [179]. Electrophoretic mobility shift assays revealed that only compound **Cu-21c** was able to cleave plasmid DNA. The compounds were active towards the A375 melanoma cell line, with the lowest $IC_{50}$ value being 2.0 ± 0.8 μM for **Cu-21c**.

Fei et al. studied two rosin-derivative based optically pure chiral Cu(II) complexes, **Cu-22a** and **Cu-22b** (Fig. 21), as potential anticancer agents [180]. Both complexes were able to inhibit A431 cells *in vitro* with $IC_{50}$ of 3.04 ± 0.84 μM and 3.98 ± 0.45 μM and were more active than cisplatin and oxaliplatin in the same assay ($IC_{50}$ = 10.50 ± 0.88 μM and 15.75 ± 3.59 μM, respectively). Complex **Cu-22a** had its anticancer activity further evaluated *in vivo* on MCF-7 subcutaneous xenograft models in BALB/c nude mice and was able to suppress tumoral growth by 62.9% against 73.5% of cisplatin. Assays with MCF-7 cells *in vitro* showed that **Cu-22a** could induce ROS production, cell-cycle arrest, matrix metalloproteinases depolarization, caspases and p53 activation, damage of DNA, lipid and protein, apoptosis and autophagy. Moreover, it showed potential to inhibit migration, invasion and angiogenesis of cancer cells. The antiproliferative assay *in vitro* suggested better results of the copper complexes against A431 cells than for MCF-7 cells. The $IC_{50}$ values against the MCF-7 cell line were 8.80 ± 0.59 μM for **Cu-22a**, 4.47 ± 0.28 μM for **Cu-22b**, 6.30 ± 0.42 μM for cisplatin and 7.59 ± 1.50 μM for oxaliplatin [180].

Copper(II) complexes of aziridine ligands, **Cu-23a** and **Cu-23b** (Fig. 21) were tested against WM-115 melanoma cells *in vitro* [134]. Compound **Cu-23a** presented high cytotoxicity ($IC_{50}$ of 5.9 ± 0.9 μM) against this cell line, whereas **Cu-23b** presented low activity ($IC_{50}$ = 51.4 ± 3.9 μM). This may be a result of deactivation by sulfur biomolecules, since **Cu-23a** is coordinatively saturated. The same trend was observed for the Pd(II) compounds **Pd-10a** to **Pd-10c**.

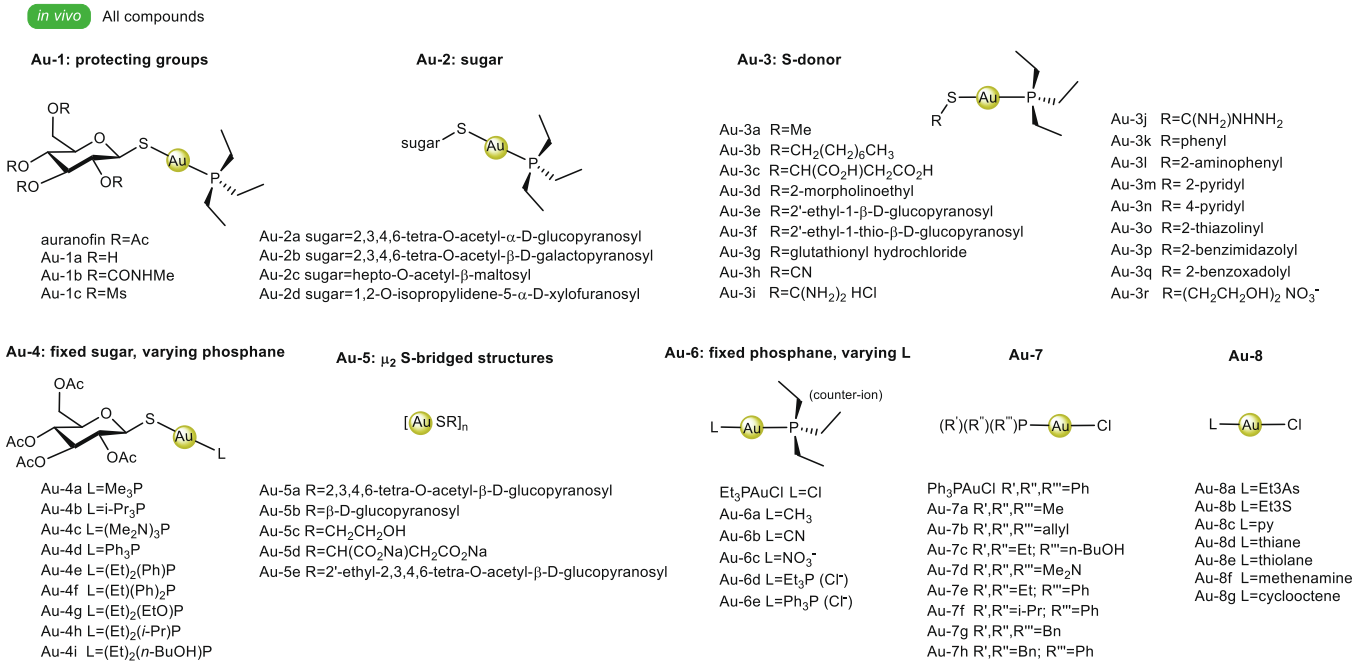


**Fig. 23.** Au(I) compounds obtained by Mirabelli and coworkers *via* the systematic variation of the chemical motif established by auranofin.

The homoleptic complexes **Cu-24a**, **Cu-24b** and **Cu-24c** (Fig. 21) with the flavonoids chrysin, apigenin and genistein, respectively, were synthesized and evaluated against 518A2 melanoma cells [181]. The choice of ligands was inspired by the structural similarities with ASA404/vadimezan, a tumor vascular disrupting agent that failed in phase III trials for treatment of advance non-small cell lung cancer in combination with carboplatin and taxol. The complexes were able to inhibit 518A cells with $IC_{50}$ between 10.9 and 13.2 μM, while non-malignant fibroblasts were not affected and the ligands were active only at concentrations >50 μM. Apigenin and genistein are able to arrest cell cycle at the G2/M transition, but the complexes **Cu-24a** to **Cu-24c** showed an even more pronounced G2/M arrest than the ligands. It is interesting to notice that antimigratory and antimetastatic activities were observed for **Cu-24a** to **Cu-24c** (particularly **Cu-24c**) in models using 518A2 cells. It is hypothesized that these effects are consequence of the inhibition of certain protein kinases in analogy to various flavonoids that lead to disruption of signaling pathways linked with proliferation and metastasis [182].

Compound **Cu-25** (Fig. 21) was investigated as a proteasome inhibitor, a strategy used for the development of antitumor and anti-angiogenic agents. **Cu-25** inhibited the proteasomal chymotrypsin-like activity in purified rabbit proteasome with an $IC_{50}$ of 6 μM [183]. It also enhanced cisplatin toxicity against cisplatin-resistant ovarian cancer cells independent of p53 and by delaying S-phase progression in the cell cycle [184,185]. This compound was also investigated against the NCI-60 panel of cancer cells. Against 10 melanoma cells, **Cu-25** showed $GI_{50}$ values between 10 and 20 μM [183]. Although the values are moderate, its potential against skin cancers could be further evaluated in combination with cisplatin for combined therapy protocols, as already demonstrated for ovarian cancers.

The use of porphyrin derivatives as ligands was also explored in the context of antiproliferative metal complexes against SCC. Metalloporphyrins of Cu(II) (**Cu-26**), Zn(II) (**Zn-1**) and Co(II) (**Co-1**), shown in Fig. 21, successfully inhibited the growth of A431 cells after 24 h of incubation in the dark, with $IC_{50}$ between 6.6 and 6.8 μM. The complexes were slightly more cytotoxic than the porphyrin ligand alone and showed very low toxicities in normal HaCaT cells, which demonstrated their significant selectivity [186].

### 3.4. Gold

Gold compounds have been extensively studied as anticancer agents in the past decades [187-190]. The two main oxidation states of gold are the linear Au(I) or as square-planar Au(III), once again isoelectronic to Pt(II). The main difference to platinum-containing compounds is the relevant redox chemistry of gold compounds [191,192]. In addition, in terms of molecular targets, gold compounds are particularly avid for cysteine residues in proteins and enzymes due to soft–soft affinity.

#### 3.4.1. Auranofin

The prototypical Au(I) compound for multi-purpose metallodrug development, auranofin (Fig. 22) is a phosphane/thiolate compound, used to treat rheumatoid arthritis, with anti-inflammatory properties and potential antineoplastic, antiviral, antiparasitic and antibacterial activities [193]. The most reported mechanism of action of auranofin is its capability to inhibit mitochondrial thioredoxin reductase (TrxR) by binding to the selenocysteine residue. This compound impairs mitochondrial function and ATP-coupled cellular respiration [194]. Induction of apoptosis by this compound occurs through ROS- and caspase-dependent mechanisms [195,196].

Early studies showed that auranofin has an $IC_{50}$ value of 1.5 μM over the B16-F10 melanoma cell line after short time periods of incubation (2 h, assessed by the trypan blue assay). However, when tested in 15 tumor models in mice, it was found to be active only in a leukemia model. Intraperitoneal or subcutaneous injection of auranofin did not prolong life span nor inhibited the growth of B16-F10-implanted melanoma tumors [197]. A recent study demonstrated that auranofin at concentrations of > 1 μM significantly inhibited melanin synthesis in B16-F10 cells [198]. This activity was attributed to inhibition of intracellular tyrosinase activity, downregulation of cAMP levels and increase in immature melanosome populations. The authors also tested the cytotoxicity

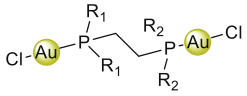

Au-9a $R_1 = R_2 = Ph$
Au-9b $R_1 = R_2 = Et$
Au-9c $R_1 = R_2 =$ Cyclohexil
Au-9d $R_1 = R_2 = C_6H_5CH_2$-
Au-9e $R_1 = R_2 =$ 2-furyl
Au-9f $R_1 = R_2 =$ 2-thienyl
Au-9g $R_1 = R_2 =$ 2-pyridyl
Au-9h $R_1 =$ Et, $R_2 = Ph$
Au-9i $R_1 = R_2 = 4\text{-}FC_6H_4$
Au-9j $R_1 = R_2 = 2\text{-}FC_6H_4$
Au-9k $R_1 = R_2 = 4\text{-}CH_3C_6H_4$
Au-9l $R_1 = R_2 = 3\text{-}CH_3C_6H_4$
Au-9m $R_1 = R_2 = 4\text{-}CH_3OC_6H_4$
Au-9n $R_1 = R_2 = C_6D_5$

*in vivo* Au-9a

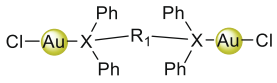

Au-10a $R_1 = CH_2$, X = P
Au-10b $R_1 =$ cis-HC=CH, X = P
Au-10c $R_1 =$ trans-HC=CH, X = P
Au-10d $R_1 = CC$, X = P
Au-10e $R_1 = CH_2CH(CH_3)$, X = P
Au-10f $R_1 = CH(CH_3)CH(CH_3)$, X = P
Au-10g $R_1 = (CH_2)_3$, X = P
Au-10h $R_1 = (CH_2)_4$, X = P
Au-10i $R_1 = (CH_2)_5$, X = P
Au-10j $R_1 = (CH_2)_6$, X = P
Au-10k $R_1 = 1,4\text{-}C_6H_4$, X = P
Au-10l $R_1 = (CH_2)_2$, X = P,As
Au-10m $R_1 = (CH_2)_2$, X = As
Au-10n $R_1 = (CH_2)_2$, X = S

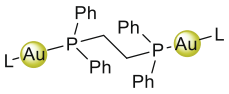

Au-11a L = $Cl_3$
Au-11b L = Br
Au-11c L = $OCOCH_3$
Au-11d* L = Cl-,$[(Ph)_2PCH_2\text{-}]_2$
Au-11e L = SCN
Au-11f L = $SCF_3$
Au-11g L = SCSOEt
Au-11h L = SGlu
Au-11i L = $SGluAc_4$
Au-11j L = $SManAc_4$
*10 membered ring

*in vivo* Au-11h

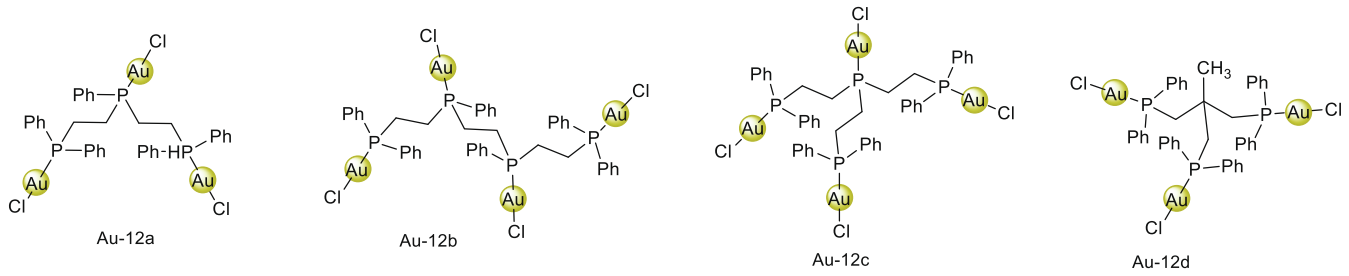


**Fig. 24.** Dinuclear Au(I) compounds with phosphane ligands.

of auranofin in B16-F10/HaCaT and MNT-1/HaCaT cocultures, which are better physiological skin models than monocultures, and it retained its activity at concentrations > 1 μM.

Auranofin has also been subject of the NCI-60 screening assay, presenting $GI_{50}$ values of 0.5 μM or lower against all melanoma cell lines of this panel (NSC number = 321521) [194,199]. It is currently undergoing several clinical trials, including one in conjunction with sirolimus (an immunosuppressant drug) for the treatment of lung-cancers, including squamous cell lung carcinoma (identifier: NCT01737502). To the best of our knowledge, no clinical trials for the treatment of skin cancer with this metallodrug have been conducted. Further testing of auranofin, in a drug repurposing strategy, may be promising for the chemotherapeutic/adjuvant treatment of skin cancers, especially since thioredoxin reductase and other selenoproteins have been associated with the pathogenesis of these diseases [200-204].

### 3.4.2. Systematic variation of the structure of auranofin

At Smith, Kline and French laboratories in 1986, Mirabelli and co-workers evaluated the effects of systematic variation of auranofin's structure [205]. A series of 63 compounds was studied, which we divide here in 8 categories (Fig. 23): **Au-1**, where the protecting groups of the thioglucose were altered; **Au-2**, where the thiosugar is changed; **Au-3**, where Et3P is fixed and a series of S-donors was incorporated into the structure; **Au-4**, where the tetraacetyl thiogluxose is fixed, and varying phosphanes were studied; **Au-5**, where no phosphane is used, and the S-donor becomes a $\mu_2$ S-bridging ligand; **Au-6**, where the $Et_3P$ phosphane is fixed, and the coligand L is changed; **Au-7**, where the chlorido ligand is fixed and the identity of the phosphane is changed; and finally **Au-8**, where the chlorido ligand is fixed, and different coligands were evaluated.

The cytotoxicity of every single compound was evaluated *in vitro* against the B16-F10 melanoma cell line by the colony formation assay.

The structure–activity relationship derived from their studies indicate that structural changes within ligand classes can have a profound effect on the *in vitro* cytotoxic potency. Auranofin, used as a benchmark, had an $IC_{50}$ of 1.5 μM against B16-F10 *in vitro*. From series **Au-1**, the replacement of the acetyl groups by other "protecting" groups produced compounds **Au-1a** and **Au-1c**, with cytotoxic potency comparable to that of auranofin, while the CONHMe group led to a less cytotoxic analogue (**Au-1b**). From series **Au-2**, the replacement of α-D-glucose in auranofin by different sugars did not have a great impact on the $IC_{50}$ values, with cytotoxic potencies ranging from 4 to 6 μM. From series **Au-3**, with a fixed $Et_3P$ ligand, the identity of the S-donor had a more profound effect on the cytotoxicity trend. The ligand $MeS^-$ in **Au-3a** led to the least active compound, with an $IC_{50}$ of 60 μM. The most remarkable activities in this series were observed for compounds **Au-3h**, **Au-3i**, **Au-3l** and **Au-3n**, all of which had $IC_{50}$ values of 1 μM against B16-F10. In the series **Au-4**, which has a fixed tetraacetyl thioglucose, the varying phosphane ligand was shown to have less impact on the cytotoxic potency, with all compounds presenting $IC_{50}$ values from 2 to 8 μM. Comparing phosphane-containing mononuclear compounds to the polymeric $\mu_2$ S-bridged counterparts present in series **Au-5** highlights the reduction of *in vitro* cytotoxicity for the polymeric compounds, which have $IC_{50}$ values varying from 60 to 166 μM against B16-F10. The removal of the $Et_3P$ moiety from auranofin reduced the cytotoxic potency of the resulting complex (**Au-5a**) 150-fold. This relationship may be in part the result of lipophilicity introduced by the alkyl- or phenylphosphane. Partition coefficient data show that $Et_3PAuCl$ (from **Au-6** series), $Me_3PAuCl$ (**Au-7a**), $Ph_3PAuCl$ (from **Au-7** series), and auranofin (from **Au-1** series) are significantly more lipophilic than aurothioglucose

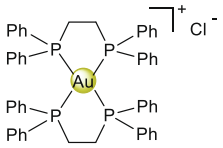

Au-12e

*in vivo*

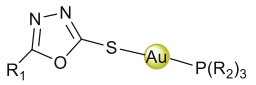

Au-13a: $R_1$ = adamantyl, $R_2$ = phenyl
Au-13b: $R_1$ = phenyl, $R_2$ = phenyl
Au-13c: $R_1$ = 4-chlorophenyl, $R_2$ = phenyl
Au-13d: $R_1$ = 4-fluorophenyl, $R_2$ = phenyl
Au-13e: $R_1$ = 4-nitrophenyl, $R_2$ = phenyl
Au-13f: $R_1$ = 4-methoxylphenyl, $R_2$ = phenyl
Au-13g: $R_1$ = *n*-heptyl, $R_2$ = phenyl
Au-13h: $R_1$ = *n*-nonyl, $R_2$ = phenyl
Au-13i: $R_1$ = *n*-undecyl, $R_2$ = phenyl
Au-13j: $R_1$ = *n*-tridecyl, $R_2$ = phenyl
Au-13k: $R_1$ = *n*-pentadecyl, $R_2$ = phenyl

Au-14a: $R_1$ = adamantyl, $R_2$ = ethyl
Au-14b: $R_1$ = phenyl, $R_2$ = ethyl
Au-14c: $R_1$ = 4-chlorophenyl, $R_2$ = ethyl
Au-14d: $R_1$ = 4-fluorophenyl, $R_2$ = ethyl
Au-14e: $R_1$ = 4-nitrophenyl, $R_2$ = ethyl
Au-14f: $R_1$ = 4-methoxylphenyl, $R_2$ = ethyl
Au-14g: $R_1$ = *n*-heptyl, $R_2$ = ethyl
Au-14h: $R_1$ = *n*-nonyl, $R_2$ = ethyl
Au-14i: $R_1$ = *n*-undecyl, $R_2$ = ethyl
Au-14j: $R_1$ = *n*-tridecyl, $R_2$ = ethyl
Au-14k: $R_1$ = *n*-pentadecyl, $R_2$ = ethyl

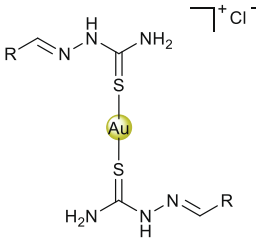

Au-17a R = phenyl
Au-17b R = p-methoxyphenyl
Au-17c R = thiophene
Au-17d R = furan
Au-17e R = pyridinyl
Au-17f R = p-hydroxyphenyl

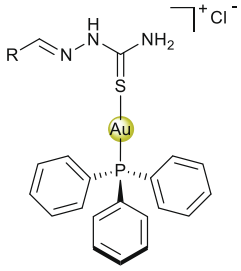

Au-17g R = phenyl
Au-17h R = p-methoxyphenyl
Au-17i R = thiophene
Au-17j R = furan
Au-17k R = pyridinyl
Au-17l R = p-hydroxyphenyl

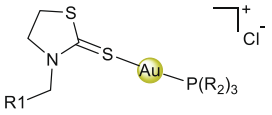

Au-15a: $R_1$ = adamantyl, $R_2$ = phenyl
Au-15b: $R_1$ = phenyl, $R_2$ = phenyl
Au-15c: $R_1$ = *n*-heptyl, $R_2$ = phenyl
Au-15d: $R_1$ = *n*-nonyl, $R_2$ = phenyl
Au-15e: $R_1$ = *n*-undecyl, $R_2$ = phenyl
Au-15f: $R_1$ = *n*-tridecyl, $R_2$ = phenyl
Au-15g: $R_1$ = *n*-pentadecyl, $R_2$ = phenyl

Au-16a: $R_1$ = adamantyl, $R_2$ = ethyl
Au-16b: $R_1$ = phenyl, $R_2$ = ethyl
Au-16c: $R_1$ = *n*-heptyl, $R_2$ = ethyl
Au-16d: $R_1$ = *n*-nonyl, $R_2$ = ethyl
Au-16e: $R_1$ = *n*-undecyl, $R_2$ = ethyl
Au-16f: $R_1$ = *n*-tridecyl, $R_2$ = ethyl
Au-16g: $R_1$ = *n*-pentadecyl, $R_2$ = ethyl

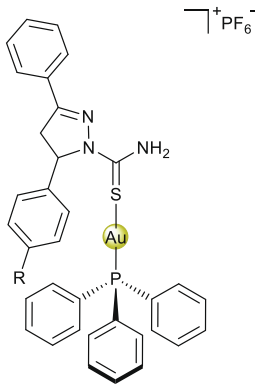

Au-18a R = methyl
Au-18b R = H
Au-18c R = methoxyl

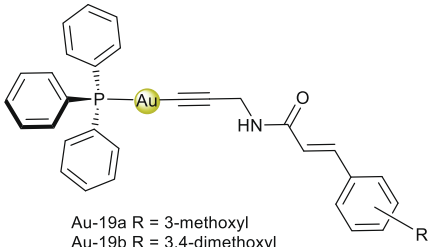

*in vivo*

Au-19a R = 3-methoxyl
Au-19b R = 3,4-dimethoxyl
Au-19c R = 3,4,5-trimethoxyl

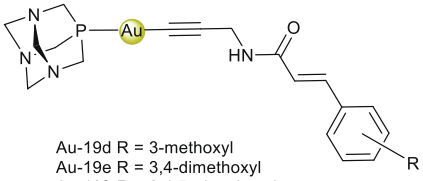

Au-19d R = 3-methoxyl
Au-19e R = 3,4-dimethoxyl
Au-19f R = 3,4,5-trimethoxyl

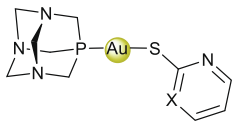

Au-20a X = C
Au-20b X = N

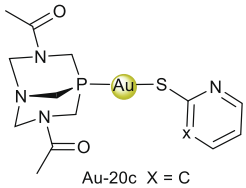

Au-20c X = C
Au-20d X = N

**Fig. 25.** Mononuclear Au(I) compounds with phosphane ligands.

(**Au-5b**) and aurothiomalate (**Au-5d**). From series **Au-6**, again with a fixed $Et_3P$, all compounds were highly cytotoxic, reaching the highest *in vitro* potency found in this study ($IC_{50}$ = 0.4 μM) with compound $Et_3PAuCN$ (**Au-6b**). Series **Au-7** and **Au-8** are both comprised of monofunctional compounds, containing a fixed chloride ligand. In this case, the presence of a phosphane of any kind (**Au-7**) is the most important factor for reaching high cytotoxic potency. Comparing the bulkiness and basicity of the phosphane, $Et_3P$ is the optimal moiety with $Et_3PAuCl$ (from **Au-6** series) displaying an $IC_{50}$ of 1 μM, while moving to $Me_3PAuCl$ (**Au-7a**) and $Ph_3PAuCl$ leads to a less cytotoxic compounds ($IC_{50}$ values of 6 μM and 12 μM respectively). **Au-7d**, $(MeN)_3PAuCl$, was also highly cytotoxic $IC_{50}$ values of 0.7 μM). Comparing the non-phosphane co-ligand varied in the **Au-8** series, the most cytotoxic compound **Au-8a** bears the $Et_3As$ motif (with an $IC_{50}$ value of 8 μM). All the other compounds evaluated in series **Au-8** were significantly less cytotoxic, with $IC_{50}$ values ranging from 60 to > 200 μM. The 63 compounds from series **Au-1** to **Au-8** were also tested for the treatment of a mouse leukemia model (P388). The SAR studies led Mirabelli and co-authors to summarize four major findings: (1) the phosphane-Au(I) moiety leads to highly active species *in vitro*, as discussed here; (2) low activity *in vitro* (as tested against the B16-F10 cell line) translated well into ineffectiveness *in vivo* for the leukemia model; (3) potent complexes *in vitro* were not necessarily potent *in vivo;* and (4) for the studied series, the most active compounds *in vivo* belonged to the phosphane-Au(I)-thiosugar class, *i.e.*, the ones following the auranofin protostructure.

### 3.4.3. Other Au(I)-phosphane compounds

Mirabelli and co-workers also evaluated a series of dinuclear Au(I) complexes of bisphosphanes (**Au-9** to **Au-12** – Fig. 24) related to dppe (1,2-bis (diphenylphosphino)ethane) [206].

In series **Au-9**, the ethane linkage was kept constant, while the other two substituents on the phosphorous atom were varied; **Au-10**, the phenyl substituents were kept constant, while the bridging group was changed; **Au-11**, the co-ligand chlorido was changed, with a fixed dppe; and finally, in series **Au-12**, triphos (bis(diphenylphosphinoethyl)phenylphosphane) and tetraphos (tris[2-(diphenylphosphino)ethyl]phosphane) and related phosphanes were studied. The compounds were evaluated against the B16-F10 cell line using the colony formation (clonogenic) assay to determine cytotoxic potency. In addition, most of the compounds were tested against leukemia P388 in a mouse model. The authors highlighted that no relationship was found between *in vitro* cytotoxicity and antitumor activity in this class of compounds; many gold complexes devoid of antitumor activity were potent cytotoxic agents. However, in the present study, a number of bisphosphane ligands with excellent antitumor activity (e.g., **Au-9c**, **Au-9f**, **Au-9i**, **Au-12a**) did not demonstrate cytotoxicity *in vitro* in the P388 model. In addition, two of the compounds, namely dppe$(AuCl)_2$ (**Au-9a**), and the thioglucose-containing analogue (**Au-11h**) were evaluated *in vivo* for the treatment of a B16 and (highly invasive) B16-F10 mouse models. Against B16, both compounds led to a 30% increase in life span of the mice in comparison to the untreated control, while both had no effect on the B16-F10 model. The Au(I) complex **Au-12e** is an unusually stable, tetrahedral compound which was able to reduce clonogenic capacity of B16 cells by 50% following a 2-h exposure at 2 μM as assessed by a colony formation assay [207]. Presence of serum in culture medium only resulted in a 2-fold decrease in activity, much lower than the 10-fold decrease observed for auranofin. The compound is also fairly unreactive towards GSH and GSSG. *In vivo* studies were performed on B6D2F mice inoculated with B16 melanoma cells. When **Au-12e** was administered intraperitoneally daily for 10 days, starting 1 day after tumor implantation, the animal models presented an average of 39% of increased lifespan at the maximum tolerated dose (1.9 μmol/kg).

More recent studies on structure–activity relationships of Au(I)-phosphane complexes were reported by Almeida and collaborators [208-211]. A series of mercapto-oxadiazole (**Au-13a-k** and **Au-14a-k**, neutral) or mercapto-thiazolidine (**Au-15a-g** and **Au-16a-g**, 1 + charge) ligands, shown in Fig. 25, had their effect on the Au(I)-phosphane moiety evaluated.

The adamantyl series (**Au-13a**, **Au-14a**, **Au-15a** and **Au-16a**) revealed that the triethylphosphane complexes were more cytotoxic over B16-F10 cells than the triphenylphospane ones. This trend was also observed on the cytotoxic profile of [AuCl$(PEt_3)$] and [AuCl$(PPh_3)$]. The adamantyl-oxadiazole ligand was not active, while the adamantyl-thiazolidine one had an $IC_{50}$ value of 9.0 ± 0.6 μM. The cytotoxicity correlated with the capacity of the metal complexes to inhibit thioredoxin reductase, even in the presence of albumin. Docking studies revealed that the adamantyl substituent is essential to stabilize the ligand–enzyme complex prior the formation of covalent bond with gold center [209].

The phenyl-substituted compounds (**Au-13b**, **Au-14b**, **Au-15b** and **Au-16b**) had almost equal and sub-micromolar (0.1 – 0.4 μM) activity on B16-F10 cell line. The ligands, in contrast to what was observed for the adamantyl series, were already quite cytotoxic, on low micromolar $IC_{50}$ values (2.3 and 6.5 μM for oxadiazol and thiazolidine ligands, respectively), being equally or more cytotoxic than cisplatin (6.4 μM) itself. **Au-15b** was 70 times selective to the melanoma cell line when compared the normal cell line (BHK-21). Further studies on the oxadiazole-phenyl series evaluated the effect on substitution on the phenyl ring. Compounds **Au-13c** to **Au-13f** and **Au-14c** to **Au-14f** showed impressive *in vitro* antiproliferative activity against B16-F10 cells with $IC_{50}$ values ranging from < 0.10 to 1.40 μM. These values were lower than for cisplatin in the same experiment ($IC_{50}$ = 6.40 ± 2.20 μM) and comparable to the precursors [AuCl$(PPh_3)$] and [AuCl$(PEt_3)$] ($IC_{50}$ = 0.90 and 0.50 μM, respectively) [210]. In all cases the antiproliferative activity of the complexes were higher than their respective oxadiazole-2-thione, even for the ligand with $NO_2$ substituent that already had a remarkable activity with $IC_{50}$ = 0.26 ± 0.1 μM. Some interesting structure–activity relationships can be obtained for these complexes. Those containing ligands with chloride or $NO_2$ moieties were more active towards B16-F10, and also the complexes with triethylphosphane ligand were generally slightly more active than the ones with triphenylphosphane, which might be related to their lipophilicity. Although the mechanism of action for these compounds is not currently know, the seleno-enzime TrxR is hypothesized as a possible target, in a similar fashion as for the adamantyl-substituted complexes [209].

Finally, the authors evaluated the effect of varying the size of an alkyl chain on the oxadiazole and thiazolidine ligands. Overall, the thiazolidine series was more active over B16-F10 cells than the oxadiazole one. A direct correlation of alkyl chain size and cytotoxicity was not verified, but compounds that had between 8 and 11 carbon atoms led to the lower $IC_{50}$ values, highlighting an ideal lipophilic character for these compounds.

Overall, this series of studies highlighted that: (1) in general, triethylphosphane compounds are slightly more active than the triphenylphosphane analogues, (2) adamantyl-substituted oxadiazole and thiazolidine ligands lead to less active compounds than phenyl or alkyl substituted ones, (3) the thiazolidine ligand may lead to more cytotoxic compounds, probably due to the cationic lipophilic nature of the resulting complexes which could improve cell uptake.

The group of Fontes [212] reported a series of homo and heteroleptic Au(I) complexes of thiosemicarbazones, **Au-17a** to **Au-17l** (Fig. 25). The cytotoxic activity of these complexes was tested over the B16-F10 melanoma cell line. The heteroleptic thiosemicarbazone-triphenylphosphane compounds were much more active (**Au-17h** being the most active: 0.2 ± 0.1 μM, MTT assay, 24 h) than the homoleptic ones, indicating that the activity originated mostly from the Au(I)-triphenylphosphane motif, as seen previously. Interestingly, the cytotoxic profiles of the compounds did not correlate with their ability to inhibit thioredoxin reductase, since the homoleptic compounds induced, in general, a higher degree of inhibition. The authors attributed these observations to the greater lipophilicity of the gold-phosphane complexes, which resulted in much higher cell uptake.

A work with similar thiocarbamoyl-pyrazoline ligands and their Au(I) complexes has recently been reported (**Au-18a-c,** Fig. 25) [213]. Cytotoxicity studies over B16-F10 cells revealed that the methoxyl substituent led to the most active compound, with $IC_{50}$ value of 1.3 ± 0.1 μM, while the values for reference compounds [AuCl$(PPh_3)$] and cisplatin were close to 6 μM. Investigation of their photophysical properties showed an intense greenish blue emission when the complexes were excited at 305 nm in solution. This property allowed the authors to track the compounds in MDA-MB-231, MCF-7 and HUVEC cells, where they showed neither preferential organelle localization, nor were they found in nuclei. Additional studies on melanoma or KC cells could be performed for their application in skin cancer.

Organometallic alkynylgold(I) phosphane complexes containing methoxy-substituted cinnamide moieties, **Au-19a-f** (Fig. 25), have been reported [214]. The PTA-containing compounds were much less active than the corresponding triphenylphosphane ones. Complex **Au-19c** possessed 20 times higher cytotoxicity than cisplatin and about 5 times higher than [AuCl$(PPh_3)$] against D24 melanoma cells, showing disruption and disaggregation of the 3D spheroidal structure of the same melanoma cells in a concentration-dependent manner. Mechanistic investigations of **Au-19c** activity

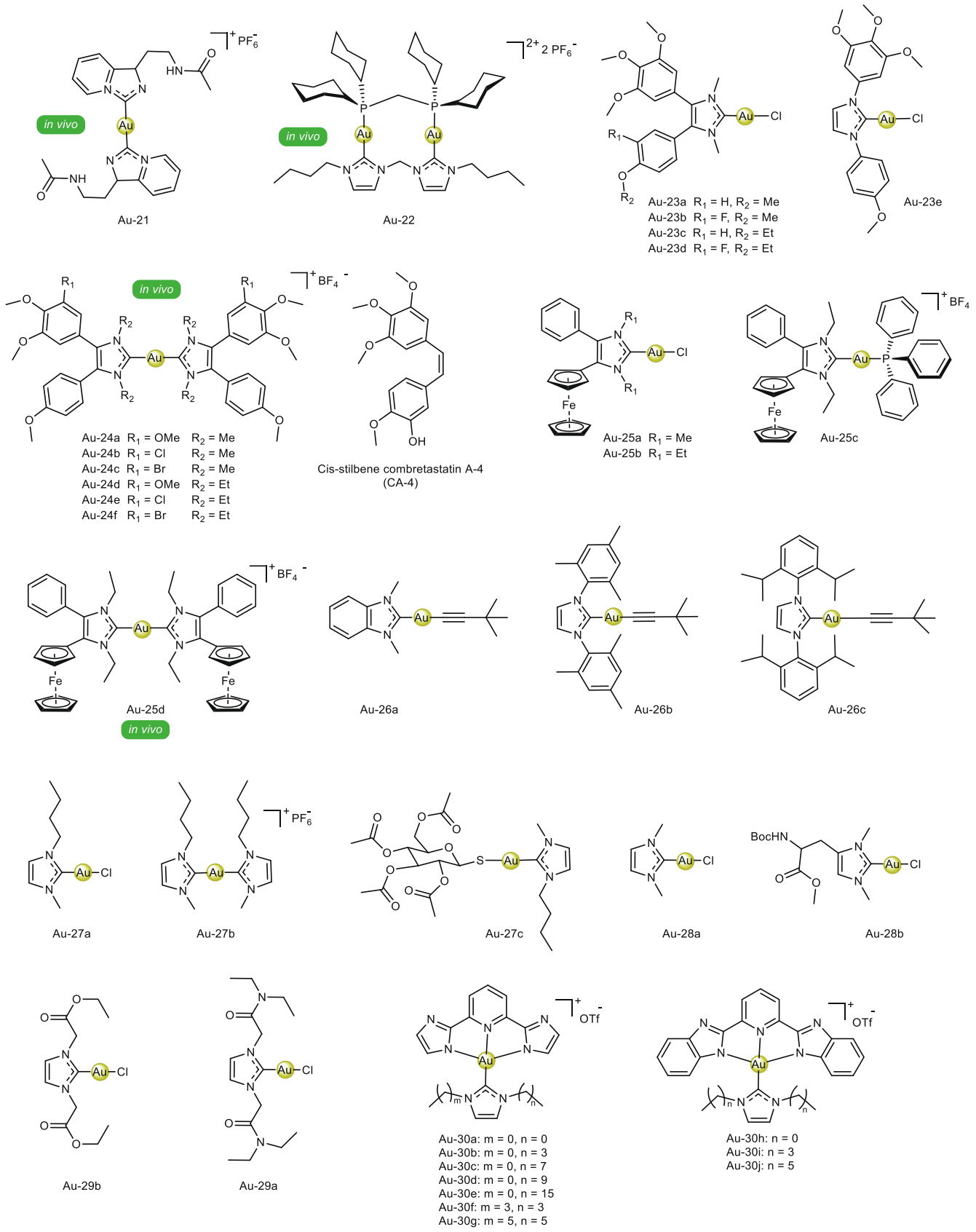


**Fig. 26.** Au(I) complexes (**Au-21** to **Au-29**) and Au(III) complexes (**Au-30a** to **Au-30j**) with NHC ligands.

indicate that DNA is not a major target of these compounds, as expected from most Au(I)-phosphane complexes, while thioredoxin reductase inhibition was observed through steric and hydrogen-bonding interactions. ROS and mitochondrial pathways of cell death were identified for D24 cells treated with **Au-19c.** Finally, the inhibition of thioredoxin reductase was correlated with angiogenesis-inhibiting properties of **Au-19c** (starting at concentrations as low as 0.1 μM) in a transgenic Tg(fli1a:EGFP) zebrafish model, which expresses enhanced green fluorescent protein in endothelial cells. Such antiangiogenic properties were not observed for cisplatin in the zebrafish model even when treated at 1 μM. The results suggested the prospect of Au(I)-phosphane as antiangiogenesis agents, with more *in vivo* data being necessary for further investigations.

Miranda et al. reported four Au(I) thionate complexes with water-soluble phosphane ligands (**Au-20a-d,** Fig. 25) [112]. The choice of phosphane ligands was made to improve aqueous solubility of the complexes in contrast to other less soluble complexes that usually contain triphenylphosphane or triethylphosphane. The authors reported $IC_{50}$ values of 3.6, 3.6, 6.3 and 12.2 μM for **Au-20a**, **Au-20b**, **Au-20c** and **Au-20d**, respectively, against M19 MEL cells. It is worth noting that similar water-soluble Pt(II) complexes (**Pt-16a** to **Pt-16d**, Fig. 10), with the same set of ligands, showed better $IC_{50}$ values than the Au(I) ones over the M19 MEL cells.

### 3.4.4. Gold(I) N-heterocyclic carbene compounds

The class of the N-heterocyclic carbene (NHC) ligands are frequently associated with Au(I) complexes, forming strong metal–ligand bonds due to their pronounced electronic σ- or π-donation as well as π-accepting properties [215].

The group of Das Saha described a Au(I) bis-NHC complex (**Au-21,** Fig. 26) with *in vitro* activity over B16-F10 mouse melanoma cell lines of $GI_{50}$ 9.4 ± 0.26 μM [216]. **Au-21** induced apoptosis with nuclear condensation, DNA fragmentation, and externalization of phosphatidylserine. This complex suppressed anti-apoptotic Bcl-2 proteins and activated pro-apoptotic Bax protein. The latter leads to disruption of the mitochondrial membrane and to the release of cytochrome *c* from mitochondria to cytosol. These events activate caspase 9 (initiator caspase) and caspase 3 (executioner caspase) that then cause the cleavage of PARP, which would be responsible for DNA repair and cell survival [217]. **Au-21** was also shown to upregulate the tumoral suppressor gene p53, and its translocation to the nucleus and to increase expression of p21 proteins that negatively regulates the G1 to S phase transition [218].

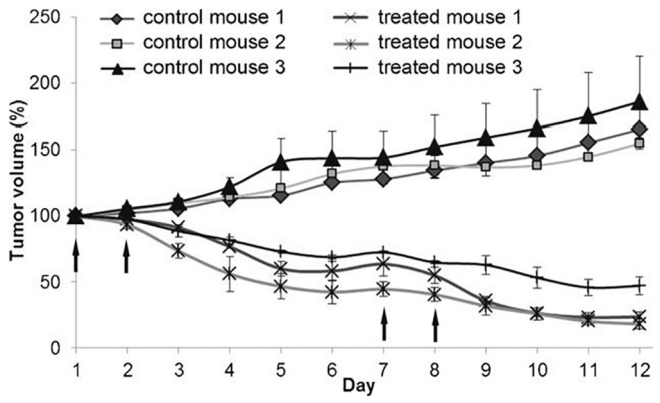


**Fig. 27.** Antitumoral activity of complex **Au-25d** in mouse xenografts of the highly metastatic B16-F10 melanoma cell line. Shown are the relative tumor responses following a repeated application of DMSO (control) or complex **Au-25d** on two consecutive days (i.p. injections of 7.5 mg/kg on days 1, 2, 7, and 8: black arrows). Data are mean values ± S.D. of the tumors implanted in both flanks of each mouse. Image retrieved from Muenzner et al [222].

The *in vivo* assays show that BALB/c mice bearing the B16-F10 tumor that were not treated with **Au-21** faced total mortality by the 40th day, whereas treatment with the complex ensured dose dependent survivability of 30% to 70% until the 60th day. Also, the mice body weight remained nearly constant, as the tumor volume decreased in a dose dependent manner. Moreover, mice treated with the complex had inhibited expressions of angiogenic and metastatic markers such as VEGF and MMP-9, respectively [216].

The **Au-22** (Fig. 26) complex is a dinuclear Au(I) coordination compound, with the metal ions bridged by a bis(NHC) and a diphosphane ligand. **Au-22** was 13.5-fold more active than cisplatin against B16-F10 cells ($IC_{50}$ = 3.2 ± 1.0 μM for **Au-22**) [219].

It reduced TrxR activity by over 90% (at concentration of 200 nM in the presence of NADH) and the mechanism of inhibition was proposed by studying the C-terminal GCUG motif (Gly-Cys-Sec-Gly) as a model for the TrxR active site. It was suggested that **Au-22** binds to GCUG motif in 1:1 M ratio through simultaneous coordination of the binuclear Au(I) metal centers to respective S and Se atoms from neighbors Cys and Sec residues, accompanied by the release of the bis(NHC) ligand but not the diphosphane ligand.

In this case, **Au-22** was also tested *in vivo* using a highly aggressive, poorly immunogenic mouse melanoma (B16- F10) model in C57BL/6N mice. While the tumors in the control group grew fast, significant tumor inhibition (62%, $p < 0.05$) was achieved after intraperitoneal injections with 15 mg/kg of **Au-22** once every 2–3 days for 8 days, with no variation of the mice body weight.

The series of Au(I) NHC complexes including **Au-23**, **Au-24** and **Au-25** (Fig. 26) [220-222] have in common the ligands which are derivatives or analogues of *cis*-stilbene combretastatin A-4 (**CA-4**), a vascular disrupting agent that induces a rapid vascular shutdown in solid tumors, leading to secondary tumor cell death. **CA-4** binds strongly to tubulin, which affects the microtubule cytoskeleton and therefore inhibits mitosis. It also inhibits cell migration and adhesion by interfering with the VE-cadherin/b-catenin/Akt signaling pathway in vascular endothelial cells [220].

Complexes **Au-23a** to **Au-23e** bearing NHC ligands inhibited 518A2 melanoma cells with $IC_{50}$ varying from 12 to 20 μM, with exception of **Au-23d** that was not active ($IC_{50}$ > 50 μM). Furthermore, **Au-23a** to **Au-23c** and **Au-23e** were selective to the cancer cells when compared to non-malignant foreskin fibroblasts (HF), specially **Au-23a** that showed SI > 8 [221].

The article describing the **Au-23** series [221] presents studies on uptake and its implications in various pathways of drug entry using 518A2 melanoma cells. Significant fractions of these Au(I) NHC complexes were internalized via organic cation transporters and the copper transporter. **Au-23b** and **Au-23e** entered the cell also by $Na^+$ and $K^+$-dependent endocytosis.

The bis-NHC analogues to the **Au-23** series were also studied by Muenzner et al [220]. Complexes **Au-24a** to **Au-24f** were able to inhibit a variety of cancer cell lines at low micromolar ranges, including 518A2 cells ($IC_{50}$ between 0.23 and 0.46 μM for 518A2) [220].

Complexes **Au-24a** to **Au-24f** exhibited distinct vascular disrupting effects both *in vitro* and *in vivo* (by CAM assay). Although the antivascular effects of the complexes are very similar to the effects of **CA-4**, they originate from different modes of action. Whereas **CA-4** targets and disrupts the microtubules of cancer and endothelial cells causing a G2/M cell-cycle arrest, complexes interfere only with the F-actin dynamics by stress fiber formation, leading to G1 phase arrest, therefore impairing cell motility. The antimetastatic properties of the **Au-24** series is further enhanced by their ability to decrease the concentration of pro-metastatic matrix metalloproteinase MMP-2, which is commonly expressed

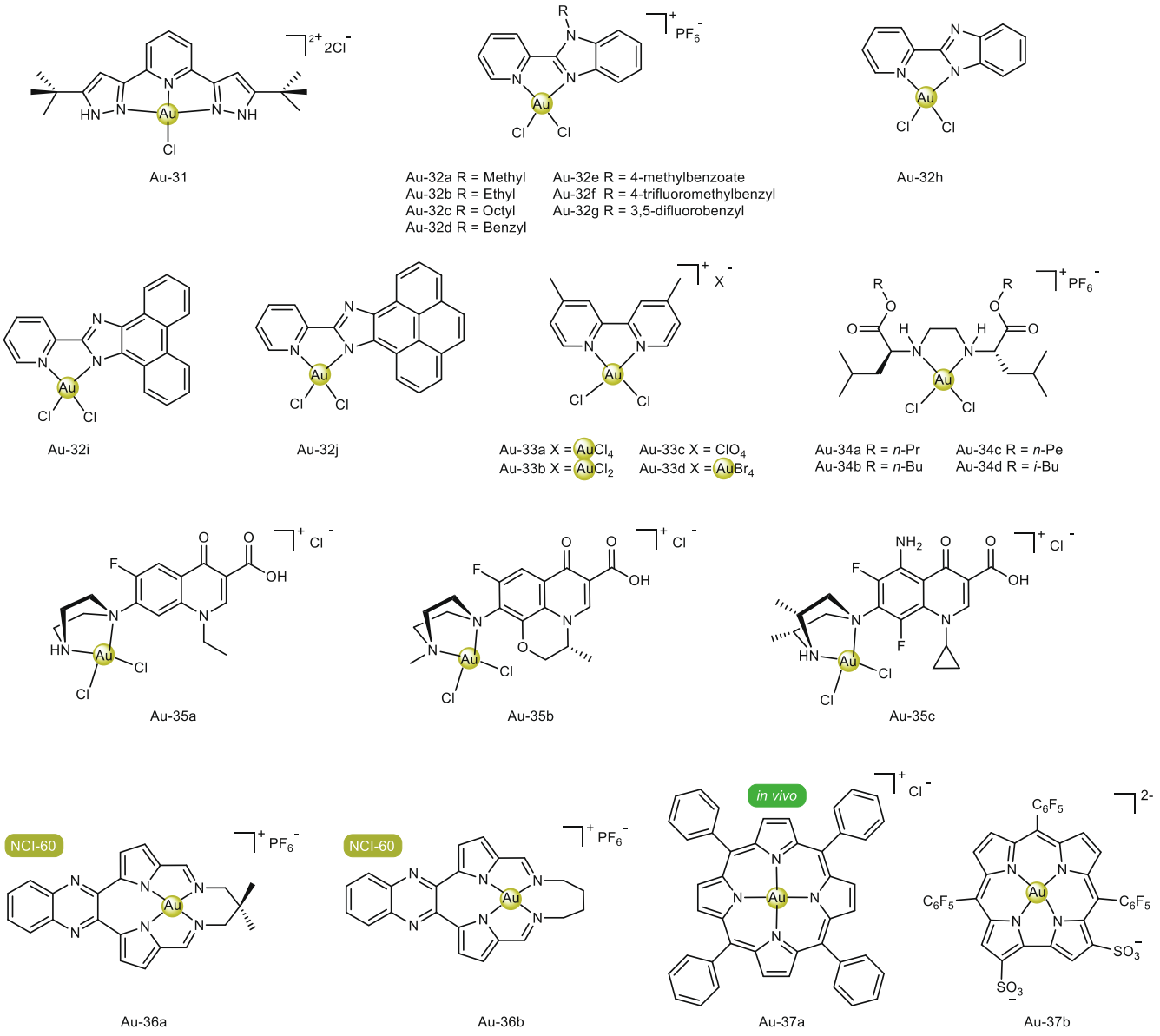


**Fig. 28.** Au(III) complexes with N^N donating ligands, including bidentate and macrocyclic compounds.

and secreted by cancer cells. Moreover, the complexes offer a prospect of recovering blood vessels after disruption as observed in the CAM assay.

The efficacy of these complexes was also confirmed in mouse xenografts of highly metastatic B16-F10 cell line, with repeatedly high dosages being tolerated by the animals.

Gold NHC complexes had also been reported to interfere with redox processes inside the cell (e.g. by interacting with thioredoxin reductase). To capitalize on that, Muenzner et al. attached an electronically coupled, redox-active ferrocenyl residue to NHC ligands of Au(I) complexes (**Au-25a** to **Au-25d**) and evaluated their antiproliferative activity against a panel of tumor cells, including 518A2 melanoma cells [222].

The complex **Au-25a** was significantly less active against 518A2 ($IC_{50}$ = 11.3 ± 0.3 μM), than the complex **Au-25b** ($IC_{50}$ = 1.3 ± 0.1 μM), which is the analogue bearing the N-ethyl NHC ligand. **Au-25c** and **Au-25d** showed even lower $IC_{50}$ values in this assay, 0.20 ± 0.03 and 0.19 ± 0.02 μM. Besides the positive charge, these two complexes do not have the chloride ligand coordinated, showing that series **Au-25** follows a trend of complexes that have increasing cytotoxicity when the chloride ligand is substituted by a phosphane or NHC ligand [223].

The mechanism of action of complexes **Au-25c** and **Au-25d** was investigated in detail. They were able to cause a significant accumulation of 518A2 cells in the G1 phase, with the effect induced by **Au-25d** being slightly more potent. This is associated with induction of a distinct reorganization of the F-actin cytoskeleton in human vascular endothelial and melanoma cells by the complexes. The fractions of cells in S and G2/M phase were distinctly reduced whereas the sub-G1 population of apoptotic cells rose slightly [222].

The complexes **Au-25c** and **Au-25d** were also shown to be potent inhibitors of the redox enzyme TrxR in accordance with other N-heterocyclic carbene Au(I) complexes reported in the literature [223,224]. Moreover, the ferrocene moiety was responsible for intracellular accumulation of ROS and decrease of mitochondrial membrane potential. Another important feature of these two complexes was their antiangiogenic potential, demonstrated by the inhibition of the formation of vessel-like structures by HUVEC (human endothelial cells) *in vitro* and also by the disrup-

tion of blood vessels in chorioallantoic membrane of fertilized chicken eggs *in vivo*. This is particularly important for the application of these derivatives against metastatic and invasive melanomas.

In addition, the antitumoral activity of **Au-25d** was also attested *in vivo* by using a Balb/c mouse xenograft model of invasive B16-F10 melanoma (Fig. 27). A reduction in tumor size of 18% to 48% was observed after twelve days whereas the volumes of untreated B16-F10 tumors increased by 1.6- to 1.9-fold. Not only the complexes were effective against the highly metastatic melanoma, they were also well tolerated by the animals as no significant weight loss was observed in the treated mice.

Oberkofler et al. systematically studied the reactivity of NHC-Au-alkynyl complexes. The stability of the compounds towards EtSH is influenced by the type of NHC scaffold and the steric hindrance of substituents in the N atom of the NHC or in the alkynyl moiety. For instance, **Au-26a** (Fig. 26) [225] (benzimidazole ligand with low steric hindrance) was much less stable than **Au-26b** [225] or **Au-26c** [226]. The antiproliferative activity of these three complexes were evaluated over A375 cells. They inhibited the cell line with $IC_{50}$ of 12 ± 4, 3.4 ± 0.5 and 10 ± 1 μM, respectively. The moderate cytotoxic activity is attributed to the relatively low reactivity of the complexes with DNA G-quadruplexes and model thiols.

Complexes **Au-27a** to **Au-27c** (Fig. 26) inhibited A375 cells with even lower $IC_{50}$ values, between 1.0 and 2.0 μM, which is comparable to auranofin ($IC_{50}$ = 1.3 ± 0.8) and cisplatin ($IC_{50}$ = 3.7 ± 0.9 μM) in the same assay [226].

Given the antiproliferative activity of **Au-27a** to **Au-27c** and **Au-26c**, their toxicity was evaluated in an *ex vivo* model of healthy rat kidney tissue. Therefore, kidney samples were incubated with various concentrations of each Au complex, and after 24 h the viability of the tissues was determined by measuring the ATP content. Compounds **Au-27a** to **Au-27c** were 6 to 12-fold more toxic to the kidneys than cisplatin, which is remarkable considering the high nephrotoxicity of cisplatin. However, complex **Au-26c** showed no toxicity up to the concentration of 50 μM and did not induce significant morphological changes in the kidneys in comparison to the control, indicating selective toxicity to cancer cells over healthy kidney tissue.

Other NHC-Au(I) complexes showed a less pronounced antiproliferative effect over melanoma cells, as **Au-28a** and **Au-28b** (Fig. 26) ($IC_{50}$ = 17 ± 1 and 15 ± 5 μM for 518A2 cells) [108] or **Au-29a** and **Au-29b** (Fig. 26) ($IC_{50}$ = 44.64 ± 3.22 and 46.33 ± 2.98 μM for A375 cells) [227]. Nonetheless, **Au-29a** and **Au-29b** were not toxic to HEK293 nontumoral human embryonic kidney cells ($IC_{50}$ > 100) and were able to decrease the TrxR enzyme activity by approximately 80% at a concentration of 90 nM.

All of these examples highlight how the choice of the NHC ligand moieties in Au(I) complexes are important to balance reactivity, toxicity, selectivity to cancer cells, antiproliferative and antimetastatic activity, as well as TrxR inhibition or DNA interaction for example.

### 3.4.5. Au(III) compounds

A series of Au(III) compounds of NHC and 2,6-bis(imidazol-2-yl) pyridine and 2,6-bis(benzimidazol-2-yl)pyridine ligands, **Au-30a** to **Au-30j** (Fig. 26), have been reported by the Che group [228]. The Au(III) complexes quickly react with reducing S-donor small molecules, such as glutathione, resulting in Au(I)–NHC and free luminescent N^N^N ligand. This fluorescence switch-on property was explored for tracking the compound in cells. HeLa cells incubated for 10 min with compound **Au-30h** resulted in significant blue fluorescence in the cytoplasm, especially localized in mitochondria. The cytotoxic activity of these compounds was screened against a panel of 6 cell lines, including the B16 melanoma one. Overall, cytotoxicity increased with lipophilicity, although in the **Au-30a** to **Au-30e** series, an ideal side-chain length was found for **Au-30d** ($IC_{50}$ = 1.60 ± 0.10 μM), with 10 carbon atoms, rather than the one with 16. Additionally, the benzimidazole-containing complexes **Au-30h** to **Au-30j** were more cytotoxic than their imidazole counterparts (**Au-30a**, **Au-30f** and **Au-30g**, respectively). An apoptotic pathway was indicated as mechanism of cell death, possibly mediated by their capability to inhibit thioredoxin reductase.

Simović and collaborators studied Au(III) complexes of tridentate pincer-type ligands [229]. The fourth coordination site was occupied by chloride. **Au-31** (Fig. 28) was the only in the series evaluated in terms of cytotoxic potency against A375, due to solubility limitations of its analogues. Although the labile chloride could be substituted by 5′-GMP, the authors identified intercalation of the planar complexes as the main type of interaction with calf-thymus DNA. The compound presented an $IC_{50}$ value of 13.1 ± 2 μM (48 h, MTT), while cisplatin had a potency of 23.1 ± 0.1 μ

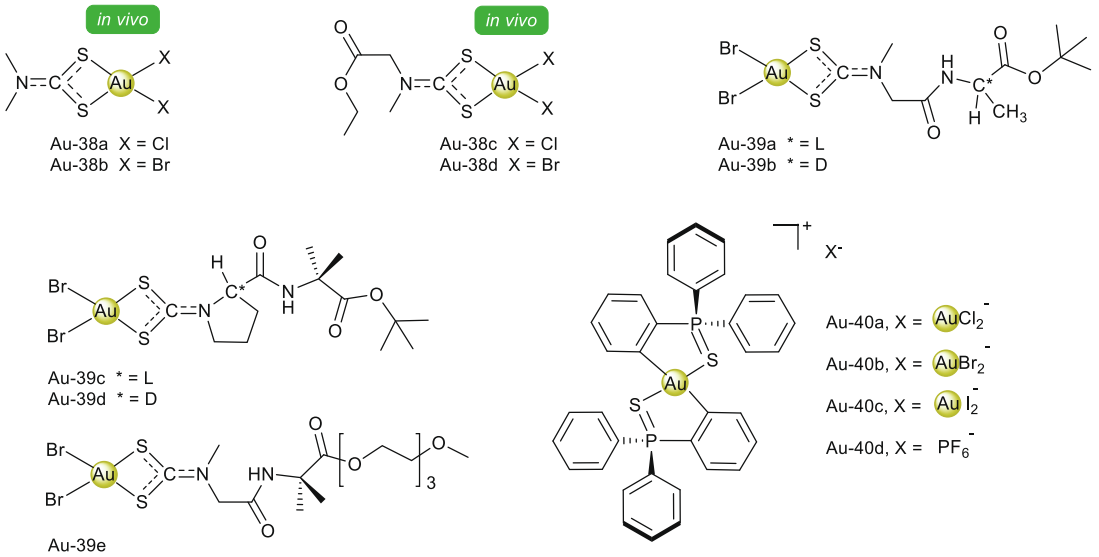


**Fig. 29.** Au(III) complexes with dithiocarbamato ligands (**Au-38** and **Au-39**) and cyclometallated Au(III) complexes of triphenylphosphane sulfide ligands (**Au-40**).

M against the same cell line. The ligand itself was cytotoxic, with an $IC_{50}$ comparable to that of cisplatin. Pre-incubation with the S-donor *N*-acetyl-*L*-cysteine resulted in protective effect when cells were treated at $IC_{50}$ concentration of **Au-31**, implying deactivation of the complex. Flow cytometry analysis using A375 cells demonstrated that **Au-31** decreased the percentage of cells in the G1 phase while increasing the accumulation in the S phase, without affecting the sub-G1 and G2 phases. Annexin-V/PI flow cytometry data revealed that the mechanism of cell death induced by compound **Au-31** is apoptotic.

The Casini and Soveral groups reported a series of 10 Au(III) complexes of pyridine-benzimidazole ligands, **Au-32a** to **Au-32j** (Fig. 28), as inhibitors of aquaporins [230]. The compounds were selective inhibitors of glycerol permeation via the aquaglyceroporin AQP3 in human red blood cells, with $IC_{50}$ values < 2.0 μM except for the neutral compound **Au-32h** ($IC_{50}$ > 50 μM). The *in vitro* cytotoxic activity of the compounds was investigated against several cell lines, including A375, which were shown to have AQP3 expression on both cell and nuclear membranes. The neutral compounds **Au-32h** to **Au-32j** were more active ($EC_{50}$ values between 5 and 13 μM) than the positively charged ones ($EC_{50}$ values > 20 μM), which may be derived from higher uptake due to their more lipophilic nature.

The Safari group [231] synthesized a series of Au(III) compounds containing the fixed $[Au(4,4\text{-dimethylbpy})X_2]^+$ motif (where X = Cl or Br) with varying counter-ions (**Au-33a** to **Au-33d,** Fig. 28). The antiproliferative activities of the compounds were assayed against A431 (72 h, MTT). The tested anions, $[AuCl_4]^-$, $[AuCl_2]^-$, $(ClO_4)^-$ and $[AuBr_4]^-$, had a profound effect on the cytotoxicity profile. The authors reported the following order of cytotoxicity, in terms of $IC_{50}$ values: **Au-33c** (0.63 ± 0.007 μM) > **Au-33b** (8.14 ± 0.03 μM) > **Au-33a** (27.63 ± 0.13 μM) > **Au-33d** (72.77 ± 5.84 μM). Remarkably, the perchlorate derivative **Au-33c**, the only one where no additional metal ion was present, was the most active. Cisplatin and carboplatin were tested for comparison and had $IC_{50}$ values of 6.83 ± 1.31 and 79.38 ± 3.72 μM respectively.

Complexes **Au-34a** to **Au-34d** (Fig. 28) were prepared by the Kaluđerovićg group [232]. The compounds are based on the bis(-carboxyalkylamino)ethane motif, with varying alkyl lengths on the ester group. These derivatives were assayed against the FEMX melanoma cell line. The compounds with the longer side chain (**Au-34b**, R = *n*-Bu; and **Au-34c**, R = *n*-Pe) were the most cytotoxic, presumably due to the higher lipophilicity. Uptake data was presented only for compound **Au-34c**, hindering further comparison. Compounds **Au-34c** (R = *n*-Pe) and **Au-34d** (R = *i*-Bu) were compared in terms of cell cycle effect in FEMX cells. Compound **Au-34d** induced an increase in the sub-G1 population in a dose-dependent manner, while treatment with **Au-34c** did not induce significant changes at 24 h.

Teixeira an co-workers [233] developed a series of fluoroquinolone ligands conjugated to a coordinating diaminocyclohexane motif. The ligands were used for the synthesis of Au(III) compounds **Au-35a** to **Au-35c** (Fig. 28), which were tested against B16-F10. The compounds were only moderately cytotoxic, with $IC_{50}$ values of 27 ± 1, 29 ± 9 and 45 ± 7 μM, respectively.

Munro and co-workers developed a series of planar cationic Au (III) macrocycles that combines two pyrrole-imine units linked by a quinoxaline moiety and a variable alkyl chain bridge (Fig. 28) [234]. In this series, compounds **Au-36a** and **Au-36b** were potent DNA intercalators, with $K_A > 10^6\ M^{-1}$ bp for calf-thymus DNA (CT-DNA). The two compounds were also tested in the NCI-60 panel. Compound **Au-36a** was particularly active against SK-MEL-5 ($GI_{50}$ = 4.68 μM), while compound **Au-36b** had a more diverse cytotoxic profile, with single-digit $GI_{50}$ against LOX-IMVI, MALME-3 M, M14, SK-MEL-2, SK-MEL-5, SK = MEL-28 and UACC-62. Hierarchical cluster analysis of NCI-60 cytotoxicity data for **Au-36b** indicated that it correlated most closely with the topoisomerase IB (Top1) poison camptothecin. The authors proceeded to investigate the mechanism of Top 1 inhibition by **Au-36b** and found through several topical enzyme inhibition assays that **Au-36b** is a catalytic inhibitor (and not a poison) of Top 1. Comparison with the catalytic inhibition of human topoisomerase IIα (Top2α) revealed that **Au-36b** is a selective type I-inhibitor. Finally, Surface plasmon resonance (SPR) studies confirmed (*i*) that Top1 does not bind to its DNA substrate in the presence of **Au-36b**, (*ii*) that **Au-36b** does not bind to Top1 itself, and (*iii*) that the **Au-36b** has specificity for 5′-TA-3′, the dinucleotide target sequence for the enzyme, as pointed out by macromolecular simulations.

The promising anticancer properties of Au(III) porphyrins were reported for the first time in 2003 by the Che group [235]. On this seminal work, the authors reported the synthesis and characterization of the complexes as well as their *in vitro* cytotoxicity over a panel of 7 cancer cell lines. These included KB-3–1 and KB-V1 (multi-drug resistant) cells, which were previously labeled as human oral squamous cell carcinoma, but attention has been called in the literature, since KB cells are actually misidentified HeLa [236]. Overall, the gold porphyrins were active on low or sub-micromolar range, while cisplatin had $IC_{50}$ values > 10 μM. DNA binding and apoptotic cell death was observed after treatment with Au(III) *meso*-tetraphenylporphyrin, **Au-37a** (Fig. 28), and this compound has, since then, been selected as prototype by the Che group and subject of additional work. **Au-37a** induces caspase dependent and independent apoptosis via depletion of mitochondrial transmembrane potential and Bcl-2 protein suppression. It can also cause cell cycle arrest at $G_0$-$G_1$, activate p38 and inhibit thioredoxin reductase [237]. Recent work on chemical proteomics revealed that the direct molecular target of **Au-37a** in mitochondria is the chaperone heat shock protein 60 (Hsp60), which has an important role in regulating protein folding and in the prevention of aggregation [238]. The safe dosage of this metalloporphyrin by intravenous injection is below 3 mg/kg and additional experiments in mice showed that it does not cause blood-vessel irritation or genotoxicity [239].

The *in vivo* effects of **Au-37a** were evaluated in a model of melanoma in mice [240]. Female C57BL/6 mice were inoculated with $2 \times 10^5$ B16-F10 cells by subcutaneous injection. Treatment with **Au-37a** (0.125 mg/kg or 0.25 mg/kg) was performed by intraperitoneal injection for ten consecutive days. The median survival rates for mice treated with **Au-37a** (lower and higher dosages), saline with 2 % DMSO and dacarbazine an antineoplastic agent used against melanoma (80 mg/kg) were 26, 32, 20 and 26 days, respectively. However, treatment with saline resulted in tumor with average volumes of 3000 $mm^3$, whereas the groups with **Au-37a** at both dosages had an average tumor volume of 1000 $mm^3$ after 20 days of inoculation. Necrosis and apoptotic cells were observed in tumor tissues treated with **Au-37a** and it was also able to inhibit angiogenesis in melanoma-affected tissues.

Corroles are major representatives of contracted porphyrins with applications from fundamental coordination chemistry to biology [241]. A hydrophilic Au(III) corrole, **Au-37b** (Fig. 28) was reported in 2014 and had its anticancer properties evaluated

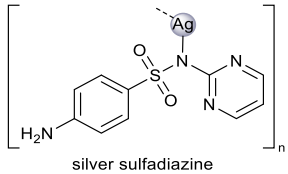

silver sulfadiazine

**Fig. 30.** Structure of silver sulfadiazine.

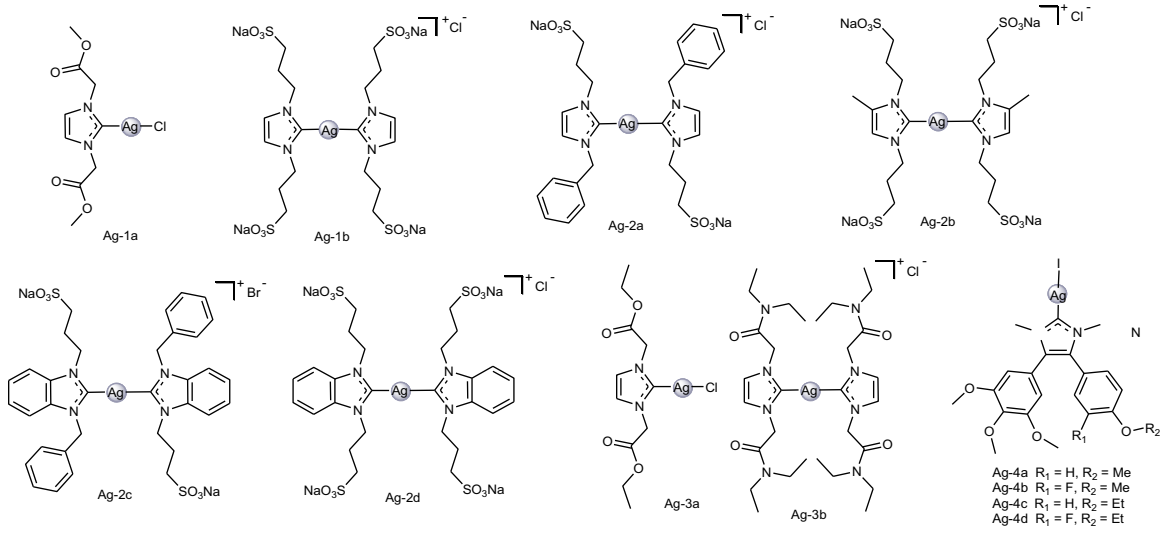


**Fig. 31.** Silver (I) complexes with NHC ligands.

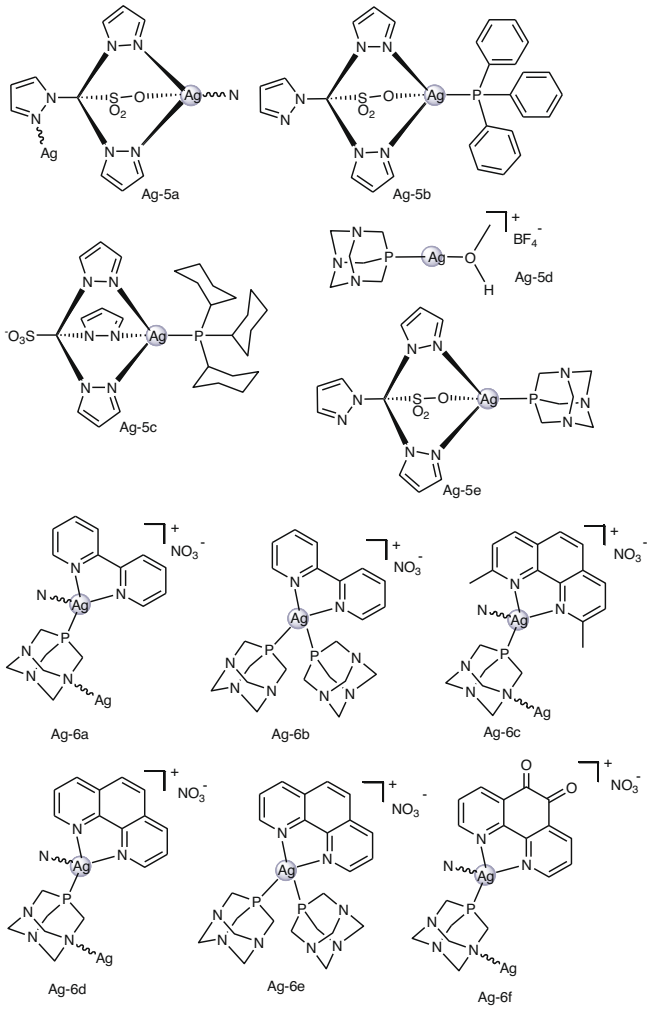


**Fig. 32.** Ag(I) complexes with phosphane or adamantyl ligands.

against SK-MEL-28 and other cell lines [242]. Results indicated that **Au-37b** was moderately cytotoxic ($IC_{50}$ = 26.8 μM) and cytostatic ($IC_{50}$ = 35.6 μM) towards the melanoma cell line. The authors hypothesized that the compound may cause M cell cycle arrest as a result of DNA replication inhibition, since this effect was observed for corresponding Al, Mn and Ga corroles. Weak albumin binding was identified as a major factor for improved cytotoxicity of **Au-37b** when compared to the correspondent Ga(III) corrole, which has a high affinity for albumins. However, the relatively high $IC_{50}$ values of **Au-37b** when compared to Au(III) porphyrin **Au-37a** was attributed to the greater lipophilicity of the latter, so that more lipophilic Au(III) corroles might result in more cytotoxic agents.

The class of Au(III)-dithiocarbamato complexes was designed to closely reproduce the main features of cisplatin and had demonstrated promising antiproliferative activity for several cancer cell lines with good safety profile [243,244]. The complexes **Au-38a** to **Au-38d** (Fig. 29) were tested against melanoma MeWo cells, SCC cisplatin-sensitive A431 cells and cisplatin-resistant A431-R cells. All four complexes were considerably more cytotoxic than cisplatin against these cells ($IC_{50,cisplatin}$ = 48 ± 2 μM, 77.4 ± 0.4 μM and 382 ± 3 μM, respectively). **Au-38b** was by far the most active complex against MeWo cells ($IC_{50}$ = 1.0 ± 0.1 nM), while **Au-38a** and **Au-38d** exhibited $IC_{50}$ values in the nM range for A431 and A431-R cells. Curiously, **Au-38a** and **Au-38d** were more active against the A431-R cells ($IC_{50}$ = 2.0 ± 0.1 nM and 1.0 ± 0.1 nM) than the cisplatin-sensitive A431 cells ($IC_{50}$ = 12.0 ± 0.1 nM and 15.0 ± 0.1 nM). Some important biological targets such as the mitochondria, proteasome and thioredoxin reductase have been identified as part of the overall mechanism of action of these Au(III) complexes. Also, they were able to trigger cell death by apoptosis rather than necrosis and neither cross-resistance nor other main drawbacks of cisplatin-based therapy were detected [187].

*In vivo* antitumor activity of **Au-38d** was evaluated against Ehrlich solid-tumor-bearing mice, MDA-MB-231 breast tumor in nude mice and xenografts of PC3 prostate tumor in nude mice, resulting in at least 50 % tumor reduction [187,245-247]. Despite the great *in vitro* results of the **Au-38** series of complexes in melanoma and SCC cells, they were not yet tested *in vivo* against skin carcinoma models.

Improvements in the antitumor properties and pharmacological aspects of this class of complexes have been made over the years [187,248-250] and more recently the Au(III)-dithiocarbamato complexes **Au-39a** to **Au-39e** (Fig. 29) were developed with anchored oligopeptides with the idea that they could be recognized and taken up by specific peptide transporters [251]. In this case the role of the amino acid chirality in the transporter recognition and

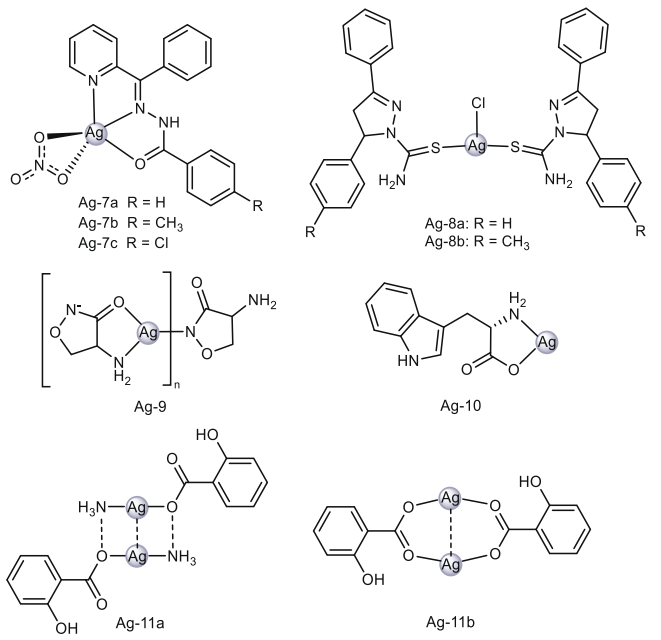


**Fig. 33.** Other Ag(I) complexes with diverse ligands.

mechanism of action was explored for the **Au-39a** to **Au-39b** and **Au-39c** to **Au-39d** pairs. The *in vitro* activity of these complexes in A431 cells was between $GI_{50}$ values of 8 and 16 μM, with **Au-39c** being the most active.

For **Au-39c** and **Au-39d**, preliminary evaluation of toxicity carried out by *ex vivo* incubation of the complexes with healthy rat tissues, showed lower toxicity than cisplatin in liver and kidney tissues. Complexes **Au-39a** to **Au-39d** were also proved to be potent and fast-acting PARP-1 inhibitors. This is important as cascade of apoptosis-promoting signals starts upon inactivation of the enzyme. Therefore, these inhibitors can be either used alone or in combination with other anticancer drugs, thus amplifying their cytotoxic effect [251].

Bhargava and coworkers [252] reported a series of cationic cyclometallated Au(III) complexes of triphenylphosphane sulfide, with varying counterions ($AuCl_2^-$ in **Au-40a**, $AuBr_2^-$ in **Au-40b**; $AuI_2^-$ in **Au-40c** and $PF_6^-$ in **Au-40d,** Fig. 29). The compounds with $AuCl_2^-$, $AuBr_2^-$ and $PF_6^-$ counterions were active over the D24 melanoma cell line with very similar $IC_{50}$ values (MTT assay, 72 h incubation) of approximately 2.4 μM. The finding highlighted that the cyclometallated species is the main responsible for such pronounced cytotoxicity. However, the compound with $AuI_2^-$ as counterion (**Au-40c**) was more active than the others ($IC_{50}$ = 0.97 ± 0.08 μM), which correlated well with its higher cell uptake and increased stability in the presence of glutathione. The compounds were able to partly inhibit cell migration in a wound healing experiment, which was attributed to their capability to disrupt actin assembly. Treatment of HeLa cells with $IC_{50}$ concentrations of the compounds led to approximately 40% of apoptotic cells and to disruption of mitochondrial membrane potential. The complexes

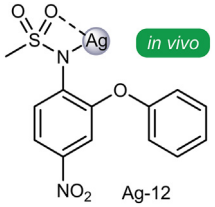


**Fig. 34.** Silver nimesulide.

showed anti-inflammatory activity, since they inhibited the secretion of pro-inflammatory cytokines in LPS-activated macrophages.

### 3.5. Silver

Silver(I) is the main oxidation state found on silver compounds. As a $d^{10}$ ion, it has access to a wide variety of coordination geometries, although linear compounds are somewhat common. Carbenes and phosphanes are recurring ligands, as well as O-donors. Sulfonamides are also a class of great significance in the history of inorganic medicinal chemistry. Represented by silver sulfadiazine, silver compounds are relevant for the treatment of skin-related conditions as topical agents. Since the introduction of silver sulfadiazine, other silver complexes have been studied not only for their antibacterial activity, but also their antitumoral properties [253,254].

#### 3.5.1. The case of silver sulfadiazine

Silver sulfadiazine [255] (Fig. 30) is a clinically approved topical antibacterial agent recommended specially for burn wound treatment [256] and is one of the hallmarks of the use of metal complexes in medicine, although at first as an antibacterial agent.

NCI-60 data for silver sulfadiazine is available through the NCI compound search (NSC 625324). It shows significant antiproliferative activity against several cancer cell lines, including the melanoma ones, especially MALME-3 M ($GI_{50}$ = 1.97 μM), UACC-257 ($GI_{50}$ = 3.11 μM) and SK-MEL-5 ($GI_{50}$ = 6.27 μM).

#### 3.5.2. Silver(I) compounds

Silver(I) NHC complexes with sulfonate, ester or amide functionalization were evaluated against A375 melanoma cells and A431 cells (**Ag-1a** and **Au-1b**, **Ag-2a** to **Ag-2d** and **Ag-3a** to **Ag-3b,** Fig. 31) [227,257,258]. The bis-NHC complex **Ag-1b** exhibited the best *in vitro* antiproliferative activity of the series for both cell lines, with $IC_{50}$ = 14.16 ± 2.76 μM for A375 and $IC_{50}$ = 8.24 ± 1.76 μM for A431, with exception of **Ag-2c** that was able to inhibit A375 cells with $IC_{50}$ = 13.0 ± 3.1 μM. However, cisplatin was significantly more active ($IC_{50}$ = 3.11 ± 0.98 μM for A375 and $IC_{50}$ = 2.26 ± 1.61 μM for A431) against the same cell line.

Mechanistic studies revealed that the antiproliferative effects induced by **Ag-1a** and **Ag-1b** correlate well with their ability to inhibit TrxR. The inhibition of the enzyme led to an increase of intracellular ROS, and to unbalance of the thiol redox status. The effects on redox homeostasis and on apoptosis signal-regulating kinase (ASK-1) activity both resulted in the activation of downstream signaling cascades, ultimately leading to mitochondrial mediated apoptosis [257].

Additionally, the Ag(I) complexes of this series exhibited similar cytotoxic profile over ovarian cell lines that are cisplatin-sensitive (2008 cells) and cisplatin-resistant (C13* cells). These tests showed the ability of these compounds to overcome acquired cisplatin resistance and reinforced that their mechanism of action is different from that of cisplatin-like drugs.

The silver analogues of **Au-23a-d** (Fig. 26) complexes with NHC ligands, **Ag-4a** to **Ag-4d** (Fig. 31) were also tested on the inhibition of 518A2 melanoma cells [221]. Interestingly, no direct correlation was observed between the cytotoxicity of the Ag and Au compounds when comparing the analogues with the same ligand. For example, while **Au-23a** was the most active of the gold series, **Ag-4c** had the lowest $IC_{50}$ value (10 ± 3 μM). Importantly, this class of compounds showed selectivity towards cancer cells, being non-toxic in normal non-malignant foreskin fibroblasts HF cells.

Five silver(I) complexes bearing a scorpionate ligand and monodentate phosphanes $PPh_3$, $PCy_3$, and PTA, **Ag-5a** to **Ag-5e** (Fig. 32), were reported by Pettinari and collaborators [259]. Compounds **Ag-5b**, **Ag-5c**, and **Ag-5e** are tetrahedral and mononuclear com-

plexes, whereas **Ag-5a** and **Ag-5d** are likely polynuclear in the solid state and dissociate in solution. The mononuclear compounds **Ag-5b** and **Ag-5c**, bearing $PPh_3$ and $PCy_3$ coligands presented submicromolar cytotoxicity against A375 melanoma cells and were at least twice more active than $AgNO_3$ ($IC_{50}$ = 2.0 μM). When comparing **Ag-5d** and **Ag-5e**, the introduction of the scorpionate ligand was fundamental to confer toxicity, so that PTA functions to improve aqueous solubility. The higher activity of **Ag-5b** and **Ag-5c** correlated well with their higher DNA binding affinity. Overall, these results show how the choice of ligands and their design were important for improving selectivity, solubility and reactivity of the complexes in biological media.

A series of water-soluble polymeric and mononuclear silver(I) compounds of N^N heterocyclic ligands and the phosphane PTA, **Ag-6a** to **Ag-6f** (Fig. 32), has been reported [260]. The bpy-containing compounds, **Ag-6a** and **Ag-6b** were less active than the ones containing phen-derivatives, similar to the trend observed of Cu(II)-bipyridyl and Cu(II)-phenanthroline complexes. The most active complexes against A375 cells were the polymeric **Ag-6c** and

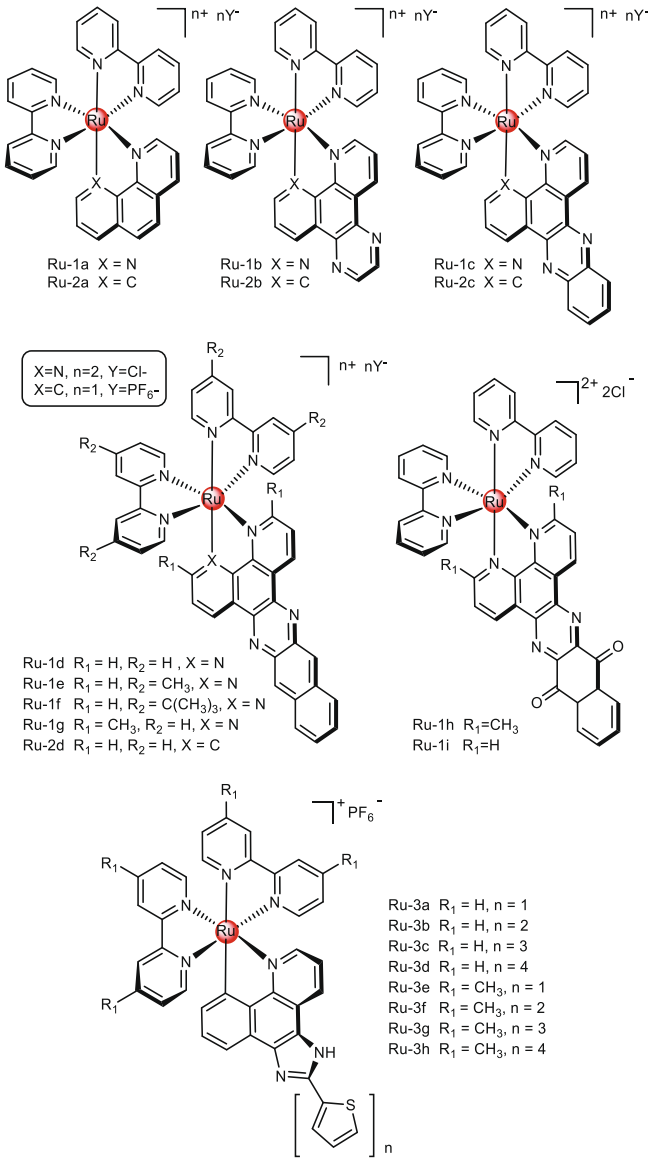


**Fig. 35.** Octahedral Ru(II) compounds with π-expansive ligands that were designed for photodynamic therapy.

**Ag-6f** ($IC_{50}$ values of 0.37 and 0.39 μM, respectively, after 72 h incubation), which contained neocuproine and 1,10-phenanthroline-5,6-dione. Both compounds were more potent than $AgNO_3$, which had an $IC_{50}$ value of 2.54 μM, indicating that the N^N ligand plays a major role for the bioactivity of this class of compounds. Their DNA binding constants correlated well with cytotoxicity, with **Ag-6c** having the highest value of the series.

The compounds **Ag-7a** to **Ag-7c,** (Fig. 33) had similar antiproliferative activity against metastatic B16-F10 cells ($IC_{50}$ between 2.00 and 2.36 μM) [261]. Against melan-A cells, the $IC_{50}$ values of **Ag-7a**, **Ag-7b** and **Ag-7c** were 54.63, 10.23 and 7.87 μM, respectively (Selectivity index - SI = 23.0, 5.1 and 3.9). These results demonstrated that, in some cases, coordination to silver(I) can be a good strategy for improving selectivity against cancer cells. The complexes were more cytotoxic than $AgNO_3$, cisplatin and their respective ligands for both cell lines.

**Ag-7a** to **Ag-7c** interacted with DNA by intercalation, which is favored by the presence of the benzene or pyridine aromatic rings in the ligand skeleton. However, no evidence was found of direct coordination of Ag(I) to the DNA, suggesting that covalent bonding to DNA structure is not part of the mechanism of action of these complexes.

Compounds **Ag-8a** and **Ag-8b** (Fig. 33) are based on thiocarbamoyl-pyrazoline ligands and display trigonal distorted trigonal pyramidal geometries, respectively [262]. Spectroscopic characterization revealed that the compounds exhibit intense blue-greenish emissions in solution and in the solid state when excited at 300 nm. *In vitro* cytotoxicity studies revealed that **Ag-8a** and **Ag-8b** have modest cytotoxicity against B16-F10 melanoma cells (approximately 20 μM), while the thiocarmoyl ligands were inactive. Although the compounds were not very effective over melanoma cells, the luminescence properties of the compounds could be further explored for tracking them *in cellulo*.

A silver complex with the amino acid cycloserine (cic) was prepared by Ciol and co-workers (**Ag-9,** Fig. 33) [263]. The structure consists of repeating (Ag-cic) units. **Ag-9** was highly active against UACC62 melanoma, with a $GI_{50}$ of 1.2 μM. For comparison, the compound was also tested against a keratinocyte (HaCaT), and the same cytotoxic potency was found. Silver nitrate had an $GI_{50}$ of 1.42 μM against both UACC62 and HaCaT. Corbi's group also reported on a silver complex with the amino acid L-tryptophan (**Ag-10,** Fig. 33) [264]. The compound was only moderately active against SK-MEL-103, with an $IC_{50}$ of 68.8 μM.

Coyle, McCann and co-workers evaluated prepared two silver compounds based on salicylic acid, and evaluated their cytotoxic activities against Cal-27, a squamous cell carcinoma of the tongue [265]. Compounds **Ag-11a** and **Ag-11b** (Fig. 33) were only moderately cytotoxic even at 96 h of incubation (MTT), with $IC_{50}$ values of 27 and 51 μM respectively.

Recently, a silver complex with the anti-inflammatory drug nimesulide (**Ag-12**, Fig. 34) was evaluated in the treatment of skin carcinomas and melanoma [266]. The silver complex was able to inhibit the UACC-62 melanoma cell line with $GI_{50}$ = 1.56 μmol/L, and no cross-inhibition of glioma, breast, lung, and colon carcinomas and leukemia cells or HaCaT keratinocytes, even at the highest concentration tested (600 μmol/L). The same complex was further evaluated *in vitro* against a panel of SCC cell lines, demonstrating relevant cytotoxicity ($GI_{50}$ = 9.68 μmol/L against SCC15 and 7.87 μmol/L against FaDu). Multicaspase activation was identified in the FaDu cell lne. Importantly, nimesulide alone did not show the same antiproliferative potential as the silver complex. Compound **Ag-12** was further evaluated *in vivo* supported in a bacterial cellulose membrane for the topical treatment of cutaneous squamous cell carcinoma in a BALB/c mouse model. The topical treatment did not induce systemic toxicity, and reduced tumour

volume by up to 100% with no relapse during the 21-day follow-up [266].

### 3.6. Ruthenium

The antitumoral properties of ruthenium complexes have been extensively studied in the last decades. It led to several ruthenium complexes to reach phase I or II clinical trials, such as Ru(III) compounds NAMI-A, KP1019 and KP1339 [267-272].

Usually in the biological environment, Ru(III) compounds may undergo reduction to the more reactive 2 + oxidation state, as it is the case for KP1019 and KP1339. The arene substituent present in many bioactive Ru(II) complexes is relatively inert towards displacement and is known to stabilize the metal in this oxidation state. Chelating N^N or N^S ligands are also generally used to lower the lability of the complexes, in order to enhance their biological activity [273].

While Ru(III) complexes and Ru(II) compounds with bidentate ligands are commonly octahedral, the Ru(II) arene complexes usually assume the pseudo-tetrahedral or "piano-stool" geometry, with a variety of N-, O-, S- and P- donors as ligands which is ideal for preparing multifunctional drugs [273,274].

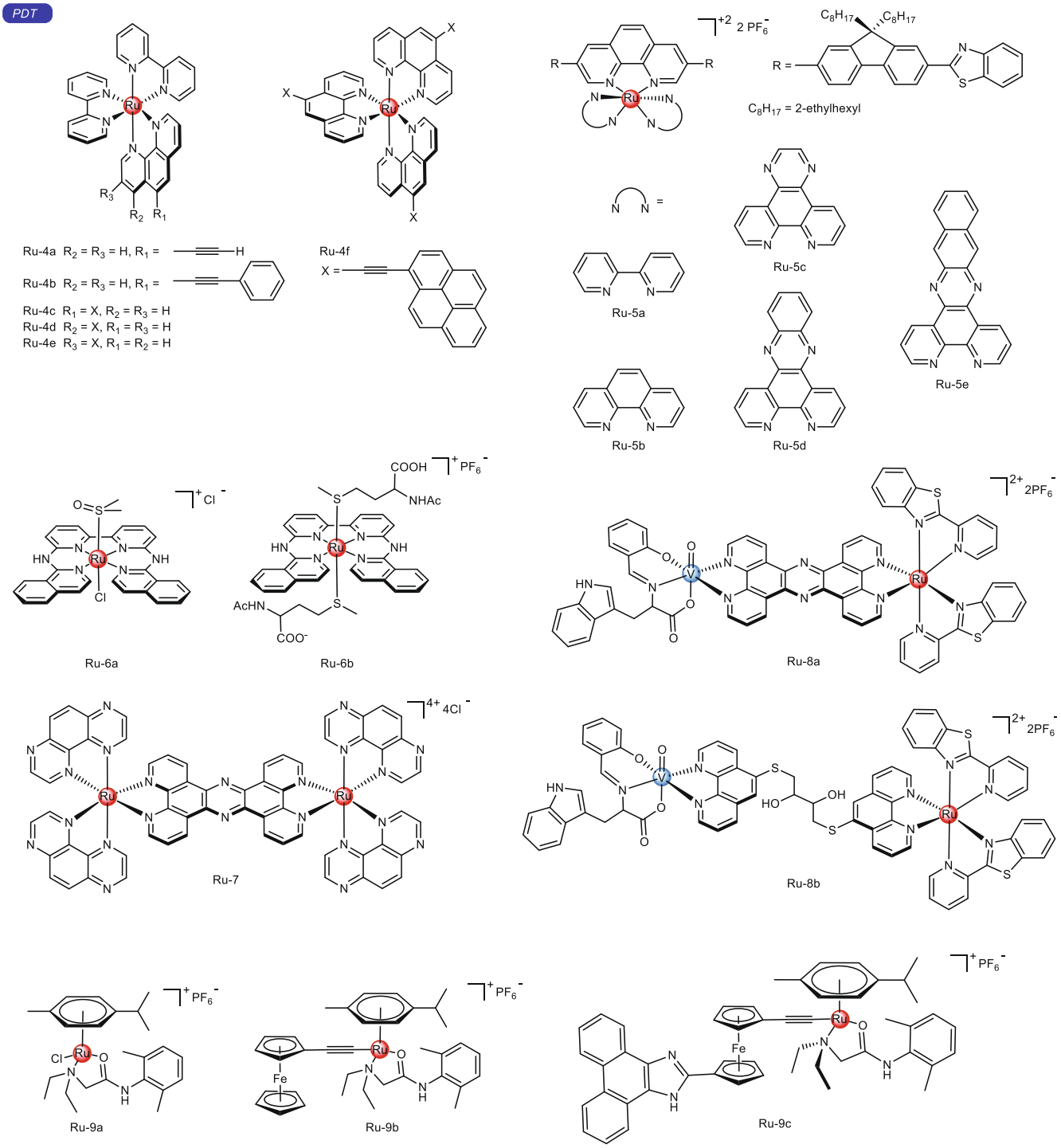


**Fig. 36.** Other Ru(II) complexes tested as part of PDT strategies. Examples vary from octahedral complexes with N^N ligands to porphyrins, arene and binuclear complexes.

Ruthenium(II) complexes with diamine and related ligands (e.g. N^S and N^C) can also be used as photosensitizers and have been studied as candidates for cancer photodynamic therapy, especially against skin cancer. These compounds have unique photochemical and photophysical properties, notably, strong absorption and emission of visible light associated with long-lived metal-to-ligand charge transfer (MLCT) and intra-ligand (IL) excited states [275].

*3.6.1. Ruthenium compounds for Photodynamic Therapy (PDT): the case of octahedral compounds with π-expansive ligands*

Photodynamic therapy (PDT) is an anticancer strategy that aims at increasing the selectivity of chemotherapeutic agents. PDT is a procedure that activates a photosensitizer at a specific wavelength in order to generate ROS and induce cancer cell death. Ideally, the photosensitizer (PS) should be inactive and minimally interact with biological molecules to limit the toxicity in non-irradiated tissues. Upon light irradiation, these prodrugs are locally activated to selectively kill tumor cells [276,277].

In this context, metal complexes can be designed as excellent photosensitizers due to the unique interactions between metal and ligands orbitals. To promote toxicity in the cancer cell, the excited state of the photosensitizer metallodrug may either interact with oxygen to produce ROS (type I reaction), or the triplet state can directly transfer its energy to oxygen atoms to form singlet oxygen species ($^1O_2$) (type II reaction) [155]. PDT is a noninvasive method that has been investigated for the past 30 years due to the fact that far less side effects are observed when compared to conventional treatments [278,279].

Currently, topical PDT with the pro-drugs 5-aminolevulinic acid (Levulan®) or methyl aminolevulinic acid (Metvix®) are being recommended by dermatologists to treat squamous cell carcinomas and actinic keratosis or basal cell carcinoma, respectively. These pro-drugs are intermediates in the biosynthetic process leading to protoporhyrin IX and then to heme, which act as photosensitizers. The protoporhyrin IX accumulates *in vivo*, especially in the cancer site, once neoplastic cells produce higher amount of porphyrins in the presence of these pro-drugs [278,280].

Topical PDT offers better safety profile over systemic photosensitizers, such as porfimer sodium, benzoporphyrin derivative monoacid ring A (BPD-MA) and *meta*-tetrahydroxyphenylchlorin, but falls short in efficacy against more invasive and metastatic tumors [279,280].

It is generally accepted that the triplet excited states of PSs exert their PDT effects through energy or electron transfer to ground state oxygen to produce ROS, most notably the cytotoxic singlet oxygen ($^1O_2$). Thus, PSs with appropriate triplet energy levels, high quantum yields for triplet state formation, and long intrinsic triplet lifetimes are highly desirable for PDT [281].

However, the reliance on $^1O_2$ for cytotoxic effects is a salient drawback and significantly diminishes the PDT effect in hypoxic tissue and solid tumors [282]. While well-oxygenated tumors that are superficial may respond well to traditional PDT, which is the case for superficial skin carcinomas, some of the most aggressive and drug-resistant tumors are a challenge that the metal complexes may be able to overcome by exerting oxygen-independent phototoxic effects by covalent modification of biomolecules such as DNA [282]. In addition, the organic PSs approved for clinical use cannot be activated by wavelengths of light that penetrate tissue best (e.g., >700 nm), limiting their use to superficial lesions [282].

Polypyridyl and cyclometalated Ru(II) complexes comprised of π-expansive ligands (**Ru-1** to **Ru-3,** Fig. 35) were explored as photocytotoxic agents in an excellent series of publications [275,283-285]. The cytotoxicity of these complexes were tested in the dark and under broadband visible light against melanoma SK-MEL-28 cells and expressed by the $EC_{50}$ values. The importance of the light activation is clear when the ratio of the dark to light $EC_{50}$ values for cytotoxicity is observed. PI values close to 1 indicate that there is no amplified effect with light, and PIs $\gg$ 1, on the other hand, indicate that light enhances the cytotoxicity of the compound.

Compounds **Ru-1a** to **Ru-1d** (Fig. 35) are the series of polypyridyl (N^N) complexes with an increasing size of the π-expansive ligand. These complexes were all essentially nontoxic in the dark ($EC_{50}$ > 100 μM) and more active in the PDT regimen, especially **Ru-1d** (PI > 650), which is the complex with the larger π-expansive ligand. Systematic structure/activity relationship for these complexes were observed for **Ru-1e** to **Ru-1i**, where modifications in the bipyridyl and π-expansive ligands were evaluated. Under visible light $EC_{50}$ values are sub-μM (0.04 – 0.16 μM) for complexes with simple modifications in the bipyridyl substituents, with increased PI (PI = 1678) for **Ru-1f** (*tert*-butyl substituent), while modification of the π-expansive ligand was not advantageous for the cytotoxicity or selectivity. The photocytotoxicities of these complexes were positively correlated with their excited-state lifetimes and their capacity to produce ROS, suggesting that these parameters could be used to reliably predict *in vitro* PDT effects from structure – activity relationships.

Moreover, an osmium(II) complex (**Os-1**) with the exact same structure of **Ru-1d** was also evaluated against SK-MEL-28 cells. Both showed very low toxicity in the dark, but **Ru-1d** is 10 times more active than **Os-1** after visible light treatment. Nonetheless, an $EC_{50,vis}$ = 0.96 ± 0.01 μM for **Os-1** is still remarkable. Another difference is that under red light treatment the activity of **Os-1** did not improve (PI ~ 1), while the cytotoxicity of **Ru-1d** improved 906-fold.

The polypyridyl series (**Ru-1a** to **Ru-i**) was then compared with Ru(II) complexes with the analogue (C^N) π-extended benzo[h]imidazo[4,5-f]quinolone ligands (**Ru-2a** to **Ru-2d,** Fig. 35). All the complexes in this series were active over SK-MEL-28 with $EC_{50}$ of approximately 0.2 μM under light irradiation. However, in the dark **Ru-2d** is not cytotoxic and therefore showing a PI > 1400, unlike **Ru-2a** to **Ru-2c**.

Another $[Ru(N^N)_2(C^N)]^+$ analogue, derived from the π-extended benzo[h]imidazo[4,5-f]quinolone ligand appended with 1 to 4 thienyl groups **Ru-3a** to **Ru-3d** (Fig. 35) [275]. Complexes **Ru-3a** to **Ru-3c** were cytotoxic to SK-MEL-28 melanoma cells with $EC_{50}$ values ranging from 1 to 20 μM, while compound **Ru-2d** was nontoxic in the dark. However, **Ru-2d** was cytotoxic under visible light, with PI > 267 ($EC_{50,vis}$ = 1.13 ± 0.07 μM). The relative cytotoxicity of the compounds could not be attributed to differences in cellular uptake according to laser scanning confocal microscopy studies using the inherent emission from the compounds.

Interestingly, the authors say that the series with thienyl groups is the third example in the literature of cyclometalated Ru(II) series based on π-expanded C^N ligands, whereby there is a critical π-conjugation length (n = 4) that leads to an abrupt change in dark cytotoxicity [275,283,285]. This opens a perspective for the development of new Ru(II) phototherapeutic complexes that would otherwise be too toxic to consider.

The Ru(II) photosensitizer TLD1433 (analogue of **Ru-3c** with methyl substituents in the bipyridyl ligands) successfully completed a human clinical trial (ClinicalTrials.gov identifier: NCT03053635) for treating bladder cancer with PDT. More on the development of TLD1433 and other complexes for photodynamic therapy can be found in a recent review by McFarland's group [286].

*3.6.2. Other ruthenium compounds for PDT*

In the search for new PDT agents, considerable effort has been made toward prolonging the excited-state lifetimes in coordination compounds. To achieve long excited-state lifetimes, Lincoln et al. [287] developed Ru(II) complexes with spatially separated

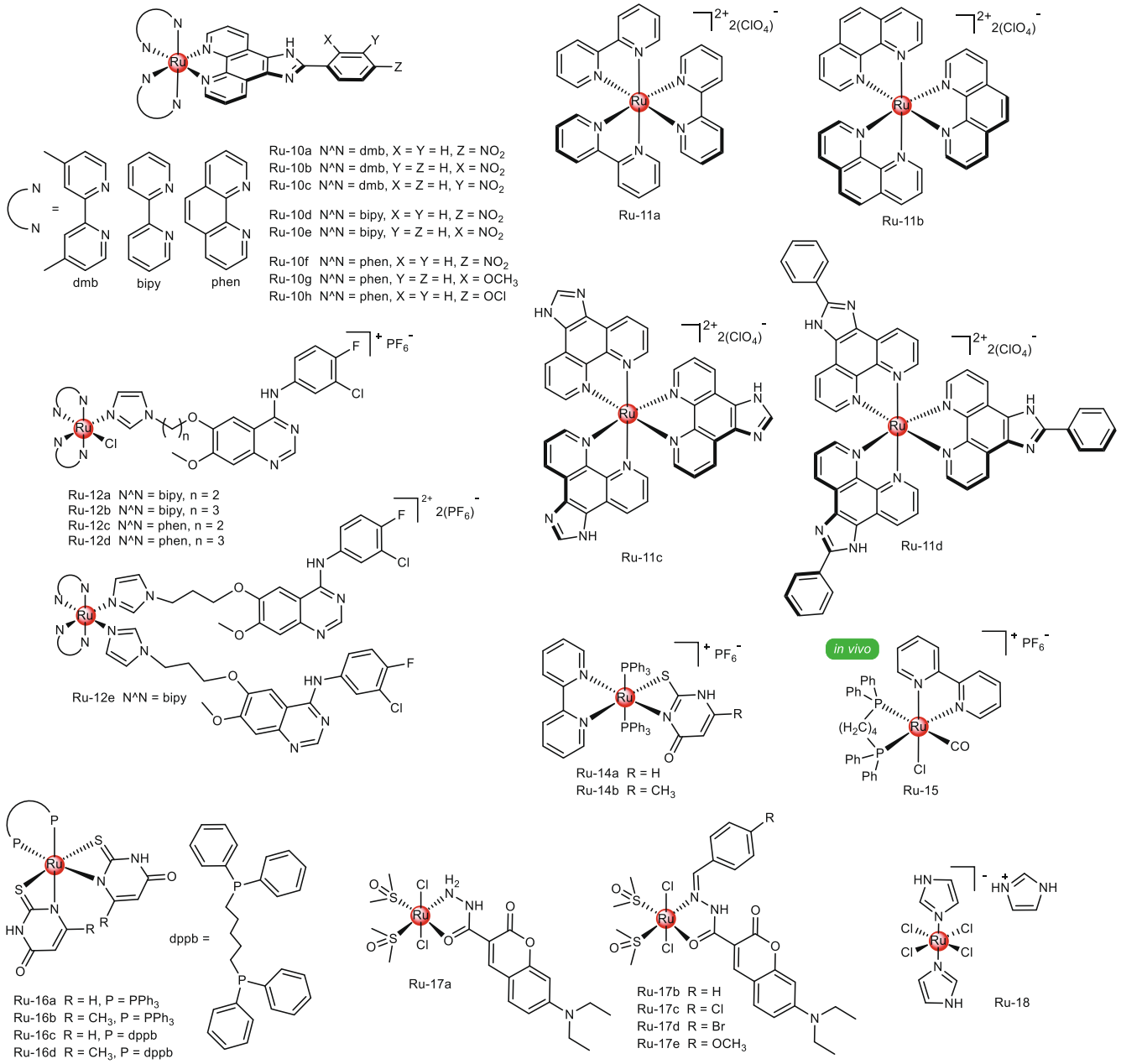


**Fig. 37.** Octahedral Ru(II) complexes (not tested for PDT).

polycyclic aromatic hydrocarbon ligands as chromophores (**Ru-4a** to **Ru-4f,** Fig. 36). These complexes were first tested against HL60 human leukemia cells and showed higher activity under light than in the dark, for **Ru-4c** to **Ru-4e** the PI were higher than 100. Given the results, these three complexes with higher PI were also evaluated over metastatic melanoma cells (Malme-3 M) in an assay that used minimal light treatment (irradiation with visible light for 15 min, 7 J $cm^{-2}$). The toxicities in the dark of these complexes ranged from 44 to 62 μM, while the low light treatment yielded an $EC_{50}$ of 200 nM for **Ru-4c**, 600 nM for **Ru-4d** and 700 nM for **Ru-4e** (PI > 70).

The $EC_{50}$ values for PDT with low light dose were 20 times lower in the melanoma cells than in the HL60 cells, which is even more impressive because the Malme-3 M cells are pigmented melanoma cells which are believed to be inherently less susceptible to PDT in comparison to amelanotic melanoma cells or other cancer cells in general [287,288].

In their work with the $[RuL(N^N)_2](PF_6)_2$ complexes (**Ru-5a** to **Ru-5e,** Fig. 36), where L is 3,8-di(benzothiazolylfluorenyl)-1,10-phenanthroline, Wang *et al.* [282] showed, that long intrinsic triplet lifetimes and high yields for triplet formation are desired features to identify promising PDT agents.

The cytotoxicity of **Ru-5a** to **Ru-5e** in the absence of a light stimulus were minimal or not observed (dark $EC_{50}$ > 100 μM for **Ru-5a**, **Ru-5b** and **Ru-5e**) over SK-MEL-28 cells. With visible light activation, $EC_{50}$ values ranged from 3.8 to 8.4 μM, while with red light activation, the range increased to 10–204 μM. **Ru-5e** was the most cytotoxic over SK-MEL-28 cells under broadband visible light and also under red light, showing once again that the longer π-extended N^N ligand yields higher photocytotoxicity.

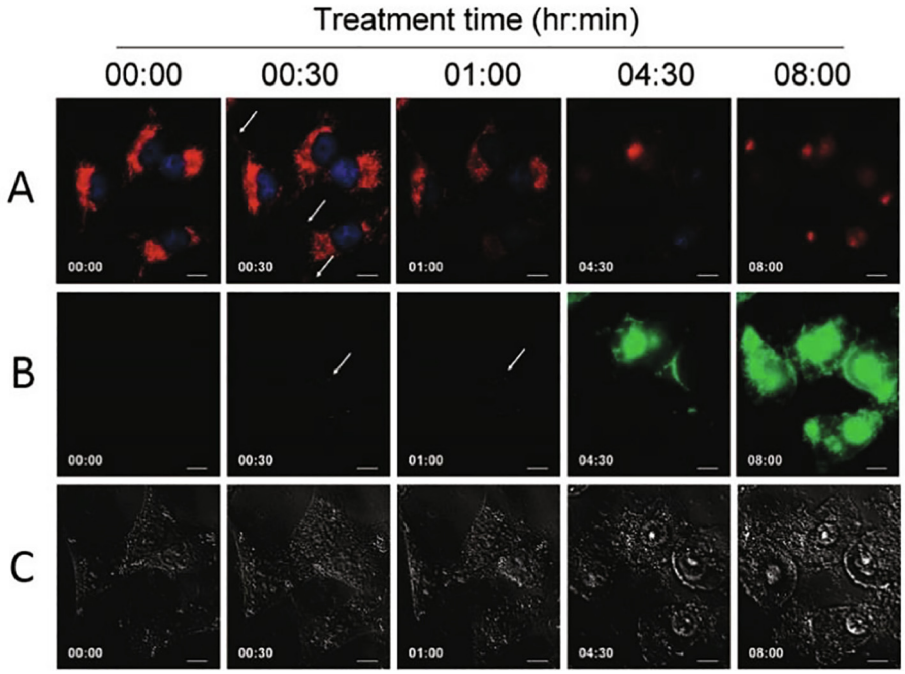


**Fig. 38.** Real-time imaging of the same cells treated with 20 μM **Ru-10h**. Mitochondria, the nucleus, and **Ru-10h** were visualized by red, blue, and green fluorescence, respectively. The **panel A** is the merged images of mitochondria and the nucleus. while **panel B** presents the images of **Ru-10h**. **Panel C** shows the cell morphology captured by a differential internal reflection (DIC) microscope. Scale bar: 10 μm. Image adapted with permission from Chen et al. Copyright 2010, American Chemical Society [295]. (For interpretation of the references to color in this figure legend, the reader is referred to the web version of this article.)

**Table 2**
Correlation of lipophilicity (Log P) with antiproliferactive activity against A375 ($IC_{50}$) and TrxR inhibition ($EC_{50}$) for complexes **Ru-11a** to **Ru-11d**.

| | $IC_{50}$ A375 (μM) | $EC_{50}$ TrxR (μM) | Log P |
|---|---|---|---|
| Ru-11a | 183.1 | >100 | −0.41 |
| Ru-11b | 153.9 | 40.2 | −0.33 |
| Ru-11c | 137.9 | 20.7 | 0.42 |
| Ru-11d | 0.9 | 2.7 | 2.67 |

For all the complexes, uptake experiments showed increased Ru accumulation with light irradiation, indicating PDT-induced uptake. The fact that cell uptake was evaluated by intrinsic bright luminescence of the complexes creates a perspective to use this kind of compounds as theranostic PDT agents, with both diagnostic and therapeutic potentials.

A different example of light activated Ru(II) complex are the tetrapyridyl prodrugs (**Ru-6a** and **Ru-6b,** Fig. 36) evaluated by van Rixel et al. against the A431 and A549 cell lines [276]. For A549 cells, apoptosis was induced by green light irradiation, and cell death was not attributed to photodynamic effect, as **Ru-6a** and **Ru-6b** are extremely poor $^1O_2$ generators.

Instead, the light induced changes in the coordination sphere of the metal, therefore modifying how the complex binds to biomolecules. Light irradiation diminished the mitochondrial membrane potential and induced chromosomal condensation in the A549 cells. The cell uptake mechanism is likely endocytosis-dependent, where high concentration of Ru(II) is found in the endosomes and lysosomes, and lipophilic species are accumulated in the mitochondrial membranes [276,289].

The cytotoxicity experiments were carried out using 6 h or 24 h of incubation and irradiation of green light (520 nm, 60 min, 75 J $cm^{-2}$). The two complexes were more active under light irradiation, and **Ru-6a** is the most potent overall, showing a PI higher than 10 for A431 and A549 and, when activated by the green light, **Ru-6a** was more cytotoxic than cisplatin.

Raza et al. reported the interesting phototoxicity of complex **Ru-7** (Fig. 36) in melanoma cancer monolayers and spheroids [290]. The strategy used in this case was to photoactivate the complex through two-photon absorption (TPA). As this requires the absorption of two photons simultaneously, activation through TPA is proportional to the square of the light source intensity and therefore only occurs at, or very close to, the focal point of the laser [291]. The TPA with a laser not only is more spatial selective, but it was also done at 900 nm to avoid a known mechanism of PDT resistance in melanoma, which is the abundance of melanin in such pigmented tumours that absorbs the light that should be used for the PS excitation. Other advantages are increased skin penetration, less local hyperthermia and less oxygen depletion that would otherwise reduce the photodynamic effect. It is also worth mentioning that the use of TPA for photosensitisers with therapeutical properties has been widely suggested, but it has overall been rendered impractical by low two-photon cross-sections [292]. Therefore, solving this problem actually represents an advancement in the field.

In monolayered 2-D cell cultures, **Ru-7** irradiated with near-infrared light (900 nm) at low power (20 mW) resulted in precisely focused phototoxicity effects in which C8161 human melanoma cells could be killed after 5 min of light exposure. The PDT effects of **Ru-7** were also evaluated in a live multicellular 3-D spheroid tumor model that has both proliferative and hypoxic regions and thus assess the therapeutic effectiveness of this PS in low oxygen conditions. It was observed that photoexcitation of the complex can be accomplished to a depth of ~240 ± 20 μm. 40 mW in the PDT-TPA regimen (900 nm) were necessary to eradicate the proliferative region of the spheroid after 30 to 45 min of exposure and 60 mW were necessary produce the same effect after only 15 min of light exposure. Most efficient phototoxic effects were observed in depths up to 80 μm, however cell death was observed

throughout the entire z-axis depth of the spheroid, showing that cell killing occurred also the hypoxic regions of the spheroid [290].

The combination of a photosensitizing ruthenium motif with bioactive vanadyl species via bridging polypyridyl ligands resulted in two heterobimetallic complexes, **Ru-8a** and **Ru-8b** (Fig. 36) [293]. The compounds presented modest cytotoxic activity against A431 cells, but cisplatin also showed a low activity profile in the same experiment (around 40 μM) and they were non cytotoxic against HFF human skin fibroblast cells. The vanadyl motif was tested for comparison, and was also marginally cytotoxic, with dark $IC_{50}$ values of 41.6 and 63.1 μM against A431 and HFF, respectively. Photoactivation using red light (710 nm) resulted in increased activity for the heterobimetallic compounds, causing profound cell (A431) morphologic changes at a lower concentration of 20 μM, although no specific $IC_{50}$ values for the cytotoxicity under light exposure were provided.

Organometallic Ru(II)-arene complexes with lidocaine (**Ru-9a** to **Ru-9c,** Fig. 36) were not toxic to A375 melanoma cells without light treatment [294]. The presence of the ferrocene moiety was essential for phototoxicity of the complexes since after broadband visible light irradiation (400– 700 nm, 10 J $cm^{-2}$), the complexes **Ru-9b** and **Ru-9c** exhibited $IC_{50}$ = 6.7 ± 0.1 μM and 2.3 ± 0.1 μM respectively, while **Ru-9a** remained non-toxic ($IC_{50}$ > 100 μM). Cell uptake of complex **Ru-9c** was significantly higher than **Ru-9d** in A375 cells, which could explain the difference in antiproliferative activity of these complexes. Furthermore, cell cycle arrest assay in the same cell line showed increased sub-G1 phase accumulation in cells treated with **Ru-9a** and **Ru-9b** only with light activation and not in the dark.

*3.6.3. Other octahedral ruthenium compounds*

Chen et al. studied the activity Ru(II) complexes (**Ru-10a**- to **Ru-10h,** Fig. 37) against A375 melanoma cells. In this case the variation of the auxiliary ligands (planar N,N-chelating diimines like bipyridine, 4,4′-dimethyl-bipiridine and phenanthroline) and changes in the positions of substituent groups (–$OCH_3$ and-$NO_2$) on the phenyl ring of the ligand designed for DNA intercalation caused interesting differences in the properties of the resulting complexes [295]. **Ru-10h** was the only complex that showed an $IC_{50}$ (5.9 ± 1.1 μM) lower than cisplatin ($IC_{50}$ = 7.3 ± 0.8 μM) in that experiment, also with better selectivity in comparison to cisplatin for melanoma versus fibroblast Hs68 (SI = 5.6).

Treatment of A375 cells with different concentrations of **Ru-10h** for 24 h resulted in a marked dose-dependent increase in the proportion of apoptotic cells, and further DNA fragmentation and nuclear condensation indicated that the complex in fact induced apoptosis. Moreover, nuclear condensation, and cytoplasmic shrinkage were also observed in A375 cells incubated with **Ru-10h** and mitochondrial fragmentation and disruption (caused by loss of mitochondrial membrane potential) were attributed to suppressed expression of prosurvival Bcl-2 proteins (Bcl-2 and Bcl-xl) and upregulation of the expression of a proapoptosis protein (Bad) also from Bcl-2 family.

The loss of membrane potential triggered the mitochondrial release of apoptogenic factors, like cytochrome *c* and AIF. Release of cytochrome *c* induced by the loss of mitochondrial membrane potential caused activation of caspases and cleavage of their specific substrate PARP. Furthermore, apoptotic cell death was significantly suppressed by a general caspase inhibitor (z-VAD-fmk), indicating the important roles of caspases in the induced apoptosis.

Morphologies of the nucleus and mitochondria were observed with the help of fluorescent dyes, along with the cellular uptake of **Ru-10h** that could be monitored due to intrinsic green fluorescence of the complex (Fig. 38).

The series of Ru(II) complexes **Ru-11a** to **Ru-11d** (Fig. 38) exhibit distinct antiproliferative activities against A375 melanoma cells. While **Ru-11a** to **Ru-11c** were able to inhibit the melanoma cells only in high concentrations ($IC_{50}$ > 130 μM), **Ru-11d** was active in the low micromolar range, with $IC_{50}$ = 0.9 μM [296].

The increasing planarity of the ligands and lipophilicity (Log P) of complexes **Ru-11a** to **Ru-11d** not only correlates with their crescent antiproliferative activity, but also with their ability to inhibit TrxR. Complex **Ru-11d** showed 7.6 to 37-fold increased TrxR-inhibitory activities in A375 cells than the other complexes of this series and was more effective than auranofin in the inhibition of the same enzyme (see Table 2). Moreover, **Ru-11d** was selective towards inhibition of TrxR in comparison to other selenoenzymes such as glutathione peroxidase and glutathione reductase, that were not inhibited by the complex [296].

Furthermore, through TrxR-mediated pathways, **Ru-11d** triggered apoptosis of A375 cells, with activation of caspases-3, 8 and 9, leading to cell death. **Ru-11d** down-regulated the expression levels of pro-survival proteins including Bcl-xL, Bcl-2 and Mcl-1, and at the same time up-regulated the pro-apoptotic proteins Bad. Increased levels of ROS were detected in cells treated with the complex, which activated the p53 signaling pathway. The vascular endothelial growth factor (VEGF) is reported to be able to prevent ceramide and starvation induced apoptosis by inhibiting JNK and activating p38 MAPK and Erk signals. Levels of phospho-VEGFR2 and VEGF in cells exposed to complex **Ru-11d** were suppressed in a dose dependent manner, showing that regulation of MAPKs and VEGFR signaling is also affected by the complex to cause cancer cell apoptosis [296].

Du et al. designed **Ru-12a** to **Ru-12e** (Fig. 38) with ligands containing 4-anilinoquinazoline pharmacophores [297]. These are known for being highly selective EGFR inhibitors by competitive insertion into its ATP-binding pocket. The EGFR is associated with a broad range of malignance, including squamous cell cancers. It can bind to epidermal growth factor (EGF) and is thus activated through dimerization and autophosphorylation of several tyrosine residues. Phosphorylation of the tyrosine residues triggers the downstream signal transduction of a number of intracellular signaling proteins, followed by the activation of a series of physiological processes associated with cell growth, differentiation, apoptosis, and migration [297].

Antiproliferation assays in A431 cells (and other 3 cell lines of lung, breast and cervical carcinomas) were carried out both in the absence and in the presence of 100 ng $mL^{-1}$ EGF with 48 h incubation time after addition of the tested Ru(II) complexes. Generally, adding EGF reduced the $IC_{50}$ values of the complexes, suggesting that EGF stimulated the repression of EGFR, which is indeed a target of the Ru complexes. Only complex **Ru-12d** showed increased activity ($IC_{50}$ = 11 ± 1 μM for -EGF and 13 ± 1 μM for + EGF) when compared to the corresponding ligand ($IC_{50}$ = 20 ± 1 μM for -EGF and 15 ± 2 μM for + EGF) for A431 cells. Complex **Ru-12d** exhibited the highest antiproliferative activity of the series, even though it was not able to inhibit EGFR as effectively as **Ru-12e**, which was 3.5-fold more potent in the inhibition of the receptor. Also, both **Ru-12d** and **Ru-12e** exhibited high affinity to DNA via strong minor groove binding and weak intercalation, demonstrating that DNA can also be a target. Finally, in A549 cells (which also overexpress EGFR), **Ru-12d** induced higher ratio of late-stage apoptosis and necrosis than the clinically available EGFR inhibitor gefitinib.

Rajendiran et al. reported mixed ligand Ru(II) complexes of dipyrido[3,2-a:2′,3′-c]phenazine (a planar N,N-chelating diimine) and bis(benzimidazol-2-yl)-dithioether (**Ru-13a,** Fig. 38) or bis (pyrid-2-yl)-dithioether (**Ru-13b,** Fig. 38), with different activities over A375 melanoma cells [298]. While **Ru-13a** showed $IC_{50}$ of 4.0 ± 0.7 μM, the complex with pyridyl ligand could not inhibit the A375 cells in the concentrations tested ($IC_{50}$ > 113 μM). Such difference of the *in vitro* activity for these complexes could be explained

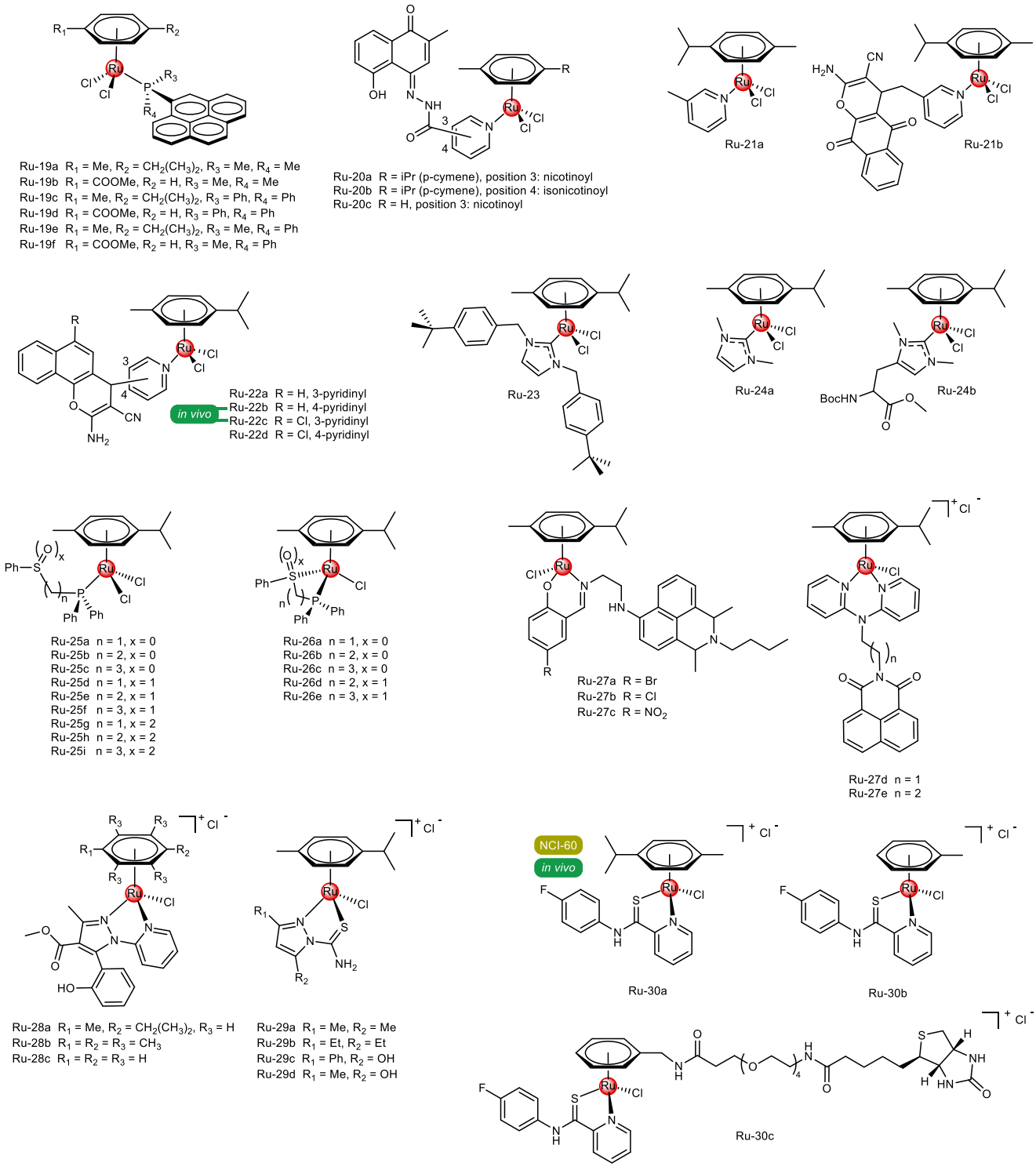


**Fig. 39.** Ru(II)-arene complexes.

by the higher reactivity of complex **Ru-13a** with DNA, but also by the lower redox potential of the Ru(II)/Ru(III) pair in **Ru-13a** complex (0.803 V) than in **Ru-13b** (1.345 V).

Complexes **Ru-14a** and **Ru-14b** (Fig. 38) were active against B16-F10 cells, with $IC_{50}$ = 5.28 and 3.07 μM, respectively. They also exhibit certain selectivity to cancer cells in contrast to non-tumoral human peripheral blood mononuclear cells (PBMC) with SI of approximately 1.3. However, the ruthenium complexes were not as potent and selective as oxaliplatin and doxorubicin. Biophysical studies reveled weak DNA binding with the complexes ($K_b$ of about $10^3$ $M^{-1}$) and flow cytometry assays in HL-60 leukemia cells showed that **Ru-14a** and **Ru-14b** altered the cell cycle, reducing the cells in G1/G0, S, and G2/M phases. They also caused DNA fragmentation, leading to cell death by apoptosis [299].

Complex **Ru-15** (Fig. 38) showed higher antiproliferative activity against B16-F10 cells ($IC_{50}$ = 2.77 ± 0.53 μM) than other four cancer cell lines (MCF-7, HeLa, MO59J and HepG2). It was more cytotoxic than cisplatin ($IC_{50}$ = 26.51 ± 0.64 μM) for the melanoma

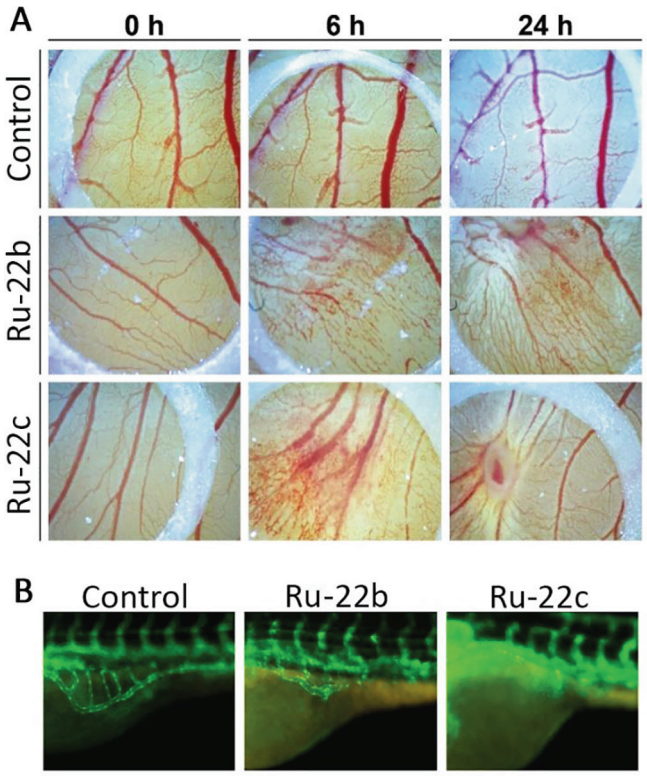


**Fig. 40.** A) Effects of complexes **Ru-22b** (5 nmol) and **Ru-22c** (5 nmol) when applied topically to the vasculature in the chorioallantoic membrane of fertilized chicken eggs (60 × magnification). B) Effect of test compounds **Ru-22b** and **Ru-22c** on angiogenesis in zebrafish embryos. 24 hpf old transgenic Tg(fli1a:EGFP) zebrafish embryos were exposed to 0.5 and 1 μM of the test compounds for 48 h at 28 °C in embryo medium. Adapted from Schmitt et al. [310].

cells and more selective when compared to non-tumor Chinese hamster lung fibroblasts V79 (SI = 3.1 for **Ru-15** and SI = 0.4 for cisplatin). Evidences of **Ru-15** interaction with CT-DNA and BSA were also reported [300]. *In vivo* assays showed that **Ru-15** inhibited melanoma tumor growth in C57BL/6 mice by 60.0% in volume compared to untreated tumors and histopathological evaluation of these tumors revealed that the number of mitoses were significantly reduced [300].

Metal complexes of nucleobase analogues are promising platforms for drug development since the ligand introduces a recognizing factor for nuclear DNA, especially non-canonical sequences observed in cancer cells. This strategy was explored in the preparation of four Ru(II) complexes of uracil nucleobase analogues, **Ru-16a** to **Ru-16d** (Fig. 38), which had their cytotoxicity against B16-F10 melanoma cells [301]. Compounds **Ru-16b** and **Ru-16d** that have a methyl substituent on the nucleobase analogue were very cytotoxic, with low micromolar $IC_{50}$ values (mean values of 0.81 and 1.34 μM, respectively). Flow cytometric studies indicated high degree of DNA fragmentation and all phases of the cell cycle decreased after treatment with these complexes, indicating cell death. Biophysical studies revealed that the most active compounds had the highest binding constants with DNA, corroborating the targeting ability of nucleobase-like ligands.

Ru(II) complexes of coumarin-*N*-acylhydrazone ligands, **Ru-17a** to **Ru-17e**, had their cytotoxicity evaluated against B16-F10 melanoma cells [302]. The complexes had only modest cytotoxicity, with the most active having an $IC_{50}$ value of 31.8 ± 0.7 μM. Interestingly, the ligands were more active over the same cell line, which the authors attributed to possible lower uptake and different mechanism of action. This could also be ascribed to partial hydrolysis in biological media, since *cis*-$[RuCl_2(DMSO)_4]$ had an $IC_{50}$ > 100 μM.

Complex **Ru-18** (KP418, Fig. 38) [303] is an example of compound that had significant antitumor activity, but did not reach clinical trials due to its hampered transmembrane transport and consequently systemic toxicity at effective doses *in vivo*. However, it was shown that higher intracellular concentration of **Ru-18** can be achieved by means of reversible electroporation *in vitro*. Electrochemotherapy (ECT) is an electroporation process in which pulsed electric field is used to increase cell-uptake of compounds that normally cannot permeate the cell [304]. ECT is approved in the clinical practice for the treatment of cutaneous and subcutaneous tumors, especially melanoma [303]. It is an interesting strategy to adapt for complexes that exhibited low activity in classic chemotherapy due to their hydrophilic nature and intracellular site of action.

Intracellular accumulation of ruthenium after ECT with **Ru-18** was dependent on electric field strength (optimal 800 $V.cm^{-1}$) and correlated well with decrease in cell viability. Complex **Ru-18** alone is not cytotoxic up to 1000 μM against three cell lines: SA-1 (murine fibrosarcoma cells), B16-F1 and B16-F10. While electroporation did not increase the cytotoxicity of **Ru-18** in SA-1 cells, it did significantly increase it in B16–F1 and B16–F10 cells ($IC_{50}$ = 600 μM). Similarly, ECT with cisplatin was more cytotoxic for B16-F1 cells ($IC_{50}$ = 70 μM) than SA-1 cells ($IC_{50}$ = 200 μM).

The effectiveness of the electroporation treatment was not maintained *in vivo*, since ECT with up to 20.8 mM **Ru-18** applied i.v. had no antitumor effect on B16-F1 and SA-1 murine tumor models. However, ECT with cisplatin i.v. caused tumor growth delay for both tumor models and also 18.8 % complete responses in case of SA-1 tumors. In conclusion, electroporation could increase *in vitro* cytotoxicity of **Ru-18** but its effectiveness *in vitro* and *in vivo* is still lower than the effectiveness of cisplatin combined with ECT [303].

### 3.6.4. Ruthenium-arene compounds

The cytotoxic activities of a series of six ruthenium half-sandwich complexes with pyrenyl-phosphane ligands (**Ru-19** series, Fig. 39) have been assessed against A375 melanoma cells. These Ru(II) complexes showed $IC_{50}$ between 2.19 and 25.01 μM, with **Ru-19b** being the most active, with methyl substituents in the phosphane and methyl benzoate $\eta^6$-ring [305]. The bulkiness of the P-ligand seemed to be important for the cytotoxicity as the Ru(II) complexes with $P(Me)_2$(1-pyrenyl) phosphane ligands were generally more active against the cancer cells. All the compounds in the series were able to induce apoptosis in A375 cells, but only **Ru-19b** arrested the cell cycle at the G2/M and S phases, like cisplatin (**Ru-19d** only produces some $G_2$/M arrest). However, the mechanism of action of **Ru-19b** is apparently different from that of cisplatin, as DNA is most likely not its cellular target [305].

Another series of Ru(II) half-sandwich complexes with *p*-cymene or toluene $\eta^6$-rings and 5-hydroxy-2-methyl-1-oxo-naphthalen-4(1H)-ylidene)nicotinohydrazide ligand (derived from Plumbagin) (**Ru-20a** to **Ru-20c,** Fig. 39) was evaluated against 518A2 melanoma cell line by Spoerlein-Guettler et al. [306]. The $IC_{50}$ of the Ru(II) complexes were between 1.3 and 2.3 μM and cell cycle arrest assays were performed in HCT-116 and KB-V1/Vbl cells. A similar complex (**Ru-21a,** Fig. 39) [307] was also cytotoxic against 518A2 cells ($IC_{50}$ = 13.5 ± 0.5 μM) and showed specificity comparable to cisplatin (SI = 4.6 and 5.2, respectively) for human melanoma cells over non-malignant human dermal fibroblasts with lower general toxicity against normal cells. **Ru-21b** (Fig. 39) however, was not able to inhibit the cancer cells ($IC_{50}$ > 100 μM). The **Ru-21a** complex was shown to interact with DNA and to induce ROS production (similarly as **Ru-20a**) and also to arrest cell cycle of 518A2 in $G_2$/M phase as consequence of DNA damage,

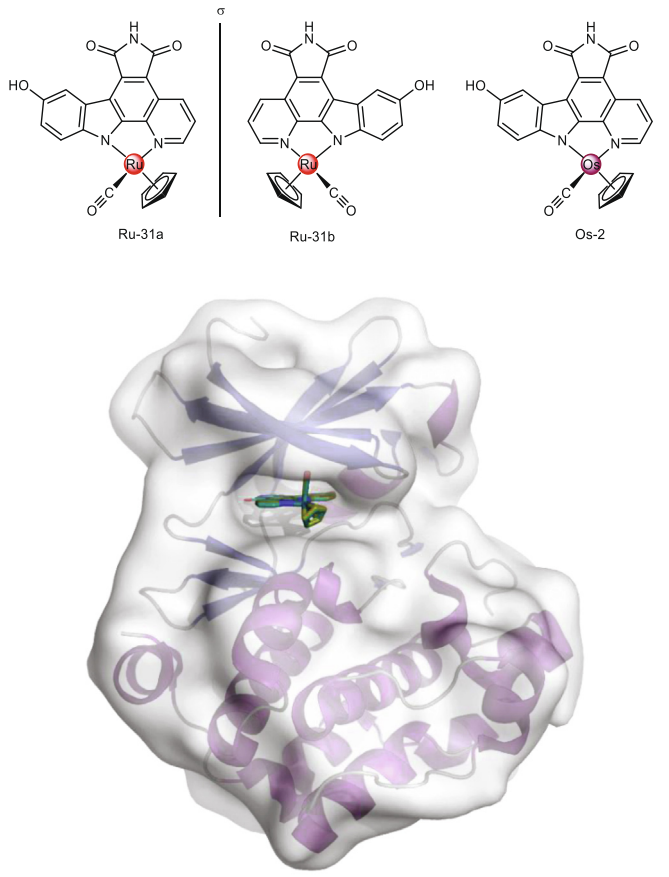


**Fig. 41.** Top: structures of the arene complexes **Ru-31a**, **Ru-31b** and **Os-2**. Bottom: aligned structures of Pim-1 co-crystallized with either **Os-2** (PDB accession code 3BFW, golden) or **Ru-31a** (PDB accession code 2BZI, green). Both compounds, irrespective of metal complex. Illustration prepared with Pymol. (For interpretation of the references to color in this figure legend, the reader is referred to the web version of this article.)

however, no evidence of apoptosis and necrosis were observed. The authors suggested a mechanism of cellular senescence, a tumor suppressor mechanism that limits the proliferation of cells at different stages of mutagenesis, which might be a potential alternative to conventional melanoma chemotherapy as most melanoma cells are highly resistant to cytotoxic, apoptosis-inducing chemotherapy [308], but have powerful pro-senescence signaling via activation of BRAF or NRAS [309].

Moreover, the series of piano stool Ru(II) complexes **Ru-22** (Fig. 39), showed remarkable cytotoxicity, with $IC_{50}$ values in the nM range over 518A2 cells [310]. The free 2 amino (pyridin 3 yl) 4H benzo[h]chromene 3 carbonitrile ligands showed $IC_{50}$ < 0.5 nM while complexes **Ru-22a** and **Ru-22b** were also active, with $IC_{50}$ = 37.8 ± 2.3 nM and 33.3 ± 2.9 nM, respectively. The substitution of a hydrogen atom in the ligand by a chloride did not improve activity the activity of the complexes when comparing **Ru-22a** to **Ru-22c** and **Ru-22b** and **Ru-22d**. It is clear that the naphthopyran ligand plays a major role in the anti-angiogenic, vascular-disruptive and cytotoxic activities of the complex, but the presence of the Ru(II) center is important to confer DNA interactions that are typical of (arene)Ru(II) complexes and in this case that happen 10 times faster than with cisplatin. In 518A2 cells, **Ru-22a** and **Ru-22b** induced dose-dependent G2/M phase accumulation, that can be attributed to the interference of naphthopyrans with the tubulin dynamics which prevents the normal microtubule formation and decrease of G1 phase. At higher concentrations there was an increase of apoptotic cells in sub-G1 phase.

The **Ru-22b** and **Ru-22c** complexes were able to cause microtubule destruction as evidenced in assays with chorioallantoic membrane of fertilized chicken eggs (Fig. 40**A**). Moreover, the anti-angiogenic effects of the complexes were evidenced by monitoring the growth of subintestinal veins in Tg(fli1a:EGFP) zebrafish embryos with casper background (Fig. 40**B**). In this experiment, **Ru-22c** showed greater anti-angiogenic potential. As observed for RAPTA compounds [311], the anti-angiogenic activity **of Ru-22b** and **Ru-22c** might be associated to the inhibition of growth factor receptors such as fibroblast growth factor receptor (FGF-R1) or vascular endothelial growth factor receptor (VEGFR).

The antiproliferative mechanism of **Ru-23** (Fig. 39) was systematically evaluated in human esophageal squamous carcinoma EC109 cells ($IC_{50}$ = 5.81 ± 0.41 μM). The complex induced cell cycle arrest at G2/M phase, with up regulation of p53 and p21 and down-regulation of cyclin D1, which regulates cell cycle and is important for malignant transformation of tumor cells. **Ru-23** also inhibited glutathione reductase, altering the balance between glutathione and oxidized glutathione and therefore triggering apoptosis by increase concentration of ROS. Moreover, mitochondria-mediated apoptosis of EC109 was observed, with increase of Bax/Bcl-2ratio, overload of $Ca^{2+}$ disruption of mitochondrial membrane potential, redistribution of cytochrome *c*, and activation of caspase-3 and caspase-9. Overall, the antiproliferative activity of **Ru-23** was very dependent on ROS generation, since the introduction of the ROS scavenger N-acetylcysteine (NAC) significantly attenuated the cytotoxic effects of the complex in the cancer cells.

**Ru-24a** and **Ru-24b** (Fig. 39) were developed by Schmitt and tested against 518A2 melanoma cells [108]. These ruthenium compounds were much less active than the Au analogues **Au-28a** and **Au-28b** (Fig. 26).

Ludwig et al. evaluated Ru(II) complexes with sulfide, sulfoxide and sulfone ligands (**Ru-25** series, Fig. 39) against 518A2 melanoma cells, among other four cancer cell lines. The coordination generally increased the antiproliferative activity of the ligands compared to their free forms [312].

The elongation of the spacer from a $CH_2$ to a $(CH_2)_3$ chain has a positive effect on the cytotoxic activity of the complexes **Ru-25d** to **Ru-25i**, while the reduction of the sulfur oxidation state increased the anticancer activity of **Ru-25a** to **Ru-25i** against melanoma cells. The complexes with sulfide ligands **Ru-25a**, **Ru-25b** and **Ru-25c** were able to inhibit 518A2 cells with lower $IC_{50}$ values of 1.8, 2.6 and 3.0 μM, respectively [312].

Moreover, the analogue cationic Ru(II) complexes with the same group of ligands (**Ru-26a** to **Ru-26e,** Fig. 39) were also tested. The cationic complexes were generally more cytotoxic against 518A2 cells than their neutral counterparts, with $IC_{50}$ values of 0.96 ± 0.12 μM for **Ru-26e** to 1.81 ± 0.11 μM for **Ru-26a**. Similarly to **Ru-25a-i**, the cytotoxic activity of **Ru-26a** to **Ru-26e** increased with the ligand length, but in this case the oxidation state of the sulfur moiety did not have a significant influence on the $IC_{50}$ values for the cationic complexes [313].

Ghebreyessus *et al.* reported another series of seven Ru(II) arene complexes with p-cymene $\eta^6$-rings and naphthalimide-tagged N, O- and N,N-based chelating ligands (**Ru-27a** to **Ru-27e,** Fig. 39) where the naphthalimide moiety functioned as chromophore and intercalating agent [314]. These were tested against the human melanoma skin cancer cell line CR7687. The Ru(II) complexes exhibit antiproliferative activities with $IC_{50}$ in the low μM range, the lowest values being for **Ru-27d** ($IC_{50}$ = 0.688 ± 0.2 μM). However, the presence of the naphthalimide moiety in the complexes did not afford more potent cytotoxic activities, with ligands and their corresponding metal complexes displaying nearly the same cytotoxicity. Nevertheless, UV–Vis and fluorescence spectroscopy, and gel electrophoresis studies suggested that the naphthalimide group was essential for DNA interaction, suggesting that the activ-

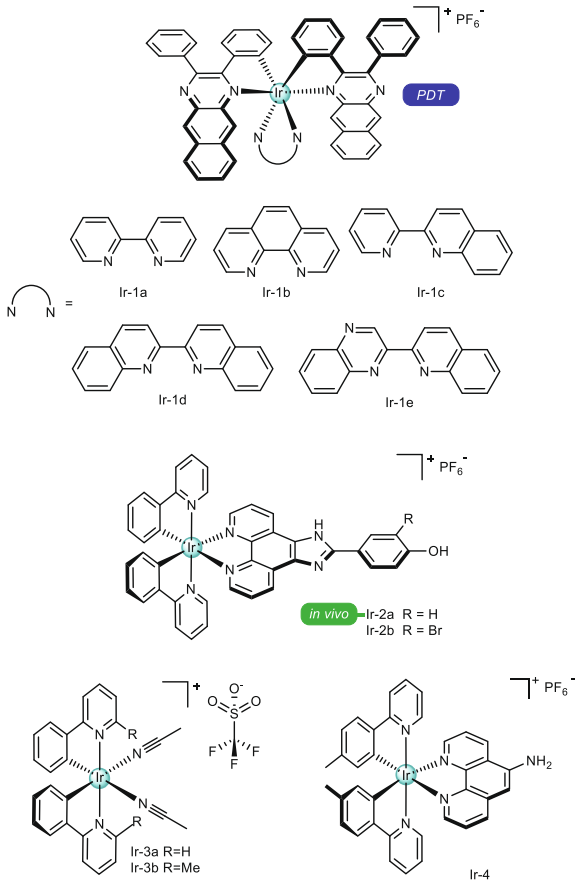


**Fig. 42.** Octahedral Ir(III) complexes.

ity of this complexes was not significantly related to their ability to bind DNA.

Ruthenium(II)-piano stool complexes containing pyrazole derivatives, **Ru-28a** to **Ru-28c** (Fig. 39), have been studied for anticancer purposes [315]. Compounds **Ru-28a** and **Ru-28c** did not show relevant activity over the WM-115 melanoma cell line (>100 μM), while **Ru-28b** was moderately active (51.9 ± 5.1 μM). A comet assay indicated that the analyzed ruthenium complexes triggered DNA damage. Modifications of the structures of the initial Ru(II)-p-cymene/pyrazole motif to give **Ru-29a-d** (Fig. 39) resulted in improved cytotoxicity [316]. Small variations on the substituent groups on the pyrazole moiety resulted in relevant changes of $IC_{50}$ values from 60.24 ± 6.30 μM in **Ru-29a** to 7.99 ± 0.87 μM in **Ru-29d**, which was more active than cisplatin (18.2 ± 4.3 μM) against the same WM-115 cells. The compounds were non-cytotoxic against human foreskin fibroblasts, which highlights a selectivity towards melanoma cells. Plasmid DNA cleavage was observed mainly for **Ru-29b** and **Ru-29d**, which could relate to their improved cytotoxicity.

Meier, Gerner and co-workers developed a series of ruthenium-arene pyridinecarbothioamide complexes referred to as plecstatins (**Ru-30a** to **Ru-30c,** Fig. 39) [317]. A proteomics-based target-response analysis revealed a surprisingly high selectivity of plecstatins for plectin, a scaffold protein and cyto-linker, with pronounced effects on the organization of non-mitotic micro-tubules (MTs). The authors highlighted that non-mitotic MTs are an underappreciated drug target and their disturbance by plectin-targeting agents affects the motility of cancer cells, which may be harnessed as a promising strategy for the development of anticancer agents. **Ru-30a** was selected for the 5-dose NCI-60 screening (NSC 776415), and the compound had single-digit μM $GI_{50}$ across all the melanoma cell lines. Importantly, COMPARE analysis showed only correlations with low significance, indicating an unprecedent mechanism of action for **Ru-30a**. Target profiling was carried out on HCT116 (colon) cancer cells. The authors used an elegant approach to address non-specific interactions with molecular targets, based on differences between cell lysates either pre-treated or not with the parent metallodrug before addition of the drug immobilized on a solid support. Pre-treatment saturated actual binding sites and results in these proteins not being able to interact with the immobilized drug. Compound **Ru-30c**, bearing a biotin motif, was prepared for immobilization on streptavidin beads. **Ru-30b** was used as a more direct analogue to **Ru-30c** for proteomics analysis. This approach led to the identification of outer dense fiber protein 2(ODF2, 210-fold) and plectin (PLEC, 160-fold) as potential targets with high enrichment factors. **Ru-30a** was also evaluated *in vivo*, with two mouse models, B6 mice bearing the highly invasive B16 melanoma; and a Balb/c mice bearing murine colon carcinoma (CT-26). In both cases, the tumor was induced by injecting the respective cells subcutaneously. **Ru-30a** was administered orally (30 mg/kg) at days 3–7 and 10–14 for both mouse models. Statistically significant tumor volume and weight reduction was observed at the last day.

Meggers and colleagues [318] studied the effect of the enantiomers **Ru-31a** and **Ru-31b** (Fig. 41), as well as the racemic mixture **Ru-31ab** as melanoma growth inhibitors. **Ru-31a** and the racemate **Ru-31ab** have $IC_{50}$ values of ∼ 0.1 μM against 1205Lu melanoma cells, while **Ru-31b** has an $IC_{50}$ of ∼ 0.5 μM (72 h growth curves are shown, but no $IC_{50}$ values are given from the plots). *In vitro* kinase inhibition assays revealed the $IC_{50}$ values for **Ru-31a** to be 2 and 2.5 nmol $L^{-1}$ for glycogen synthase kinase GSK3α and GSK3β, respectively, and the $IC_{50}$ values for **Ru-31b** to be 9 and 15 nmol $L^{-1}$ for GSK3α and GSK3β, respectively, at an ATP concentration of 100 μmol $L^{-1}$. The 1205Lu growth inhibition potency was found to directly correlate with the kinase inhibition potency of the compounds. The racemic mixture **Ru-31ab**, having a similar potency to **Ru-31a**, was selected for further testing against melanoma cells that were WT for p53 (WM793, 1205Lu, and WM115) or harbored p53 mutations (WM852 and WM164). Mechanistic analysis of the p53-dependent cell death indicated an apoptotic mechanism involving depolarization of mitochondrial membrane potential, caspase cleavage, and elevated NOXA expression. To investigate the possible role of p53 in the proapoptotic activity of **Ru-31ab**, melanoma cells that were p53-WT (1205Lu) and p53-mut (WM852) were treated with **Ru-31ab** (1 μmol $L^{-1}$) for 24 h and stained for p53 expression. It was found that **Ru-31ab** up-regulated nuclear levels of p53 in the 1205Lu cells but not the WM852 cells. Treatment of 1205Lu cells for 0, 2, 6, or 24 h (1 μmol $L^{-1}$) did not lead to an increase in the nuclear staining of phosphorylated H2AX or phosphorylated ataxia-telangiectasia mutated (ATM), which are both markers of DNA damage. Knockdown of p53 also reduces **Ru-31ab**-induced apoptosis in p53-WT melanoma cells.

In a follow up study, Meggers and co-workers studied **Ru-31a** in comparison to the osmium analogue, **Os-2** (Fig. 41) [319]. The compounds were developed within the framework of unreactive metal complexes, where the inert metal center has only a structural function. Within the experimental error, the two isostructural compounds **Ru-31a** and **Os-2** had the same inhibitory potency against 1205Lu melanoma cells (no $IC_{50}$ values were given). The effect of the Os analogue on the inhibition of GSK-3β was also studied, and **Os-2** was found to be a slightly more potent inhibitor an $IC_{50}$ of (0.60 ± 0.2) nmol $L^{-1}$ at 100 mmol $L^{-1}$ ATP. Finally, to support the conclusion that **Ru-31a** and **Os-2** have almost identical anticancer properties as consequence of similar protein kinase inhibition profiles, the authors co-crystallized **Os-2** with a model protein kinase (Pim-1) (PDB 3BWF).

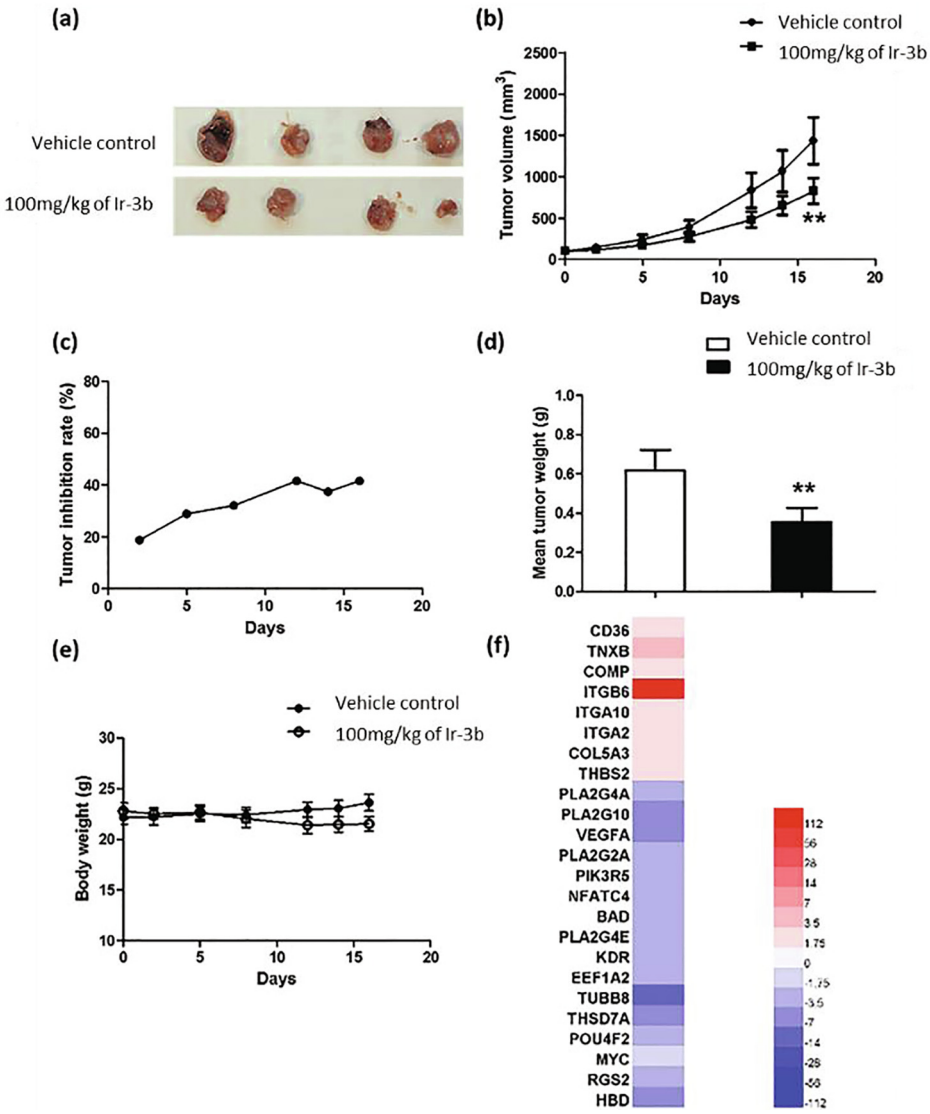


**Fig. 43.** Anti-proliferative activity of **Ir-3b** in an *in vivo* xenograft model of melanoma. (a) Photographs of dissected tumors from the control (vehicle) and treatment (**Ir-3b**, 100 mg/kg). (b) Average A375 tumor volume in the control group and treatment group (**Ir-3b**, 100 mg/kg). Each group contained six mice and results are reported as the values of the mean ± SEM. (c) Tumor inhibition of A375 xenografts in the treatment group (**Ir-3b**, 100 m/kg) expressed as percentage reduction in tumor volume compared to the control group. The results were analyzed using the Student's *t*-test. Significantly different at $0.01 < {}^{**}p < 0.05$. (d) Average tumor weight of the vehicle control group versus the treatment group (**Ir-3b**, 100 mg/kg). (e) Average body weight of the two groups. Each group contained six mice, and results were reported as the values of the mean ± SEM. The results were analyzed using the Student's *t*-test. Significantly different at $0.01 < {}^{**}p < 0.05$. (f) Heat map of regulated genes of the ECM pathway and VEGF signaling pathway following treatment with **Ir-3b**. The color scale in the inset represents the log-fold change of expression compared with untreated control. Adapted from Leung *et al.* [325].

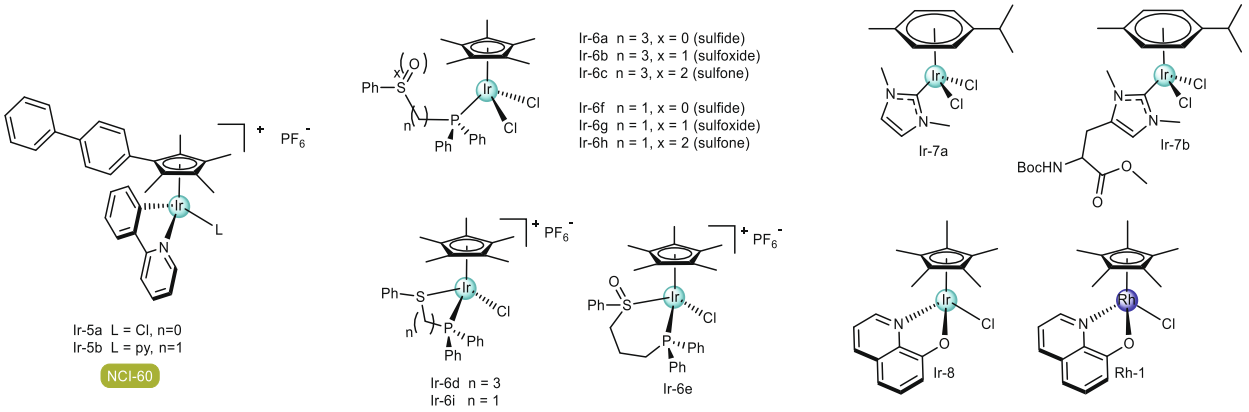


**Fig. 44.** Arene Ir(III) complexes.

The structure was compared to an already existent Pim-1 adduct with **Ru-31a** (PDB 2BZI). This represented the first crystal structure an osmium complex bound to an enzyme. Both structures have the metal complexes occupying almost identical positions within the binding pocket and, importantly, the metal centers are not involved in any direct interaction with the kinase active site (Fig. 41).

### 3.7. Iridium

Ir(III) complexes are considered very inert towards ligand substitution reactions due to the low-spin $5d^6$ electron configuration (low-spin). However, the introduction of a cyclopentadienyl ligand in Ir(III) complexes can increase the ligand exchange rate by 14 orders of magnitude [320]. This is an important feature that has been exploited for both inert and labile Ir(III) complexes as anticancer agents.

While Ir(III) complexes have been extensively studied in organic light-emitting diodes and light-emitting electrochemical cells, as photosensitizers (PSs) and in photocatalysts [321-323], few Ir(III) complexes were explored in PDT. This is despite of Ir (III) having very high quantum yields for triplet state formation, which is important for the energy or electron transfer to the ground state of oxygen to produce $^1O_2$ and other reactive oxygen species (ROS) [281]. Moreover, Ir(III) complexes also have the potential to be used as theranostic agents [281], with large luminescence quantum yields and tunable and excitation/emission energies.

#### 3.7.1. Octahedral iridium complexes

Near-infrared (NIR) emitting Ir(III) complexes are examples of potential theranostic agents studied by Wang et al. [281], using π-expansive 2,3-diphenylbenzo[g]quinoxaline as cyclometalating (C^N) ligands and probing the effects of systematic changes to the identity of auxiliary diimine ligands (**Ir-1a** to **Ir-1e,** Fig. 42) on the photophysical and photobiological properties of these complexes. Complexes **Ir-1b** and **Ir-1c** were selective toward melanoma cells (SK-MEL-28) and showed activity in the nanomolar range after light activation (15 and 18 nM, respectively) with PI higher than 10. The higher PI observed was for the complex **Ir-1e** with 2-(quinolin-2-yl)quinoxaline as auxiliary ligand (PI = 275).

Although the changes in the auxiliary ligands altered the cytotoxicity of the complexes, not many differences were observed regarding their mechanism of action. All these complexes induced DNA aggregation and production of $^1O_2$ in cell-free experiments, and were taken up readily by melanoma cells [281].

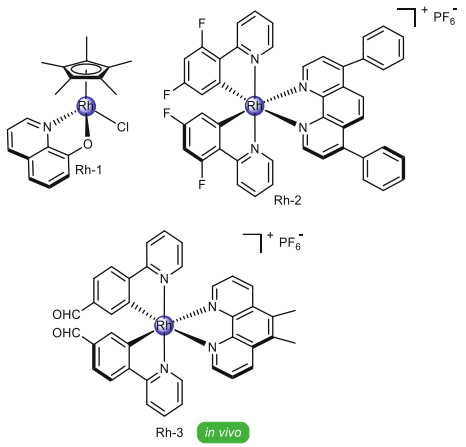


**Fig. 45.** Structure of Rh(III) complexes.

Two Ir(III) polypyridyl complexes, **Ir-2a** and **Ir-2b** (Fig. 42), and their liposome formulations, **Ir-2a/lipo** and **Ir-2b/lipo**, have been reported and had their anticancer activity evaluated [324]. While the unloaded metal complexes showed no cytotoxic activity over B16 melanoma cells, their liposome formulations presented $IC_{50}$ values of 5.2 ± 0.8 and 10.8 ± 1.5 μM for **Ir-2a/lipo** and **Ir-2b/lipo**, respectively. It was verified that, in these melanoma cells, **Ir-2a/lipo** and **Ir-2b/lipo** induced apoptosis in B16 through ROS-mediated lysosomal-mitochondrial dysfunction, which was corroborated by the detection of increased intracellular levels of $Ca^{2+}$ and cytochrome *c* and up-regulation of protein caspase-3 and PARP expression. Comet assay also revealed DNA damage after exposure to the liposomes. Flow cytometry experiments corroborated the low cytotoxicity of unloaded **Ir-2a** and **Ir-2b** in B16 cells due to low percentages of cell population in early apoptosis. Treatment with **Ir-2a/lipo** and **Ir-2b/lipo** induced a 2-fold increase in apoptotic cells when compared to the treatment with the unloaded complexes and S-phase cell cycle arrest. The liposomes also showed antiangiogenic activity, possibly by triggering cell morphology collapse because of microtubule polymerization inhibition. *In vivo* studies were performed in mice bearing a B16 tumor xenograft model. The mice were treated by intraperitoneal injection of different doses of **Ir-2a/lipo** (4.8 and 9.6 mg/kg) or **Ir-2a** (6.0 mg/kg) every day for 7 days. By the end of the treatment period, mice that received the higher dose of **Ir-2a/lipo** had 39 % of tumor volume decrease as compared with **Ir-2a-**treated mice. Additionally, the rate of tumor growth induced by the lipid formulation at higher dose was 72 % lower when compared to the control group. This study brings interesting insights into the use of nanocarriers to improve the cytotoxicity of otherwise inactive metal complexes, especially against melanoma.

The Leung group was the first to screen a series of 27 Ir(III) organometallic compounds in the inhibition of bromodomain-containing protein 4 (BRD4) [325]. Bromodomain-containing proteins are involved in the regulation of gene expression though several factors that include histone modification and recognition. BRDs deregulation and mutations are frequently observed in cancer [326]. BRD4 plays an important role in metastatic melanoma, which makes it a possible target for therapy. Compound **Ir-3a** (Fig. 42) was identified as a promising initial motif for the design of fine-tuned inhibitors of BRD4-acetylated histone protein–protein interactions. In the same manuscript, the authors modified the parent compound **Ir-3a** and prepared an additional series of 10 fine-tuned Ir(III) and Rh(III) compounds. From this improved series, complex **Ir-3b** was a selective inhibitor of BRD4-tetra-acetylated lysine histone 4 peptide (H4AcK4) binding and was comparably potent to the positive control JQ1, a potent inhibitor of bromodomains. The molecular interaction of complex **Ir-3b** with BRD4 occurs by ligand substitutions, where selective histidine binding on the first *N*-terminal bromodomain BRD4(1) is observed after loss of its acetonitrile ligands. *In cellulo* studies by a chromatin immunoprecipitation assay at the *Myc* promoter revealed that a concentration of 10 nM of **Ir-3b** decreased the recruitment of BRD4. Moreover, expression of c-*myc* and *Bcl-2* proteins, which are involved in cancer progression and apoptosis, was reduced by **Ir-3b** in a dose-dependent manner. The direct effect of the compounds in melanoma cells was assessed *in vitro* by the MTT assay. The results showed cytotoxicity of compound **Ir-3b** against A375 ($IC_{50}$ = 12.5 μM) and A2058 ($IC_{50}$ = 3 μM) cell lines. Contrastingly, the colony formation assay showed much higher activity, with estimated $IC_{50}$ values of 5 nM and 1 nM, against the same cell lines.

*In vivo* studies (Fig. 43) were performed in CB.17 SCID mice that were injected subcutaneously with human malignant melanoma A375 cells. Treatment was performed with **Ir-3b** at a dose of 100 mg/kg or vehicle (13% DMSO in normal saline) intraperitoneally once daily for 16 days. A significant reduction in tumour

volume of 40% was observed on the treated models, with no significant loss of body weight. Analysis of the excised tumours revealed downregulation of *MYC* and expression of the *c-myc*, as verified *in vitro*. Additionally, up-regulation of genes in the extracellular matrix pathway was observed and assigned as a potential result of BRD4 inhibition *in vivo*.

Leung and colleagues reported the antiproliferative activity of **Ir-4** (Fig. 42), a cyclometallated compound, against A375 and A2058 melanoma cells [327]. The compound was highly active, with $IC_{50}$ below 1.6 μM for both cell lines. **Ir-4** showed a log P value of 0.629, characteristic related to a slightly lipophilic compound.

### 3.7.2. Iridium-arene compounds

Another strategy to induce oxidative stress in melanoma cells with iridium complexes is demonstrated by Sadler and colleagues [320]. In their work, two half-sandwich biphenyltetramethylcyclopentadienyl complexes with 2-phenylpyridine bidentate ligand and either chloride (**Ir-5a,** Fig. 44) or pyridine (**Ir-5b,** Fig. 44) monodentate ligands are compared. The antiproliferative profile of **Ir-5a** and **Ir-5b** were evaluated against the NCI-60 panel.

The **Ir-5b** complex was especially selective and active against all the melanoma cell lines tested, with $GI_{50}$ between 0.1 and 0.5 μM, and in all cases being more cytotoxic than cisplatin and oxaliplatin. With assays in A2780 ovarian carcinoma cells it was possible to determine that the mode of action of **Ir-5b** involves redox processes, high amount of ROS and superoxide production was observed at low doses in only one hour (no increase was observed for higher concentrations of complex). In the case of **Ir-5a** for instance, the level of superoxide induction was significantly lower than for **Ir-5b**, indicating that ROS generation is correlated with the anticancer activity. Moreover, the introduction of pyridine in **Ir-5b** significantly slowed down the hydrolysis rate, in contrast to the chloride in **Ir-5a**, which leads to an activation time that is more compatible with transport to biological target sites.

Complex **Ir-5a** was more reactive towards hydrolysis, GSH, and NADH than **Ir-5b**. Complex **Ir-5b** showed enhanced accumulation in cancer cells, which was followed by the reaction with NADH and the generation of the ROS hydrogen peroxide, also leading to the build-up of superoxide.

Ludwig et al. studied a distinct class of iridium complexes bearing sulfide, sulfoxide, and sulfone ligands (**Ir-6** series, Fig. 44) and evaluated their *in vitro* antiproliferative effects over 518A2 melanoma cells [328]. The complexes were generally more active than cisplatin ($IC_{50}$ = 1.5 ± 0.2 μM) against the melanoma cell line, with the exception of **Ir-6c**. A trend is observed in the antiproliferative

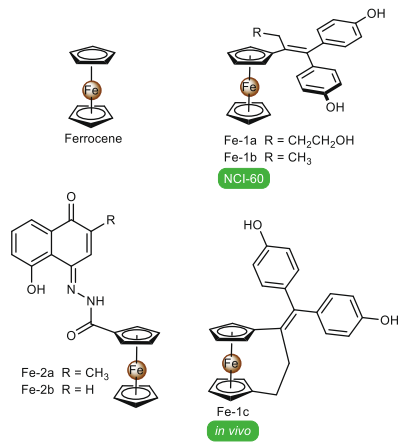


**Fig. 46.** Structure of Ferrocene and derivative complexes.

activities of the complexes where they decreased slightly from **Ir-6a** (sulfide ligand, $IC_{50}$ = 0.3 ± 0.1 μM) to **Ir-6b** (sulfoxide ligand, $IC_{50}$ = 0.7 ± 0.4 μM) and significantly reduced for **Ir-6c** (sulfone ligand, $IC_{50}$ = 4.4 ± 2.5 μM). For the cationic complexes **Ir-6d** and **Ir-6e**, the opposite is observed and the activity of the complex **Ir-6e** with sulfoxide ligand ($IC_{50}$ = 0.4 ± 0.2 μM) is slightly better than **Ir-6d** (sulfide ligand, $IC_{50}$ = 1.0 ± 0.6 μM). However, the change from mono coordination in **Ir-6a-c** to bis coordination in **Ir-6d** and **Ir-6e** does not significantly affect the cytotoxic activity. It is worth noting that due to a probable oxidation of the pendant sulfur groups in living organisms, the order of activities could vary *in vivo*.

Not only the oxidation state of sulfur in the ligands is important for cytotoxicity, but also the length of the carbon chain between the P and S atoms, as seen for **Ir-6f**, **Ir-6g**, **Ir-6h** ($IC_{50}$ = 14.3 ± 3.6 μM, 26.1 ± 1.3 μM and 22.5 ± 2.1 μM, respectively) [329]. Results demonstrated that the complexes with longer ligands yield more pronounced antiproliferative activity, as previously observed for the Ru(II) complexes with the same ligands (**Ru-25** series, Fig. 39) [312].

Complexes **Ir-6a to Ir-6c** exhibited higher activities (up to two orders of magnitude) against 518A2 cells than the related Ru(II) complexes, **Ru-25c**, **Ru-25f** and **Ru-25i** [312]. In contrast, complexes **Ir-6d** and **Ir-6e** exhibited only a similar or slightly better cytotoxic activity in comparison with the corresponding cationic ruthenium complexes **Ru-26c** and **Ru-26e** [313].

Schmitt and colleagues designed **Ir-7a** and **Ir-7b** (Fig. 44) as part of a panel that evaluated the same two imidazole-2-ylidene and histidine-2-ylidene NHC ligands combined with different metal centers [108]. **Ir-7a** and **Ir-7b** were not cytotoxic against 518A2 melanoma, the same behavior observed for the Ru analogues **Ru-24a** and **Ru-24b** (Fig. 39).

Complexes **Ir-8** and **Rh-1** (Figs. 44 and 45) with quinoline ligands were tested against three melanoma cell lines: SK-MEL, C-32 and SH-4. The antiproliferative activity of these two complexes are different for the C-32 cells, as **Ir-8** exhibited $ID_{50}$ = 4.9 μM and **Rh-1** inhibited the same cells with $ID_{50}$ = 0.9 μM. Both complexes showed $ID_{50}$ values of 0.8 μM and 100 μM for the SK-MEL and SH-4 cell lines, respectively [330].

### 3.8. Rhodium

Rhodium compounds can be classified in inert Rh(III) compounds (octahedral, piano stool), labile Rh(II) compounds and the $d^8$, square-planar Rh(I). Additionally, the photochemistry of rhodium compounds has been widely explored. Rhodium(I,II) compounds tend to dimerize when dicarboxylate ligands are present, forming a paddlewheel dirhodium species. [331].

Leung's group developed **Rh-2** (Fig. 45) as part of a series of compounds that were studied as autotaxin (ATX) inhibitors [332]. ATX, also known as ectonucleotidepyrophosphatase/ phosphodiesterase 2 (ENPP2), regulates physiological and pathological functions of lysophosphatidic acid. **Rh-2** was the most potent ATX inhibitor identified in this study, with 69.3% inhibition observed at 3 μM. In contrast, the Ir(III) analogue showed only 25% inhibitory activity at the same concentration. **Rh-2** also exhibited strong antiproliferative activity against A2058 melanoma cells ($IC_{50}$ = 0.58 μM). The antiproliferative activity observed for **Rh-2** was further evaluated looking at its effect on ERK and AKT signaling in A2058 melanoma cells. Phosphorylated proteins and total proteins were measured after 1 and 24 h exposures. The level of p-ERK was decreased to 51.49% and 87.19% upon 0.3 and 1 μM **Rh-2** treatments. Additionally, **Rh-2** decreased p-AKT levels in a dose-dependent fashion. Finally, **Rh-2** also suppressed STAT3 and NF-κB via inhibition of ATX activity. Taken together, these data suggested that the significant antiproliferative activity of **Rh-2** in A2058 could partially related to the inhibition of ATX down-

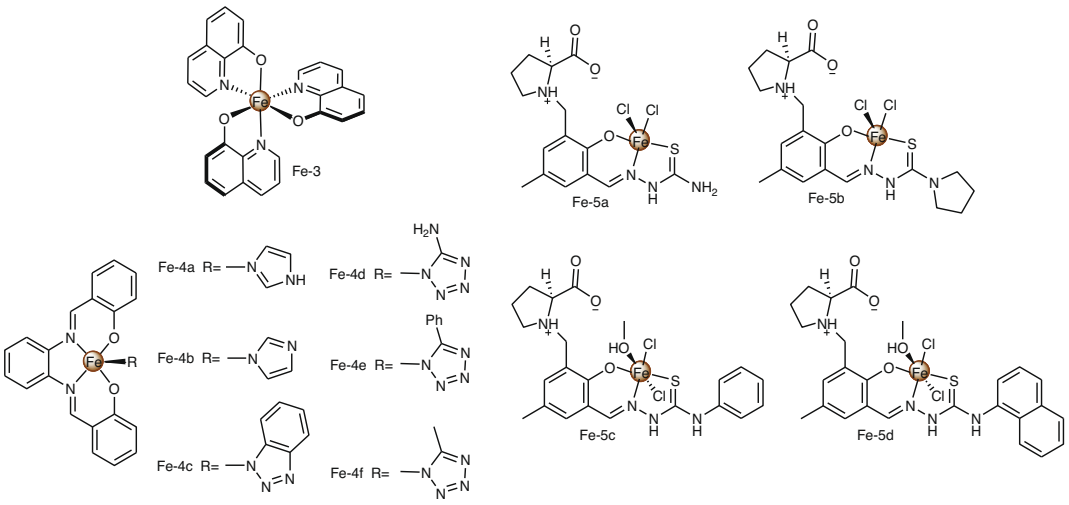


**Fig. 47.** Structure of Fe(III) complexes and the Fe(II) complex.

stream signaling partners that are responsible for mediating cellular survival. Structure-activity relationship analysis indicated that both the presence of the cyclometallated C^N motif, the 4,7-dpphen co-ligand as well as the nature of the metal center are relevant for the biological endpoint observed.

Leung and colleagues reported a series of 35 Ir(III) and Rh(III) complexes [333]. On the initial cytotoxicity screening, the authors found one compound (**Rh-3,** Fig. 45) with a promising activity profile over the A375.S2 ($IC_{50}$ = 6.6 ± 3.0 μM), A2058 ($IC_{50}$ < 1 μM) and A375 ($IC_{50}$ = 17.2 ± 4.9 μM) human melanoma cells lines [333]. Additionally, **Rh-3** displayed low cytotoxicity towards normal human dermal fibroblasts ($IC_{50}$ > 100 μM). *In vivo* studies showed that **Rh-3** was effective in treating Balb/c mice with induced malignant A375 melanoma. Subcutaneous administration of the compound at 75 mg/kg four times a week for 35 days resulted in 60 % of average reduced tumor weight after sacrifice. No signs of acute toxicity were detected, and mean weights of the heart, liver and kidney were not affected with the treatment regime. The authors hypothesized that the anti-tumor effects of the compound are related to the inhibition of the signal transducer and activator of transcription 3 (STAT3), which plays an important role in the development of skin cancers [333].

The **Rh-3** complex targets a key domain (SH2 domain) for the formation of the activated STAT3 dimer and therefore inhibits STAT3 DNA-binding activity. In the *in vivo* assay, the mice tumor tissues showed repressed STAT3 phosphorylation, VEGF expression, and angiogenesis. Furthermore, anti-inflammatory activity of the complex was also observed in these tissues as it reduced the expression of COX-2 and inducible nitric oxide synthase. These results highlighted that the inhibition of STAT3 dimerization is a promising target for the development of novel anti-neoplastic agents due to its implication also in angiogenesis and inflammatory processes [333].

### 3.9. Iron

Iron is not only the most abundant transition metal on the Earth's crust but also the most abundant in living organisms. It is one of the only two transition metals in the gram-scale in our bodies (~4g in a 70 kg male) [334]. Its prevalence reflects its involvement in a plethora of biological processes, from the transport of $O_2$ in the blood, to energy production in the cells and synthesis of DNA. From heme to non-heme proteins, the use of iron by nature exploits the ability of the metal to cycle between iron(II) and iron(III). This cycling in the presence of $O_2$ can lead to toxic ROS, therefore its homeostasis requires tight regulation. We have specialized proteins for iron transport (transferrin) and storage (ferritin). This tight regulation means that metallodrugs based on iron can explore any of the biological processes where iron is involved as part of their mechanism of action [335-337]. The two most common classes of iron compounds studied as metallodrugs are ferrocene derivatives and coordination compounds with chelating ligands.

#### 3.9.1. Ferrocene-based compounds

Ferrocene complexes (Fig. 46) were among the first examples of antiproliferative iron complexes reported in the literature [338], with more in-depth studies explored in the recent years. Their mechanism of action are generally different than the clinically established Pt(II) complexes. For instance, they often target the mitochondrial system or inhibit kinases or redox proteins overexpressed in cancer cells [339,340].

Ferrocene (single dose administered i.p.), had an antitumor effect on mice bearing established lung metastases of B-16 melanoma. The maximal antitumor effect, observed by the changes in the weight of the lungs with the metastases, was attained at doses of 0.05–0.2 mg/kg. Ferrocene was also effective when administrated in the mice's drinking water. At low doses, Ferrocene activated the protooncogene p21ras (increased GTPase) and the kinase ERK1/2 (downstream of p21ras activation), stimulated lymphocyte proliferation, and activated peritoneal macrophages. Also, immune stimulation effects by ferrocene were observed as peritoneal mononuclear cells from ferrocene-treated mice were more effective than cells from untreated mice in eliciting an antitumor effect [340].

Complexes **Fe-1a** and **Fe-1b** (Fig. 46) were designed to combine the properties of the ferrocene moiety with ligands that are analogues to hydroxytamoxifen [339], known for its antagonist effect on MCF-7 hormone-dependent (ERα + ) breast cancer cells and for its lack of activity on hormone-independent (ERα-) MDA-MB-231 breast cancer cells. However, **Fe-1b** was shown to exert antiproliferative effect on both ERα + and ERα- breast cancer cells *via* mechanism of cellular senescence [341].

These two Fe(II) complexes were evaluated in the NCI-60 cell panel. The **Fe-1a** complex inhibited M14, SK-MEL-5 and UACC-62 cells with $GI_{50}$ values lower than 0.08 μM (NSC identifier 775548). Although not as cytotoxic as **Fe-1a**, complex **Fe-1b** was able to inhibit LOX IMVI, M14, SK-MEL-5 and UACC-62 cells with $GI_{50}$ between 0.1 and 0.5 μM.

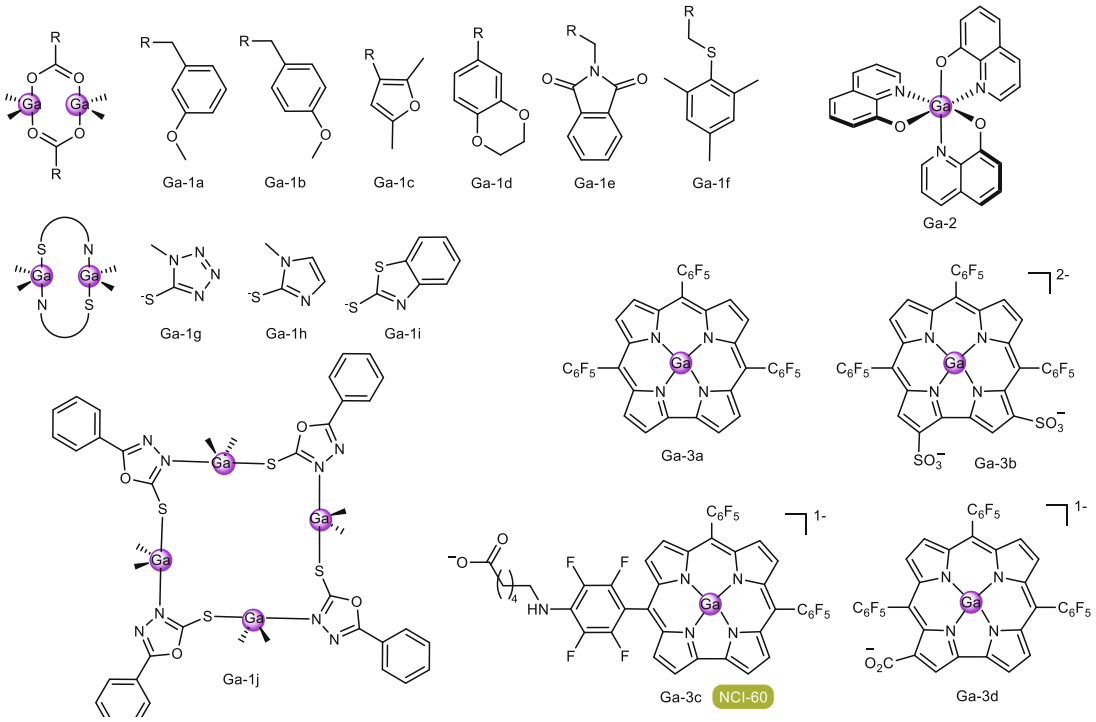


**Fig. 48.** Structure of Ga(III) complexes.

Two ferrocene complexes **Fe-1b** and **Fe-1c** were associated with lipid nanocapsules (LNCs) against melanoma cells *in vitro* and *in vivo*. The LNCs were adapted with small Bcl-2 interfering RNA (siRNA) encapsulation, to provide specific extinction of the Bcl-2, which is a key regulator in apoptosis pathways. Bcl-2 is up-regulated in melanoma metastasis, and its high level is associated to chemoresistance, poor prognoses and short survival rates in melanoma victims [342].

The efficacy of LNCs to deliver Bcl-2 siRNA and the Fe(II) complexes was tested on human SK-MEL-28 melanoma cells, in comparison to dacarbazine, the reference chemotherapy agent used in cases of metastatic melanomas. **Fe-1b** and **Fe-1c** showed significantly high cytotoxicity compared to dacarbazine on SK-MEL-28 melanoma cells with estimated $IC_{50}$ values of 3.0 μM and 1.2 μM, respectively. No difference in cytotoxicity was observed for these complexes administrated alone or in the LCN formulation. The LCNs with incorporated Bcl-2 siRNA did not influenced cell viability significantly. The only considerable synergic effect observed was in SK-MEL-28 cells treated with Bcl-2 siRNA and **Fe-1c** loaded LCNs, that reduced cell viability to 46%.

These formulations were also assessed *in vivo* by repeated intravenous injections in nude mice. It was found that LCN formulation with Bcl-2 siRNA alone was able to reduce tumor size by 25%, LCNs with **Fe-1c** caused the reduction in approximately 30% of tumor volume and concomitant treatment using LCNs loaded with Bcl-2 siRNA and **Fe-1c** was able to inhibit melanoma tumor growth by 50%, demonstrating synergic effects also *in vivo*.

Ferrocene complexes with juglone (**Fe-2a**) and plumbagin (**Fe-2b**) derivatives were evaluated against 518A2 cells in comparison to **Ru-20a** to **Ru-20c** [306]. Interestingly, **Fe-2a** was more cytotoxic to 518A2 cells ($IC_{50}$ = 0.5 ± 0.1 μM) than cisplatin ($IC_{50}$ = 4.1 ± 1.0 μM), plumbagin ($IC_{50}$ = 1.1 ± 0.2 μM), juglone ($IC_{50}$ = 1.9 ± 0.5 μM) and all the ligands and other Ru(II) complexes tested. On the other hand, **Fe-2b** was the only compound tested in this work that was not toxic to 518A2 cells ($IC_{50}$ > 50 μM), and it only differs from **Fe-2a** by the absence of one methyl substituent. This difference in

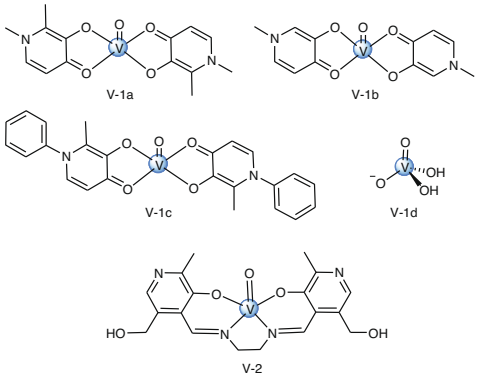


**Fig. 49.** Structure of the Vanadium complexes.

antiproliferative effects can be attributed to the nature of the ligands, however the presence of the ferrocene moiety considerably influences the toxicity of these two complexes, for reasons that are still unknown [306]. These ferrocenyl complexes also induced senescence in glioma and melanoma cell models. Interestingly, the effect was accompanied by secretion of various cytokines, including IL-1α, IL-1β, IL-6, IL-8, as well as TNF-α, suggesting an immune-stimulatory role of these Fe compounds [341].

### *3.9.2. Other Fe(II) and Fe(III) compounds*

The Fe(III) complex with 8-hydroxyquinoline ligands (**Fe-3,** Fig. 47) was studied by Chan *et al.* [343] specifically for application against head and neck SCC, BCC and melanoma. The complex was active in the micromolar range for A431, SCC25 and SCC9 squamous cancer cells ($IC_{50}$ between 1.8 and 2.5 μM), A375 melanoma cells ($IC_{50}$ = 2.9 μM) and BCC cancer cells ($IC_{50}$ = 5.3 μM), with only 24 h of incubation.

**Fe-3** caused apoptosis of SCC9 cells by cell cycle arrest during the G2/M phase and the arrest of SCC25 cells in the G0/G1 and

G2/M phases, which was associated with decreased cyclin B1/cdc2 and cyclin D/cdk4 expressions. Moreover, this compound also increases (ROS) and reduced glutathione (GSH) levels, and responds to increased p53 and p21 expressions. In summary, the complex induced the apoptotic cell death via cell cycle arrest, oxidative stress, intrinsic mitochondrial pathway and extrinsic death receptor signaling pathway activation in SCC cells.

The antiproliferative activity of Fe(II) (**Fe-4a**) and Fe(III) (**Fe-4b-f**) complexes, shown in Fig. 47, with the salophen ligand and varied azole-derived ligands was reported for G361 melanoma cells [344]. The complexes exhibited $IC_{50}$ values from 0.32 to 0.43 μM for the melanoma cells, while the $IC_{50}$ of cisplatin was 7.0 μM. The iron complexes were less toxic to LH32 normal human hepatocytes ($IC_{50}$ between 3.52 and 20 μM) than to G361 cells, showing some selectivity, especially **Fe-4f** (SI = 60.6). However, they are more toxic than cisplatin in LH32 cells ($IC_{50}$ > 50 μM). The complex **Fe-4f** is also distinct from the other complexes in this series due to its remarkable high activity over A2780 ovarian carcinoma cells ($IC_{50}$ = 58 nM) [344].

The effects of Fe(III) coordination on the cytotoxicity of thiosemicarbazones bearing a *L*-proline substituent was evaluated (Fig. 47) [345]. The ligands and the corresponding complexes showed a wide range of $IC_{50}$ values depending on the tested cell line. Against the FemX melanoma cells, ligands from **Fe-5a** and **Fe-5b** were not active, while those from **Fe-5c** and **Fe-5d** had average $IC_{50}$ values of 31 and 15 μM, respectively. Interestingly, while coordination to Fe(III) ions highly improved cytotoxicity for the first two compounds (mean $IC_{50}$ values of 53 and 25 μM for **Fe-5a** and **Fe-5b**, respectively), **Fe-5c** and **Fe-5d** were almost 1.5-fold less active than the corresponding ligands, which can be a result from different coordination geometries in solution and fine-tuning of lipophilicity.

### 3.10. Gallium

Gallium is similar in size (ionic radius) and coordination chemistry-related properties to iron, in particular Fe(III). This translates into gallium occupying the same protein binding sites as endogenous iron, but without the defining redox properties of the latter [346,347].

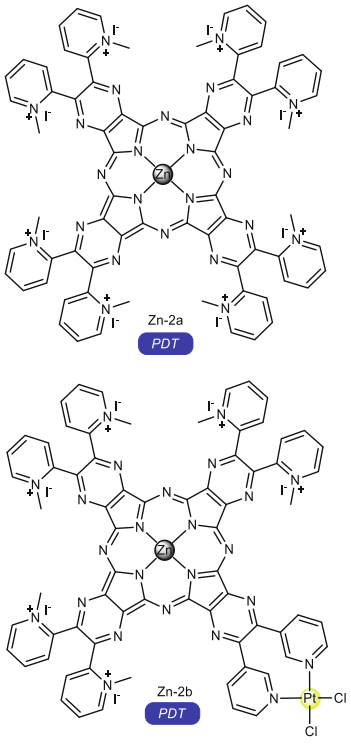


**Fig. 50.** Structure of the Zn(II) porphyrin complexes.

Ten polynuclear organogallium(III) complexes bearing carboxylate or N^S donor ligands, **Ga-1a** to **Ga-1j** (Fig. 48), were tested over a panel of head and neck squamous cell carcinoma cell lines by Kaluăerović *et al.* [348]. Cytotoxicity was determined by the SRB assay after 96 h of incubation and demonstrated modest to high $IC_{50}$ values, in the range 4–30 μM. Compound **Ga-1h** was the most active of the series against 4 of 5 tested cell lines (lowest $IC_{50}$ value of 4.33 ± 0.11 μM for FaDu cells and highest $IC_{50}$ of 13.74 ± 1.53 μM against A253 cells), which indicated that the 2-mercaptoimidazole moiety is important for the resulting activity. Interestingly a structural change from the 2-mercaptoimidazole motif to 2-mercaptobenzothiazole, **Ga-1i**, resulted in the least active compound. While all compounds were more active than $Ga(NO_3)_3$, only **Ga-1h** had a cytotoxic profile close to cisplatin. Further studies were performed with compounds **Ga-1c**, **Ga-1e** and **Ga-1h** on Cal27 (tongue) and FaDu (nasopharyngeal) squamous cells. Treatment with the compounds resulted in DNA fragmentation and formation of ladder-like fragments, which is a biochemical hallmark of apoptosis. Moreover, morphological analysis revealed that treatment with the Ga compounds and cisplatin led to chromatin condensation, loss of nuclear envelope and formation of apoptotic bodies. Different effects on the apoptotic pathway and cell cycle perturbation were observed depending on the tested cell line. For Cal27, the Ga compounds were able to induce apoptosis via a caspase independent pathway and they did not induce cell cycle arrest, but provoked a direct increase in the number of apoptotic cells. Contrastingly, treatment of FaDu cells resulted in apoptosis via a caspase dependent pathway, with effects on the G1 phase.

The Ga(III)-tris(8-hydroxyquinolinato) complex **KP46**, identified here as **Ga-2** (Fig. 48) was investigated against a panel of several melanoma cells, showing low $IC_{50}$ values (<4 μM) and higher activity than Ga(III) nitrate in all cases [349]. **Ga-2** is a lipophilic orally available complex that has strong bonds with the chelate quinoline ligands, which protect the gallium center from hydrolysis and allow facilitated gastrointestinal absorption [350].

**Ga-2** was tested in untreated melanoma cells from primary explants. Colony growth was inhibited in a concentration-dependent manner, where all samples treated with 15 and 5.0 μM of **Ga-2** showed 50 % growth inhibition and 4 out of 10 samples treated at 0.50 μM resulted in the same percentage of inhibition. **Ga-2** induced cell-cycle arrest in both 518A2 and A375 melanoma cells at the S-phase, with concomitant reduction in $G_0/G_1$ phase fraction. Microscopic analysis indicated signs of apoptosis in SK-MEL-28 cells treated with **Ga-2** for 48 h, including cell blebbing and fragmentation. Changes in the electrophoretic mobility of a circular double-strand DNA plasmid were not observed after incubation with **Ga-2**, indicating that this biomolecule is not a direct target of the gallium compound.

*I*n vivo studies showed that **Ga-2** had improved cytotoxicity and bioavailability when compared to simple gallium salts. The same compound displayed synergistic activities with cisplatin and might beneficial for combination approaches [350]. A 7-patient safety and pharmacokinetic study with **Ga-2** showed that it is tolerated at relatively high concentrations (480 $mg/m^2$), without expressive toxicity.

Gallium(III) corroles, **Ga-3a** to **Ga-3d** (Fig. 48), are luminescent macrocyclic molecules that have been investigated as anticancer agents [351]. The carboxylated compounds **Ga-3c** and **Ga-3d** showed $IC_{50}$ values against SK-MEL-28 melanoma cells of 14.4 ± 0.7 μM and 4.8 ± 0.3 μM, respectively. Contrastingly, the bis-sulfonated compound **Ga-3b** had an $IC_{50}$ value > 100 μM. The intense fluorescence of the compounds was explored to determine their uptake by SK-MEL-28 cells. Fluorescence imaging revealed the following order for cell uptake kinetics: **Ga-3d** ≫ **Ga-3c** > **Ga-**

**3b** ≫ **Ga-3a**, suggesting that carboxylate substitutions led to increased corrole permeability in cells. A single-dose experiment at 10 μM of **Ga-3c** was performed against the NCI-60 cell line panel. **Ga-3c** presented cytostatic activity against most of the NCI-60 cell line panel, inhibiting proliferation by 30% to 99%. Interestingly, lethality was only observed against 2 melanoma cells, LOX IMVI and SK-MEL-28, which indicated that this compound may be a selective chemotherapeutic agent for this type of skin cancer, an observation that requires further investigation.

### 3.11. Vanadium

Under biological conditions, vanadium can appear in oxidation states from 3 + to 5+ [352]. Vanadium(V) acts as a phosphate analogue, while vanadium(IV) behaves as a "divalent metal" [353], being able to replace either Zn(II) or Ca(II). Although not an essential micronutrient for humans, this structural similarity to ubiquitous biological species enables the use of vanadium compounds as enzyme inhibitors, anticancer agents and many other applications such as antidiabetic and antiparasitic.

Pisano, Rozzo and co-workers studied the effect of a series of vanadyl compounds on melanoma cells (**V-1a** to **V-1c,** Fig. 49) [354]. Vanadate (**V-1d**) was also included in this study, for comparison. The antiproliferative effects of these compounds were studied against A375 and CN-mel melanoma cell lines and a BJ fibroblast as a non-tumorigenic control. A375 was the most sensitive cell line to the vanadium compounds. **V-1b** and **V-1d** had $IC_{50}$ values of 2.6 and 4.7 μM, respectively. The compounds were also cytotoxic against CN-mel ($IC_{50}$ between 6.5 and 14 μM) and the non-tumorigenic BJ fibroblast, with $IC_{50}$ in the range 10.5 to 60.1 μM. In terms of selectivity (tumorigenic vs. non-tumorigenic), vanadate (**V-1d**) was identified as the best compound (A375 $IC_{50}$ = 4.2 μM; BJ $IC_{50}$ = 60.1 μM). **V-1b** and **V-1d** were the most promising compounds, and were evaluated in further detail to determine their mechanism of cell death. Cell cycle arrest was observed in A375, with G0/G1 arrest observed for **V-1b** and G2 checkpoint arrest for **V-1d**. PARP cleavage was also demonstrated by western blot for **V-1b**, confirming apoptosis as the mechanism of cell death induced on A375 cells.

Pyridoxal, a form of vitamin B6, has been explored as a ligand of vanadyl(IV) in the preparation of a complex with anticancer properties, **V-2a** (Fig. 48) [355]. The cytotoxicity of the complex against A375 melanoma cells was evaluated by the MTT assay, with varying incubation times. Remarkably, the $IC_{50}$ values decreased from 61.5 ± 1.5 μM at 24 h incubation to 6 ± 0.6 μM after 72 h. The authors also evaluated the cytotoxic effects of **V-2a** against NEK cells (human epidermal keratinocytes) and the $IC_{50}$ value after 72 h incubation was 68 ± 1.0 μM, demonstrating high selectivity. The complex induced apoptosis in A375 cells via ROS generation, mitochondrial membrane depolarization and caspase 3 activation. A375 cells treated with **V-2a** for 24 h showed a 140-fold increase in ROS levels when compared to controls. The long-term effects were evaluated by a clonogenic assay, which revealed that the number of colonies in A375 cells treated for 72 h with **V-2a** was suppressed by 99 %.

### 3.12. Zinc

The metalloporphyrins **Zn-2a** and **Zn-2b** (Fig. 50) are multicharged, water-soluble complexes that are able to act as excellent photosensitizers for the generation of singlet oxygen as cytotoxic agent for photodynamic therapy (PDT). **Zn-2b** differentiates itself from **Zn-2a** by the presence of a cisplatin-like functionality and the overall + 6 positive charge instead of + 8. The viabilities of C8161 and CA-1 cells were tested upon treatment with both complexes under irradiation with red light (660 nm) for 900 s (45 J/cm$^2$). **Zn-2a** and **Zn-2b** greatly inhibited the C8161 cells with $IC_{50}$ = 0.030 ± 0.010 μM and 0.075 ± 0.007 μM and CA-1 cells with $IC_{50}$ = 0.055 ± 0.008 μM and 0.105 ± 0.003 μM, respectively. Both complexes show similar cell uptake in the melanoma and SCC cells [356].

## 4. Results of clinical trials

### 4.1. Cisplatin and combination therapies containing cisplatin.

Cisplatin-containing treatments are by far the most reported in the literature for the therapy of SCC, BCC or melanoma. In this section, we highlight the most important findings of clinical trial results involving these compounds.

Carboplatin and cisplatin have been investigated as single-agent for treatment in chemotherapy-naive patients (patients that had little or no experience with chemotherapy) in a number of Phase II trials for melanoma, in which carboplatin has demonstrated an ORR of 19% [357], and cisplatin an ORR of 16% [358] (ORR = objective response rates; the proportion of patients with tumor size reduction of a predefined amount and for a minimum time period) that is similar to the ORR of dacarbazine [74].

The combination of carboplatin plus paclitaxel has been assessed as both first-line and second-line chemotherapy treatment for advanced melanoma. In a randomized Phase II trial as first-line treatment for advanced melanoma this combination exhibited an ORR of 16.4%, while same treatment with carboplatin plus paclitaxel and bevacizumab increased the ORR to 25.5%. However, no significant difference was observed in median progression-free survival (PFS) or overall survival (OS) [359].

In a retrospective review of 32 patients, carboplatin plus paclitaxel was efficient in treating patients with both cutaneous and non-cutaneous metastatic melanoma, including mucosal melanoma, after failure of a median of three previous systemic therapies in these patients. Carboplatin plus paclitaxel had a response rate of 22% and no significant difference between cutaneous and non-cutaneous cases. Median PFS was 2.5 months and OS was 5.3 months [74,360].

In Phase III trials in patients with advanced metastatic melanoma, carboplatin plus paclitaxel demonstrated, in a first-line setting, an ORR of 18%, median PFS of 4.2 months and median OS of 11.3 months [361]. In a second-line setting, on patients with unresectable stage III and stage IV melanoma, similar results for carboplatin plus paclitaxel were observed, with ORR of 11%, median PFS of 4.2 months and median OS of 10 months[362]. In both of these phase III trials there was no significant benefit seen with adding sorafenib to the combination. Due to the antitumoral activity of carboplatin plus paclitaxel, this treatment is widely used in the clinic for advanced melanoma, even though it is not a licensed therapy [74].

Carboplatin plus nab–paclitaxel has also been tested in another Phase II trial in patients with unresectable stage IV melanoma, in which an ORR of 26% and median PFS of 4.5 months was observed in 41 chemo-naive patients. Additionally, in 35 previously treated patients with metastatic melanoma, the ORR was 9% and median PFS was 4.1 months [74,363].

Cisplatin has also been tested in clinical trials in combination with two or more other drugs [364]. Chemotherapy combination regimens including cisplatin, vinblastine, and dacarbazine (CVD) as well as the dacarbazine, cisplatin, carmustine, and tamoxifen (Dartmouth Regimen) in patients with metastatic melanoma have yielded response rates of 30% to 40% in phase III trials, but conferred no significant advantage over dacarbazine in terms of response rate or survival time of the patients. Moreover, the combination therapies were significantly more toxic, showing hematologic and gastrointestinal toxicity and also peripheral neuropathy [364,365].

In a Phase III trial with 240 patients with metastatic melanoma [366], the Dartmouth regimen showed no statistically significant

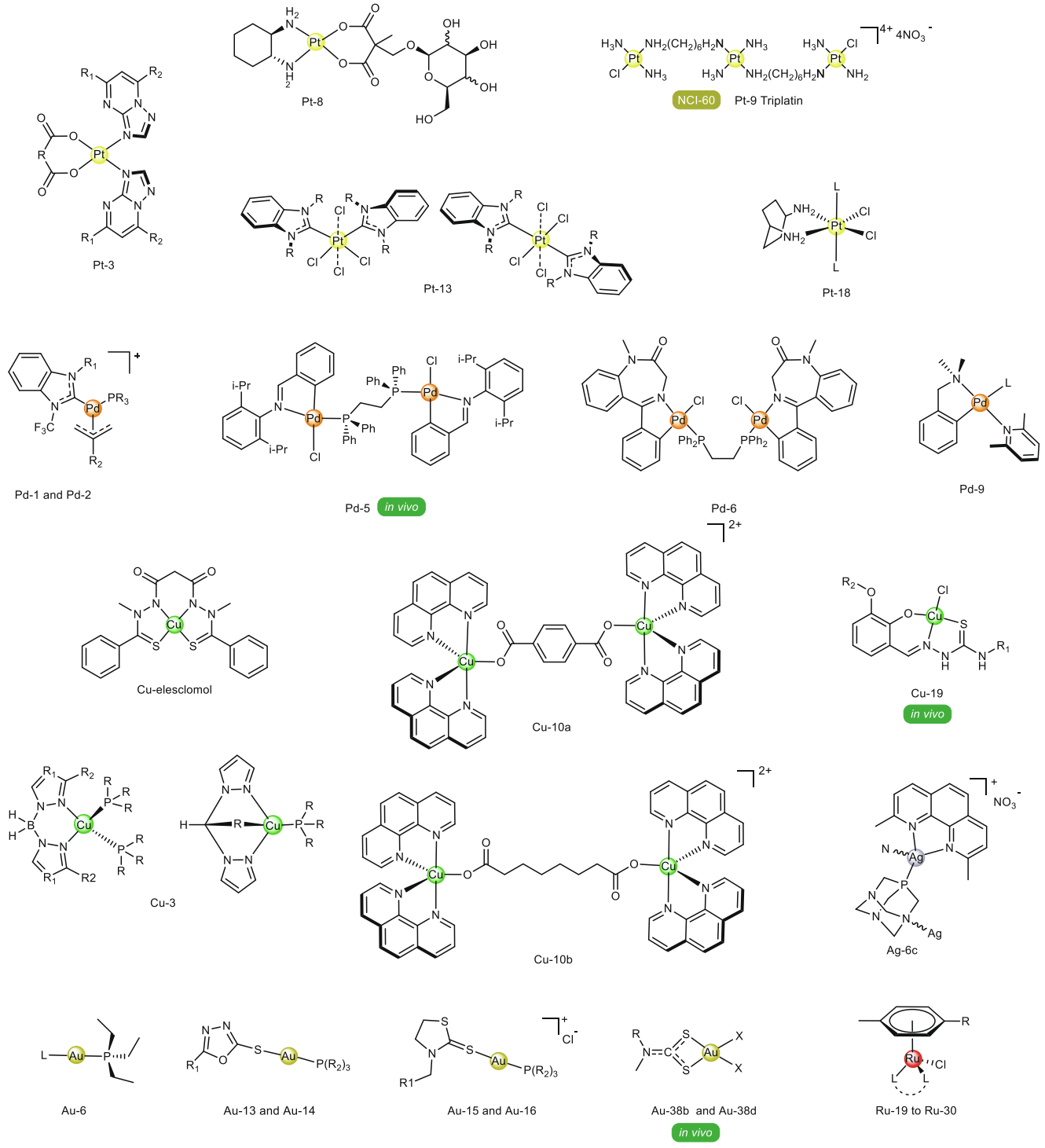


**Fig. 51.** General motifs of some of the most active metallodrugs identified throughout this review. These compounds ahve high potency *in vitro* against skin cancer cell lines without requiring light activation.

difference in ORR and OS over the standard treatment with dacarbazine and was also more toxic to the patients. Similar results were seen in a Phase III trial comparing the Dartmouth regimen with dacarbazine plus interferon (IFN) [367].

The effectiveness of the liposomal formulation of cisplatin, lipoplatin, have been tested in patients with SCC of the head and neck in low dosages. In this phase III randomized study, lipoplatin plus 5-fluorouracil was compared with the combination of cisplatin and 5-fluorouracil. In this case, lipoplatin plus 5-fluorouracil showed lower toxicity, specially nephrotoxicity and myelotoxicity. Mucositis and peripheral neuropathy were also much higher in the cisplatin group. However, response rates were higher in the cisplatin arm, showing that the liposomal formulation lowers the overall toxicity but might also decrease the effectiveness of cisplatin [368,369].

A phase II clinical study was performed to evaluate the effectiveness of electrochemotherapy with cisplatin administrated intratumorally on cutaneous tumour nodules in malignant mela-

noma patients. Four weeks after the treatment, 78% objective responses were obtained in the electrochemotherapy group (cisplatin plus electric pulses), and 38% objective responses were obtained in the group treated only with cisplatin. Tumour nodules exposed only to the electric pulses were not affected at all. Not only electrochemotherapy was well tolerated by the patients, but also good cosmetic effects were achieved, with minimal scarring and slight skin depigmentation. A follow up for 124 weeks showed a control rate 58% higher in the group treated with electrochemotherapy in comparison to monotherapy with cisplatin. Overall the procedure with electric pulses required lower doses of cisplatin, showed less side effects, had shorter duration and was well tolerated by the patients [370].

Pembrolizumab is an immunotherapeutic drug that has been shown to be active in head and neck squamous cell carcinoma (HNSCC), with the expression of programmed cell death ligand 1 (PD-L1) being associated with improved response [371]. Based on these promising results, a randomised, open-label, phase 3 study (KEYNOTE-048; registered at clinicaltrials.gov NCT02358031) of pembrolizumab given alone or in combination with a chemotherapy regimen of platinum and 5-fluorouracil for the treatment of locally incurable recurrent or metastatic SCC has just been carried out [372]. Pembrolizumab given with cisplatin or carboplatin and 5-fluorouracil significantly improved overall survival in the PD-L1 CPS of 20 or more population, PD-L1 CPS of 1 or more population, and total population compared with cetuximab, cisplatin/carboplatin, and 5-fluorouracil. Compared with standard therapy, the incidence of adverse events of any grade and of grade 3 or worse was lower with pembrolizumab monotherapy and similar with pembrolizumab plus chemotherapy. Statistical analysis demonstrated a significant survival benefit for pembrolizumab combined with cisplatin/carboplatin and 5-fluorouracil in the total and PD-L1-positive populations along with a manageable safety profile compared with standard therapy. The authors summarized that pembrolizumab plus chemotherapy represents a new standard-of-care treatment for patients with recurrent or metastatic HNSCC.

### 4.2. Elesclomol

Pre-clinical results indicated synergism between elesclomol and taxol, leading elesclomol to Phase III clinical trials in a paclitaxel combination for treatment of patients with advanced melanoma (NCT00522834) [373]. In the trial, 651 patients with stage IV melanoma were randomly treated 1:1 to paclitaxel 80 mg/m$^2$ either alone or in combination with elesclomol 213 mg/m$^2$. The study was stopped when an early overall survival data analysis indicated an imbalance in total deaths favoring paclitaxel, predominantly in patients with high lactate dehydrogenase levels. Therefore, the combination of elesclomol with paclitaxel did not significantly improve progression-free survival in patients. However, the study indicated a negative correlation between baseline LDH and elesclomol against melanoma.

## 5. Discussion and perspectives

### 5.1. Identifying lead compounds and their key features for the development of the next generation of active metallodrugs against skin cancer.

In this section we highlight what can be rationalized from the structures of the most active compounds found throughout this review, as illustrated in Fig. 51.

#### 5.1.1. Pt(II) and Pt(IV) complexes

The chemical motifs highlighted for these classes of compounds had dramatically better antiproliferative results than cisplatin. A general correlation with lipophilicity is often made, with emphasis given to the co-ligands of choice.

Nuclearity seems to play a major role on the cytotoxicity of platinum compounds against skin cancer cell lines. One of the best *in vitro* results for Pt(II) complexes is the antiproliferative activity of triplatin (**Pt-9**), which was the pioneer for the class of polynuclear Pt(II) complexes that have different mechanism of action and toxicity profile than the mononuclear complexes like cisplatin. Triplatin was able to inhibit SK-MEL-5, UACC-257 and UACC-62 cells at concentrations in the nanomolar range. Tetranuclear complexes **Pt-6a** and **Pt-6b** also exhibited outstanding $IC_{50}$ values in the nanomolar range against WM1366 human cutaneous melanoma cells, after light activation. The *in vitro* activity and the affinity of these porphyrin complexes to low density lipoproteins encourages further studies about their antitumor activity against melanoma.

Many Pt(II) complexes with distinct classes of ligands showed very low $IC_{50}$ values *in vitro* against skin carcinoma cells. It demonstrates how advanced is the research of anticancer Pt(II) complexes that was historically driven by cisplatin and its derivatives. It is important to highlight some complexes in these publications that were also tested *in vivo*, such as **Pt-8a**, a glycoconjugate that was very well tolerated in studies with DBA/2 mice models, and **Pt-3d** that had a much higher lethal dose than cisplatin and oxaliplatin in BALB/3C mice.

As for the Pt(IV) complexes, the pro-drug analogues to kiteplatin **Pt-18a** and **Pt-18b** had one of the best antiproliferative profiles *in vitro*, followed by the dimeric organometallic **Pt-21b** and the NHC-complex **Pt-13i**. Curiously, not much information was given about these complexes beyond *in vitro* antiproliferative assays, therefore it would be interesting to know more about the mechanism of action and even *in vivo* activity of these Pt(IV) complexes. In fact, no *in vivo* assays against skin cancer were identified in the publications of Pt(IV) complexes (**Pt-13g-f** and **Pt-17**–**21**).

#### 5.1.2. Pd(II) complexes

Most of the palladium(II) compounds studied as anti-skin cancer drugs with significative $IC_{50}$ values were organometallic compounds. Although there is not a clear pattern in the *in vitro* results for the Pd(II) complexes, some examples are highlighted. For example, **Pd-1** and **Pd-2** have unique chemical structures, containing NHC, phosphane and $\eta^3$-allyl ligands, and exhibited great antiproliferative activity ($IC_{50}$ in the single-digit μM or as low as 40 nM depending on the combination of co-ligands) against A375 melanoma cells. Therefore, these complexes might be part of a promising class of Pd(II) compounds to be further explored against melanoma.

Moreover, the binuclear complex **Pd-5** showed great activity *in vitro* against 501mel, ME1402 and WM1158 cells ($IC_{50}$ < 0.25 μM) with modulation of the ERK1/2 and p38 signaling pathway. This compound also displayed promising results *in vivo* in nude mice injected with ME1402. **Pd-6**, also a binuclear Pd(II) complex with a bridging phosphane ligand was able to inhibit a B16 cell line in the nanomolar range but was not yet tested *in vivo*. This shows that this class of Pd(II) complexes are also very promising and should soon be investigated further against melanoma *in vitro* and *in vivo*.

Finally, **Pd-9a** to **Pd-9d** are structurally simple organometallic complexes that were able to inhibit the murine melanoma B16-F10-nex2 cells at very low concentrations, with only 24 h of incubation. Also, they were able to inhibit SK-MEL-110 cells, that are resistant to apoptosis induction, in a time dependent manner with concentrations much lower than cisplatin.

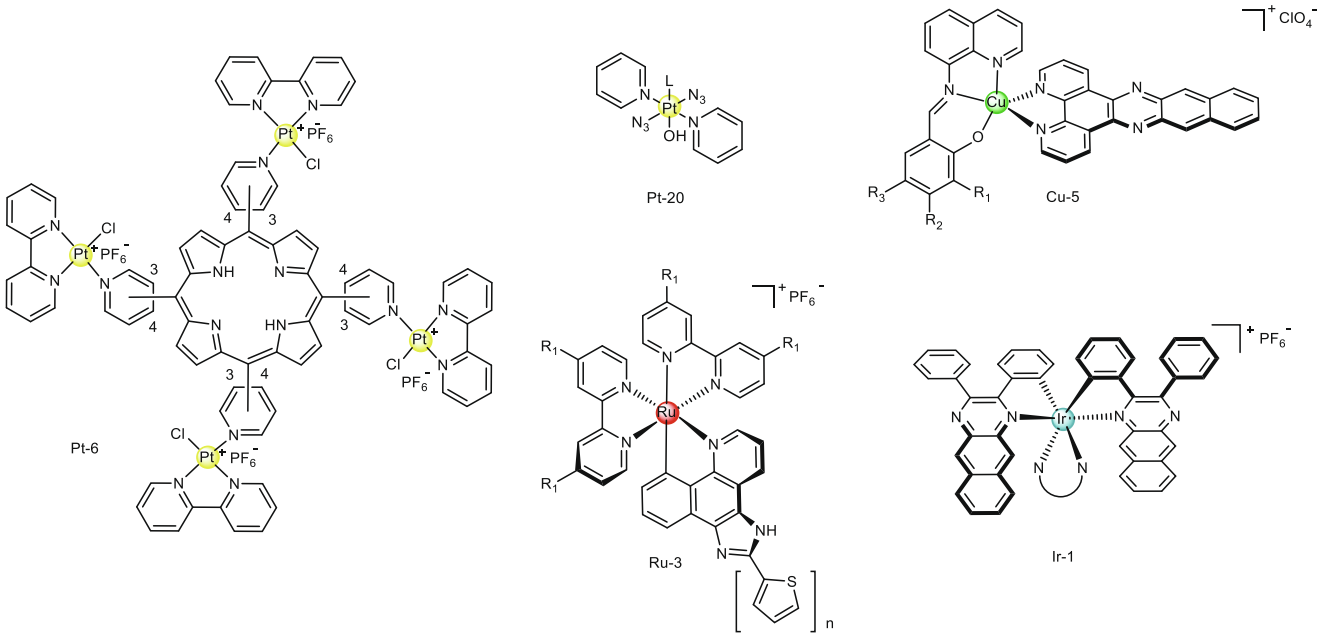


**Fig. 52.** Most active metallodrug motifs used for PDT of skin cancer cell lines *in vitro* identified throughout this review.

*5.1.3. Cu(I) and Cu(II) complexes*

Once again lipophilicity plays a major role in the activity of the compounds. Furthermore, disruption of mitochondrial function was often found for the most active compounds.

Analyzing the $IC_{50}$ values for the copper complexes in this review it is noticeable that the Cu(II) had generally higher activity than the Cu(I) ones, but also the number of Cu(I) examples reported here was much lower (only **Cu-1** to **Cu-3**). Complexes **Cu-2** and **Cu-3j** for example show very good antiproliferative activity *in vitro*.

The series **Cu-3** was rationally designed by combining either a bidentate or tridentate diazole/triazole with a phosphane co-ligand. The neutral compounds were more active than the cationic. **Cu-3j** was the most lipophilic and the most active in the series.

The Cu(II) complexes show consistent high antiproliferative activity *in vitro* against both melanoma and SCC cells. Complexes such as **Cu-elesclomol** and **Cu-19** not only show $IC_{50}$ lower than 0.1 μM, but also exhibited great potential *in vivo*. **Cu-elesclomol** may be used against melanoma once the advanced studies that already exist with the ligand elesclomol show that the binding to copper ions is essential for its anticancer activity. Interestingly, both **Cu-elesclomol** and **Cu-19** were found to bind or localize in the mitochondria.

The Cu(I/II) redox cycle is a marked characteristic often exploited in the mechanism of action of copper metallodrugs [374]. ROS production can be tuned depending on the ligand class and oxidative cleavage of biomolecules can be attained [143,144]. **Cu-9** interacted with DNA in an intercalative mode, preferentially to G-C rich regions of DNA, and was also responsible for ROS generation that caused DNA damage, such as double strand breaks. The superoxide anion radical is the main ROS generated by the complex and acts significantly on the decrease of cell viability. Another distinct class able to inhibit melanoma cells very efficiently was the Cu(II) metallonucleases **Cu-10a** and **Cu-10b**. The delocalized cationic charge and lipophilic nature of **Cu-10a** and **Cu-10b** was correlated with the preferential targeting of mitochondria and its membrane depolarization caused by ROS production. They were tested over the NCI-60 panel of cancer cells, where **Cu-10a** showed remarkable selectivity towards the SK-MEL-5 melanoma cells, with a $GI_{50}$ value of 46 nM. These results should encourage further biological evaluation of these complexes, apart from their already established ability to induce DNA breaks.

*5.1.4. Au(I) and Au(III)*

Au(I) represents the best example of efforts dedicated towards a systematic structural variation of a fixed motif (for example, the Au(I)-phosphane motif), and evaluation of the consequences on the activity of the compound. From classical studies, **Au-1** to **Au-12** were active against B16-F10, in particular the $Et_3P$-containing series **Au-6** as the most active, with $IC_{50}$ values as low as 0.4 μM (**Au-6b**, where the co-ligand is cyanide), followed by **Au-7**, where the labile chloride is fixed, and different phosphanes were evaluated (**Au-7d** is noteworthy, where the phosphane is $(Me_2N)_3P$). It becomes evident here that a combination of Au(I) with a highly basic phosphane (with electron-donating groups) leads to more cytotoxic agents. **Au-8** was much more inactive, where the chloride ligand was kept, and other ligands instead of phophane were evaluated (such as $Et_3As$, py, cod and others).

The Au(I)-phosphane motif remains highly investigated. In more recent examples, complexes **Au-13** and **Au-14**, that contain phosphane and mercaptooxadiazole ligands, showed the overall lowest $IC_{50}$ values between the Au(I) complexes (some complexes with $IC_{50}$ < 0.1 μM) against B16-F10 cells. For the same cell line, **Au-16b** and **Au-17h** also exhibited $IC_{50}$ < 0.2 μM. These complexes had antiproliferative results *in vitro* that are similar to auranofin, however none of them were tested *in vivo*. Comparing the **Au-13**, **Au-14**, **Au-16** and **Au-17**, it could be observed that: (1) in general, triethylphosphane compounds are slightly more active than the triphenylphosphane analogues, (2) adamantyl-substituted oxadiazole and thiazolidine ligands lead to less active compounds than phenyl or alkyl substituted ones, (3) the thiazolidine ligand may lead to more cytotoxic compounds, probably due to the cationic lipophilic nature of the resulting complexes which could improve cell uptake.

Interestingly, complexes **Au-24a-f** ($IC_{50}$ < 0.4 μM in 518A2 cells, tested *in vivo* on mouse xenografts of highly metastatic B16-F10 cells) are distinguished by one of the few examples of Au(I) complexes that show very low $IC_{50}$ values and do not contain phos-

phane ligands. Instead, these are high molecular weight bis-NHC complexes. Other interesting examples are the Au(I)/ferronece complexes **Au-25c**, that contain a phosphane and a NHC ligand, and **Au-25d** that is a complex with bis-NHC ligands. They inhibited 518A2 cells with $IC_{50}$ of approximately 0.2 μM and were also tested *in vivo* on a mouse xenograft model of invasive B16-F10 melanoma.

The whole data on gold complexes reveled that the best *in vitro* results with Au(I) complexes were achieved when they were stabilized by either a phosphane and a S-donor ligand or two NHC ligands (or in the case of **Au-25c** a phosphane and a NHC ligand). When one of these ligands is substituted by a halide for example, the antiproliferative activity of the corresponding complexes tends to be lower. Studies on Au(I)-phosphane derivatives indicated that the co-ligand can be introduced to add a functionality to this cytotoxic moiety, such as selectivity and improved cell uptake or luminescence.

On the other hand, looking at the least active Au(I) compounds, we identified most of the **Au-5** series, bearing $\mu_2$-S-bridged ligands (**Au-5a**, **Au-5b**, **Au-5c** and **Au-5e**); the **Au-8** series, Au(I)chlorido combined with miscellaneous ligands (**Au-8b**, **Au-8c**, **Au-8f** and **Au-8g**); and the **Au-17** series, where Au(I) is coordinated to two thiosemicarbazone ligands, each one by the = S (**Au-17c**, **Au-17e** and **Au-17f**).

The best *in vitro* activities of Au(III) complexes were identified for **Au-38a**, **Au-38b** and **Au-38d** against A431-R SCC cells ($IC_{50}$ values as low as 1 nM in the case of **Au-38d**), which are dithiocarbamato complexes designed to reproduce the main features of cisplatin. To the best of our knowledge, they were not evaluated *in vivo* against SCC, BCC or melanoma models so far.

Moreover, the cyclometallated **Au-40c** complex also exhibited outstanding *in vitro* activity, in this case against D24 melanoma cells ($IC_{50}$ = 0.97 ± 0.08 μM), with **Au-40a**, **Au-40b** and **Au-40d** not far behind. Even though complexes **Au-40a-c** are very promising against skin cancers *in vitro*, they were not yet tested *in vivo*.

#### 5.1.5. Ag(I) complexes

Although silver sulfadiazine is a classic example of a metallodrug administered topically for treating skin conditions (bacterial infections in burns), none of the compounds listed here have been assayed based on topical administration. Interestingly, NCI-60 data is available for silver sulfadiazine, with $IC_{50}$ melanoma cell lines MALME-3 M and UACC-257, of approximately 2 μM. Although the $IC_{50}$ values were not particularly low, silver sulfadiazine is well tolerated and a vast literature is already available on its biodistribution [256,375]. No data was found for silver sulfadiazine against SCC and BCC, leaving this opportunity open to be explored.

Most reports on the antiproliferative activity of silver(I) complexes found throughout this review were on melanoma cell lines, with only few examples found against SCC cells (A431 [257,258] and Cal-27 [265]).

Based on $IC_{50}$ values only, complexes **Ag-5b**, **Ag-5c**, **Ag-6c**, **Ag-6f** and **Ag-9** were the most potent. Similarly to what was observed for Au(I) complexes, the Ag(I) complexes **Ag-5b** and **Ag-5c** with phosphane ligands exhibited better antiproliferative profile than others. In the series **Ag-6**, compounds **Ag-6c** and **Ag-6f** showed lower $IC_{50}$ values, which can be attributed to their more favorable DNA interaction introduced by the N-heterocyclic ligands.

Additionally, complexes **Ag-9** and **Ag7a-c** are good examples of Ag(I) complexes that showed good antiproliferative activity in melanoma cells ($IC_{50} \leq 2$ μM) but do not include phosphane nor NHC ligands in their structure.

#### 5.1.6. Ru(II) complexes

Looking at the Ru(II) complexes that are not light-activated, the best *in vitro* results in general were achieved with arene complexes. Especially **Ru-22a-d** showed very low $IC_{50}$ values over 518A2 cells ($IC_{50}$ < 0.5 μM) and **Ru-27a-e** against CA-M75 and CRL7687 cells ($IC_{50}$ < 1.2 μM). Other examples of arene Ru(II) complexes with exceptional *in vitro* activity are **Ru-20a-c** ($IC_{50}$ < 2.3 μM), **Ru-25a** ($IC_{50}$ = 1.8 μM) and **Ru-26a-e** ($IC_{50}$ < 1.9 μM), all against 518A2 cells. The only Ru(II) compounds with $IC_{50}$ < 2.0 μM that do not coordinate arene ligands in this list are **Ru-11d**, **Ru-16b** and **Ru-16d**.

It is worth highlighting that the bifunctional Ru-arene compounds **Ru-22b** and **Ru-22c** [310], bearing the anti-angiogenic ligand naphthopyran had excellent antiproliferative results (**Ru-22b**, 518-A2, $IC_{50}$ 33 nM) and anti-angiogenic activity in chicken eggs and zebrafish models. The RAPTA compounds, (arene)Ru(II) complexes, have also antiangiogenic properties by inhibition of growth factor receptors such as fibroblast growth factor receptor (FGF-R1) or VEGFR [310,311] that could be explored against skin cancer cell lines and models.

In series **Ru-25** and **Ru-26**, lipophilicity also played a role on cytotoxicity. Both series have a phosphane ligand combined with a dangling (**Ru-25**) or coordinated (**Ru-26**) sulfide, sulfoxide or sulfone sidechain and systematically elongating $CH_2$ linkers. In both series, the longer the linker, the higher the activity of the compounds in the series against 518A2 melanoma cells. Some of the compounds in the series **Ir-6** (**a**,**b**,**c**,**f**,**g**,**h**) are analogues to compound **Ru-25**, with a dangling sulfide, sulfoxide or sulfone. The same SAR about the length of the linker is valid here.

In series **Ru-11**, the increasing planarity of the ligands and lipophilicity (Log P) of complexes when moving from **Ru-11a** to **Ru-11d** not only correlated with a more potent antiproliferative activity against A375, but also with their ability to inhibit TrxR. **Ru-11d** was an even more potent TrxR inhibitor than auranofin. VEGFR inhibition was also observed in this series.

### 5.2. Photodynamic therapy

Photodynamic therapy (PDT) is a procedure that activates a photosensitizer at a specific wavelength in order to generate ROS and induce cancer cell death [277]. In this context, metal complexes can be designed as excellent photosensitizers due to the unique interactions between metal and ligands orbitals. To promote toxicity in the cancer cell, the excited state of the photosensitizer metallodrug may either interact with oxygen to produce ROS (type I reaction), or the triplet state can directly transfer its energy to oxygen atoms to form singlet oxygen species ($^1O_2$) (type II reaction) [155]. PDT is a noninvasive method that has been investigated for the past 30 years due to the fact that far less side effects are observed when compared to conventional treatments [278,279].

Currently, topical PDT with the pro-drugs 5-Aminolevulinic acid (Levulan®) or methyl aminolevulinic acid (Metvix®) are being recommended by dermatologists to treat squamous cell carcinomas and actinic keratosis or basal cell carcinoma, respectively. These pro-drugs are intermediates in the biosynthetic process leading to protoporhyrin IX and then to heme, which act as photosensitizers. The protoporhyrin IX accumulates *in vivo*, especially in the cancer site, once neoplastic cells produce higher amount of porphyrins in the presence of these pro-drugs [278,280].

Topical PDT offers better safety profile over systemic photosensitizers, such as porfimer sodium, benzoporphyrin derivative monoacid ring A (BPD-MA) and *meta*-tetrahydroxyphenylchlorin, but falls short in efficacy against more invasive and metastatic tumors [279,280].

It is generally accepted that the triplet excited states of PSs exert their PDT effects through energy or electron transfer to ground state oxygen to produce ROS, most notably the cytotoxic singlet oxygen ($^1O_2$). Thus, PSs with appropriate triplet energy levels, high quantum yields for triplet state formation, and long intrinsic triplet lifetimes are highly desirable for PDT [281].

However, the reliance on $^1O_2$ for cytotoxic effects is a salient drawback and significantly diminishes the PDT effect in hypoxic tissue and solid tumors [282]. While well-oxygenated tumors that are superficial may respond well to traditional PDT, which is the case for superficial skin carcinomas, some of the most aggressive and drug-resistant tumors are a challenge that the metal complexes may be able to overcome by exerting oxygen-independent phototoxic effects by covalent modification of biomolecules such as DNA [282]. In addition, the organic PSs approved for clinical use cannot be activated by wavelengths of light that penetrate tissue best (e.g., >700 nm), limiting their use to superficial lesions [282].

For an overview of all the metallodrugs discussed throughout this review that used light activation for PDT of melanoma or KCs, see Fig. 36 (Ru compounds) and **Figure S3** (non-Ru compounds). The most active motifs are shown in Fig. 52.

Some metal coordination compounds may offer strategies that are different from $^1O_2$ generation, such as the photoactivated chemotherapy agents (PACT) that rely on light activation to release a toxic ligand, modify part of a ligand, change the oxidation state of the metal, or generate open coordination sites on the metal center to trigger its toxicity [276,294]. **Ru-6a** and **Ru-6b** for example are poor $^1O_2$ generators, however the light treatment activates these complexes by causing changes in the coordination sphere of the metal and allowing them to exert their antiproliferative activity, reaching $IC_{50}$ values as low as 0.88 μM for **Ru-6a** against A431 SCC. **Pt-20a-d** also do not rely on $^1O_2$ production as the light induces the change in oxidation state of the complexes from Pt (IV) to Pt(II), which leads to their toxicity. Other interesting examples are the complexes **Ru-5a** to **Ru-5e**, that not only exhibit phototoxicity, but also PDT-induced uptake, which created the prospect of using these complexes as theranostic agents.

Even though melanoma is highly resistant to traditional chemotherapy and also generally resistant to PDT [288], many examples of coordination compounds were able to selectively inhibit melanoma cells *in vitro* by PDT. The series of complexes **Ru-1**, **Ru-2** and **Ru-3** show the considerable advance in the development of Ru(II) complexes for PDT to obtain complexes with very low toxicity before light activation, using π-expansive ligands with a critical length higher than 4 repeating units. It allows these compounds to be, in some cases, >1000 times more cytotoxic when activated by the visible light treatment. For example, **Ru-3a** has an $IC_{50}$ of 0.087 μM when irradiated in the visible range in SK-MEL-28, vs. 1 μM in the dark. None of these compounds have been evaluated against either SCC or BCC cell lines to date, which represents an excellent opportunity for further studies.

The complexes **Pt-6a**, **Pt-6b**, **Ir-1b**, **Ir-1c** and **Ir-1e** exhibited even higher activities against melanoma cells after light activation ($IC_{50}$ < 20 nM), than the series of Ru(II) complexes with π-

**Table 3**
The skin-specific proteome. Information based on the Human Protein Atlas and related publications [377,378].

| Unique to the Skin | Gene | Description of the expressed protein |
|---|---|---|
| Stratum basale | COL17A1 | Collagen type XVII alpha 1 chain |
| | TP73 | Tumor protein p73; participates in the apoptotic response to DNA damage; $Cys_3His$ Zn(II) binding domain |
| Stratum spinosum | KRT10 | Keratin, type I cytoskeletal 10; plays a role in the establishment of the epidermal barrier on plantar skin |
| | CASP14 | Cysteine-aspartic acid protease (CASPASE) 14; a non-apoptotic CASPASE; the expression and processing of this caspase may be involved in keratinocyte terminal differentiation, which is important for the formation of the skin barrier. Regulates maturation of the epidermis by proteolytically processing filaggrin (FLG). |
| Stratum granulosum | FLG | Filaggrin; aggregates keratin intermediate filaments and promotes disulfide-bond formation among the intermediate filaments during terminal differentiation of mammalian epidermis. |
| | KPRP | Keratinocyte Proline Rich Protein; possibly involved in keratinocyte differentiation |
| Stratum corneum | CDSN | Corneodesmosin; undergoes a series of cleavages during corneocyte maturation. This gene is highly polymorphic in human populations. |
| | KLK5 | Kallikrein related peptidase 5; a serine protease with strong evidence to be implicated in skin desquamation and cancer. |
| Melanocytes | MLANA | Melan-A; involved in melanosome biogenesis. |
| | DCT | Dopachrome Tautomerase; catalyzes the conversion of L-dopachrome into 5,6-dihydroxyindole-2-carboxylic acid (DHICA). Related to oculocutaneous albinism. |
| | TYR | Tyrosinase; catalyzes the initial steps of the conversion of tyrosine to melanin. The enzyme has both tyrosine hydroxylase and dopa oxidase catalytic activities, and requires copper for function. Related to oculocutaneous albinism. |
| Langerhans cells | CD1A | Part of the CD1 family of transmembrane glycoproteins; structurally related to the major histocompatibility complex (MHC) proteins and form heterodimers with beta-2-microglobulin. The CD1 proteins mediate the presentation of primarily lipid and glycolipid antigens of self or microbial origin to T cells |
| | CD207 | Calcium-dependent lectin; displays mannose-binding specificity. Induces the formation of Birbeck granules (BGs); is a potent regulator of membrane superimposition and zippering. It binds to sulfated as well as mannosylated glycans, keratan sulfate (KS) and beta-glucans. It facilitates uptake of antigens and is involved in the routing and/or processing of antigen for presentation to T cells. |
| Hair | KRT75 and KRT71 | Type II cytoskeletal keratins; KRT75 is expressed in the outer root sheath, while KRT71 is expressed in the internal root sheath (Fig. 2) |
| | KRT34 | The type I keratin 34 (KRT34) is a protein expressed in the cortex. KRT34 heterodimerizes with type II keratins to form hair. |
| Skin glands | DCD | Dermcidin. Antimicrobial peptide important for the innate immune system. |
| | ELOVL3 | Elongation of very long chain fatty acids protein 3. Expressed in sebaceous glands, plays a role in the elongation of long chain fatty acids. |
| **Shared with** | **Gene** | **Description of the expressed protein** |
| Tongue | KRT15 | Kerating KRT15; component of the cytoskeleton and associated with epidermis development and keratinization. |
| | SLURP1 | a member of the Ly6/uPAR family of proteins, is suggested to be involved in late differentiation, predominantly expressed in the granular layer of skin. |
| | LGALS7 | Galectin 7; a member of the family of beta-galactoside-binding proteins known for playing a role in cell–cell and cell-matrix interactions. This particular galectin is specific to keratinocytes. The desmocollin protein family is known to be mainly found in epithelial cells. |
| | DSC3 | The desmocollin protein family is known to be mainly found in epithelial cells. This protein in particular is a component of desmosomes and thus essential for cell-to-cell adhesion. |

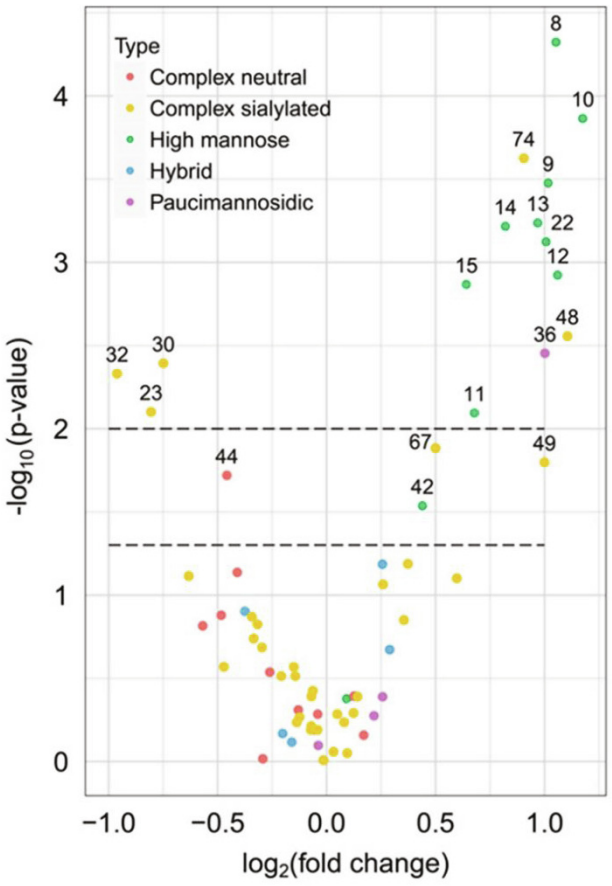


**Fig. 53.** N-glycan level changes in basal cell carcinoma. Volcano plot for the quantified N-glycan species indicating significant changes of relative abundance levels for individual N-glycan species. Two p-value thresholds are indicated (p = 0.05 and p = 0.01). N-glycan abundance levels above the second threshold were considered as significantly changed. Adapted from Kolarich et al.[380].

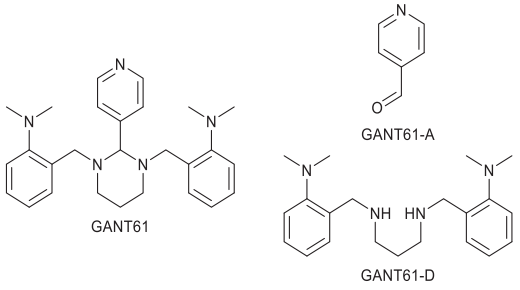


**Fig. 54.** Chemical structue of the Gli1 and Gli2 inhibitor GANT61 and its hydrolyses products: the molecule GANT61-A and the bioactive species GANT61-D.

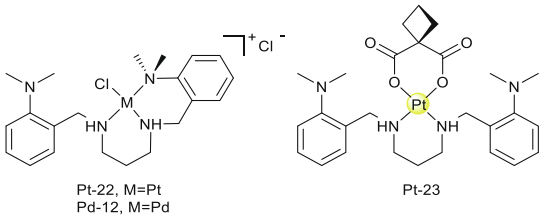


**Fig. 55.** The molecule GANT61-D as a coordination motif for Pt(II) and Pd(II) complexes.

expansive ligands. These are excellent candidates for more in-depth studies, including animal and potential clinical studies, as part of PDT regimens for the management of local melanoma.

The complexes **Cu-5a** to **Cu-5f**, that were tested under PDT conditions, also show outstanding activity, this time against SCC cells *in vitro* ($IC_{50}$ < 0.1 μM, PI values between 100 and 300). The series **Cu-5b** to **Cu-5f** is a rare example found in the literature where the antiproliferative activity was assessed against a BCC line. The compounds had remarkable phototoxicities, with $IC_{50}$ < 0.1 μM upon light activation, with PI > 100 in all cases.

Although considerable advance have been made in the development of PDT agents, there are some reasons why PDT is not a mainstream strategies for cancer treatment in the clinic, such as the extensive therapeutic protocols needed (light and drug dose, light source, interval of irradiation and drug administration), the lack of existing standardized protocols and the fact that large randomized clinical trials have either not been carried out or could not prove significant advantage over existing therapies [287,376]. Nonetheless, there is an opportunity to develop some of these complexes as PDT agents that are specific to skin malignances, given the general topic nature of non-invasive skin carcinomas. Therefore, PDT combined with other target strategies could lead to more complexes going to clinical trials and eventually being approved.

### *5.3. New directions and unexplored strategies for skin cancer targeted therapies using metallodrugs*

#### *5.3.1. The Chemical Structure of the Skin: insights from modern 'omics' and implications for the development of new therapy strategies targeting skin cancers*

In-depth analysis of the genes elevated in skin, using antibody-based protein profiling, is available through the Human Protein Atlas [377,378]. It has untapped potential for the development of targeted therapies based on metallodrugs, exploiting the unique (chemical) characteristics of the skin. A summary of proteins specific for the keratinocytes in different layers of the epidermis [377,378], e.g. stratum basale, stratum spinosum, stratum granulosum and stratum corneum, and other specific cell types present in the skin, e.g. melanocytes and Langerhans cells is given in Table 3.

For information on the human pathogeny proteome of melanoma, the reader is directed to the Human Protein Atlas.

A detailed characterization of the glycan composition of the skin upon alterations related to skin cancer have attracted much interest in the past decade.

Atomic Force Microscopy (AFM) has been used to investigate the distribution of proteoglycans in the skin using a cantilever tip functionalized with either the anti-heparan sulfate or the plant lectin wheat germ agglutinin (WGA) antibody [379]. Heparan sulfate proteoglycans and glycosylated corneodesmosin proteins such as corneodesmosin are distributed evenly on the surface of corneocytes in the lower layers of the stratum corneum, whereas in the

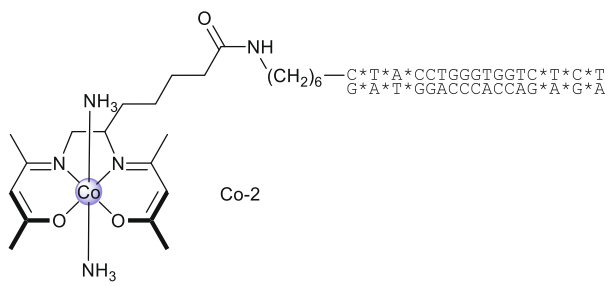


**Fig. 56.** Co(III) Schiff base-DNA conjugates developed by Meade and co-workers for targeting the Drosophila Gli-analogue protein Ci.

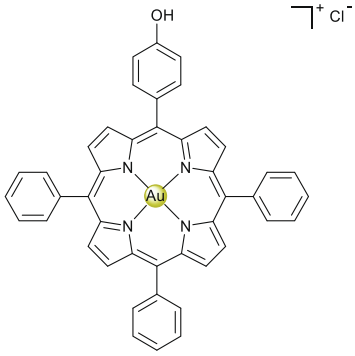


Au-41

**Fig. 57.** Chemical structure of Au(III) porphyrin complex **Au-41**.

upper layers, these glycans are found typically at the periphery of corneocytes [379].

Changes in the human skin glycome upon the development of SCC and BCC is a topic that has started to be investigated just recently.

Kolarich and coworkers [380] have demonstrated alterations in the human N- and O-glicome in tissue samples from patients with SCC and BCC, in comparison to biopsies of healthy cutaneous tissue. Analysis of the healthy skin from cancer patients was found to consist mainly of glycoproteins carrying sialylated N-glycans. Biantennary, sialylated N-glycans were the dominating structures, comprising on average about 82% of the human skin N-glycome. Interestingly, approximately half of all detected human skin N-glycans were fucosylated with the fucose residue being almost exclusively attached to the N-glycan core. The skin tissue O-glycome was less diverse, consisting of simple Core 1 and 2 type O-glycans. The authors compared the glycome profile of healthy skin samples with that of both BCC or cutaneous SCC obtained from the same patient to minimize per patient variations.

In BCC, the authors identified that virtually all oligomannosidic N-glycans had increased (2x) abundance, resulting in the whole class being differently expressed in BCC. Oligomannose type N-glycans exhibited the highest fold change (2 × ) followed by an α2-3/2–6-sialylated structure (ID 74), a bisected, α2-3/2–6-sialylated (ID 48), and a paucimannosidic N-glycan (ID 36), Fig. 53. Regarding the O-glycans profile, BCC tissue samples showed significant level changes for various structures. Core 1 type O-glycan levels were reduced while core 2 type O-glycans experienced upregulation.

In SCC oligomannose carrying N-glycans showed increased levels, while α2-3-NeuAc N-glycans were less abundant compared with healthy tissue. With an average 1.56-fold upregulation in tumor samples, oligomannose N-glycans showed a similar trend in SCC as demonstrated for BCC. The total abundance of sialylated N-glycans was reduced from 70% in healthy tissue to 64% in SCC. 2 type O-glycan levels were also increased in SCC, albeit to a lesser extent than in BCC. Qualitative analysis indicated that most of the identified glycoproteins were involved in binding activities such as receptor binding, protein complex binding, or cell adhesion and molecule binding.

These results highlight the potential of exploiting mannose-targeting compounds in the development of anti-BCC and anti-SCC metallodrugs.

In the case of melanoma, the most frequently used model to study the connection between glycosylation and metastatic behaviour is the B16 murine melanoma cell line and its sub-lines of a different metastatic potential [381]. Detailed analysis of B16 sub-lines with high- and low-metastatic potentials has revealed that although these sub-lines expressed comparable amount of sialic acids, α2,3-linked sialic acids were predominantly found in high-metastatic sub-line, while α2,6-linked sialic acids were observed in low-metastatic sub-line [382].

Within this context, exploiting the different glycan composition of the healthy skin vs. skin cancers represents a promising field that expands on the field of metalloglycomics [383-387].

*5.3.2. The Hedgehog pathway*

As previously mentioned, mutations on the patched 1 (PTCH 1) gene [43] and p53 [44] aberrant Hedgehog signaling are pivotal defects leading to formation of BCC [42,45]. It was also shown that an aberrant hedgehog/Gli1 signal pathway facilitates proliferation, invasion, and migration of cutaneous SCC through regulating vascular endothelial growth factors [72].

Many small molecules have been developed or identified as Hedgehog signalling inhibitors or modulators *in vitro* and *in vivo*. In addition to vismodegib and sonidegib (shown in Fig. 3), both SMO-inhibitors, other examples include Robotnikinin, which targets Sonic hedgehog (Shh) *in vitro*; and Gant-58 and Gant-61, which acts on Gli [388,389].

As explored in the Introduction, signalling in the canonical Hh pathway has at the distal end the Gli genes Gli1 and Gli2. Both Gli1 and Gli2 are oncogenes, constitutively activated in many types of human cancers [390]. It has been demonstrated that targeting Gli1 and Gli2 (zinc finger transcription factors) can even restore sensitivity to vemurafenib in human melanoma cells resistant to the drug [391]. For targeting Gli, the molecule Gli-antagonist 61 (GANT61, Fig. 54) was identified as a Gli1 and Gli2 inhibitor [392]. GANT61 hydrolyses under physiological conditions, leading to the formation of the bioactive diamine species GANT61-D and the bridging species GANT61-A [393]. Surface plasmon resonance (SPR) and molecular docking studies indicated that GANT61-D binds to the 5-zinc finger Gli1 between the second and third ZnF domains, effectively inhibiting Gli1 binding to DNA [390,392].

Griffith and co-workers explored GANT61-D as a coordination motif for Pt(II) (**Pt-22** and **Pt-23**), Pd(II) (**Pd-12**) and Ni(II) (Fig. 55) [394]. The authors evaluated the antiproliferative activity of the compounds against medulloblastoma cell lines (which have aberrant Hh signaling). Interestingly, only the complexes of labile metals (Pd(II) and Ni(II)) had appreciable cytotoxicity, which was also comparable to that of the free GANT61 and GANT-61D. This data strongly suggests the release of the GANT61-D ligand. The compounds were not assayed against skin cancer cell lines yet. This is the very first example found in the literature of a metal complex with a hedgehog pathway modulator and the study of this class of compounds against melanoma and BCC cell lines is of high interest.

Still on the Hedgehog pathway, Meade and colleagues have developed a strategy for introducing selectivity in a cobalt compound by targeting a $Cys_2His_2$ transcription factor (Fig. 56) [395]. The Drosophila analogue to the human Gli proteins is the single Cubitus Interruptus (Ci), with an identical DNA binding consensus sequence. To exploit this interaction, Meade's group combined a Co (III) Schiff base compound with the Ci's consensus sequence (**Co-2**, Fig. 56). This compound was found to selective inhibitor of Ci by irreversibly binding the Ci zinc finger domain and preventing it from binding DNA *in vitro*. Reduced transcriptional activity of Ci was found *in vitro*, and using wild type Drosophila embryos, the activity of the conjugate was also demonstrated *in vivo* [395].

*5.3.3. Wnt/ β-catenin signaling pathway*

Alterations of β-catenin pathway in non-melanoma skin cancers have been identified by Doglioni and co-authors [396]. In the nucleus, β -catenin mediates the extremely complex T-cell factor/-lymphoid enhancer factor (Wnt/TCF) signaling. The study demonstrated that among human skin neoplasms, β-catenin gene

mutations are a peculiar feature of the tumors of matrical origin. β-catenin nuclear accumulation was found in BCC [396] and the authors summarized that abnormalities of Wnt/ β-catenin signalling pathway play a role in a large spectrum of skin neoplasms, although mutations of β-catenin seem to be a specific hallmark of tumors with matrical differentiation [396]. In melanoma, Shakova and colleagues demonstrated that the activation of Wnt signaling has a profound effect on melanoma growth and is able to counteract Sox10-dependent melanoma maintenance both *in vitro* and *in vivo* [397]. In this context, to the best of our knowledge the Wnt/ β-catenin signalling pathway has not been explored in the development of metallodrugs targeting skin cancers, although Che's group demonstrated that the Au(III) porphyrin complex (**Au-41,** Fig. 57) attenuated the Wnt/β-catenin pathway [398] through inhibition of class I HDAC activity in a panel of breast cancer cells.

*5.3.4. Protein Disulfide Isomerase*

The protein disulfide isomerase (PDI) family is a group of abundant redox proteins found in endoplasmic reticulum, cell surfaces, cytosol and extracellularly. PDI plays a key role in the defense against general protein misfolding due to its redox-dependent chaperone activity. PDI also catalyzes the isomerization, formation and rearrangement of disulfide bonds [175,399]. Overexpression of some PDI family members occurs in a wide variety of cancer types, including melanoma, and frequently correlates with metastasis and invasiveness. The oncogenic effects of PDI proteins are apparently mediated by their role in the unfolded protein response (UPR) signaling pathway, which involves endoplasmic reticulum stress response caused by disturbances in proteostasis. Therefore, PDI inhibitors can potentially damage their pro-survival role and enhance apoptosis in cancer cells or sensitize them to anti-cancer agents [174,176].

Heffeter and co-workers recently associated the anticancer activity of some clinically-relevant thiosemicarbazones, a class of ligands that has been used for many years in coordination chemistry, to their capability of disrupting endoplasmic reticulum homeostasis by *in situ* formation of highly stable and slowly reducible Cu(II) complexes that can target PDI and induce paraptosis [400,401]. Among the examples discussed in this review, one single study has evaluated the anti-PDI activity of a series of metallodrugs and how it was correlated to the antiproliferative activity of the compounds against a melanoma cell line. Gandin and coworkers have recently reported Cu(II) complexes of thiosemicarbazones that inhibited PDI *in vitro* (**Cu-19a to Cu-19f**) and displayed nanomolar $IC_{50}$ values against a panel of cancer cell lines that included A375 melanoma cells [173]. These results show that PDI is an emerging target for metallodrugs that can be further explored specifically for skin cancer therapy.

*5.3.5. Bromodomain and extra-terminal domain (BET) proteins*

The Bromodomain and Extra-Terminal Domain (BET) family of proteins is characterized by the presence of two bromodomains and an extra-terminal domain. Bromodomains can specifically bind to acetylated lysine residues in histones and they are epigenetic readers that regulate gene transcription [402,403]. BET proteins have been reported as drivers of tumorigenesis in many human cancers, including melanoma and cutaneous SCC, therefore targeting them with inhibitors may result in antiproliferative and antimetastatic effects [404-406]. **Ir-3a** and **Ir-3b** were the first metal-containing compounds reported as inhibitors of protein–protein interaction between BRD4 (bromodomain-containing protein 4) and H4AcK4 (tetra-acetylated lysine histone 4 peptide). This effect was associated to its ability to repress cancer cell growth and high activity against *in vitro* and *in vivo* melanoma models [325]. Coordination complexes and organometallic compounds have structural and electronic properties that can be tuned to target protein–protein interactions; therefore, BET proteins may be further explored as targets of metallodrugs, especially in skin cancer.

*5.3.6. Hypoxia-inducible factor and glucose transporters*

Hypoxia is a major feature of most human cancers, and it results from the limited diffusion of oxygen in poorly vascularized tumors. Under hypoxia, glycolysis becomes the major glucose metabolism in tumors, a phenomenon known as "the Warburg effect". Glycolysis results in reduced yield of ATP when compared to mitochondrial oxidative phosphorylation, which correlates with the increased consumption of glucose by tumor cells to maintains abnormal growth rates [407]. This metabolic adaptation in tumor cells affects oxygen-responsive pathways, especially the hypoxia-inducible factor (HIF) family. Hypoxia-inducible factor 1 (HIF-1) becomes active in hypoxic conditions promoting the transcription of a number of genes, including of glucose transporters (GLUT). GLUTs are a family of proteins that transport sugars along the concentration gradient [407,408]. Overexpression of GLUTs could be a possible target for development of inhibitors, thus blocking glucose uptake [407]. Another strategy is to exploit GLUT overexpression for targeted delivery of drugs based on conjugation of the (metallo)drug to a glucose or glucose-like substrate [407]. Compounds **Pt-8a** to **Pt-8c** were developed using this strategy of glycoconjugation, resulting in compounds with improved uptake by cancer cells.

Even though postnatal human epidermis is the only epithelium in direct contact with atmospheric oxygen, lack of tissue vasculature results in a mildly hypoxic microenvironment that favors increased expression of HIFs, especially in the basal layer [409]. Since HIF-1 plays a role in tumor glycolysis and has low activity in normal tissues, it is an attractive target in selective cancer chemotherapy [407]. There are reports correlating overexpression of HIF-1 with BCC, cSCC and melanoma, making this pathway promising to target in skin cancer [410-412]. This is further reinforced by the influence of UV radiation exposure, a proved environmental risk factor for KCs, and expression of HIF-1 [412,413].

*5.3.7. Inflammation and skin cancers*

It is important to highlight that SCC can be prevented by treating the precursor inflammatory condition known as actinic keratosis, with use of retinoids, cyclooxygenase-2 (COX-2) inhibitors, difluoromethylornithine, and epigallocatechin gallate (EGCG, a green tea catechin) [414]. Topical therapy of KC with nonsteroidal anti-inflammatory agents (NSAIDs) has proven to inhibit neoplastic cell proliferation by inducing apoptosis, and it seems that there is a very strong link between COX2 activity and the expression of antiapoptotic proteins of the Bcl-2 family [415,416].

Normal skin has low levels of COX2 and PGE2 (prostaglandin E2), but COX2 is overexpressed in several epithelial tumors according to the severity of the malignancy [415]. The activity of COX2 results in the release of several prostaglandins including PGE2 which is the major mediator of acute inflammatory responses, as well as tumor growth. PGE2 is associated with cancer mainly because it mediates processes that play essential roles in tumor cell proliferation, invasion, angiogenesis, and immunosuppression [280,417].

In that context, the development of metal complexes with anti-inflammatory properties may play an important role. Auranofin, for example, was successful in treating cutaneous staphylococcal infections in a mouse model of MRSA (Methicillin-resistant *Staphylococcus aureus*) skin infection. The same work also shows that Auranofin reduces inflammatory cytokines induced by MRSA skin infection [418], which is an interesting property against inflammation but also to inhibit growth of skin carcinomas [418].

In a large-scale screening performed by the US National Cancer Institute, Auranofin was tested against 9 melanoma cell lines, and

for all of them the $GI_{50}$ was $\leq$ 0.5 μmol/L [82]. Later, Sachweh and coworkers suggested that Auranofin should be a candidate to treat malignant melanoma due to the inhibition of selenoprotein thioredoxin reductase 1 (TrxR1), which is important for redox regulation of cellular function [199]. The antitumoral activity of Auranofin had been reported for many types of cancer, including an ongoing clinical trial against leukemia [193]. However, Auranofin has been underexplored for the treat skin carcinomas by itself or as part of topical formulations.

Besides Auranofin, complexes **Au-40a-d** also showed anti-inflammatory activity, by inhibiting the secretion of pro-inflammatory cytokines in LPS-activated macrophages. Additionally, these complexes were able to inhibit the D24 melanoma cell line with concentrations 10-fold lower than cisplatin [252].

The complex **Rh-3**, that was effective against malignant A375 melanoma both *in vitro* and *in vivo* (Balb/c mice), also showed anti-inflammatory potential as it was able to reduce the expression of COX-2 and inducible nitric oxide synthase (iNOS) in the tumor tissues. The antitumoral, antiangiogenic and anti-inflammatory activities of this complexes are linked to its ability to inhibit STAT3, which plays an important role in the development of skin cancer [333].

Very few examples of Ag(I) complexes applied for skin cancer therapy were found in the recent literature, which is surprising given the very established anti-tumoral and anti-inflammatory properties of silver ions [419,420]. The anti-inflammatory properties of Ag(I) ions in wound surface for example are recognized for centuries and have been demonstrated histologically [253]. The most obvious reason for the lack of interest in Ag(I) ions for topical treatments of cancer seems to be the low stability when exposed to light, producing typical black stains on the skin [256]. However, silver sulphadiazine is an example of a stable complex used with FDA approval as antibacterial agent for topical treatment of burns and wounds [256].

Ag-nimesulide (**Ag-12**), the silver compound based on the anti-inflammatory drug nimesulide, administered topically was active *in vivo* on Balb/c mice bearing SCC [266]. Although it is still not fully elucidated, the presence of the anti-inflammatory ligand might play a role on the treatment of the SCC in mice by inhibiting the inflammation process in the vicinity of the lesions and therefore aiding in the suppression of the tumor. The topical administration might also increase the already existent selectivity of the complex against SCC by releasing a constant small concentration of the drug during a very long time, reducing the chances of acute toxicity, accumulation of the drug in internal organs of the mice and general adverse effects.

#### *5.3.8. Antibody-drug conjugates*

Our literature search reveals the untapped opportunity for development of metallodrugs-antibody conjugates with the typical ipilimumab [75], pembrolizumab [76] and nivolumab [77], that are inhibitors of the PD1/PDL1 interaction [74] and proposed for melanoma immunotherapy. No examples of works dealing with the topic have been found so far.

## 6. Outlook

Here we have presented the many advances made on the development of metallodrugs as antiproliferative agents against skin cancer in the previous two decades. We compiled > 1100 entries of *in vitro* antiproliferative data spanning 15 metals against 45 melanoma, squamous cell carcinoma and basal cell carcinoma cell lines. This compilation is available to the community as smart table on the open-source repository Zenodo (https://zenodo.org/record/5055531) [81]. We encourage the community to add extra information to this table whenever new data on metallodrugs against skin cancer cell lines are available. We believe this could help fomenting new advances in the area. The information is compiled along with structural parameters for each of the compounds, such as molecular weight with and without the counter-ion, charge of the compound, oxidation state of the metal center and ligand type. Information on the antiproliferative assay is also given, such as cell line and incubation time. Additional details, such as when the compounds have been tested under PDT settings, against the NCI-60 panel of cancer cells and in *in vivo* models are also provided in the table. This set of data can be easily further explored by computation chemists using deep learning [421,422] and fragment-based drug discovery [7] strategies for example, to obtain further information on structure–activity relationships to guide new developments in the area.

In terms of new directions, we believe that all the recent advances on the understanding on the many signaling pathways are unique to skin cancers and melanoma, and can be exploited for the development of more selective therapeutic compounds. In addition, in recent years the unique glycome and proteome of the skin affected by skin cancers has been elucidated, opening even further avenues to drug design. This knowledge has untapped potential that can guide the development of new chemotypes to exploit the molecular biology of the skin for the rational design of even more potent and selective metallodrugs.

Following the history of development of metallodrugs, the only examples of metallodrugs in clinical trials for the specific treatment of skin cancers are platinum compounds. The remarkable advances of ruthenium compounds in clinical settings (NAMI-A, KP1019, KP1339 and, more recently, TLD1433 for PDT) highlight a promising future for non-platinum metallodrugs for cancer treatment. Despite a few cases in safety and pharmacokinetic phase I studies that included melanoma-bearing patients, these Ru compounds are yet to be fully tested for efficacy in clinical settings specifically against skin cancers. Many other promising chemotypes identified throughout this review are also excellent starting points for further structural modifications.

Finally, studies of topical treatments for KCs and local melanoma using metallodrugs are extremely rare and deserve further attention of the community.

## 7. Skin cancer and related cell lines for *in vitro* screening

Our searches included melanoma, squamous cell carcinoma and basal cell carcinoma cell lines. However, only a few studies reported cytotoxicity values over KC cell lines. This seems a result of the intrinsic difficulty to propagate skin carcinoma cells *in vitro* and to establish cell lines [423]. Therefore, examples involving KCs also included those containing cell lines derived from other tissues (for example, head and neck SCC). Established cutaneous SCC cell lines are recently being published and *in vitro* models are becoming more complex and more representative of real skin and are worth to be evaluated as models for skin cancer. Table 4 lists all the cell lines mentioned throughout this Review.

One cell line that has been historically misidentified as a nasopharyngeal epidermoid carcinoma (squamous cell carcinoma) is called KB [236]. The KB cell line actually corresponds to a HeLa cell line. We found some papers that make the evaluate the cytotoxic activities of metal complexes against the misidentified cell line KB [424].

**Table 4**
List of cell lines discussed here.

| | |
|---|---|
| **Squamous Cell Carcinoma** | |
| A253 | Salivary gland squamous cell carcinoma |
| A431 | Squamous cell carcinoma of the skin/epidermis (sometimes also referred as vulvar squamous cell carcinoma) |
| Cal27 | Tongue squamous cell carcinoma |
| Cal33 | Tongue squamous cell carcinoma |
| EC109 | Esophageal squamous cell carcinoma |
| FaDu | Hypopharyngeal squamous cell carcinoma |
| HN | Oral cavity squamous cell carcinoma |
| HSC-2 | Oral cavity squamous cell carcinoma |
| HSC-3 | Tongue squamous cell carcinoma |
| HSC-4 | Tongue squamous cell carcinoma |
| SCC9 | Tongue squamous cell carcinoma |
| SCC15 | Tongue squamous cell carcinoma |
| SCC25 | Tongue squamous cell carcinoma |
| **Basal Cell Carcinoma** | |
| BCC | Basocellular carcinoma cell line |
| **Melanoma** | |
| 518A2 | melanoma |
| A2058 | melanoma, derived from metastatic site: lymph node |
| A375 | Amelanotic melanoma |
| B16-F10 | Murine melanoma |
| B16-F10 Nex2 | Murine melanoma |
| C8161 | Cutaneous melanoma, derived from metastatic site: abdominal wall |
| CN-mel | Melanoma, derived from metastatic site: lymph node |
| CRL7687 | Human skin melanoma |
| D24 | Melanoma |
| FEMX | Melanoma, derived from metastatic site: lymph node |
| G361 | Malignant melanoma |
| JR8 | |
| LOX-IMVI | Amelanotic melanoma, derived from metastatic site: axillary lymph node |
| M14 | Amelanotic melanoma, derived from metastatic site: subcutaneous |
| M19-MEL | Amelanotic melanoma |
| Malme-3M | Human malignant melanoma, derived from metastatic site (lung). |
| MDA-MB-435 | Amelanotic melanoma, derived from metastatic site: subcutaneous |
| MDA-N | Amelanotic melanoma, derived from metastatic site: subcutaneous; right buttock. |
| ME665/2/20 | |
| ME665/2/21 | Melanoma, derived from metastatic site: Subcutaneous nodules. |
| ME665/2/60 | Melanoma, derived from metastatic site: Subcutaneous nodules. |
| ME1402 (INT-MEL-15/2) | Melanoma |
| MeWo | Cutaneous melanoma, derived from metastatic site: lymph node |
| SK-MEL-2 | Melanoma |
| SK-MEL-5 | Melanoma |
| SK-MEL-28 | Melanoma |
| SK-MEL 110 | Melanoma |
| UACC-62 | Melanoma |
| UACC-257 | Melanoma |
| WM-115 | Melanoma, derived from metastatic site: right anterior leg. |
| **Other malignant cell lines** | |
| A549 | Adenocarcinomic human alveolar basal epithelial cells (lung adenocarcinoma) |
| A549/DDP | Cisplatin-resistant lung adenocarcinoma |
| HK-1 | Nasopharyngeal carcinoma |
| TM1G3 | Melan-a derived TM1 cells transfected with pEF1-neo-Gal3 plasmid |
| TM1MNG3 | Melan-a derived TM1 cells transfected with pEF1-neo plasmid |
| KB | HeLa cell line, misidentified as nasopharyngeal epidermoid carcinoma (squamous cell carcinoma) |
| **Non-tumoral** | |
| CA-M75 | Normal skin melanocyte |
| HDFa | Nonmalignant human dermal fibroblasts |
| GM22275 | Human skin melanocyte |
| Melan-A | Murine melanocyte |
| NP69 | Immortalized human nasopharyngeal epithelial cell line |
| NEK | Normal human epidermal keratinocytes |

## Declaration of Competing Interest

The authors declare that they have no known competing financial interests or personal relationships that could have appeared to influence the work reported in this paper.

## Acknowledgements

The São Paulo Research Foundation (FAPESP, São Paulo, Brazil) is acknowledged (grant 18/21537-6 to REFP and 17/25995-6 to CMM). REFP acknowledges funding from the Irish Research Council (GOIPD/2021/909). The authors thank Professors Luca Salassa from the Donostia International Physics Center and Walter Berger from the Medical University of Vienna for the engaging scientific discussions and comments on this review.

## Appendix A. Supplementary data

Supplementary data to this article can be found online at https://doi.org/10.1016/j.ccr.2022.214506.

## References


[1] O. Rixe, W. Ortuzar, M. Alvarez, R. Parker, E. Reed, K. Paull, T. Fojo, Oxaliplatin, tetraplatin, cisplatin, and carboplatin: Spectrum of activity in drug-resistant cell lines and in the cell lines of the national cancer institute's anticancer drug screen panel, Biochem. Pharmacol. 52 (1996) 1855–1865, https://doi.org/10.1016/S0006-2952(97)81490-6.

[2] G. Mattia, R. Puglisi, B. Ascione, W. Malorni, A. Carè, P. Matarrese, Cell death-based treatments of melanoma:conventional treatments and new therapeutic strategies, Cell Death Dis. 9 (2018) 112, https://doi.org/10.1038/s41419-017-0059-7.

[3] S. Dasari, P. Bernard Tchounwou, Cisplatin in cancer therapy: Molecular mechanisms of action, Eur. J. Pharmacol. 740 (2014) 364–378, https://doi.org/10.1016/j.ejphar.2014.07.025.

[4] M. Fanelli, M. Formica, V. Fusi, L. Giorgi, M. Micheloni, P. Paoli, New trends in platinum and palladium complexes as antineoplastic agents, Coord. Chem. Rev. 310 (2016) 41–79, https://doi.org/10.1016/j.ccr.2015.11.004.

[5] X. Sun, B. Shi, H. Zheng, L. Min, J. Yang, X. Li, X. Liao, W. Huang, M. Zhang, S. Xu, Z. Zhu, H. Cui, X. Liu, Senescence-associated secretory factors induced by cisplatin in melanoma cells promote non-senescent melanoma cell growth through activation of the ERK1/2-RSK1 pathway, Cell Death Dis. 9 (2018) 260, https://doi.org/10.1038/s41419-018-0303-9.

[6] I. Romero-Canelón, P.J. Sadler, Next-Generation Metal Anticancer Complexes: Multitargeting via Redox Modulation, Inorg. Chem. 52 (2013) 12276–12291, https://doi.org/10.1021/ic400835n.

[7] C.N. Morrison, K.E. Prosser, R.W. Stokes, A. Cordes, N. Metzler-Nolte, S.M. Cohen, Expanding medicinal chemistry into 3D space: Metallofragments as 3D scaffolds for fragment-based drug discovery, Chem. Sci. 11 (2020) 1216–1225, https://doi.org/10.1039/c9sc05586j.

[8] A.K. Renfrew, Transition metal complexes with bioactive ligands: mechanisms for selective ligand release and applications for drug delivery, Metallomics. 6 (2014) 1324–1335, https://doi.org/10.1039/C4MT00069B.

[9] K.D. Mjos, C. Orvig, Metallodrugs in medicinal inorganic chemistry, Chem. Rev. 114 (2014) 4540–4563, https://doi.org/10.1021/cr400460s.

[10] E.J. Anthony, E.M. Bolitho, H.E. Bridgewater, O.W.L. Carter, J.M. Donnelly, C. Imberti, E.C. Lant, F. Lermyte, R.J. Needham, M. Palau, P.J. Sadler, H. Shi, F.X. Wang, W.Y. Zhang, Z. Zhang, Metallodrugs are unique: Opportunities and challenges of discovery and development, Chem. Sci. 11 (2020) 12888–12917, https://doi.org/10.1039/d0sc04082g.

[11] K.C. Madison, Barrier function of the skin: "La Raison d'Être" of the epidermis, J, Invest. Dermatol. 121 (2003) 231–241, https://doi.org/10.1046/j.1523-1747.2003.12359.x.

[12] E. Proksch, J.M. Brandner, J.-M. Jensen, The skin: an indispensable barrier, Exp. Dermatol. 17 (2008) 1063–1072, https://doi.org/10.1111/j.1600-0625.2008.00786.x.

[13] R.B. Weller, H.J.A. Hunter, M.W. Mann, Clinical Dermatology, fifth ed., Wiley Blackwell, Chichester, UK, 2015, 10.1002/9781118938164.

[14] P.A.J. Kolarsick, M.A. Kolarsick, C. Goodwin, Anatomy and Physiology of the Skin, J. Dermatol. Nurses. Assoc. 3 (2011) 203–213, https://doi.org/10.1097/JDN.0b013e3182274a98.

[15] D.D. Bikle, Vitamin D metabolism and function in the skin, Mol. Cell. Endocrinol. 347 (2011) 80–89, https://doi.org/10.1016/j.mce.2011.05.017.

[16] C.C. Zouboulis, The skin as an endocrine organ, Dermatoendocrinol. 1 (2009) 250–252, https://doi.org/10.4161/derm.1.5.9499.

[17] K.A.U. Gonzales, E. Fuchs, Skin and Its Regenerative Powers: An Alliance between Stem Cells and Their Niche, Dev. Cell 43 (2017) 387–401, https://doi.org/10.1016/j.devcel.2017.10.001.

[18] M.T. Martin, A. Vulin, J.H. Hendry, Human epidermal stem cells: Role in adverse skin reactions and carcinogenesis from radiation, Mutat. Res. - Rev, Mutat. Res. 770 (2016) 349–368, https://doi.org/10.1016/j.mrrev.2016.08.004.

[19] F. Larcher, E. Dellambra, L. Rico, S. Bondanza, R. Murillas, C. Cattoglio, F. Mavilio, J.L. Jorcano, G. Zambruno, M. Del Rio, Long-term engraftment of single genetically modified human epidermal holoclones enables safety pre-assessment of cutaneous gene therapy, Mol. Ther. 15 (2007) 1670–1676, https://doi.org/10.1038/sj.mt.6300238.

[20] C.L. Simpson, D.M. Patel, K.J. Green, Deconstructing the skin: Cytoarchitectural determinants of epidermal morphogenesis, Nat. Rev. Mol. Cell Biol. 12 (2011) 565–580, https://doi.org/10.1038/nrm3175.

[21] J.Y. Lin, D.E. Fisher, Melanocyte biology and skin pigmentation, Nature 445 (2007) 843–850, https://doi.org/10.1038/nature05660.

[22] Y. Yamaguchi, V.J. Hearing, Melanocytes and their diseases, Cold Spring Harb. Perspect. Med. 4 (2014), https://doi.org/10.1101/cshperspect.a017046, a017046-a017046.

[23] M. Cichorek, M. Wachulska, A. Stasiewicz, A. Tymińska, Skin melanocytes: biology and development, Adv. Dermatol. Allergol. 1 (2013) 30–41, https://doi.org/10.5114/pdia.2013.33376.

[24] N. Agar, A.R. Young, Melanogenesis: A photoprotective response to DNA damage?, Mutat Res. - Fundam. Mol. Mech. Mutagen. 571 (2005) 121–132, https://doi.org/10.1016/j.mrfmmm.2004.11.016.

[25] S. Maksimovic, M. Nakatani, Y. Baba, A.M. Nelson, K.L. Marshall, S.A. Wellnitz, P. Firozi, S.H. Woo, S. Ranade, A. Patapoutian, E.A. Lumpkin, Epidermal Merkel cells are mechanosensory cells that tune mammalian touch receptors, Nature 509 (2014) 617–621, https://doi.org/10.1038/nature13250.

[26] N. Boulais, L. Misery, Merkel cells, J. Am. Acad. Dermatol. 57 (2007) 147–165, https://doi.org/10.1016/j.jaad.2007.02.009.

[27] J. Abraham, S. Mathew, Merkel Cells: A Collective Review of Current Concepts, Int. J. Appl. Basic Med. Res. 9 (2019) 9–13, https://doi.org/10.4103/ijabmr.IJABMR_34_18.

[28] K. Clayton, A.F. Vallejo, J. Davies, S. Sirvent, M.E. Polak, Langerhans cells-programmed by the epidermis, Front. Immunol. 8 (2017) 1676, https://doi.org/10.3389/fimmu.2017.01676.

[29] M. Merad, F. Ginhoux, M. Collin, Origin, homeostasis and function of Langerhans cells and other langerin-expressing dendritic cells, Nat. Rev. Immunol. 8 (2008) 935–947, https://doi.org/10.1038/nri2455.

[30] H.C. West, C.L. Bennett, Redefining the role of langerhans cells as immune regulators within the skin, Front. Immunol. 8 (2018) 1941, https://doi.org/10.3389/fimmu.2017.01941.

[31] K. Kabashima, T. Honda, F. Ginhoux, G. Egawa, The immunological anatomy of the skin, Nat. Rev. Immunol. 19 (2019) 19–30, https://doi.org/10.1038/s41577-018-0084-5.

[32] C. Karimkhani, L.N. Boyers, R.P. Dellavalle, M.A. Weinstock, It's time for "keratinocyte carcinoma" to replace the term "nonmelanoma skin cancer", J. Am. Acad. Dermatol. 72 (2015) 186–187, https://doi.org/10.1016/j.jaad.2014.09.036.

[33] D.L. Longo, K.S. Nehal, C.K. Bichakjian, Update on Keratinocyte Carcinomas, N. Engl. J. Med. 379 (4) (2018) 363–374.

[34] C. Garbe, U. Leiter, Epidemiology of melanoma and nonmelanoma skin cancer-the role of sunlight, Adv. Exp. Med. Biol. 624 (2008) 89–103, https://doi.org/10.1007/978-0-387-77574-6_8.

[35] K.S. Nehal, C.K. Bichakjian, Update on Keratinocyte Carcinomas, N. Engl. J. Med. 379 (2018) 363–374, https://doi.org/10.1056/NEJMRA1708701/SUPPL_FILE/NEJMRA1708701_DISCLOSURES.PDF.

[36] Z.C. Venables, T. Nijsten, K.F. Wong, P. Autier, J. Broggio, A. Deas, C.A. Harwood, L.M. Hollestein, S.M. Langan, E. Morgan, C.M. Proby, J. Rashbass, I.M. Leigh, Epidemiology of basal and cutaneous squamous cell carcinoma in the U.K. 2013–15: a cohort study, Br. J. Dermatol. 181 (2019) 474–482, https://doi.org/10.1111/BJD.17873.

[37] E. Pavez Loriè, H.J. Stark, M. Berning, P. Boukamp, Skin squamous cell carcinoma models: The role in combating the disease, in: Ski. Tissue Model., Elsevier Inc., 2018, pp. 151–173, doi:10.1016/B978-0-12-810545-0.00007-3.

[38] P. Nagarajan, M.M. Asgari, A.C. Green, S.M. Guhan, S.T. Arron, C.M. Proby, D.E. Rollison, C.A. Harwood, A.E. Toland, Keratinocyte carcinomas: Current concepts and future research priorities, Clin. Cancer Res. 25 (2019) 2379–2391, https://doi.org/10.1158/1078-0432.CCR-18-1122.

[39] J. Donovan, Review of the hair follicle origin hypothesis for basal cell Carcinoma, Dermatologic Surg. 35 (2009) 1311–1323, https://doi.org/10.1111/j.1524-4725.2009.01236.x.

[40] K.K. Youssef, A. Van Keymeulen, G. Lapouge, B. Beck, C. Michaux, Y. Achouri, P. A. Sotiropoulou, C. Blanpain, Identification of the cell lineage at the origin of basal cell carcinoma, Nat. Cell Biol. 12 (2010) 299–305, https://doi.org/10.1038/ncb2031.

[41] C. Köhler, D. Nittner, F. Rambow, E. Radaelli, F. Stanchi, N. Vandamme, A. Baggiolini, L. Sommer, G. Berx, J.J. van den Oord, H. Gerhardt, C. Blanpain, J.C. Marine, Mouse Cutaneous Melanoma Induced by Mutant BRaf Arises from Expansion and Dedifferentiation of Mature Pigmented Melanocytes, Cell Stem Cell 21 (2017) 679–693.e6, https://doi.org/10.1016/j.stem.2017.08.003.

[42] E.H. Epstein, Basal cell carcinomas: Attack of the hedgehog, Nat. Rev. Cancer 8 (2008) 743–754, https://doi.org/10.1038/nrc2503.

[43] H. Hahn, C. Wicking, P.G. Zaphiropoulos, M.R. Gailani, S. Shanley, A. Chidambaram, I. Vorechovsky, E. Holmberg, A.B. Unden, S. Gillies, K. Negus, I. Smyth, C. Pressman, D.J. Leffell, B. Gerrard, A.M. Goldstein, M. Dean, R. Toftgard, G. Chenevix-Trench, B. Wainwright, A.E. Bale, Mutations of the human homolog of drosophila patched in the nevoid basal cell carcinoma syndrome, Cell 85 (1996) 841–851, https://doi.org/10.1016/S0092-8674(00)81268-4.

[44] G. Ling, A. Ahmadian, Å. Persson, A.B. Undén, G. Afink, C. Williams, M. Uhlén, R. Toftgård, J. Lundeberg, F. Pontén, Patched and p53 gene alterations in sporadic and hereditary basal cell cancer, Oncogene 20 (2001) 7770–7778, https://doi.org/10.1038/sj.onc.1204946.

[45] P.R. Hoban, S. Ramachandran, R.C. Strange, Environment, phenotype and genetics: risk factors associated with BCC of the skin, Expert Rev. Anticancer Ther. 2 (2002) 570–579, https://doi.org/10.1586/14737140.2.5.570.

[46] E.Y.-X. Tay, Y.-L. Teoh, M.S.-W. Yeo, Hedgehog pathway inhibitors and their utility in basal cell carcinoma: A comprehensive review of current evidence, Dermatol. Ther. 91 (9) (2018) 33–49, https://doi.org/10.1007/S13555-018-0277-7.

[47] A.A. Jacobsen, A.S. Aldahan, O.B. Hughes, V.V. Shah, J. Strasswimmer, Hedgehog pathway inhibitor therapy for locally advanced and metastatic basal cell carcinoma: A systematic review and pooled analysis of interventional studies, JAMA Dermatol. 152 (2016) 816–824, https://doi.org/10.1001/JAMADERMATOL.2016.0780.

[48] C.S. Sander, F. Hamm, P. Elsner, J.J. Thiele, Oxidative stress in malignant melanoma and non-melanoma skin cancer, Br. J. Dermatol. 148 (2003) 913–922, https://doi.org/10.1046/j.1365-2133.2003.05303.x.

[49] B. Domingues, J. Lopes, P. Soares, H. Populo, Melanoma treatment in review, ImmunoTargets Ther. 7 (2018) 35–49, https://doi.org/10.2147/ITT.S134842.

[50] T.L. Tello, K. Coggshall, S.S. Yom, S.S. Yu, Merkel cell carcinoma: An update and review: Current and future therapy, J. Am. Acad. Dermatol. 78 (2018) 445–454, https://doi.org/10.1016/j.jaad.2017.12.004.

[51] J.A. Neville, E. Welch, D.J. Leffell, Management of nonmelanoma skin cancer, Nat. Clin. Pract. Oncol. 4 (2007) (2007) 462–469, https://doi.org/10.1038/ncponc0883.
[52] C. Potenza, N. Bernardini, V. Balduzzi, L. Losco, A. Mambrin, A. Marchesiello, E. Tolino, S. Zuber, N. Skroza, I. Proietti, A review of the literature of surgical and nonsurgical treatments of invasive squamous cells carcinoma, Biomed Res. Int. 2018 (2018) 1–9, https://doi.org/10.1155/2018/9489163.
[53] V. Lazareth, Management of non-melanoma skin cancer, Semin. Oncol. Nurs. 29 (3) (2013) 182–194.
[54] G.S. Wood, Y.G. Xu, J.L. Aylward, V. Spiegelman, E. Vanness, J.M.C. Teng, S.N. Snow, Nonmelanoma Skin Cancers: Basal Cell and Squamous Cell Carcinomas, Sixth ed., Elsevier Inc., 2013, doi:10.1016/B978-1-4557-2865-7.00070-9.
[55] J. Caddick, L. Green, J. Stephenson, G. Spyrou, The psycho-social impact of facial skin cancers, J. Plast. Reconstr. Aesthetic Surg. 65 (2012) e257–e259, https://doi.org/10.1016/j.bjps.2012.02.022.
[56] E. Zelin, I. Zalaudek, M. Agozzino, C. Dianzani, A. Dri, N. Di Meo, R. Giuffrida, G. F. Marangi, N. Neagu, P. Persichetti, L. Toffoli, C. Conforti, Neoadjuvant Therapy for Non-melanoma Skin Cancer: Updated Therapeutic Approaches for Basal, Squamous, and Merkel Cell Carcinoma, Curr. Treat. Options Oncol. 22 (2021) 35, https://doi.org/10.1007/s11864-021-00826-3.
[57] A.I. Reeder, Non-melanoma skin cancer, N. Z. Med. J. 124 (2011) 99–100.
[58] S.S. Alessi, J.A. Sanches, W.R. de Oliveira, M.C. Messina, R. de A. Pimentel, C.F. Neto, Treatment of cutaneous tumors with topical 5% imiquimod cream, Clinics. 64 (2009) 961–966, https://doi.org/10.1590/S1807-59322009001000005.
[59] H. Suzuki, B. Wang, G.M. Shivji, P. Toto, P. Amerio, M.A. Tomai, R.L. Miller, D.N. Sauder, Imiquimod, a topical immune response modifier, induces migration of Langerhans cells, J, Invest. Dermatol. 114 (2000) 135–141, https://doi.org/10.1046/j.1523-1747.2000.00833.x.
[60] R.L. Miller, J.F. Gerster, M.L. Owens, H.B. Slade, M.A. Tomai, Review article Imiquimod applied topically: A novel immune response modifier and new class of drug, Int. J. Immunopharmacol. 21 (1999) 1–14, https://doi.org/10.1016/S0192-0561(98)00068-X.
[61] S. Doğruk Kaçar, P. Özuğuz, F. Erkan, Ş. Karaca, Treatment of various types of basal cell carcinoma with topical 5% imiquimod in the elderly who refused surgical intervention: a case series, J. Dermatolog. Treat. 26 (2015) 165–167, https://doi.org/10.3109/09546634.2014.915003.
[62] M. Alam, A. Armstrong, C. Baum, J.S. Bordeaux, M. Brown, K.J. Busam, D.B. Eisen, V. Iyengar, C. Lober, D.J. Margolis, J. Messina, A. Miller, S. Miller, E. Mostow, C. Mowad, K. Nehal, K. Schmitt-Burr, A. Sekulic, P. Storrs, J. Teng, S. Yu, C. Huang, K. Boyer, W.S. Begolka, C. Bichakjian, J.Y.S. Kim, J.H. Kozlow, B. Mittal, J. Moyer, T. Olenecki, P. Rodgers, Guidelines of care for the management of cutaneous squamous cell carcinoma, J. Am. Acad. Dermatol. 78 (2018) 560–578, https://doi.org/10.1016/j.jaad.2017.10.007.
[63] S. Li, K.R. Schmitz, P.D. Jeffrey, J.J.W. Wiltzius, P. Kussie, K.M. Ferguson, Structural basis for inhibition of the epidermal growth factor receptor by cetuximab, Cancer Cell 7 (2005) 301–311, https://doi.org/10.1016/j.ccr.2005.03.003.
[64] U.A. Ramagopal, W. Liu, S.C. Garrett-Thomson, J.B. Bonanno, Q. Yan, M. Srinivasan, S.C. Wong, A. Bell, S. Mankikar, V.S. Rangan, S. Deshpande, A.J. Korman, S.C. Almo, Structural basis for cancer immunotherapy by the first-in-class checkpoint inhibitor ipilimumab, Proc. Natl. Acad. Sci. U. S. A. 114 (2017) E4223–E4232, https://doi.org/10.1073/pnas.1617941114.
[65] J.Y. Lee, H.T. Lee, W. Shin, J. Chae, J. Choi, S.H. Kim, H. Lim, T. Won Heo, K.Y. Park, Y.J. Lee, S.E. Ryu, J.Y. Son, J.U. Lee, Y.S. Heo, Structural basis of checkpoint blockade by monoclonal antibodies in cancer immunotherapy, Nat. Commun. 7 (2016) 1–10, https://doi.org/10.1038/ncomms13354.
[66] D.S. Goodsell, L. Autin, A.J. Olson, Illustrate: Software for Biomolecular Illustration, Structure. 27 (2019) 1716–1720.e1, https://doi.org/10.1016/j.str.2019.08.011.
[67] S.R. Ahmed, E. Petersen, R. Patel, M.R. Migden, Cemiplimab-rwlc as first and only treatment for advanced cutaneous squamous cell carcinoma, Expert Rev. Clin. Pharmacol. 12 (2019) 947–951, https://doi.org/10.1080/17512433.2019.1665026.
[68] M.R. Migden, D. Rischin, C.D. Schmults, A. Guminski, A. Hauschild, K.D. Lewis, C.H. Chung, L. Hernandez-Aya, A.M. Lim, A.L.S. Chang, G. Rabinowits, A.A. Thai, L.A. Dunn, B.G.M. Hughes, N.I. Khushalani, B. Modi, D. Schadendorf, B. Gao, F. Seebach, S. Li, J. Li, M. Mathias, J. Booth, K. Mohan, E. Stankevich, H.M. Babiker, I. Brana, M. Gil-Martin, J. Homsi, M.L. Johnson, V. Moreno, J. Niu, T.K. Owonikoko, K.P. Papadopoulos, G.D. Yancopoulos, I. Lowy, M.G. Fury, PD-1 blockade with cemiplimab in advanced cutaneous squamous-cell carcinoma, N. Engl. J. Med. 379 (2018) 341–351, https://doi.org/10.1056/NEJMoa1805131.
[69] T. Yanagi, S. Kitamura, H. Hata, Novel therapeutic targets in cutaneous squamous cell carcinoma, Front, Oncol. 8 (2018) 1–5, https://doi.org/10.3389/fonc.2018.00079.
[70] M.R. Migden, A.L.S. Chang, L. Dirix, A.J. Stratigos, J.T. Lear, Emerging trends in the treatment of advanced basal cell carcinoma, Cancer Treat. Rev. 64 (2018) 1–10, https://doi.org/10.1016/j.ctrv.2017.12.009.
[71] L. Feller, R.A.G. Khammissa, B. Kramer, M. Altini, J. Lemmer, Basal cell carcinoma, squamous cell carcinoma and melanoma of the head and face, Head Face Med. 12 (2016) 11, https://doi.org/10.1186/s13005-016-0106-0.
[72] S.V. Mohan, J. Chang, S. Li, A.S. Henry, D.J. Wood, A.L.S. Chang, Increased risk of cutaneous squamous cell carcinoma after vismodegib therapy for basal cell carcinoma, JAMA Dermatol. 152 (2016) 527, https://doi.org/10.1001/jamadermatol.2015.4330.
[73] K.M. Joyce, Surgical management of melanoma, in: Cutan. Melanoma Etiol. Ther., Codon Publications, 2017, pp. 91–100, doi:10.15586/codon.cutaneousmelanoma.2017.ch7.
[74] A. Gupta, F. Gomes, P. Lorigan, The role for chemotherapy in the modern management of melanoma, Melanoma Manag. 4 (2017) 125–136, https://doi.org/10.2217/mmt-2017-0003.
[75] F.S. Hodi, S.J. O'Day, D.F. McDermott, R.W. Weber, J.A. Sosman, J.B. Haanen, R. Gonzalez, C. Robert, D. Schadendorf, J.C. Hassel, W. Akerley, A.J.M. van den Eertwegh, J. Lutzky, P. Lorigan, J.M. Vaubel, G.P. Linette, D. Hogg, C.H. Ottensmeier, C. Lebbé, C. Peschel, I. Quirt, J.I. Clark, J.D. Wolchok, J.S. Weber, J. Tian, M.J. Yellin, G.M. Nichol, A. Hoos, W.J. Urba, Improved Survival with Ipilimumab in Patients with Metastatic Melanoma, N. Engl. J. Med. 363 (2010) 711–723, https://doi.org/10.1056/NEJMoa1003466.
[76] C. Robert, J. Schachter, G.V. Long, A. Arance, J.J. Grob, L. Mortier, A. Daud, M.S. Carlino, C. McNeil, M. Lotem, J. Larkin, P. Lorigan, B. Neyns, C.U. Blank, O. Hamid, C. Mateus, R. Shapira-Frommer, M. Kosh, H. Zhou, N. Ibrahim, S. Ebbinghaus, A. Ribas, Pembrolizumab versus Ipilimumab in Advanced Melanoma, N. Engl. J. Med. 372 (2015) 2521–2532, https://doi.org/10.1056/NEJMoa1503093.
[77] C. Robert, G.V. Long, B. Brady, C. Dutriaux, M. Maio, L. Mortier, J.C. Hassel, P. Rutkowski, C. McNeil, E. Kalinka-Warzocha, K.J. Savage, M.M. Hernberg, C. Lebbé, J. Charles, C. Mihalcioiu, V. Chiarion-Sileni, C. Mauch, F. Cognetti, A. Arance, H. Schmidt, D. Schadendorf, H. Gogas, L. Lundgren-Eriksson, C. Horak, B. Sharkey, I.M. Waxman, V. Atkinson, P.A. Ascierto, Nivolumab in Previously Untreated Melanoma without BRAF Mutation, N. Engl. J. Med. 372 (2015) 320–330, https://doi.org/10.1056/NEJMoa1412082.
[78] C. Robert, B. Karaszewska, J. Schachter, P. Rutkowski, A. Mackiewicz, D. Stroiakovski, M. Lichinitser, R. Dummer, F. Grange, L. Mortier, V. Chiarion-Sileni, K. Drucis, I. Krajsova, A. Hauschild, P. Lorigan, P. Wolter, G.V. Long, K. Flaherty, P. Nathan, A. Ribas, A.-M. Martin, P. Sun, W. Crist, J. Legos, S.D. Rubin, S.M. Little, D. Schadendorf, Improved Overall Survival in Melanoma with Combined Dabrafenib and Trametinib, N. Engl. J. Med. 372 (2015) 30–39, https://doi.org/10.1056/NEJMoa1412690.
[79] G.V. Long, D. Stroyakovskiy, H. Gogas, E. Levchenko, F. de Braud, J. Larkin, C. Garbe, T. Jouary, A. Hauschild, J.-J. Grob, V. Chiarion-Sileni, C. Lebbe, M. Mandalà, M. Millward, A. Arance, I. Bondarenko, J.B.A.G. Haanen, J. Hansson, J. Utikal, V. Ferraresi, N. Kovalenko, P. Mohr, V. Probachai, D. Schadendorf, P. Nathan, C. Robert, A. Ribas, D.J. DeMarini, J.G. Irani, S. Swann, J.J. Legos, F. Jin, B. Mookerjee, K. Flaherty, Dabrafenib and trametinib versus dabrafenib and placebo for Val600 BRAF-mutant melanoma: a multicentre, double-blind, phase 3 randomised controlled trial, Lancet 386 (2015) 444–451, https://doi.org/10.1016/S0140-6736(15)60898-4.
[80] C. Robert, J.J. Grob, D. Stroyakovskiy, B. Karaszewska, A. Hauschild, E. Levchenko, V. Chiarion Sileni, J. Schachter, C. Garbe, I. Bondarenko, H. Gogas, M. Mandalá, J.B.A.G. Haanen, C. Lebbé, A. Mackiewicz, P. Rutkowski, P. D. Nathan, A. Ribas, M.A. Davies, K.T. Flaherty, P. Burgess, M. Tan, E. Gasal, M. Voi, D. Schadendorf, G.V. Long, Five-Year Outcomes with Dabrafenib plus Trametinib in Metastatic Melanoma, N. Engl. J. Med. 381 (2019) 626–636, https://doi.org/10.1056/NEJMoa1904059.
[81] R.E.F. de Paiva, C.M. Manzano, D.H. Nakahata, In vitro antiproliferative data of metallodrugs in skin cancer cell lines (2021), https://doi.org/10.5281/ZENODO.5055531.
[82] R.H. Shoemaker, The NCI60 human tumour cell line anticancer drug screen, Nat. Rev. Cancer 6 (2006) 813–823, https://doi.org/10.1038/nrc1951.
[83] X. Jiang, A. Kopp-Schneider, Summarizing EC50 estimates from multiple dose-response experiments: A comparison of a meta-analysis strategy to a mixed-effects model approach, Biometrical J. 56 (2014) 493–512, https://doi.org/10.1002/bimj.201300123.
[84] V. Gold, ed., The IUPAC Compendium of Chemical Terminology, International Union of Pure and Applied Chemistry (IUPAC), Research Triangle Park, NC, 2019. doi:10.1351/goldbook.
[85] K.D. Paull, E. Hamel, L. Malspeis, COMPARE analysis - Methodology, (2015). https://dtp.cancer.gov/databases_tools/docs/compare/compare_methodology.htm (accessed September 10, 2021).
[86] A. Manuscript, Cisplatin in cancer therapy : molecular mechanisms of action, (2015) 364–378. doi:10.1016/j.ejphar.2014.07.025.Cisplatin.
[87] B. Englinger, C. Pirker, P. Heffeter, A. Terenzi, C.R. Kowol, B.K. Keppler, W. Berger, Metal drugs and the anticancer immune response, Chem. Rev. 119 (2019) 1519–1624, https://doi.org/10.1021/acs.chemrev.8b00396.
[88] D.Y.Q. Wong, W.W.F. Ong, W.H. Ang, Induction of immunogenic cell death by chemotherapeutic platinum complexes, Angew. Chemie - Int. Ed. 54 (2015) 6483–6487, https://doi.org/10.1002/anie.201500934.
[89] S.J. Park, W. Ye, R. Xiao, C. Silvin, M. Padget, J.W. Hodge, C. Van Waes, N.C. Schmitt, Cisplatin and oxaliplatin induce similar immunogenic changes in preclinical models of head and neck cancer, Oral Oncol. 95 (2019) 127–135, https://doi.org/10.1016/j.oraloncology.2019.06.016.
[90] A. Terenzi, C. Pirker, B.K. Keppler, W. Berger, Anticancer metal drugs and immunogenic cell death, J. Inorg. Biochem. 165 (2016) 71–79, https://doi.org/10.1016/J.JINORGBIO.2016.06.021.
[91] X. Huang, S. Cui, Y. Shu, Cisplatin selectively downregulated the frequency and immunoinhibitory function of myeloid-derived suppressor cells in a murine B16 melanoma model, Immunol. Res. 64 (2016) 160–170, https://doi.org/10.1007/s12026-015-8734-1.
[92] X. Huang, D. Guan, Y.Q. Shu, L.K. Liu, F. Ni, Effect of cisplatin on the frequency and immuno-inhibitory function of myeloid-derived suppressor cells in A375

melanoma model, Asian Pacific, J Cancer Prev. 16 (2015) 4329–4333, https://doi.org/10.7314/APJCP.2015.16.10.4329.
[93] R. Křikavová, L. Hanousková, Z. Dvořák, Z. Trávníček, Dichlorido-platinum(II) complexes with kinetin derivatives as promising cytotoxic agents avoiding resistance of cancer cells: Contrasting results between cisplatin and oxaliplatin analogues, Polyhedron 90 (2015) 7–17, https://doi.org/10.1016/j.poly.2015.01.033.
[94] I. Łakomska, K. Hoffmann, A. Wojtczak, J. Sitkowski, E. Maj, J. Wietrzyk, Cytotoxic malonate platinum(II) complexes with 1,2,4-triazolo[1,5-a] pyrimidine derivatives: Structural characterization and mechanism of the suppression of tumor cell growth, J. Inorg. Biochem. 141 (2014) 188–197, https://doi.org/10.1016/j.jinorgbio.2014.08.005.
[95] K. Hoffmann, J. Wiśniewska, A. Wojtczak, J. Sitkowski, A. Denslow, J. Wietrzyk, M. Jakubowski, I. Łakomska, Rational design of dicarboxylato platinum(II) complexes with purine-mimetic ligands as novel anticancer agents, J. Inorg. Biochem. 172 (2017) 34–45, https://doi.org/10.1016/j.jinorgbio.2017.04.003.
[96] B.J. Pages, J. Sakoff, J. Gilbert, A. Rodger, N.P. Chmel, N.C. Jones, S.M. Kelly, D.L. Ang, J.R. Aldrich-Wright, Multifaceted Studies of the DNA Interactions and In Vitro Cytotoxicity of Anticancer Polyaromatic Platinum(II) Complexes, Chem. - A Eur. J. 22 (2016) 8943–8954, https://doi.org/10.1002/chem.201601221.
[97] N. Margiotta, S. Savino, V. Gandin, C. Marzano, G. Natile, Monofunctional platinum(II) complexes with potent tumor cell growth inhibitory activity: The effect of a hydrogen-bond donor/acceptor N-heterocyclic ligand, ChemMedChem 9 (2014) 1161–1168, https://doi.org/10.1002/cmdc.201402028.
[98] G.K. Couto, B.S. Pacheco, V.M. Borba, J.C.R. Junior, T.L. Oliveira, N.V. Segatto, F. K. Seixas, T.V. Acunha, B.A. Iglesias, T. Collares, Tetra-cationic platinum(II) porphyrins like a candidate photosensitizers to bind, selective and drug delivery for metastatic melanoma, J. Photochem. Photobiol. B Biol. 202 (2020), https://doi.org/10.1016/j.jphotobiol.2019.111725 111725.
[99] R.A. Firestone, Low-Density Lipoprotein as a Vehicle for Targeting Antitumor Compounds to Cancer Cells, Bioconjug. Chem. 5 (1994) 105–113, https://doi.org/10.1021/bc00026a002.
[100] A. Curci, V. Gandin, C. Marzano, J.D. Hoeschele, G. Natile, N. Margiotta, Novel Kiteplatin Pyrophosphate Derivatives with Improved Efficacy, Inorg. Chem. 56 (2017) 7482–7493, https://doi.org/10.1021/acs.inorgchem.7b00931.
[101] J. Kasparkova, T. Suchankova, A. Halamikova, L. Zerzankova, O. Vrana, N. Margiotta, G. Natile, V. Brabec, Cytotoxicity, cellular uptake, glutathione and DNA interactions of an antitumor large-ring PtII chelate complex incorporating the cis-1,4-diaminocyclohexane carrier ligand, Biochem. Pharmacol. 79 (2010) 552–564, https://doi.org/10.1016/j.bcp.2009.09.019.
[102] X. Gao, S. Liu, Y. Shi, Z. Huang, Y. Mi, Q. Mi, J. Yang, Q. Gao, Mechanistic and biological characteristics of different sugar conjugated 2-methyl malonatoplatinum(II) complexes as new tumor targeting agents, Eur. J. Med. Chem. 125 (2017) 372–384, https://doi.org/10.1016/j.ejmech.2016.09.047.
[103] A.G. Abdou, M.M.S. Eldien, D. Elsakka, GLUT-1 Expression in Cutaneous Basal and Squamous Cell Carcinomas, Int. J. Surg. Pathol. 23 (2015) 447–453, https://doi.org/10.1177/1066896915589968.
[104] A. Koch, S.A. Lang, P.J. Wild, S. Gantner, A. Mahli, G. Spanier, M. Berneburg, M. Müller, A.K. Bosserhoff, C. Hellerbrand, Glucose transporter isoform 1 expression enhances metastasis of malignant melanoma cells, Oncotarget. 6 (2015) 32748–32760, https://doi.org/10.18632/oncotarget.4977.
[105] C. Manzotti, G. Pratesi, E. Menta, R. Di Domenico, E. Cavalletti, H.H. Fiebig, L.R. Kelland, N. Farrell, D. Polizzi, R. Supino, G. Pezzoni, F. Zunino, BBR 3464: a novel triplatinum complex, exhibiting a preclinical profile of antitumor efficacy different from cisplatin, Clin. Cancer Res. 6 (2000) 2626–2634. http://www.ncbi.nlm.nih.gov/pubmed/10914703.
[106] H. Daghriri, F. Huq, P. Beale, Studies on activities, cell up take and DNA binding of four multinuclear complexes of the form: [{trans-PtCl(NH3)2}2μ-{trans-Pd(NH3)2-(H2N(CH2)nNH2)2}]Cl4 where n=4–7, J. Inorg. Biochem. 98 (2004) 1722–1733, https://doi.org/10.1016/j.jinorgbio.2004.07.008.
[107] L.J. Teixeira, M. Seabra, E. Reis, M.T.G. Da Cruz, M.C.P. De Lima, E. Pereira, M.A. Miranda, M.P.M. Marques, Cytotoxic activity of metal complexes of biogenic polyamines: Polynuclear platinum(II) chelates, J. Med. Chem. 47 (2004) 2917–2925, https://doi.org/10.1021/jm0311238.
[108] F. Schmitt, K. Donnelly, J.K. Muenzner, T. Rehm, V. Novohradsky, V. Brabec, J. Kasparkova, M. Albrecht, R. Schobert, T. Mueller, Effects of histidin-2-ylidene vs. imidazol-2-ylidene ligands on the anticancer and antivascular activity of complexes of ruthenium, iridium, platinum, and gold, J. Inorg. Biochem. 163 (2016) 221–228, https://doi.org/10.1016/j.jinorgbio.2016.07.021.
[109] T. Rehm, M. Rothemund, T. Dietel, R. Kempe, R. Schobert, Synthesis, structures and cytotoxic effects: In vitro of cis-and trans-[PtIVCl4(NHC)2] complexes and their PtII precursors, Dalton Trans. 48 (2019) 16358–16365, https://doi.org/10.1039/c9dt02438g.
[110] A. Zamora, S.A. Pérez, M. Rothemund, V. Rodríguez, R. Schobert, C. Janiak, J. Ruiz, Exploring the Influence of the Aromaticity on the Anticancer and Antivascular Activities of Organoplatinum(II) Complexes, Chem. - A Eur. J. 23 (2017) 5614–5625, https://doi.org/10.1002/chem.201700717.
[111] A.G. Quiroga, J.M. Pérez, I. López-Solera, J.R. Masaguer, A. Luque, P. Román, A. Edwards, C. Alonso, C. Navarro-Ranninger, Novel tetranuclear orthometalated complexes of Pd(II) and Pt(II) derived from p-isopropylbenzaldehyde thiosemicarbazone with cytotoxic activity in cis-DDP resistant tumor cell lines. Interaction of these complexes with DNA, J. Med. Chem. 41 (1998) 1399–1408, https://doi.org/10.1021/jm970520d.
[112] S. Miranda, E. Vergara, F. Mohr, D. De Vos, E. Cerrada, A. Mendía, M. Laguna, Synthesis, characterization, and in vitro cytotoxicity of some gold(I) and trans platinum(II) thionate complexes containing water-soluble PTA and DAPTA ligands. X-ray crystal structures, Inorg. Chem. 47 (2008) 5641–5648, https://doi.org/10.1021/ic7021903.
[113] A.R.Z. Almotairy, V. Gandin, L. Morrison, C. Marzano, D. Montagner, A. Erxleben, Antitumor platinum(IV) derivatives of carboplatin and the histone deacetylase inhibitor 4-phenylbutyric acid, J. Inorg. Biochem. 177 (2017) 1–7, https://doi.org/10.1016/j.jinorgbio.2017.09.009.
[114] N. Garmpis, C. Damaskos, A. Garmpi, D. Dimitroulis, E. Spartalis, G.A. Margonis, D. Schizas, I. Deskou, C. Doula, E. Magkouti, N. Andreatos, E.A. Antoniou, A. Nonni, K. Kontzoglou, D. Mantas, Targeting histone deacetylases in malignant melanoma: A future therapeutic agent or just great expectations?, Anticancer Res 37 (2017) 5355–5362, https://doi.org/10.21873/anticanres.11961.
[115] N. Margiotta, S. Savino, C. Marzano, C. Pacifico, J.D. Hoeschele, V. Gandin, G. Natile, Cytotoxicity-boosting of kiteplatin by Pt(IV) prodrugs with axial benzoate ligands, J. Inorg. Biochem. 160 (2016) 85–93, https://doi.org/10.1016/j.jinorgbio.2015.11.028.
[116] A. Barbanente, V. Gandin, N. Ditaranto, C. Marzano, J.D. Hoeschele, G.P. Suranna, P. Papadia, G. Natile, N. Margiotta, A Pt(IV) prodrug of kiteplatin with the bone-targeting pyrophosphate ligand, Inorganica Chim. Acta. 494 (2019) 98–104, https://doi.org/10.1016/j.ica.2019.05.011.
[117] A. Barbanente, V. Gandin, N. Ditaranto, C. Marzano, J.D. Hoeschele, G.P. Suranna, P. Papadia, G. Natile, N. Margiotta, A Pt(IV)prodrug of kiteplatin with the bone-targeting pyrophosphate ligand, Inorganica Chim. Acta. 494 (2019) 98–104, https://doi.org/10.1016/j.ica.2019.05.011.
[118] E. Shaili, M. Fernández-Giménez, S. Rodríguez-Astor, A. Gandioso, L. Sandín, C. García-Vélez, A. Massaguer, G.J. Clarkson, J.A. Woods, P.J. Sadler, V. Marchán, A Photoactivatable Platinum(IV) Anticancer Complex Conjugated to the RNA Ligand Guanidinoneomycin, Chem. - A Eur. J. 21 (2015) 18474–18486, https://doi.org/10.1002/chem.201502373.
[119] A. Gandioso, E. Shaili, A. Massaguer, G. Artigas, A. González-Cantó, J.A. Woods, P.J. Sadler, V. Marchán, An integrin-targeted photoactivatable Pt(IV) complex as a selective anticancer pro-drug: synthesis and photoactivation studies, Chem. Commun. 51 (2015) 9169–9172, https://doi.org/10.1039/C5CC03180J.
[120] R. Lindner, G.N. Kaluderović, R. Paschke, C. Wagner, D. Steinborn, Synthesis and characterization of dinuclear pyrazolato bridged platinum(IV) complexes, Polyhedron 27 (2008) 914–922, https://doi.org/10.1016/j.poly.2007.11.020.
[121] N. Cutillas, G.S. Yellol, C. de Haro, C. Vicente, V. Rodríguez, J. Ruiz, Anticancer cyclometalated complexes of platinum group metals and gold, Coord. Chem. Rev. 257 (2013) 2784–2797, https://doi.org/10.1016/j.ccr.2013.03.024.
[122] M.N. Alam, F. Huq, Comprehensive review on tumour active palladium compounds and structure–activity relationships, Coord. Chem. Rev. 316 (2016) 36–67, https://doi.org/10.1016/j.ccr.2016.02.001.
[123] A.R. Kapdi, I.J.S. Fairlamb, Anti-cancer palladium complexes: a focus on PdX 2 L 2, palladacycles and related complexes, Chem. Soc. Rev. 43 (2014) 4751–4777, https://doi.org/10.1039/C4CS00063C.
[124] T.J. Carneiro, A.S. Martins, M.P.M. Marques, A.M. Gil, Metabolic Aspects of Palladium(II) Potential Anti-Cancer Drugs, Front. Oncol. 10 (2020) 2218, https://doi.org/10.3389/FONC.2020.590970/BIBTEX.
[125] T. Scattolin, V.A. Voloshkin, F. Visentin, S.P. Nolan, A critical review of palladium organometallic anticancer agents, Cell Rep. Phys. Sci. 2 (2021), https://doi.org/10.1016/J.XCRP.2021.100446.
[126] F. Visentin, T. Scattolin, E. Bortolamiol, I. Caligiuri, T. Perin, V. Canzonieri, S. Pluda, A. Angelini, N. Demitri, F. Rizzolio, A. Togni, S. Palazzolo, Palladium(II)-η3-allyl complexes bearing N-trifluoromethyl N-heterocyclic carbenes:a new generation of anticancer agents which restrain the growth of high grade serous ovarian cancer tumoroids, Chem. – A Eur. J. (2020), https://doi.org/10.1002/chem.202002199, chem.202002199.
[127] T. Scattolin, I. Caligiuri, N. Mouawad, M. El Boustani, N. Demitri, F. Rizzolio, F. Visentin, Synthesis and in-depth studies on the anticancer activity of novel palladacyclopentadienyl complexes stabilized by N-Heterocyclic carbene ligands, Eur. J. Med. Chem. 179 (2019) 325–334, https://doi.org/10.1016/j.ejmech.2019.06.065.
[128] A. Blanckenberg, S. Aliwaini, S.W. Kimani, A. van Niekerk, A. Neumann-Mufweba, S. Prince, S.F. Mapolie, Preparation, characterization and evaluation of novel 1,3,5-triaza-7-phosphaadamantane (PTA)-based palladacycles as anti-cancer agents, J. Organomet. Chem. 851 (2017) 68–78, https://doi.org/10.1016/j.jorganchem.2017.09.005.
[129] S. Aliwaini, A.J. Swarts, A. Blanckenberg, S. Mapolie, S. Prince, A novel binuclear palladacycle complex inhibits melanoma growth in vitro and in vivo through apoptosis and autophagy, Biochem. Pharmacol. 86 (2013) 1650–1663, https://doi.org/10.1016/j.bcp.2013.09.020.
[130] D.L. Dai, M. Martinka, G. Li, Prognostic Significance of Activated Akt Expression in Melanoma: A Clinicopathologic Study of 292 Cases, J. Clin. Oncol. 23 (2005) 1473–1482, https://doi.org/10.1200/JCO.2005.07.168.
[131] J. Spencer, R.P. Rathnam, M. Motukuri, A.K. Kotha, S.C.W. Richardson, A. Hazrati, J.A. Hartley, L. Male, M.B. Hursthouse, Synthesis of a 1,4-benzodiazepine containing palladacycle with in vitro anticancer and cathepsin B activity, Dalton Trans. (2009) 4299, https://doi.org/10.1039/b819061e.
[132] R.F.F. de Souza, G.A. da Cunha, J.C.M. Pereira, D.M. Garcia, C. Bincoletto, R.N. Goto, A.M. Leopoldino, I.C. da Silva, F.R. Pavan, V.M. Deflon, E.T. de Almeida, A. E. Mauro, A.V.G. Netto, Orthopalladated acetophenone oxime compounds

bearing thioamides as ligands: Synthesis, structure and cytotoxic evaluation, Inorganica Chim. Acta. 486 (2019) 617–624, https://doi.org/10.1016/j.ica.2018.11.022.
[133] G.A. da Cunha, R.F.F. de Souza, R.L. de Farias, M.B. Moreira, D.E.S. Silva, R.D. Zanetti, D.M. Garcia, D.G. Spindola, L.F.G. Michelin, C. Bincoletto, A.A. de Souza, A.A. Antunes, W.A.d.S. Judice, R.C.F. Leitao, V.M. Deflon, A.E. Mauro, A. V.G. Netto, Cyclopalladated compounds containing 2,6-lutidine: Synthesis, spectral and biological studies, J. Inorg. Biochem. 203 (2020) 110944.
[134] E. Budzisz, R. Bobka, A. Hauss, J.N. Roedel, S. Wirth, I.P. Lorenz, B. Rozalska, M. Więckowska-Szakiel, U. Krajewska, M. Rozalski, Synthesis, structural characterization, antimicrobial and cytotoxic effects of aziridine, 2-aminoethylaziridine and azirine complexes of copper(ii) and palladium(ii), Dalton Trans. 41 (2012) 5925–5933, https://doi.org/10.1039/c2dt12107g.
[135] A.R. Kapdi, A.C. Whitwood, D.C. Williamson, J.M. Lynam, M.J. Burns, T.J. Williams, A.J. Reay, J. Holmes, I.J.S. Fairlamb, The elusive structure of Pd2(dba)3. Examination by isotopic labeling, NMR spectroscopy, and X-ray diffraction analysis: Synthesis and characterization of Pd2(dba-Z)3 complexes, J. Am. Chem. Soc. 135 (2013) 8388–8399, https://doi.org/10.1021/ja403259c.
[136] S.S. Bhandarkar, J. Bromberg, C. Carrillo, P. Selvakumar, R.K. Sharma, B.N. Perry, B. Govindarajan, L. Fried, A. Sohn, K. Reddy, J.L. Arbiser, Tris (dibenzylideneacetone) dipalladium, a N-myristoyltransferase-1 inhibitor, is effective against melanoma growth in vitro and in vivo, Clin. Cancer Res. 14 (2008) 5743–5748, https://doi.org/10.1158/1078-0432.CCR-08-0405.
[137] N.E. Kay, T. Sassoon, C. Secreto, S. Sinha, T.D. Shanafelt, A.K. Ghosh, J.L. Arbiser, Tris (dibenzylideneacetone) dipalladium: a small-molecule palladium complex is effective in inducing apoptosis in chronic lymphocytic leukemia B-cells, Leuk. Lymphoma 57 (2016) 2409–2416, https://doi.org/10.3109/10428194.2016.1161186.
[138] B. Díaz, K.T. Ostapoff, J.E. Toombs, J. Lo, M.Y. Bonner, A. Curatolo, V. Adsay, R. A. Brekken, J.L. Arbiser, Tris DBA palladium is highly effective against growth and metastasis of pancreatic cancer in an orthotopic model, Oncotarget. 7 (2016) 51569–51580, https://doi.org/10.18632/oncotarget.10514.
[139] E. Musi, G.K. Schwartz, J.H. Yoo, S.J. Odelberg, D.Y. Li, M.Y. Bonner, P. Selvakumar, S. Rao, L.C. Gilbert, J. Elsey, J.L. Arbiser, Tris DBA palladium is an orally available inhibitor of GNAQ mutant uveal melanoma in vivo, Oncotarget. 10 (2019) 4424–4436, https://doi.org/10.18632/oncotarget.27040.
[140] E.I. Solomon, D.E. Heppner, E.M. Johnston, J.W. Ginsbach, J. Cirera, M. Qayyum, M.T. Kieber-Emmons, C.H. Kjaergaard, R.G. Hadt, L. Tian, Copper active sites in biology, Chem. Rev. 114 (2014) 3659–3853, https://doi.org/10.1021/cr400327t.
[141] T.D. Rae, P.J. Schmidt, R.A. Pufahl, V.C. Culotta, T. V. O'Halloran, Undetectable Intracellular Free Copper: The Requirement of a Copper Chaperone for Superoxide Dismutase, Science 284 (5415) (1999) 805–808.
[142] E.J. Ge, A.I. Bush, A. Casini, P.A. Cobine, J.R. Cross, G.M. DeNicola, Q.P. Dou, K.J. Franz, V.M. Gohil, S. Gupta, S.G. Kaler, S. Lutsenko, V. Mittal, M.J. Petris, R. Polishchuk, M. Ralle, M.L. Schilsky, N.K. Tonks, L.T. Vahdat, L. Van Aelst, D. Xi, P. Yuan, D.C. Brady, C.J. Chang, Connecting copper and cancer: from transition metal signalling to metalloplasia, Nat. Rev. Cancer 22 (2) (2022) 102–113.
[143] D.S. Sigman, D.R. Graham, V. D'Aurora, A.M. Stern, Oxygen-dependent cleavage of DNA by the 1,10-phenanthroline. cuprous complex. Inhibition of Escherichia coli DNA polymerase I, J. Biol. Chem. 254 (24) (1979) 12269–12272.
[144] C.H. Chen, D.S. Sigman, Nuclease activity of 1,10-phenanthroline-copper: sequence-specific targeting, Proc. Natl. Acad. Sci. U. S. A. 83 (19) (1986) 7147–7151.
[145] A.P. Borges, Z.A. Carneiro, F.S. Prado, J.R. Souza, L.H. Furlan e Silva, C.G. Oliveira, V.M. Deflon, S. de Albuquerque, N.B. Leite, A.E.H. Machado, A.O.T. Patrocinio, P.I.S. Maia, complexes with thiosemicarbazides derived from p-toluenesulfohydrazide: Structural, luminescence and biological studies, Polyhedron 155 (2018) 170–179.
[146] F. Tisato, C. Marzano, V. Peruzzo, M. Tegoni, M. Giorgetti, M. Damjanovic, A. Trapananti, A. Bagno, C. Santini, M. Pellei, M. Porchia, V. Gandin, Insights into the cytotoxic activity of the phosphane copper(I) complex [Cu(thp) 4 ][PF 6 ], J. Inorg. Biochem. 165 (2016) 80–91, https://doi.org/10.1016/j.jinorgbio.2016.07.007.
[147] M. Porchia, A. Dolmella, V. Gandin, C. Marzano, M. Pellei, V. Peruzzo, F. Refosco, C. Santini, F. Tisato, Neutral and charged phosphine/scorpionate copper(I) complexes: Effects of ligand assembly on their antiproliferative activity, Eur. J. Med. Chem. 59 (2013) 218–226, https://doi.org/10.1016/j.ejmech.2012.11.022.
[148] S. Chen, L. Sun, K. Koya, N. Tatsuta, Z. Xia, T. Korbut, Z. Du, J. Wu, G. Liang, J. Jiang, M. Ono, D. Zhou, A. Sonderfan, Syntheses and antitumor activities of N′1, N′3-dialkyl-N′1, N′3-di- (alkylcarbonothioyl) malonohydrazide: The discovery of elesclomol, Bioorganic Med, Chem. Lett. 23 (2013) 5070–5076, https://doi.org/10.1016/j.bmcl.2013.07.032.
[149] M. Nagai, N.H. Vo, L.S. Ogawa, D. Chimmanamada, T. Inoue, J. Chu, B.C. Beaudette-Zlatanova, R. Lu, R.K. Blackman, J. Barsoum, K. Koya, Y. Wada, The oncology drug elesclomol selectively transports copper to the mitochondria to induce oxidative stress in cancer cells, Free Radic. Biol. Med. 52 (2012) 2142–2150, https://doi.org/10.1016/j.freeradbiomed.2012.03.017.
[150] A.A. Yadav, D. Patel, X. Wu, B.B. Hasinoff, Molecular mechanisms of the biological activity of the anticancer drug elesclomol and its complexes with Cu(II), Ni(II) and Pt(II), J. Inorg. Biochem. 126 (2013) 1–6, https://doi.org/10.1016/j.jinorgbio.2013.04.013.
[151] B.B. Hasinoff, A.A. Yadav, D. Patel, X. Wu, The cytotoxicity of the anticancer drug elesclomol is due to oxidative stress indirectly mediated through its complex with Cu(II), J. Inorg. Biochem. 137 (2014) 22–30, https://doi.org/10.1016/j.jinorgbio.2014.04.004.
[152] B.B. Hasinoff, X. Wu, A.A. Yadav, D. Patel, H. Zhang, D.S. Wang, Z.S. Chen, J.C. Yalowich, Cellular mechanisms of the cytotoxicity of the anticancer drug elesclomol and its complex with Cu(II), Biochem. Pharmacol. 93 (2015) 266–276, https://doi.org/10.1016/j.bcp.2014.12.008.
[153] R.K. Blackman, K. Cheung-Ong, M. Gebbia, D.A. Proia, S. He, J. Kepros, A. Jonneaux, P. Marchetti, J. Kluza, P.E. Rao, Y. Wada, G. Giaever, C. Nislow, Mitochondrial electron transport is the cellular target of the oncology drug elesclomol, PLoS One. 7 (2012), https://doi.org/10.1371/journal.pone.0029798.
[154] C. Al Hageh, M. Al Assaad, Z. El Masri, N. Samaan, M. El-Sibai, C. Khalil, R.S. Khnayzer, A long-lived cuprous bis-phenanthroline complex for the photodynamic therapy of cancer, Dalton Trans. 47 (2018) 4959–4967, https://doi.org/10.1039/c8dt00140e.
[155] R.-K. Lin, C.-I. Chiu, C.-H. Hsu, Y.-J. Lai, P. Venkatesan, P.-H. Huang, P.-S. Lai, C.-C. Lin, Photocytotoxic Copper(II) Complexes with Schiff-Base Scaffolds for Photodynamic Therapy, Chem. - A Eur. J. 24 (2018) 4111–4120, https://doi.org/10.1002/chem.201705640.
[156] R. Křikavová, J. Vančo, Z. Trávníček, J. Hutyra, Z. Dvořák, Design and characterization of highly in vitro antitumor active ternary copper(II) complexes containing 2′-hydroxychalcone ligands, J. Inorg. Biochem. 163 (2016) 8–17, https://doi.org/10.1016/j.jinorgbio.2016.07.005.
[157] H.H. Hammud, U. Kortz, S. Bhattacharya, S. Demirdjian, E. Hariri, S. Isber, E. Sang Choi, B. Mirtamizdoust, M. Mroueh, C.F. Daher, Structure, DFT studies, Magnetism and Biological activity of Bis[(μ2-azido)-chloro-(1,10-phenanthroline)-copper(II)] complex, Inorganica Chim. Acta. (2020), https://doi.org/10.1016/j.ica.2020.119533 119533.
[158] C.-H. Ng, W.-S. Wang, K.-V. Chong, Y.-F. Win, K.-E. Neo, H.-B. Lee, S.-L. San, R. N.Z. Raja Abd, W.K.L. Rahman, Ternary copper(ii)-polypyridyl enantiomers: aldol-type condensation, characterization, DNA-binding recognition, BSA-binding and anticancer property, Dalton Trans. 42 (2013) 10233, https://doi.org/10.1039/c3dt50884f.
[159] C. Slator, N. Barron, O. Howe, A. Kellett, [Cu(o -phthalate)(phenanthroline)] Exhibits Unique Superoxide-Mediated NCI-60 Chemotherapeutic Action through Genomic DNA Damage and Mitochondrial Dysfunction, ACS Chem. Biol. 11 (2016) 159–171, https://doi.org/10.1021/acschembio.5b00513.
[160] C. Slator, Z. Molphy, V. McKee, C. Long, T. Brown, A. Kellett, Di-copper metallodrugs promote NCI-60 chemotherapy via singlet oxygen and superoxide production with tandem TA/TA and AT/AT oligonucleotide discrimination, Nucleic Acids Res. 46 (2018) 2733–2750, https://doi.org/10.1093/nar/gky105.
[161] M. Ahmad, S.-N. Suhaimi, T.-L. Chu, N. Abdul Aziz, N.-K. Mohd Kornain, D.S. Samiulla, K.-W. Lo, C.-H. Ng, A.S.-B. Khoo, Ternary copper(II) complex: NCI60 screening, toxicity studies, and evaluation of efficacy in xenograft models of nasopharyngeal carcinoma, PLoS One. 13 (2018), https://doi.org/10.1371/journal.pone.0191295.
[162] S. Barrett, M. De Franco, A. Kellett, E. Dempsey, C. Marzano, A. Erxleben, V. Gandin, D. Montagner, Anticancer activity, DNA binding and cell mechanistic studies of estrogen-functionalised Cu(II) complexes, J. Biol. Inorg. Chem. 25 (2020) 49–60, https://doi.org/10.1007/s00775-019-01732-8.
[163] D.H. Nakahata, R.E.F. de Paiva, W.R. Lustri, C.M. Ribeiro, F.R. Pavan, G.G. da Silva, A.L.T.G. Ruiz, J.E. de Carvalho, P.P. Corbi, Sulfonamide-containing copper(II) metallonucleases: Correlations with in vitro antimycobacterial and antiproliferative activities, J. Inorg. Biochem. 187 (2018) 85–96, https://doi.org/10.1016/j.jinorgbio.2018.07.011.
[164] R.H.G. Teles, A.E. Graminha, C.M. Rivera-Cruz, D.H. Nakahata, A.L.B. Formiga, P.P. Corbi, M.L. Figueiredo, M.R. Cominetti, Copper transporter 1 affinity as a delivery strategy to improve the cytotoxic profile of rationally designed copper(II) complexes for cancer treatment, Toxicol. Vitr. 67 (2020), https://doi.org/10.1016/j.tiv.2020.104922 104922.
[165] M. Jopp, J. Becker, S. Becker, A. Miska, V. Gandin, C. Marzano, S. Schindler, Anticancer activity of a series of copper(II) complexes with tripodal ligands, Eur. J. Med. Chem. 132 (2017) 274–281, https://doi.org/10.1016/j.ejmech.2017.03.019.
[166] L.J.H. Borges, É.S. Bull, C. Fernandes, A. Horn, N.F. Azeredo, J.A.L.C. Resende, W. R. Freitas, E.C.Q. Carvalho, L.S. Lemos, H. Jerdy, M.M. Kanashiro, In vitro and in vivo studies of the antineoplastic activity of copper (II) compounds against human leukemia THP-1 and murine melanoma B16–F10 cell lines, Eur. J. Med. Chem. 123 (2016) 128–140, https://doi.org/10.1016/j.ejmech.2016.07.018.
[167] C. Fernandes, A. Horn, B.F. Lopes, E.S. Bull, N.F.B. Azeredo, M.M. Kanashiro, F. V. Borges, A.J. Bortoluzzi, B. Szpoganicz, A.B. Pires, R.W.A. Franco, J.C.D.A. Almeida, L.L.F. Maciel, J.A.L.C. Resende, G. Schenk, Induction of apoptosis in leukemia cell lines by new copper(II) complexes containing naphthyl groups via interaction with death receptors, J. Inorg. Biochem. 153 (2015) 68–87, https://doi.org/10.1016/j.jinorgbio.2015.09.014.
[168] J.P. Rada, B.S.M. Bastos, L. Anselmino, C.H.J. Franco, M. Lanznaster, R. Diniz, C. O. Fernández, M. Menacho-Márquez, A.M. Percebom, N.A. Rey, Binucleating Hydrazonic Ligands and Their μ-Hydroxodicopper(II) Complexes as Promising Structural Motifs for Enhanced Antitumor Activity, Inorg. Chem. 58 (2019) 8800–8819, https://doi.org/10.1021/acs.inorgchem.9b01195.
[169] C.J. Nunes, B.E. Borges, L.S. Nakao, E. Peyroux, R. Hardré, B. Faure, M. Réglier, M. Giorgi, M.B. Prieto, C.C. Oliveira, A.M. Da Costa Ferreira, Reactivity of

dinuclear copper(II) complexes towards melanoma cells: Correlation with its stability, tyrosinase mimicking and nuclease activity, J. Inorg. Biochem. 149 (2015) 49–58, https://doi.org/10.1016/j.jinorgbio.2015.05.007.
[170] C.J. Nunes, A.H. Otake, S.O. Bustos, R.B. Fazzi, R. Chammas, A.M. Da Costa Ferreira, Unlike reactivity of mono- and binuclear imine-copper(II) complexes toward melanoma cells via a tyrosinase-dependent mechanism, Chem. Biol. Interact. 311 (2019), https://doi.org/10.1016/j.cbi.2019.108789 108789.
[171] E.E. Aranda, T.A. Matias, K. Araki, A.P. Vieira, E.A. de Mattos, P. Colepicolo, C.P. Luz, F.L.N. Marques, A.M. da Costa Ferreira, Design, syntheses, characterization, and cytotoxicity studies of novel heterobinuclear oxindolimine copper(II)-platinum(II) complexes, J. Inorg. Biochem. 165 (2016) 108–118, https://doi.org/10.1016/j.jinorgbio.2016.08.001.
[172] E.E. Aranda, J.S. da Luz, C.C. Oliveira, P.A. Divina Petersen, H.M. Petrilli, A.M. da Costa Ferreira, Heterobinuclear copper(II)-platinum(II) complexes with oxindolimine ligands: Interactions with DNA, and inhibition of kinase and alkaline phosphatase proteins, J. Inorg. Biochem. 203 (2020), https://doi.org/10.1016/j.jinorgbio.2019.110863.
[173] M. Carcelli, M. Tegoni, J. Bartoli, C. Marzano, G. Pelosi, M. Salvalaio, D. Rogolino, V. Gandin, In vitro and in vivo anticancer activity of tridentate thiosemicarbazone copper complexes: Unravelling an unexplored pharmacological target, Eur. J. Med. Chem. 194 (2020), https://doi.org/10.1016/j.ejmech.2020.112266 112266.
[174] S. Xu, S. Sankar, N. Neamati, Protein disulfide isomerase: A promising target for cancer therapy, Drug Discov. Today. 19 (2014) 222–240, https://doi.org/10.1016/j.drudis.2013.10.017.
[175] S. Parakh, J.D. Atkin, Novel roles for protein disulphide isomerase in disease states: A double edged sword?, Front Cell Dev. Biol. 3 (2015) 30, https://doi.org/10.3389/fcell.2015.00030.
[176] E. Lee, D.H. Lee, Emerging roles of protein disulfide isomerase in cancer, BMB Rep. 50 (2017) 401–410, https://doi.org/10.5483/BMBRep.2017.50.8.107.
[177] P.E. Lovat, M. Corazzari, J.L. Armstrong, S. Martin, V. Pagliarini, D. Hill, A.M. Brown, M. Piacentini, M.A. Birch-Machin, C.P.F. Redfern, Increasing melanoma cell death using inhibitors of protein disulfide isomerases to abrogate survival responses to endoplasmic reticulum stress, Cancer Res. 68 (2008) 5363–5369, https://doi.org/10.1158/0008-5472.CAN-08-0035.
[178] D. Senthil Raja, N.S.P. Bhuvanesh, K. Natarajan, Effect of N(4)-Phenyl Substitution in 2-Oxo-1,2-dihydroquinoline-3-carbaldehyde Semicarbazones on the Structure, DNA/Protein Interaction, and Antioxidative and Cytotoxic Activity of Cu(II) Complexes, Inorg. Chem. 50 (2011) 12852–12866, https://doi.org/10.1021/ic2020308.
[179] M. Grazul, E. Besic-Gyenge, C. Maake, M. Ciolkowski, M. Czyz, R.K.O. Sigel, E. Budzisz, Synthesis, physico-chemical properties and biological analysis of newly obtained copper(II) complexes with pyrazole derivatives, J. Inorg. Biochem. 135 (2014) 68–76, https://doi.org/10.1016/j.jinorgbio.2014.02.014.
[180] B.L. Fei, S. Tu, Z. Wei, P. Wang, C. Qiao, Z.F. Chen, Optically pure chiral copper (II) complexes of rosin derivative as attractive anticancer agents with potential anti-metastatic and anti-angiogenic activities, Eur. J. Med. Chem. 176 (2019) 175–186, https://doi.org/10.1016/j.ejmech.2019.05.030.
[181] C. Spoerlein, K. Mahal, H. Schmidt, R. Schobert, Effects of chrysin, apigenin, genistein and their homoleptic copper(II) complexes on the growth and metastatic potential of cancer cells, J. Inorg. Biochem. 127 (2013) 107–115, https://doi.org/10.1016/j.jinorgbio.2013.07.038.
[182] Y.-T. Huang, J.J. Hwang, P.-P. Lee, F.C. Ke, J.-H. Huang, C.J. Huang, C. Kandaswami, E. Middleton, M.T. Lee, Effects of luteolin and quercetin, inhibitors of tyrosine kinase, on cell growth and metastasis-associated properties in A431 cells overexpressing epidermal growth factor receptor, Br. J. Pharmacol. 128 (1999) 999–1010, https://doi.org/10.1038/sj.bjp.0702879.
[183] K.G. Daniel, P. Gupta, R.H. Harbach, W.C. Guida, Q.P. Dou, Organic copper complexes as a new class of proteasome inhibitors and apoptosis inducers in human cancer cells, Biochem. Pharmacol. 67 (2004) 1139–1151, https://doi.org/10.1016/j.bcp.2003.10.031.
[184] D. Jain, N. Patel, M. Shelton, A. Basu, R. Roque, W. Siede, Enhancement of cisplatin sensitivity by NSC109268 in budding yeast and human cancer cells is associated with inhibition of S-phase progression, Cancer Chemother. Pharmacol. 66 (2010) 945–952, https://doi.org/10.1007/s00280-010-1246-8.
[185] E. Shankar, C. Basu, B. Adkins, W. Siede, A. Basu, NSC109268 potentiates cisplatin-induced cell death in a p53-independent manner, J. Mol. Signal. 5 (2010) 1–7, https://doi.org/10.1186/1750-2187-5-4.
[186] Y.-H. Yao, Y. Luo, J. Li, F.-X. Zhang, Synthesis of Novel Porphyrin Derivatives and Their Cytotoxic Activities against A431 Cells, Helv. Chim. Acta 99 (2016) 24–29, https://doi.org/10.1002/hlca.201500184.
[187] C. Nardon, D. Fregona, Gold(III) Complexes in the Oncological Preclinical Arena: From Aminoderivatives to Peptidomimetics, Curr. Top. Med. Chem. 16 (2015) 360–380, https://doi.org/10.2174/1568026615666150827094500.
[188] P.J. Barnard, S.J. Berners-Price, Targeting the mitochondrial cell death pathway with gold compounds, Coord. Chem. Rev. 251 (2007) 1889–1902, https://doi.org/10.1016/j.ccr.2007.04.006.
[189] I. Ott, On the medicinal chemistry of gold complexes as anticancer drugs, Coord. Chem. Rev. 253 (2009) 1670–1681, https://doi.org/10.1016/j.ccr.2009.02.019.
[190] A. Bindoli, M.P. Rigobello, G. Scutari, C. Gabbiani, A. Casini, L. Messori, Thioredoxin reductase: A target for gold compounds acting as potential anticancer drugs, Coord. Chem. Rev. 253 (2009) 1692–1707, https://doi.org/10.1016/j.ccr.2009.02.026.
[191] T. Zou, A. Ching, T. Lum, C.-N. Lok, J.-J. Zhang, C.-M. Che, Chemical biology of anticancer gold(III) and gold(I) complexes, Chem. Soc. Rev. 44 (2015) 8786–8801, https://doi.org/10.1039/c5cs00132c.
[192] B. Huang, M. Hu, F.D. Toste, Homogeneous Gold Redox Chemistry: Organometallics, Catalysis, and Beyond, Trends Chem. 2 (2020) 707–720, https://doi.org/10.1016/j.trechm.2020.04.012.
[193] C. Roder, M.J. Thomson, Auranofin: Repurposing an Old Drug for a Golden New Age, Drugs R D. 15 (2015) 13–20, https://doi.org/10.1007/s40268-015-0083-y.
[194] W.C. Stafford, X. Peng, M.H. Olofsson, X. Zhang, D.K. Luci, L. Lu, Q. Cheng, L. Trésaugues, T.S. Dexheimer, N.P. Coussens, M. Augsten, H.-S.-M. Ahlzén, O. Orwar, A. Östman, S. Stone-Elander, D.J. Maloney, A. Jadhav, A. Simeonov, S. Linder, E.S.J. Arnér, Irreversible inhibition of cytosolic thioredoxin reductase 1 as a mechanistic basis for anticancer therapy, Sci. Transl. Med. 10 (2018), https://doi.org/10.1126/scitranslmed.aaf7444.
[195] J. Wang, J. Wang, E. Lopez, H. Guo, H. Zhang, Y. Liu, Z. Chen, S. Huang, S. Zhou, A. Leeming, R.J. Zhang, D. Jung, H. Shi, H. Grundman, D. Doakes, K. Cui, C. Jiang, M. Ahmed, K. Nomie, B. Fang, M. Wang, Y. Yao, L. Zhang, Repurposing auranofin to treat TP53-mutated or PTEN-deleted refractory B-cell lymphoma, Blood, Cancer J. 9 (2019) 1–6, https://doi.org/10.1038/s41408-019-0259-8.
[196] C. Fan, W. Zheng, X. Fu, X. Li, Y.S. Wong, T. Chen, Enhancement of auranofin-induced lung cancer cell apoptosis by selenocystine, a natural inhibitor of TrxR1 in vitro and in vivo, Cell Death Dis. 5 (2014), https://doi.org/10.1038/cddis.2014.132, e1191–e1191.
[197] C.K. Mirabelli, R.K. Johnson, C.M. Sung, L. Faucette, K. Muirhead, S.T. Crooke, Evaluation of the in vivo antitumor activity and in vitro cytotoxic properties of auranofin, a coordinated gold compound, murine tumor models, Cancer Res. 45 (1985) 32–39.
[198] S. Goenka, S.R. Simon, Organogold drug Auranofin exhibits anti-melanogenic activity in B16F10 and MNT-1 melanoma cells, Arch. Dermatol. Res. 312 (2020) 213–221, https://doi.org/10.1007/s00403-019-01974-1.
[199] M.C.C. Sachweh, W.C. Stafford, C.J. Drummond, A.R. McCarthy, M. Higgins, J. Campbell, B. Brodin, E.S.J. Arnér, S. Laín, Redox effects and cytotoxic profiles of MJ25 and auranofin towards malignant melanoma cells, Oncotarget. 6 (2015) 16488–16506, https://doi.org/10.18632/oncotarget.4108.
[200] P.B. Cassidy, S.A. Leachman, P.J. Moos, CHAPTER 23. Selenium and Skin Cancer, in: Food Nutr. Components Focus, Royal Society of Chemistry, 2015: pp. 391–407. doi:10.1039/9781782622215-00391.
[201] S. Iwasawa, Y. Yamano, Y. Takiguchi, H. Tanzawa, K. Tatsumi, K. Uzawa, Upregulation of thioredoxin reductase 1 in human oral squamous cell carcinoma, Oncol. Rep. 25 (2011) 637–644, https://doi.org/10.3892/or.2010.1131.
[202] A. Ecker, N.V. Barbosa, D. Ardisson-Araujo, Accessing the transcriptional status of selenoproteins in skin cancer-derived cell lines, J. Trace Elem. Med Biol. 60 (2020), https://doi.org/10.1016/j.jtemb.2020.126476 126476.
[203] P.B. Cassidy, M. Honeggar, R.L. Poerschke, K. White, S.R. Florell, R.H.I. Andtbacka, J. Tross, M. Anderson, S.A. Leachman, P.J. Moos, The role of thioredoxin reductase 1 in melanoma metabolism and metastasis, Pigment Cell Melanoma Res. 28 (2015) 685–695, https://doi.org/10.1111/pcmr.12398.
[204] M. Sobhani, A.R. Taheri, A.H. Jafarian, S.I. Hashemy, The activity and tissue distribution of thioredoxin reductase in basal cell carcinoma, J. Cancer Res. Clin. Oncol. 142 (2016) 2303–2307, https://doi.org/10.1007/s00432-016-2242-0.
[205] C.K. Mirabelli, D.T. Hill, R.K. Johnson, L.F. Faucette, C.M. Sung, S.T. Crooke, G.R. Girard, G.Y. Kuo, Correlation of the in Vitro Cytotoxic and in Vivo Antitumor Activities of Gold(I) Coordination Complexes, J. Med. Chem. 29 (1986) 218–223, https://doi.org/10.1021/jm00152a009.
[206] C.K. Mirabelli, D.T. Hill, L.F. Faucette, F.L. Mccabe, G.R. Girard, R.K. Johnson, S. T. Crooke, J.O.L. Bartus, B.M. Sutton, D.B. Bryan, Antitumor Activity of Bis (diphenylphosphino)alkanes, Their Gold(I) Coordination Complexes, and Related Compounds, J. Med. Chem. 30 (1987) 2181–2190, https://doi.org/10.1021/jm00395a004.
[207] S.J. Berners-Price, C.K. Mirabelli, R.K. Johnson, M.R. Mattern, F.L. McCabe, L.F. Faucette, C.M. Sung, S.M. Mong, P.J. Sadler, S.T. Crooke, In vivo antitumor activity and in vitro cytotoxic properties of bis[1,2-bis(diphenylphosphino) ethane]gold(I) chloride, Cancer Res. 46 (1986) 5486–5493. http://www.ncbi.nlm.nih.gov/pubmed/3756897.
[208] J.D.S. Chaves, F. Neumann, T.M. Francisco, C.C. Corrêa, M.T.P. Lopes, H. Silva, A. P.S. Fontes, M.V. De Almeida, Synthesis and cytotoxic activity of gold(I) complexes containing phosphines and 3-benzyl-1,3-thiazolidine-2-thione or 5-phenyl-1,3,4-oxadiazole-2-thione as ligands, Inorganica Chim. Acta. 414 (2014) 85–90, https://doi.org/10.1016/j.ica.2014.01.042.
[209] A. Garcia, R.C. Machado, R.M. Grazul, M.T.P. Lopes, C.C. Corrêa, H.F. Dos Santos, M.V. De Almeida, H. Silva, Novel antitumor adamantane-azole gold(I) complexes as potential inhibitors of thioredoxin reductase, J. Biol. Inorg. Chem. 21 (2016) 275–292, https://doi.org/10.1007/s00775-016-1338-y.
[210] J.D.S. Chaves, L.G. Tunes, C.H. de J. Franco, T.M. Francisco, C.C. Corrêa, S.M.F. Murta, R.L. Monte-Neto, H. Silva, A.P.S. Fontes, M.V. de Almeida, Novel gold(I) complexes with 5-phenyl-1,3,4-oxadiazole-2-thione and phosphine as potential anticancer and antileishmanial agents, Eur. J. Med. Chem. 127 (2017) 727–739.
[211] A.M. de Almeida, B.A. de Oliveira, P.P. de Castro, C.C. de Mendonça, R.A. Furtado, H.D. Nicolella, V.L. da Silva, C.G. Diniz, D.C. Tavares, H. Silva, M.V. de Almeida, Lipophilic gold(I) complexes with 1,3,4-oxadiazol-2-thione or 1,3-thiazolidine-2-thione moieties: synthesis and their cytotoxic and

antimicrobial activities, Biometals 30 (2017) 841–857, https://doi.org/10.1007/s10534-017-0046-6.
[212] T.T. Tavares, G.C. Azevedo, A. Garcia, A.G. Carpanez, P.M. Lewer, D. Paschoal, B.L. Müller, H.F. Dos Santos, R.C. Matos, H. Silva, R.M. Grazul, A.P.S. Fontes, Gold(I) complexes with aryl-thiosemicarbazones: Molecular modeling, synthesis, cytotoxicity and TrxR inhibition, Polyhedron 132 (2017) 95–104, https://doi.org/10.1016/j.poly.2017.05.004.
[213] L.R.V. Favarin, G.B. Laranjeira, C.F.A. Teixeira, H. Silva, A.C. Micheletti, L. Pizzuti, A. Machulek Júnior, A.R.L. Caires, V.M. Deflon, R.B.P. Pesci, C.N.L. Rocha, J.R. Correa, L.M.C. Pinto, G.A. Casagrande, Harvesting greenish blue luminescence in gold(i) complexes and their application as promising bioactive molecules and cellular bioimaging agents, New J. Chem. 44 (2020) 6862–6871, https://doi.org/10.1039/d0nj01339k.
[214] V. Ganga Reddy, T. Srinivasa Reddy, S.H. Privér, Y. Bai, S. Mishra, D. Wlodkowic, N. Mirzadeh, S. Bhargava, Synthesis of Gold(I) Complexes Containing Cinnamide. In Vitro Evaluation of Anticancer Activity in 2D and 3D Spheroidal Models of Melanoma and in Vivo Angiogenesis, Inorg. Chem. 58 (2019) 5988–5999, https://doi.org/10.1021/acs.inorgchem.9b00281.
[215] H.V. Huynh, Electronic properties of N-heterocyclic carbenes and their experimental determination, Chem. Rev. 118 (2018) 9457–9492, https://doi.org/10.1021/acs.chemrev.8b00067.
[216] A. Nandy, S.K. Dey, S. Das, R.N. Munda, J. Dinda, K.D. Saha, Gold (I) N-heterocyclic carbene complex inhibits mouse melanoma growth by p53 upregulation, Mol. Cancer. 13 (2014) 1–14, https://doi.org/10.1186/1476-4598-13-57.
[217] Z. Herceg, Z.Q. Wang, Functions of poly(ADP-ribose) polymerase (PARP) in DNA repair, genomic integrity and cell death, Mutat. Res. - Fundam. Mol. Mech. Mutagen. 477 (2001) 97–110, https://doi.org/10.1016/S0027-5107(01)00111-7.
[218] A.B. Niculescu, X. Chen, M. Smeets, L. Hengst, C. Prives, S.I. Reed, Effects of p21Cip1/Waf1 at Both the G1/S and the G2/M Cell Cycle Transitions: pRb Is a critical determinant in blocking DNA replication and in preventing endoreduplication, Mol. Cell. Biol. 18 (1998), https://doi.org/10.1128/MCB.18.3.1763, 1763-1763.
[219] T. Zou, C.T. Lum, C.N. Lok, W.P. To, K.H. Low, C.M. Che, A binuclear gold(I) complex with mixed bridging diphosphine and bis(N-heterocyclic carbene) ligands shows favorable thiol reactivity and inhibits tumor growth and angiogenesis in vivo, Angew. Chemie - Int. Ed. 53 (2014) 5810–5814, https://doi.org/10.1002/anie.201400142.
[220] J.K. Muenzner, B. Biersack, H. Kalie, I.C. Andronache, L. Kaps, D. Schuppan, F. Sasse, R. Schobert, Gold(I) biscarbene complexes derived from vascular-disrupting combretastatin A-4 address different targets and show antimetastatic potential, ChemMedChem 9 (2014) 1195–1204, https://doi.org/10.1002/cmdc.201400049.
[221] L. Kaps, B. Biersack, H. Müller-Bunz, K. Mahal, J. Münzner, M. Tacke, T. Mueller, R. Schobert, Gold(I)-NHC complexes of antitumoral diarylimidazoles: Structures, cellular uptake routes and anticancer activities, J. Inorg. Biochem. 106 (2012) 52–58, https://doi.org/10.1016/j.jinorgbio.2011.08.026.
[222] J.K. Muenzner, B. Biersack, A. Albrecht, T. Rehm, U. Lacher, W. Milius, A. Casini, J.-J. Zhang, I. Ott, V. Brabec, O. Stuchlikova, I.C. Andronache, L. Kaps, D. Schuppan, R. Schobert, Ferrocenyl-coupled N-heterocyclic carbene complexes of gold(I): A successful approach to multinuclear anticancer drugs, Chem. - A Eur. J. 22 (2016) 18953–18962, https://doi.org/10.1002/chem.201604246.
[223] R. Rubbiani, S. Can, I. Kitanovic, H. Alborzinia, M. Stefanopoulou, M. Kokoschka, S. Mönchgesang, W.S. Sheldrick, S. Wölfl, I. Ott, Comparative in vitro evaluation of n-heterocyclic carbene gold(I) complexes of the benzimidazolylidene type, J. Med. Chem. 54 (2011) 8646–8657, https://doi.org/10.1021/jm201220n.
[224] R. Rubbiani, I. Kitanovic, H. Alborzinia, S. Can, A. Kitanovic, L.A. Onambele, M. Stefanopoulou, Y. Geldmacher, W.S. Sheldrick, G. Wolber, A. Prokop, S. Wölfl, I. Ott, Benzimidazol-2-ylidene gold(I) complexes are thioredoxin reductase inhibitors with multiple antitumor properties, J. Med. Chem. 53 (2010) 8608–8618, https://doi.org/10.1021/jm100801e.
[225] J. Oberkofler, B. Aikman, R. Bonsignore, A. Pöthig, J. Platts, A. Casini, F.E. Kühn, Exploring the reactivity and biological effects of heteroleptic N-heterocyclic carbene gold(I)-Alkynyl Complexes, Eur. J. Inorg. Chem. 2020 (11-12) (2020) 1040–1051.
[226] N. Estrada-Ortiz, F. Guarra, I.A.M. de Graaf, L. Marchetti, M.H. de Jager, G.M.M. Groothuis, C. Gabbiani, A. Casini, Anticancer gold N-heterocyclic carbene complexes: A comparative in vitro and ex vivo study, ChemMedChem 12 (2017) 1429–1435, https://doi.org/10.1002/cmdc.201700316.
[227] M. Pellei, V. Gandin, M. Marinelli, C. Marzano, M. Yousufuddin, H.V.R. Dias, C. Santini, Synthesis and biological activity of ester- and amide-functionalized imidazolium salts and related water-soluble coinage metal N-heterocyclic carbene complexes, Inorg. Chem. 51 (2012) 9873–9882, https://doi.org/10.1021/ic3013188.
[228] T. Zou, C.T. Lum, S.S.Y. Chui, C.M. Che, Gold(III) complexes containing N-heterocyclic carbene ligands: Thiol "switch-on" fluorescent probes and anti-cancer agents, Angew. Chemie - Int. Ed. 52 (2013) 2930–2933, https://doi.org/10.1002/anie.201209787.
[229] S. Radisavljević, I. Bratsos, A. Scheurer, J. Korzekwa, R. Masnikosa, A. Tot, N. Gligorijević, S. Radulović, A. Rilak Simović, New gold pincer-type complexes: Synthesis, characterization, DNA binding studies and cytotoxicity, Dalton Trans. 47 (2018) 13696–13712, https://doi.org/10.1039/c8dt02903b.
[230] B. Aikman, M. Wenzel, A. Mósca, A. de Almeida, W. Klooster, S. Coles, G. Soveral, A. Casini, Gold(III) Pyridine-Benzimidazole Complexes as Aquaglyceroporin Inhibitors and Antiproliferative Agents, Inorganics. 6 (2018) 123, https://doi.org/10.3390/inorganics6040123.
[231] V. Amani, A. Abedi, S. Ghabeshi, H.R. Khavasi, S.M. Hosseini, N. Safari, Synthesis and characterization of a series of gold(III) complexes with the 4,4′-dimethyl-2,2′-bipyridine ligand: Counterion influence on the cytotoxicity of gold(III) complexes, Polyhedron 79 (2014) 104–115, https://doi.org/10.1016/j.poly.2014.04.064.
[232] N. Pantelić, B.B. Zmejkovski, B. Kolundžija, M.Đ. Crnogorac, J.M. Vujić, B. Dojčinović, S.R. Trifunović, T.P. Stanojković, T.J. Sabo, G.N. Kaluđerović, In vitro antitumor activity, metal uptake and reactivity with ascorbic acid and BSA of some gold(III) complexes with N, N′-ethylenediamine bidentate ester ligands, J. Inorg. Biochem. 172 (2017) 55–66, https://doi.org/10.1016/j.jinorgbio.2017.04.001.
[233] L.R. Gouvea, L.S. Garcia, D.R. Lachter, P.R. Nunes, F. De Castro Pereira, E.P. Silveira-Lacerda, S.R.W. Louro, P.J.S. Barbeira, L.R. Teixeira, Atypical fluoroquinolone gold(III) chelates as potential anticancer agents: Relevance of DNA and protein interactions for their mechanism of action, Eur. J. Med. Chem. 55 (2012) 67–73, https://doi.org/10.1016/j.ejmech.2012.07.004.
[234] K.J. Akerman, A.M. Fagenson, V. Cyril, M. Taylor, M.T. Muller, M.P. Akerman, O.Q. Munro, Gold(III) Macrocycles: Nucleotide-Specific Unconventional Catalytic Inhibitors of Human Topoisomerase I, J. Am. Chem. Soc. 136 (2014) 5670–5682, https://doi.org/10.1021/ja412350f.
[235] C.M. Che, R.W.Y. Sun, W.Y. Yu, C.B. Ko, N. Zhu, H. Sun, Gold(III) porphyrins as a new class of anticancer drugs: Cytotoxicity, DNA binding and induction of apoptosis in human cervix epitheloid cancer cells, Chem. Commun. 3 (2003) 1718–1719, https://doi.org/10.1039/b303294a.
[236] L. Vaughan, W. Glänzel, C. Korch, A. Capes-Davis, Widespread use of misidentified cell line KB (HeLa): Incorrect attribution and its impact revealed through mining the scientific literature, Cancer Res. 77 (2017) 2784–2788, https://doi.org/10.1158/0008-5472.CAN-16-2258.
[237] R.W.Y. Sun, C.K.L. Li, D.L. Ma, J.J. Yan, C.N. Lok, C.H. Leung, N. Zhu, C.M. Che, Stable anticancer gold(III)-porphyrin complexes: Effects of porphyrin structure, Chem. - A Eur. J. 16 (2010) 3097–3113, https://doi.org/10.1002/chem.200902741.
[238] D. Hu, Y. Liu, Y.T. Lai, K.C. Tong, Y.M. Fung, C.N. Lok, C.M. Che, Anticancer Gold (III) Porphyrins Target Mitochondrial Chaperone Hsp60, Angew. Chemie - Int. Ed. 55 (2016) 1387–1391, https://doi.org/10.1002/anie.201509612.
[239] C.T. Lum, A.S.T. Wong, M.C.M. Lin, C.M. Che, R.W.Y. Sun, A gold(iii) porphyrin complex as an anti-cancer candidate to inhibit growth of cancer-stem cells, Chem. Commun. 49 (2013) 4364–4366, https://doi.org/10.1039/c2cc37366a.
[240] C.T. Lum, L. Huo, R.-W.-Y. Sun, M. Li, H.F. Kung, C.-M. Che, M.C.M. Lin, Gold(III) porphyrin 1a prolongs the survival of melanoma-bearing mice and inhibits angiogenesis, Acta Oncol. (Madr) 50 (2011) 719–726, https://doi.org/10.3109/0284186X.2010.537693.
[241] R.D. Teo, J.Y. Hwang, J. Termini, Z. Gross, H.B. Gray, Fighting Cancer with Corroles, Chem. Rev. 117 (2017) 2711–2729, https://doi.org/10.1021/acs.chemrev.6b00400.
[242] R.D. Teo, H.B. Gray, P. Lim, J. Termini, E. Domeshek, Z. Gross, A cytotoxic and cytostatic gold(III) corrole, Chem. Commun. 50 (2014) 13789–13792, https://doi.org/10.1039/c4cc06577h.
[243] L. Ronconi, C. Maccato, D. Barreca, R. Saini, M. Zancato, D. Fregona, Gold(III) dithiocarbamate derivatives of N-methylglycine: An experimental and theoretical investigation, Polyhedron 24 (2005) 521–531, https://doi.org/10.1016/j.poly.2004.12.015.
[244] L. Ronconi, L. Giovagnini, C. Marzano, F. Bettìo, R. Graziani, G. Pilloni, D. Fregona, Gold Dithiocarbamate Derivatives as Potential Antineoplastic Agents: Design, Spectroscopic Properties, and in Vitro Antitumor Activity, Inorg. Chem. 44 (2005) 1867–1881, https://doi.org/10.1021/ic048260v.
[245] C. Marzano, L. Ronconi, F. Chiara, M.C. Giron, I. Faustinelli, P. Cristofori, A. Trevisan, D. Fregona, Gold(III)-dithiocarbamato anticancer agents: Activity, toxicology and histopathological studies in rodents, Int. J. Cancer 129 (2011) 487–496, https://doi.org/10.1002/ijc.25684.
[246] V. Milacic, D. Chen, L. Ronconi, K.R. Landis-Piwowar, D. Fregona, Q.P. Dou, A Novel Anticancer Gold(III) Dithiocarbamate Compound Inhibits the Activity of a Purified 20S Proteasome and 26S Proteasome in Human Breast Cancer Cell Cultures and Xenografts, Cancer Res. 66 (2006) 10478–10486, https://doi.org/10.1158/0008-5472.CAN-06-3017.
[247] L. Cattaruzza, D. Fregona, M. Mongiat, L. Ronconi, A. Fassina, A. Colombatti, D. Aldinucci, Antitumor activity of gold(III)-dithiocarbamato derivatives on prostate cancer cells and xenografts, Int. J. Cancer 128 (2011) 206–215, https://doi.org/10.1002/ijc.25311.
[248] M. Negom Kouodom, L. Ronconi, M. Celegato, C. Nardon, L. Marchiò, Q.P. Dou, D. Aldinucci, F. Formaggio, D. Fregona, Toward the Selective Delivery of Chemotherapeutics into Tumor Cells by Targeting Peptide Transporters: Tailored Gold-Based Anticancer Peptidomimetics, J. Med. Chem. 55 (2012) 2212–2226, https://doi.org/10.1021/jm201480u.
[249] M.N. Kouodom, G. Boscutti, M. Celegato, M. Crisma, S. Sitran, D. Aldinucci, F. Formaggio, L. Ronconi, D. Fregona, Rational design of gold(III)-dithiocarbamato peptidomimetics for the targeted anticancer chemotherapy, J. Inorg. Biochem. 117 (2012) 248–260, https://doi.org/10.1016/j.jinorgbio.2012.07.001.
[250] D. Fregona, L. Ronconi, F. Formaggio, Q.P. Dou, D. Aldinucci, Gold(III) complexes with oligopeptides functionalized with sulfur donors and use

thereof as antitumor agents, WO2010105691A1, 2010. doi: WO2010105691A1.
[251] G. Boscutti, C. Nardon, L. Marchiò, M. Crisma, B. Biondi, D. Dalzoppo, L. Dalla Via, F. Formaggio, A. Casini, D. Fregona, Anticancer Gold(III) Peptidomimetics: From Synthesis to in vitro and ex vivo Biological Evaluations, ChemMedChem 13 (2018) 1131–1145, https://doi.org/10.1002/cmdc.201800098.
[252] T.S. Reddy, D. Pooja, S.H. Privér, R.B. Luwor, N. Mirzadeh, S. Ramesan, S. Ramakrishna, S. Karri, M. Kuncha, S.K. Bhargava, Potent and Selective Cytotoxic and Anti-inflammatory Gold(III) compounds containing cyclometalated phosphine sulfide ligands, Chem. – A Eur. J. 25 (2019) 14089–14100, https://doi.org/10.1002/chem.201903388.
[253] C.N. Banti, S.K. Hadjikakou, Anti-proliferative and anti-tumor activity of silver (I) compounds, Metallomics. 5 (2013) 569–596, https://doi.org/10.1039/c3mt00046j.
[254] S. Medici, M. Peana, G. Crisponi, V.M. Nurchi, J.I. Lachowicz, M. Remelli, M.A. Zoroddu, Silver coordination compounds: A new horizon in medicine, Coord. Chem. Rev. 327–328 (2016) 349–359, https://doi.org/10.1016/J.CCR.2016.05.015.
[255] C.L. Fox, Silver sulfadiazine—A new topical therapy for pseudomonas in burns, Arch. Surg. 96 (1968) 184, https://doi.org/10.1001/archsurg.1968.01330200022004.
[256] B.S. Atiyeh, M. Costagliola, S.N. Hayek, S.A. Dibo, Effect of silver on burn wound infection control and healing: Review of the literature, Burns. 33 (2007) 139–148, https://doi.org/10.1016/j.burns.2006.06.010.
[257] V. Gandin, M. Pellei, M. Marinelli, C. Marzano, A. Dolmella, M. Giorgetti, C. Santini, Synthesis and in vitro antitumor activity of water soluble sulfonate- and ester-functionalized silver(I) N-heterocyclic carbene complexes, J. Inorg. Biochem. 129 (2013) 135–144, https://doi.org/10.1016/j.jinorgbio.2013.09.011.
[258] M. Marinelli, M. Pellei, C. Cimarelli, H.V.R. Dias, C. Marzano, F. Tisato, M. Porchia, V. Gandin, C. Santini, Novel multicharged silver(I)–NHC complexes derived from zwitterionic 1,3-symmetrically and 1,3-unsymmetrically substituted imidazoles and benzimidazoles: Synthesis and cytotoxic properties, J. Organomet. Chem. 806 (2016) 45–53, https://doi.org/10.1016/j.jorganchem.2016.01.018.
[259] C. Pettinari, F. Marchetti, G. Lupidi, L. Quassinti, M. Bramucci, D. Petrelli, L.A. Vitali, M.F.C. Guedes Da Silva, L.M.D.R.S. Martins, P. Smoleński, A.J.L. Pombeiro, Synthesis, antimicrobial and antiproliferative activity of novel silver(I) tris(pyrazolyl)methanesulfonate and 1,3,5-triaza-7-phosphadamantane complexes, Inorg. Chem. 50 (2011) 11173–11183, https://doi.org/10.1021/ic201714c.
[260] P. Smoleński, S.W. Jaros, C. Pettinari, G. Lupidi, L. Quassinti, M. Bramucci, L.A. Vitali, D. Petrelli, A. Kochel, A.M. Kirillov, New water-soluble polypyridine silver(i) derivatives of 1,3,5-triaza-7-phosphaadamantane (PTA) with significant antimicrobial and antiproliferative activities, Dalton Trans. 42 (2013) 6572–6581, https://doi.org/10.1039/c3dt33026e.
[261] A.F. Santos, I.P. Ferreira, C.B. Pinheiro, V.G. Santos, M.T.P. Lopes, L.R. Teixeira, W.R. Rocha, G.L.S. Rodrigues, H. Beraldo, [Ag(L)$NO_3$] Complexes with 2-Benzoylpyridine-Derived Hydrazones: Cytotoxic Activity and Interaction with Biomolecules, ACS Omega 3 (2018) 7027–7035, https://doi.org/10.1021/acsomega.8b00533.
[262] L.R.V. Favarin, L.B. Oliveira, H. Silva, A.C. Micheletti, L. Pizzuti, A. Machulek-Júnior, A.R.L. Caires, D.F. Back, S.M. Lima, L.H.C. Andrade, L.F.B. Duarte, L.M.C. Pinto, G. Antônio Casagrande, Sonochemical synthesis of highly luminescent silver complexes: Photophysical properties and preliminary in vitro antitumor and antibacterial assays, Inorganica Chim. Acta. 492 (2019) 235–242, https://doi.org/10.1016/j.ica.2019.04.043.
[263] M.R. Ciol, C.M. Manzano, A. Cuin, F.R. Pavan, C.M. Ribeiro, A.L.T.G. Ruiz, E.C.S. de Oliveira, W.R. Lustri, N.F. Fregonezi, F.A.R. Nogueira, P.P. Corbi, A silver complex with cycloserine: synthesis, spectroscopic characterization, crystal structure and in vitro biological studies, ChemistrySelect. 3 (2018) 1719–1726, https://doi.org/10.1002/slct.201703078.
[264] M.A. Carvalho, R.E.F. de Paiva, F.R.G. Bergamini, A.F. Gomes, F.C. Gozzo, W.R. Lustri, A.L.B. Formiga, S.M. Shishido, C.V. Ferreira, P.P. Corbi, A silver complex with tryptophan: Synthesis, structural characterization, DFT studies and antibacterial and antitumor assays in vitro, J. Mol. Struct. 1031 (2013) 125–131, https://doi.org/10.1016/j.molstruc.2012.07.044.
[265] B. Coyle, M. McCann, K. Kavanagh, M. Devereux, V. McKee, N. Kayal, D. Egan, C. Deegan, G.J. Finn, Synthesis, X-ray crystal structure, anti-fungal and anti-cancer activity of [Ag2(NH3)2(salH)2] (salH2=salicylic acid), J. Inorg. Biochem. 98 (2004) 1361–1366, https://doi.org/10.1016/j.jinorgbio.2004.04.016.
[266] T.Z. Candido, R.E.F. de Paiva, M.C. Figueiredo, L. de Oliveira Coser, S.C.L. Frajácomo, C. Abbehausen, I.A. Cardinalli, W.R. Lustri, J.E. Carvalho, A.L.T.G. Ruiz, P.P. Corbi, C.S.P. Lima, Silver Nimesulide Complex in Bacterial Cellulose Membranes as an Innovative Therapeutic Method for Topical Treatment of Skin Squamous Cell Carcinoma, Pharmaceutics 14 (2022) 462, https://doi.org/10.3390/pharmaceutics14020462.
[267] J. Iida, E.T. Bell-Loncella, M.L. Purazo, Y. Lu, J. Dorchak, R. Clancy, J. Slavik, M. Lou Cutler, C.D. Shriver, Inhibition of cancer cell growth by ruthenium complexes, J. Transl. Med. 14 (2016) 1–10, https://doi.org/10.1186/s12967-016-0797-9.
[268] R.G. Kenny, C.J. Marmion, Toward multi-targeted platinum and ruthenium drugs - A new paradigm in cancer drug treatment regimens?, Chem Rev. 119 (2019) 1058–1137, https://doi.org/10.1021/ACS.CHEMREV.8B00271/SUPPL_FILE/CR8B00271_SI_001.PDF.
[269] R. Trondl, P. Heffeter, C.R. Kowol, M.A. Jakupec, W. Berger, B.K. Keppler, NKP-1339, the first ruthenium-based anticancer drug on the edge to clinical application, Chem. Sci. 5 (2014) 2925–2932, https://doi.org/10.1039/C3SC53243G.
[270] E. Alessio, L. Messori, NAMI-A and KP1019/1339, Two iconic ruthenium anticancer drug candidates face-to-face: A case story in medicinal inorganic chemistry, Molecules 24 (2019) 1995, https://doi.org/10.3390/molecules24101995.
[271] L. Zeng, P. Gupta, Y. Chen, E. Wang, L. Ji, H. Chao, Z.S. Chen, The development of anticancer ruthenium(II) complexes: from single molecule compounds to nanomaterials, Chem. Soc. Rev. 46 (2017) 5771–5804, https://doi.org/10.1039/C7CS00195A.
[272] Pragti, B.K. Kundu, S. Mukhopadhyay, Target based chemotherapeutic advancement of ruthenium complexes, Coord. Chem. Rev. 448 (2021), https://doi.org/10.1016/J.CCR.2021.214169.
[273] E. Namiecińska, B. Sadowska, M. Więckowska-Szakiel, A. Dołęga, B. Pasternak, M. Grazul, E. Budzisz, Anticancer and antimicrobial properties of novel η6-: P -cymene ruthenium(ii) complexes containing a N, S-type ligand, their structural and theoretical characterization, RSC Adv. 9 (2019) 38629–38645, https://doi.org/10.1039/c9ra08736b.
[274] W.D.J. Tremlett, D.M. Goodman, T.R. Steel, S. Kumar, A. Wieczorek-Błauż, F.P. Walsh, M.P. Sullivan, M. Hanif, C.G. Hartinger, Design concepts of half-sandwich organoruthenium anticancer agents based on bidentate bioactive ligands, Coord. Chem. Rev. 445 (2021), https://doi.org/10.1016/J.CCR.2021.213950 213950.
[275] J. McCain, K.L. Colón, P.C. Barrett, S.M.A. Monro, T. Sainuddin, J. Roque III, M. Pinto, H. Yin, C.G. Cameron, S.A. McFarland, Photophysical Properties and Photobiological Activities of Ruthenium(II) Complexes Bearing π-Expansive Cyclometalating Ligands with Thienyl Groups, Inorg. Chem. 58 (2019) 10778–10790. doi:10.1021/acs.inorgchem.9b01044.
[276] V.H.S. van Rixel, B. Siewert, S.L. Hopkins, S.H.C. Askes, A. Busemann, M.A. Siegler, S. Bonnet, Green light-induced apoptosis in cancer cells by a tetrapyridyl ruthenium prodrug offering two trans coordination sites, Chem. Sci. 7 (2016) 4922–4929, https://doi.org/10.1039/C6SC00167J.
[277] C.N. Honors, C.A. Kruger, H. Abrahamse, Photodynamic therapy for metastatic melanoma treatment: A review, Technol. Cancer Res. Treat. 17 (2018) 1–15, https://doi.org/10.1177/1533033818791795.
[278] A.T.P.C. Gomes, M.G.P.M.S. Neves, JOSÉ.A.S. Cavaleiro, Photodynamic Therapy and Porphyrin-Type Derivatives, An. Acad. Bras. Cienc. 90 (1 suppl 2) (2018) 993–1026.
[279] C. Naidoo, C.A. Kruger, H. Abrahamse, Photodynamic therapy for metastatic melanoma treatment: A review, Technol. Cancer Res. Treat. 17 (2018), https://doi.org/10.1177/1533033818791795, 153303381879179.
[280] J. Lanoue, G. Goldenberg, Basal cell carcinoma: A comprehensive review of existing and emerging nonsurgical therapies, J. Clin. Aesthet. Dermatol. 9 (2016) 26–36. http://www.ncbi.nlm.nih.gov/pubmed/27386043.
[281] L. Wang, H. Yin, P. Cui, M. Hetu, C. Wang, S. Monro, R.D. Schaller, C.G. Cameron, B. Liu, S. Kilina, S.A. McFarland, W. Sun, Near-infrared-emitting heteroleptic cationic iridium complexes derived from 2,3-diphenylbenzo[g] quinoxaline as in vitro theranostic photodynamic therapy agents, Dalton Trans. 46 (2017) 8091–8103, https://doi.org/10.1039/C7DT00913E.
[282] L. Wang, H. Yin, M.A. Jabed, M. Hetu, C. Wang, S. Monro, X. Zhu, S. Kilina, S.A. McFarland, W. Sun, π-Expansive Heteroleptic Ruthenium(II) Complexes as Reverse Saturable Absorbers and Photosensitizers for Photodynamic Therapy, Inorg. Chem. 56 (2017) 3245–3259, https://doi.org/10.1021/acs.inorgchem.6b02624.
[283] G. Ghosh, K.L. Colón, A. Fuller, T. Sainuddin, E. Bradner, J. McCain, S.M.A. Monro, H. Yin, M.W. Hetu, C.G. Cameron, S.A. McFarland, Cyclometalated Ruthenium(II) Complexes Derived from α-Oligothiophenes as Highly Selective Cytotoxic or Photocytotoxic Agents, Inorg. Chem. 57 (2018) 7694–7712, https://doi.org/10.1021/acs.inorgchem.8b00689.
[284] C. Reichardt, S. Monro, F.H. Sobotta, K.L. Colón, T. Sainuddin, M. Stephenson, E. Sampson, J. Roque, H. Yin, J.C. Brendel, C.G. Cameron, S. McFarland, B. Dietzek, Predictive Strength of Photophysical Measurements for in Vitro Photobiological Activity in a Series of Ru(II) Polypyridyl Complexes Derived from π-Extended Ligands, Inorg. Chem. 58 (5) (2019) 3156–3166.
[285] T. Sainuddin, J. McCain, M. Pinto, H. Yin, J. Gibson, M. Hetu, S.A. McFarland, Organometallic Ru(II) Photosensitizers Derived from π-Expansive Cyclometalating Ligands: Surprising Theranostic PDT Effects, Inorg. Chem. 55 (2016) 83–95, https://doi.org/10.1021/acs.inorgchem.5b01838.
[286] S. Monro, K.L. Colón, H. Yin, J. Roque, P. Konda, S. Gujar, R.P. Thummel, L. Lilge, C.G. Cameron, S.A. McFarland, Transition Metal Complexes and Photodynamic Therapy from a Tumor-Centered Approach: Challenges, Opportunities, and Highlights from the Development of TLD1433, Chem. Rev. 119 (2) (2019) 797–828.
[287] R. Lincoln, L. Kohler, S. Monro, H. Yin, M. Stephenson, R. Zong, A. Chouai, C. Dorsey, R. Hennigar, R.P. Thummel, S.A. McFarland, Exploitation of long-lived 3IL excited states for metal-organic photodynamic therapy: Verification in a metastatic melanoma model, J. Am. Chem. Soc. 135 (2013) 17161–17175, https://doi.org/10.1021/ja408426z.
[288] Y.-Y. Huang, D. Vecchio, P. Avci, R. Yin, M. Garcia-Diaz, M.R. Hamblin, Melanoma resistance to photodynamic therapy: new insights, Biol. Chem. 394 (2013) 239–250, https://doi.org/10.1515/hsz-2012-0228.
[289] M. Groessl, O. Zava, P.J. Dyson, Cellular uptake and subcellular distribution of ruthenium-based metallodrugs under clinical investigation versus cisplatin, Metallomics. 3 (2011) 591, https://doi.org/10.1039/c0mt00101e.

[290] A. Raza, S.A. Archer, S.D. Fairbanks, K.L. Smitten, S.W. Botchway, J.A. Thomas, S. Macneil, J.W. Haycock, A Dinuclear Ruthenium(II) Complex Excited by Near-Infrared Light through Two-Photon Absorption Induces Phototoxicity Deep within Hypoxic Regions of Melanoma Cancer Spheroids, J. Am. Chem. Soc. 142 (2020) 4639–4647, https://doi.org/10.1021/jacs.9b11313.
[291] M. Pawlicki, H. Collins, R. Denning, H. Anderson, Two-photon absorption and the design of two-photon dyes, Angew. Chemie - Int. Ed. 48 (18) (2009) 3244–3266.
[292] H.A. Collins, M. Khurana, E.H. Moriyama, A. Mariampillai, E. Dahlstedt, M. Balaz, M.K. Kuimova, M. Drobizhev, V.X.D. Yang, D. Phillips, A. Rebane, B.C. Wilson, H.L. Anderson, Blood-vessel closure using photosensitizers engineered for two-photon excitation, Nat. Photonics 2 (2008) 420–424, https://doi.org/10.1038/nphoton.2008.100.
[293] A.A. Holder, P. Taylor, A.R. Magnusen, T. Mo, K. Meyer, Y. Hong, S.E. Ramsdale, M. Gordon, J. Stubbs, L.A. Seymour, D. Acharya, R.T. Weber, P.F. Smith, G.C. Dismukes, P. Ji, L. Menocal, F. Bai, J.L. Williams, D.M. Cropek, W.L. Jarrett, E.T. Moffett, K. Meyer, Y. Hong, S.E. Ramsdale, M. Gordon, J. Stubbs, L.A. Seymour, D. Acharya, R.T. Weber, P.F. Smith, G.C. Dismukes, P. Ji, L. Menocal, F. Bai, J.L. Williams, D.M. Cropek, W.L. Jarrett, Preliminary anti-cancer photodynamic therapeutic in vitro studies with mixed-metal binuclear ruthenium(ii)–vanadium(iv) complexes, Dalton Trans. 42 (2013) 11881, https://doi.org/10.1039/c3dt50547b.
[294] L. Tabrizi, H. Chiniforoshan, Discovery of organometallic Ruthenium(II)-arene complexes of lidocaine as improved photocytotoxic agents, Polyhedron 119 (2016) 575–583, https://doi.org/10.1016/j.poly.2016.09.031.
[295] T. Chen, Y. Liu, W.J. Zheng, J. Liu, Y.S. Wong, Ruthenium polypyridyl complexes that induce mitochondria-mediated apoptosis in cancer cells, Inorg. Chem. 49 (2010) 6366–6368, https://doi.org/10.1021/ic100277w.
[296] Z. Luo, L. Yu, F. Yang, Z. Zhao, B. Yu, H. Lai, K.H. Wong, S.M. Ngai, W. Zheng, T. Chen, Ruthenium polypyridyl complexes as inducer of ROS-mediated apoptosis in cancer cells by targeting thioredoxin reductase, Metallomics. 6 (2014) 1480–1490, https://doi.org/10.1039/c4mt00044g.
[297] J. Du, Y. Kang, Y. Zhao, W. Zheng, Y. Zhang, Y. Lin, Z. Wang, Y. Wang, Q. Luo, K. Wu, F. Wang, Synthesis, Characterization, and in Vitro Antitumor Activity of Ruthenium(II) Polypyridyl Complexes Tethering EGFR-Inhibiting 4-Anilinoquinazolines, Inorg. Chem. 55 (2016) 4595–4605, https://doi.org/10.1021/acs.inorgchem.6b00309.
[298] V. Rajendiran, M. Murali, E. Suresh, S. Sinha, K. Somasundaram, M. Palaniandavar, Mixed ligand ruthenium(ii) complexes of bis(pyrid-2-yl)-/bis(benzimidazol- 2-yl)-dithioether and diimines: Study of non-covalent DNA binding and cytotoxicity, Dalton Trans. (2008) 148–163, https://doi.org/10.1039/b710578a.
[299] D.E.L. Carvalho, K.M. Oliveira, L.M. Bomfim, M.B.P. Soares, D.P. Bezerra, A.A. Batista, R.S. Correa, Nucleobase Derivatives as Building Blocks to Form Ru(II)-Based Complexes with High Cytotoxicity, ACS Omega 5 (2020) 122–130, https://doi.org/10.1021/acsomega.9b01921.
[300] A.P. Carnizello, M.I.F. Barbosa, M. Martins, N.H. Ferreira, P.F. Oliveira, G.M. Magalhães, A.A. Batista, D.C. Tavares, In vitro and in vivo antitumor activity of a novel carbonyl ruthenium compound, the ct-[RuCl(CO)(dppb)(bipy)]PF-6 [dppb = 1,4-bis(diphenylphosphine)butane and bipy = 2,2'-bipyridine], J. Inorg. Biochem. 164 (2016) 42–48, https://doi.org/10.1016/j.jinorgbio.2016.08.010.
[301] R.S. Correa, L.M. Bomfim, K.M. Oliveira, D.R.M. Moreira, M.B.P. Soares, J. Ellena, D.P. Bezerra, A.A. Batista, Ru(II) complexes containing uracil nucleobase analogs with cytotoxicity against tumor cells, J. Inorg. Biochem. 198 (2019), https://doi.org/10.1016/j.jinorgbio.2019.110751 110751.
[302] P.S.V.B. de Almeida, T.M. Pereira, A.E. Kummerle, G.P. Guedes, H. Silva, L.L. de Oliveira, A.P. Neves, New Ru(II)–DMSO complexes containing coumarin-N-acylhydrazone hybrids: Synthesis, X-ray structures, cytotoxicity and antimicrobial activities, Polyhedron 171 (2019) 20–31, https://doi.org/10.1016/j.poly.2019.06.053.
[303] R. Hudej, D. Miklavcic, M. Cemazar, V. Todorovic, G. Sersa, A. Bergamo, G. Sava, A. Martincic, J. Scancar, B.K. Keppler, I. Turel, Modulation of Activity of Known Cytotoxic Ruthenium(III) Compound (KP418) with Hampered Transmembrane Transport in Electrochemotherapy In Vitro and In Vivo, J. Membr. Biol. 247 (2014) 1239–1251, https://doi.org/10.1007/s00232-014-9696-2.
[304] G. Sersa, D. Miklavcic, M. Cemazar, Z. Rudolf, G. Pucihar, M. Snoj, Electrochemotherapy in treatment of tumours, Eur. J. Surg. Oncol. 34 (2) (2008) 232–240.
[305] R.F. Brissos, P. Clavero, A. Gallen, A. Grabulosa, L.A. Barrios, A.B. Caballero, L. Korrodi-Gregório, R. Pérez-Tomás, G. Muller, V. Soto-Cerrato, P. Gamez, Highly Cytotoxic Ruthenium(II)-Arene Complexes from Bulky 1-Pyrenylphosphane Ligands, Inorg. Chem. 57 (2018) 14786–14797, https://doi.org/10.1021/acs.inorgchem.8b02541.
[306] C. Spoerlein-Guettler, K. Mahal, R. Schobert, B. Biersack, Ferrocene and (arene)ruthenium(II) complexes of the natural anticancer naphthoquinone plumbagin with enhanced efficacy against resistant cancer cells and a genuine mode of action, J. Inorg. Biochem. 138 (2014) 64–72, https://doi.org/10.1016/j.jinorgbio.2014.04.020.
[307] M. Gold, Y. Mujahid, K. Ahmed, H. Kostrhunova, J. Kasparkova, V. Brabec, B. Biersack, R. Schobert, A new 4-(pyridinyl)-4H-benzo[g]chromene-5,10-dione ruthenium(II) complex inducing senescence in 518A2 melanoma cells, J. Biol. Inorg. Chem. 24 (2019) 647–657, https://doi.org/10.1007/s00775-019-01677-y.
[308] M.S. Soengas, S.W. Lowe, Apoptosis and melanoma chemoresistance, Oncogene 22 (20) (2003) 3138–3151.
[309] D. Zhuang, S. Mannava, V. Grachtchouk, W.-H. Tang, S. Patil, J.A. Wawrzyniak, A.E. Berman, T.J. Giordano, E.V. Prochownik, M.S. Soengas, M.A. Nikiforov, C-MYC overexpression is required for continuous suppression of oncogene-induced senescence in melanoma cells, Oncogene 27 (2008) 6623–6634, https://doi.org/10.1038/onc.2008.258.
[310] F. Schmitt, J. Kasparkova, V. Brabec, G. Begemann, R. Schobert, B. Biersack, New (arene)ruthenium(II) complexes of 4-aryl-4H-naphthopyrans with anticancer and anti-vascular activities, J. Inorg. Biochem. 184 (2018) 69–78, https://doi.org/10.1016/j.jinorgbio.2018.03.013.
[311] P. Nowak-Sliwinska, J.R. van Beijnum, A. Casini, A.A. Nazarov, G. Wagnières, H. van den Bergh, P.J. Dyson, A.W. Griffioen, Organometallic Ruthenium(II) Arene Compounds with Antiangiogenic Activity, J. Med. Chem. 54 (2011) 3895–3902, https://doi.org/10.1021/jm2002074.
[312] G. Ludwig, G.N. Kaluderović, M. Bette, M. Block, R. Paschke, D. Steinborn, Highly active neutral ruthenium(II) arene complexes: Synthesis, characterization, and investigation of their anticancer properties, J. Inorg. Biochem. 113 (2012) 77–82, https://doi.org/10.1016/j.jinorgbio.2012.04.003.
[313] G. Ludwig, G.N. Kaluderović, T. Rüffer, M. Bette, M. Korb, M. Block, R. Paschke, H. Lang, D. Steinborn, Cationic arene ruthenium(ii) complexes with chelating P-functionalized alkyl phenyl sulfide and sulfoxide ligands as potent anticancer agents, Dalton Trans. 42 (2013) 3771–3774, https://doi.org/10.1039/c3dt33064h.
[314] K. Ghebreyessus, A. Peralta, M. Katdare, K. Prabhakaran, S. Paranawithana, Ruthenium(II)-arene complexes with naphthalimide-tagged N, O- and N, N-chelating ligands: Synthesis and biological evaluation, Inorganica Chim. Acta. 434 (2015) 239–251, https://doi.org/10.1016/j.ica.2015.05.025.
[315] A. Skoczyńska, B. Pasternak, M. Małecka, U. Krajewska, M. Mirowski, A. Merecz-Sadowska, B.T. Karwowski, J. Kusz, E. Budzisz, The cytotoxic effect of Ru(II) complexes with 5-(2-hydroxyphenyl)-3-methyl-1-(2-pyridyl)-1H-pyrazole-4-carboxylic acid methyl ester: Synthesis, X-ray structure and DNA damage potential, Polyhedron 169 (2019) 228–238, https://doi.org/10.1016/j.poly.2019.04.065.
[316] E. Namiecińska, B. Sadowska, M. Więckowska-Szakiel, A. Dołęga, B. Pasternak, M. Grazul, E. Budzisz, Anticancer and antimicrobial properties of novel η 6 - p -cymene ruthenium(ii) complexes containing a N, S-type ligand, their structural and theoretical characterization, RSC Adv. 9 (2019) 38629–38645, https://doi.org/10.1039/C9RA08736B.
[317] S.M. Meier, D. Kreutz, L. Winter, M.H.M. Klose, K. Cseh, T. Weiss, A. Bileck, B. Alte, J.C. Mader, S. Jana, A. Chatterjee, A. Bhattacharyya, M. Hejl, M.A. Jakupec, P. Heffeter, W. Berger, C.G. Hartinger, B.K. Keppler, G. Wiche, C. Gerner, An Organoruthenium Anticancer Agent Shows Unexpected Target Selectivity For Plectin, Angew. Chemie Int. Ed. 56 (2017) 8267–8271, https://doi.org/10.1002/anie.201702242.
[318] K.S.M. Smalley, R. Contractor, N.K. Haass, A.N. Kulp, G.E. Atilla-Gokcumen, D. S. Williams, H. Bregman, K.T. Flaherty, M.S. Soengas, E. Meggers, M. Herlyn, An Organometallic Protein Kinase Inhibitor Pharmacologically Activates p53 and Induces Apoptosis in Human Melanoma Cells, Cancer Res. 67 (2007) 209–217, https://doi.org/10.1158/0008-5472.CAN-06-1538.
[319] J. Maksimoska, D.S. Williams, G.E. Atilla-Gokcumen, K.S.M. Smalley, P.J. Carroll, R.D. Webster, P. Filippakopoulos, S. Knapp, M. Herlyn, E. Meggers, Similar Biological Activities of Two Isostructural Ruthenium and Osmium Complexes, Chem. - A Eur. J. 14 (2008) 4816–4822, https://doi.org/10.1002/chem.200800294.
[320] Z. Liu, I. Romero-Canelõn, B. Qamar, J.M. Hearn, A. Habtemariam, N.P.E. Barry, A.M. Pizarro, G.J. Clarkson, P.J. Sadler, The potent oxidant anticancer activity of organoiridium catalysts, Angew. Chemie - Int. Ed. 53 (2014) 3941–3946, https://doi.org/10.1002/anie.201311161.
[321] Y. Kuramochi, O. Ishitani, An Ir(III) Complex Photosensitizer With Strong Visible Light Absorption for Photocatalytic CO2 Reduction, Front. Chem. 7 (2019), https://doi.org/10.3389/fchem.2019.00259.
[322] V. Mdluli, S. Diluzio, J. Lewis, J.F. Kowalewski, T.U. Connell, D. Yaron, T. Kowalewski, S. Bernhard, High-throughput Synthesis and Screening of Iridium(III) Photocatalysts for the Fast and Chemoselective Dehalogenation of Aryl Bromides, ACS Catal. 10 (2020) 6977–6987, https://doi.org/10.1021/acscatal.0c02247.
[323] R.C.W. Lier, A.D. Bruijn, G. Roelfes, A Water-Soluble Iridium Photocatalyst for Chemical Modification of Dehydroalanines in Peptides and Proteins, Chem. – A Eur. J. 27 (2021) 1430–1437, https://doi.org/10.1002/chem.202002599.
[324] W.-Y. Zhang, F. Du, M. He, L. Bai, Y.-Y. Gu, L.-L. Yang, Y.-J. Liu, Studies of anticancer activity in vitro and in vivo of iridium(III) polypyridyl complexes-loaded liposomes as drug delivery system, Eur. J. Med. Chem. 178 (2019) 390–400, https://doi.org/10.1016/j.ejmech.2019.06.009.
[325] H.J. Zhong, L. Lu, K.H. Leung, C.C.L. Wong, C. Peng, S.C. Yan, D.L. Ma, Z. Cai, H. M. David Wang, C.H. Leung, An iridium(III)-based irreversible protein-protein interaction inhibitor of BRD4 as a potent anticancer agent, Chem. Sci. 6 (2015) 5400–5408, https://doi.org/10.1039/c5sc02321a.
[326] T. Fujisawa, P. Filippakopoulos, Functions of bromodomain-containing proteins and their roles in homeostasis and cancer, Nat. Rev. Mol. Cell Biol. 18 (2017) 246–262, https://doi.org/10.1038/nrm.2016.143.
[327] L. Lu, L.J. Liu, W.C. Chao, H.J. Zhong, M. Wang, X.P. Chen, J.J. Lu, R.N. Li, D.L. Ma, C.H. Leung, Identification of an iridium(III) complex with anti-bacterial and anti-cancer activity, Sci. Rep. 5 (2015) 1–9, https://doi.org/10.1038/srep14544.

[328] G. Ludwig, I. Ranđelović, D. Maksimović-Ivanić, S. Mijatović, M.Z. Bulatović, D. Miljković, M. Korb, H. Lang, D. Steinborn, G.N. Kaluđerović, Anticancer Potential of (Pentamethylcyclopentadienyl)chloridoiridium(III) Complexes Bearing κ P and κ P, κ S -Coordinated Ph 2 PCH 2 CH 2 CH 2 S(O) x Ph (x =0-2) Ligands, ChemMedChem 9 (2014) 1586–1593, https://doi.org/10.1002/cmdc.201300479.
[329] G. Ludwig, S. Mijatović, I. Ranđelović, M. Bulatović, D. Miljković, D. Maksimović-Ivanić, M. Korb, H. Lang, D. Steinborn, G.N. Kaluđerović, Biological activity of neutral and cationic iridium(III) complexes with κP and κP, κS coordinated Ph2PCH2S(O)xPh (x = 0–2) ligands, Eur. J. Med. Chem. 69 (2013) 216–222, https://doi.org/10.1016/j.ejmech.2013.08.025.
[330] U. Śliwińska, F.P. Pruchnik, S. Ułaszewski, M. Latocha, D. Nawrocka-Musiał, Properties of η5-pentamethylcyclopentadienyl rhodium(III) and iridium(III) complexes with quinolin-8-ol and their cytostatic activity, Polyhedron 29 (2010) 1653–1659, https://doi.org/10.1016/j.poly.2010.02.013.
[331] N. Katsaros, A. Anagnostopoulou, Rhodium and its compounds as potential agents in cancer treatment, Crit. Rev. Oncol. Hematol. 42 (2002) 297–308, https://doi.org/10.1016/S1040-8428(01)00222-0.
[332] T.-S. Kang, W. Wang, H.-J. Zhong, J.-X. Liang, C.-N. Ko, J.-J. Lu, X.-P. Chen, D.-L. Ma, C.-H. Leung, A rhodium(III)-based inhibitor of autotaxin with antiproliferative activity, Biochim. Biophys. Acta - Gen. Subj. 2017 (1861) 256–263, https://doi.org/10.1016/j.bbagen.2016.11.032.
[333] D.L. Ma, L.J. Liu, K.H. Leung, Y.T. Chen, H.J. Zhong, D.S.H. Chan, H.M.D. Wang, C.H. Leung, Antagonizing STAT3 dimerization with a rhodium(III) complex, Angew. Chemie - Int. Ed. 53 (2014) 9178–9182, https://doi.org/10.1002/anie.201404686.
[334] W. Kaim, B. Schwederski, A. Klein, Bioinorganic Chemistry - Inorganic Elements in the Chemistry of Life: An Introduction and Guide, 2nd Edition | Wiley, 2nd Editio,., 2013.
[335] K. Pantopoulos, S.K. Porwal, A. Tartakoff, L. Devireddy, Mechanisms of Mammalian Iron Homeostasis, Biochemistry 51 (2012) 5705–5724, https://doi.org/10.1021/bi300752r.
[336] C. Camaschella, A. Nai, L. Silvestri, Iron metabolism and iron disorders revisited in the hepcidin era, Haematologica 105 (2020) 260–272, https://doi.org/10.3324/haematol.2019.232124.
[337] U. Abbasi, S. Abbina, A. Gill, L.E. Takuechi, J.N. Kizhakkedathu, Role of iron in the molecular pathogenesis of diseases and therapeutic opportunities, ACS Chem. Biol. 16 (2021) 945–972, https://doi.org/10.1021/acschembio.1c00122.
[338] P. Kpf-Maier, H. Kpf, E.W. Neuse, Ferricenium complexes: A new type of water-soluble antitumor agent, J. Cancer Res. Clin. Oncol. 108 (1984) 336–340, https://doi.org/10.1007/BF00390468.
[339] Y. Wang, P.M. Dansette, P. Pigeon, S. Top, M.J. McGlinchey, D. Mansuy, G. Jaouen, A new generation of ferrociphenols leads to a great diversity of reactive metabolites, and exhibits remarkable antiproliferative properties, Chem. Sci. 9 (2018) 70–78, https://doi.org/10.1039/C7SC04213B.
[340] R. Kovjazin, T. Eldar, M. Patya, A. Vanichkin, H.M. Lander, A. Novogrodsky, Ferrocene-induced lymphocyte activation and antitumor activity is mediated by redox-sensitive signaling, FASEB J. 17 (2003) 1–16, https://doi.org/10.1096/fj.02-0558fje.
[341] C. Bruyère, V. Mathieu, A. Vessières, P. Pigeon, S. Top, G. Jaouen, R. Kiss, Ferrocifen derivatives that induce senescence in cancer cells: selected examples, J. Inorg. Biochem. 141 (2014) 144–151, https://doi.org/10.1016/j.jinorgbio.2014.08.015.
[342] P. Resnier, N. Galopin, Y. Sibiril, A. Clavreul, J. Cayon, A. Briganti, P. Legras, A. Vessières, T. Montier, G. Jaouen, J.P. Benoit, C. Passirani, Efficient ferrocifen anticancer drug and Bcl-2 gene therapy using lipid nanocapsules on human melanoma xenograft in mouse, Pharmacol. Res. 126 (2017) 54–65, https://doi.org/10.1016/j.phrs.2017.01.031.
[343] L.-P. Chan, Y.-P. Tseng, H.-Y. Ding, S.-M. Pan, F.-Y. Chiang, L.-F. Wang, T.-H. Chou, P.-J. Lien, C. Liu, P.-L. Kuo, C.-H. Liang, Tris(8-Hydroxyquinoline)iron induces apoptotic cell death via oxidative stress and by activating death receptor signaling pathway in human head and neck carcinoma cells, Phytomedicine 63 (2019), https://doi.org/10.1016/j.phymed.2019.153005 153005.
[344] J. Vančo, Z. Šindelář, Z. Dvořák, Z. Trávníček, Iron-salophen complexes involving azole-derived ligands: A new group of compounds with high-level and broad-spectrum in vitro antitumor activity, J. Inorg. Biochem. 142 (2015) 92–100, https://doi.org/10.1016/j.jinorgbio.2014.10.002.
[345] M.N.M. Milunović, A. Dobrova, G. Novitchi, N. Gligorijević, S. Radulović, J. Kožišek, P. Rapta, E.A. Enyedy, V.B. Arion, Effects of terminal substitution and iron coordination on antiproliferative activity of l-proline-salicylaldehyde–thiosemicarbazone hybrids, Eur. J. Inorg. Chem. 2017 (2017) 4773–4783, https://doi.org/10.1002/ejic.201700962.
[346] C.R. Chitambar, Gallium and its competing roles with iron in biological systems, Biochim. Biophys. Acta - Mol. Cell Res. 2016 (1863) 2044–2053, https://doi.org/10.1016/j.bbamcr.2016.04.027.
[347] X.-X. Peng, S. Gao, J.-L. Zhang, Gallium (III) complexes in cancer chemotherapy, Eur. J. Inorg. Chem. 2022 (6) (2022), https://doi.org/10.1002/ejic.202100953.
[348] M.R. Kaluäerović, G.N. Kaluäerović, S. Gómez-Ruiz, R. Paschke, A. Hemprich, J. Kühling, T.W. Remmerbach, Organogallium(III) complexes as apoptosis promoting anticancer agents for head and neck squamous cell carcinoma (HNSCC) cell lines, J. Inorg. Biochem. 105 (2011) 164–170, https://doi.org/10.1016/j.jinorgbio.2010.10.013.
[349] S.M. Valiahdi, P. Heffeter, M.A. Jakupec, R. Marculescu, W. Berger, K. Rappersberger, B.K. Keppler, The gallium complex KP46 exerts strong activity against primary explanted melanoma cells and induces apoptosis in melanoma cell lines, Melanoma Res. 19 (2009) 283–293, https://doi.org/10.1097/CMR.0b013e32832b272d.
[350] B.K.K. and W.B. Isabella Pötsch, Dina Baier, Challenges and Chances in the Preclinical to Clinical Translation of Anticancer Metallodrugs, in: A. Casini, A. Vessières, S.M. Meier-Menches (Eds.), Met. Anticancer Agents, The Royal Society of Chemistry, 2019: pp. 308–336. doi:10.1039/9781788016452-FP001.
[351] M. Pribisko, J. Palmer, R.H. Grubbs, H.B. Gray, J. Termini, P. Lim, Cellular uptake and anticancer activity of Carboxylated gallium corroles, Proc. Natl. Acad. Sci. USA 113 (2016) E2258–E2266, https://doi.org/10.1073/pnas.1517402113.
[352] D.C. Crans, J.J. Smee, E. Gaidamauskas, L. Yang, The chemistry and biochemistry of vanadium and the biological activities exerted by vanadium compounds, Chem. Rev. 104 (2004) 849–902, https://doi.org/10.1021/cr020607t.
[353] E. Bellomo, K. Birla Singh, A. Massarotti, C. Hogstrand, W. Maret, The metal face of protein tyrosine phosphatase 1B, Coord. Chem. Rev. 327–328 (2016) 70–83, https://doi.org/10.1016/j.ccr.2016.07.002.
[354] C. Rozzo, D. Sanna, E. Garribba, M. Serra, A. Cantara, G. Palmieri, M. Pisano, Antitumoral effect of vanadium compounds in malignant melanoma cell lines, J. Inorg. Biochem. 174 (2017) 14–24, https://doi.org/10.1016/j.jinorgbio.2017.05.010.
[355] M. Strianese, A. Basile, A. Mazzone, S. Morello, M.C. Turco, C. Pellecchia, Therapeutic potential of a pyridoxal-based vanadium(IV) complex showing selective cytotoxicity for cancer versus healthy cells, J. Cell. Physiol. 228 (2013) 2202–2209, https://doi.org/10.1002/jcp.24385.
[356] E. Viola, M.P. Donzello, F. Sciscione, K. Shah, C. Ercolani, G. Trigiante, Tetra-2,3-pyrazinoporphyrazines with externally appended pyridine rings. 17. Photosensitizing properties and cellular effects of ZnII octacationic and ZnII/PtII hexacationic macrocycles in aqueous media: Perspectives of multimodal anticancer potentialities, J. Photochem. Photobiol. B Biol. 169 (2017) 101–109, https://doi.org/10.1016/j.jphotobiol.2017.03.005.
[357] L.M. Evans, E.S. Casper, R. Rosenbluth, Phase II trial of carboplatin in advanced malignant melanoma, Cancer Treat. Rep. 71 (1987) 171–172. http://www.ncbi.nlm.nih.gov/pubmed/3542209.
[358] D. Glover, J. Ibrahim, J. Kirkwood, J. Glick, D. Karp, J. Stewart, M. Ewell, E. Borden, Phase II randomized trial of cisplatin and WR-2721 versus cisplatin alone for metastatic melanoma, Melanoma Res. 13 (2003) 619–626, https://doi.org/10.1097/00008390-200312000-00012.
[359] K.B. Kim, J.A. Sosman, J.P. Fruehauf, G.P. Linette, S.N. Markovic, D.F. McDermott, J.S. Weber, H. Nguyen, P. Cheverton, D. Chen, A.C. Peterson, W. E. Carson, S.J. O'Day, BEAM: A randomized phase II study evaluating the activity of bevacizumab in combination with carboplatin plus paclitaxel in patients with previously untreated advanced melanoma, J. Clin. Oncol. 30 (1) (2012) 34–41.
[360] W. Chang, S.J. Lee, S. Park, M.K. Choi, J.Y. Hong, Y.S. Kim, C.H. Maeng, H.A. Jung, S. Kim, J. Lee, Effect of paclitaxel/carboplatin salvage chemotherapy in noncutaneous versus cutaneous metastatic melanoma, Melanoma Res. 23 (2013) 147–151, https://doi.org/10.1097/CMR.0b013e32835efd8d.
[361] K.T. Flaherty, S.J. Lee, F. Zhao, L.M. Schuchter, L. Flaherty, R. Kefford, M.B. Atkins, P. Leming, J.M. Kirkwood, Phase III trial of carboplatin and paclitaxel with or without sorafenib in metastatic melanoma, J. Clin. Oncol. 31 (2013) 373–379, https://doi.org/10.1200/JCO.2012.42.1529.
[362] A. Hauschild, S.S. Agarwala, U. Trefzer, D. Hogg, C. Robert, P. Hersey, A. Eggermont, S. Grabbe, R. Gonzalez, J. Gille, C. Peschel, D. Schadendorf, C. Garbe, S. O'Day, A. Daud, J.M. White, C. Xia, K. Patel, J.M. Kirkwood, U. Keilholz, Results of a phase III, randomized, placebo-controlled study of sorafenib in combination with carboplatin and paclitaxel as second-line treatment in patients with unresectable stage III or stage IV melanoma, J. Clin. Oncol. 27 (2009) 2823–2830, https://doi.org/10.1200/JCO.2007.15.7636.
[363] L.A. Kottschade, V.J. Suman, T. Amatruda, R.R. McWilliams, B.I. Mattar, D.A. Nikcevich, R. Behrens, T.R. Fitch, A.J. Jaslowski, S.N. Markovic, A phase II trial of nab-paclitaxel (ABI-007) and carboplatin in patients with unresectable stage IV melanoma, Cancer 117 (8) (2011) 1704–1710.
[364] N.E. Papadopoulos, A. Bedikian, S. Ring, K.B. Kim, W.-J. Hwu, D.L. Gerber, J. Homsi, P. Hwu, Phase I/II Study of a Cisplatin-Taxol-Dacarbazine Regimen in Metastatic Melanoma, Am. J. Clin. Oncol. 32 (2009) 509–514, https://doi.org/10.1097/COC.0b013e3181942a1f.
[365] S.S. Legha, S. Ring, N. Papadopoulos, C. Plager, S. Chawla, R. Benjamin, A prospective evaluation of a triple-drug regimen containing cisplatin, vinblastine, and dacarbazine (CVD) for metastatic melanoma, Cancer 64 (1989) 2024–2029, https://doi.org/10.1002/1097-0142(19891115)64:10<2024::AID-CNCR2820641010>3.0.CO;2-V.
[366] P.B. Chapman, L.H. Einhorn, M.L. Meyers, S. Saxman, A.N. Destro, K.S. Panageas, C.B. Begg, S.S. Agarwala, L.M. Schuchter, M.S. Ernstoff, A.N. Houghton, J.M. Kirkwood, Phase III Multicenter Randomized Trial of the Dartmouth Regimen Versus Dacarbazine in Patients With Metastatic Melanoma, J. Clin. Oncol. 17 (1999) 2745–2745. doi:10.1200/JCO.1999.17.9.2745.
[367] M.R. Middleton, P. Lorigan, J. Owen, L. Ashcroft, S.M. Lee, P. Harper, N. Thatcher, A randomized phase III study comparing dacarbazine, BCNU, cisplatin and tamoxifen with dacarbazine and interferon in advanced

melanoma, Br. J. Cancer 82 (2000) 1158–1162, https://doi.org/10.1054/bjoc.1999.1056.
[368] G.P. Stathopoulos, T. Boulikas, Lipoplatin formulation review article, J. Drug Deliv. 2012 (2012) 1–10, https://doi.org/10.1155/2012/581363.
[369] C.F. Jehn, T. Boulikas, A. Kourvetaris, K. Possinger, D. Lüftner, Pharmacokinetics of liposomal cisplatin (lipoplatin) in combination with 5-FU in patients with advanced head and neck cancer: first results of a phase III study, Anticancer Res. 27 (2007) 471–475. http://www.ncbi.nlm.nih.gov/pubmed/17352269.
[370] G. Sersa, B. Stabuc, M. Cemazar, D. Miklavcic, Z. Rudolf, Electrochemotherapy with cisplatin: clinical experience in malignant melanoma patients, Clin. Cancer Res. 6 (2000) 863–867. http://www.ncbi.nlm.nih.gov/pubmed/10741708.
[371] M.G. McCusker, D. Orkoulas-Razis, R. Mehra, Potential of Pembrolizumab in Metastatic or Recurrent Head and Neck Cancer: Evidence to Date, Onco. Targets. Ther. 13 (2020) 3047–3059, https://doi.org/10.2147/OTT.S196252.
[372] B. Burtness, K.J. Harrington, R. Greil, D. Soulières, M. Tahara, G. de Castro, A. Psyrri, N. Basté, P. Neupane, Å. Bratland, T. Fuereder, B.G.M. Hughes, R. Mesía, N. Ngamphaiboon, T. Rordorf, W.Z. Wan Ishak, R.-L. Hong, R. González Mendoza, A. Roy, Y. Zhang, B. Gumuscu, J.D. Cheng, F. Jin, D. Rischin, G. Lerzo, M. Tatangelo, M. Varela, J.J. Zarba, M. Boyer, H. Gan, B.o. Gao, B. Hughes, G. Mallesara, D. Rischin, A. Taylor, M. Burian, T. Fuereder, R. Greil, C.H. Barrios, D. O. de Castro Junior, G. Castro, F.A. Franke, G. Girotto, I.P.F. Lima, U.R. Nicolau, G.D.J. Pinto, L. Santos, A.-P. Victorino, N. Chua, F. Couture, R. Gregg, A. Hansen, J. Hilton, J. McCarthy, D. Soulieres, R. Ascui, P. Gonzalez, L. Villanueva, M. Torregroza, A. Zambrano, P. Holeckova, Z. Kral, B. Melichar, J. Prausova, M. Vosmik, M. Andersen, N. Gyldenkerne, H. Jurgens, K. Putnik, P. Reinikainen, V. Gruenwald, S. Laban, G. Aravantinos, I. Boukovinas, V. Georgoulias, A. Psyrri, D. Kwong, Y. Al-Farhat, T. Csoszi, J. Erfan, G. Horvai, L. Landherr, E. Remenar, A. Ruzsa, J. Szota, S. Billan, I. Gluck, O. Gutfeld, A. Popovtzer, M. Benasso, S. Bui, V. Ferrari, L. Licitra, F. Nole, T. Fujii, Y. Fujimoto, N. Hanai, H. Hara, K. Matsumoto, K. Mitsugi, N. Monden, M. Nakayama, K. Okami, N. Oridate, K. Shiga, Y. Shimizu, M. Sugasawa, M. Tahara, M. Takahashi, S. Takahashi, K. Tanaka, T. Ueda, H. Yamaguchi, T. Yamazaki, R. Yasumatsu, T. Yokota, T. Yoshizaki, I. Kudaba, Z. Stara, W.Z. Wan Ishak, S.K. Cheah, J. Aguilar Ponce, R. Gonzalez Mendoza, C. Hernandez Hernandez, F. Medina Soto, J. Buter, A. Hoeben, S. Oosting, K. Suijkerbuijk, A. Bratland, M. Brydoey, R. Alvarez, L. Mas, P. Caguioa, J. Querol, E.E. Regala, M.B. Tamayo, E.M. Villegas, A. Kawecki, A. Karpenko, A. Klochikhin, A. Smolin, O. Zarubenkov, B.C. Goh, G. Cohen, J. du Toit, C. Jordaan, G. Landers, P. Ruff, W. Szpak, N. Tabane, I. Brana, L. Iglesias Docampo, J. Lavernia, R. Mesia, E. Abel, V. Muratidu, N. Nielsen, V. Cristina, T. Rordorf, S. Rothschild, R.-L. Hong, H.-M. Wang, M.-H. Yang, S.-P. Yeh, C.-J. Yen, N. Ngamphaiboon, N. Soparattanapaisarn, V. Sriuranpong, S. Aksoy, I. Cicin, M. Ekenel, H. Harputluoglu, O. Ozyilkan, K. Harrington, S. Agarwala, H. Ali, R. Alter, D. Anderson, J. Bruce, B. Burtness, N. Campbell, M. Conde, J. Deeken, W. Edenfield, L. Feldman, E. Gaughan, B. Goueli, B. Halmos, U. Hegde, B. Hunis, R. Jotte, A. Karnad, S. Khan, N. Laudi, D. Laux, D. Martincic, S. McCune, D. McGaughey, K. Misiukiewicz, D. Mulford, E. Nadler, P. Neupane, J. Nunnink, J. Ohr, M. O'Malley, B. Patson, D. Paul, E. Popa, S. Powell, R. Redman, V. Rella, C. Rocha Lima, A. Sivapiragasam, Y. Su, A. Sukari, S. Wong, E. Yilmaz, J. Yorio, Pembrolizumab alone or with chemotherapy versus cetuximab with chemotherapy for recurrent or metastatic squamous cell carcinoma of the head and neck (KEYNOTE-048): a randomised, open-label, phase 3 study, Lancet 394 (10212) (2019) 1915–1928.
[373] S.J. O'Day, A.M.M. Eggermont, V. Chiarion-Sileni, R. Kefford, J.J. Grob, L. Mortier, C. Robert, J. Schachter, A. Testori, J. Mackiewicz, P. Friedlander, C. Garbe, S. Ugurel, F. Collichio, W. Guo, J. Lufkin, S. Bahcall, V. Vukovic, A. Hauschild, Final results of phase III SYMMETRY study: Randomized, double-blind trial of elesclomol plus paclitaxel versus paclitaxel alone as treatment for chemotherapy-naive patients with advanced melanoma, J. Clin. Oncol. 31 (2013) 1211–1218, https://doi.org/10.1200/JCO.2012.44.5585.
[374] C. Santini, M. Pellei, V. Gandin, M. Porchia, F. Tisato, C. Marzano, Advances in Copper Complexes as Anticancer Agents, Chem. Rev. 114 (2014) 815–862, https://doi.org/10.1021/cr400135x.
[375] C.L. Fox, Silver sulfadiazine–a new topical therapy for Pseudomonas in burns. Therapy of Pseudomonas infection in burns, Arch. Surg. 96 (1968) 184–188, https://doi.org/10.1001/archsurg.1968.01330200022004.
[376] K. Plaetzer, B. Krammer, J. Berlanda, F. Berr, T. Kiesslich, Photophysics and photochemistry of photodynamic therapy: Fundamental aspects, Lasers Med. Sci. 24 (2) (2009) 259–268.
[377] M. Uhlén, L. Fagerberg, B.M. Hallström, C. Lindskog, P. Oksvold, A. Mardinoglu, Å. Sivertsson, C. Kampf, E. Sjöstedt, A. Asplund, IngMarie Olsson, K. Edlund, E. Lundberg, S. Navani, C.-K. Szigyarto, J. Odeberg, D. Djureinovic, J.O. Takanen, S. Hober, T. Alm, P.-H. Edqvist, H. Berling, H. Tegel, J. Mulder, J. Rockberg, P. Nilsson, J.M. Schwenk, M. Hamsten, K. von Feilitzen, M. Forsberg, L. Persson, F. Johansson, M. Zwahlen, G. von Heijne, J. Nielsen, F. Pontén, Tissue-based map of the human proteome, Science 347 (6220) (2015).
[378] P.J. Thul, L. Åkesson, M. Wiking, D. Mahdessian, A. Geladaki, H. Ait Blal, T. Alm, A. Asplund, L. Björk, L.M. Breckels, A. Bäckström, F. Danielsson, L. Fagerberg, J. Fall, L. Gatto, C. Gnann, S. Hober, M. Hjelmare, F. Johansson, S. Lee, C. Lindskog, J. Mulder, C.M. Mulvey, P. Nilsson, P. Oksvold, J. Rockberg, R. Schutten, J.M. Schwenk, Å. Sivertsson, E. Sjöstedt, M. Skogs, C. Stadler, D.P. Sullivan, H. Tegel, C. Winsnes, C. Zhang, M. Zwahlen, A. Mardinoglu, F. Pontén, K. von Feilitzen, K.S. Lilley, M. Uhlén, E. Lundberg, A subcellular map of the human proteome, Science 356 (6340) (2017).
[379] J. Danzberger, M. Donovan, C. Rankl, R. Zhu, S. Vicic, C. Baltenneck, R. Enea, P. Hinterdorfer, G.S. Luengo, Glycan distribution and density in native skin's stratum corneum, Ski. Res. Technol. 24 (2018) 450–458, https://doi.org/10.1111/srt.12453.
[380] U. Möginger, S. Grunewald, R. Hennig, C.-W. Kuo, F. Schirmeister, H. Voth, E. Rapp, K.-H. Khoo, P.H. Seeberger, J.C. Simon, D. Kolarich, Alterations of the Human Skin N- and O-Glycome in Basal Cell Carcinoma and Squamous Cell Carcinoma, Front. Oncol. 8 (2018), https://doi.org/10.3389/fonc.2018.00070.
[381] M. Przybylo, M.E. Janik, D. Hoja-Lukowicz, Bitter sweetness of malignant melanoma: deciphering the role of cell surface glycosylation in tumour progression and metastasis, Hum. Ski. Cancer, Potential Biomarkers Ther. Targets, InTech (2016), https://doi.org/10.5772/64406.
[382] A. Passaniti, G.W. Hart, Cell surface sialylation and tumor metastasis. Metastatic potential of B16 melanoma variants correlates with their relative numbers of specific penultimate oligosaccharide structures, J. Biol. Chem. 263 (1988) 7591–7603. http://www.ncbi.nlm.nih.gov/pubmed/3372501.
[383] N.P. Farrell, A.K. Gorle, E.J. Peterson, S.J. Berners-Price, 4. Metalloglycomics, in: A. Sigel, H. Sigel, E. Freisinger, R.K.O. Sigel (Eds.), Met. Dev. Action Anticancer Agents, De Gruyter, Berlin, Boston, 2018: pp. 109–140. doi:10.1515/9783110470734-010.
[384] A.K. Gorle, S.J. Katner, W.E. Johnson, D.E. Lee, A.G. Daniel, E.P. Ginsburg, M. von Itzstein, S.J. Berners-Price, N.P. Farrell, Substitution-inert polynuclear platinum complexes as metalloshielding agents for heparan sulfate, Chem. - A Eur. J. 24 (2018) 6606–6616, https://doi.org/10.1002/chem.201706030.
[385] B. Bailly, A.K. Gorle, L. Dirr, A.K. Malde, N.P. Farrell, S.J. Berners-Price, M. von Itzstein, Platinum complexes act as shielding agents against virus infection, Chem. Commun. 57 (38) (2021) 4666–4669.
[386] M. Shoup, A. Ourahmane, E.P. Ginsburg, N.P. Farrell, M.A. McVoy, Substitution-inert polynuclear platinum compounds inhibit human cytomegalovirus attachment and entry, Antiviral Res. 184 (2020), https://doi.org/10.1016/j.antiviral.2020.104957 104957.
[387] E.J. Peterson, A.G. Daniel, S.J. Katner, L. Bohlmann, C.-W. Chang, A. Bezos, C.R. Parish, M. von Itzstein, S.J. Berners-Price, N.P. Farrell, Antiangiogenic platinum through glycan targeting, Chem. Sci. 8 (2017) 241–252, https://doi.org/10.1039/C6SC02515C.
[388] C. Li, S. Chi, J. Xie, Hedgehog signaling in skin cancers, Cell. Signal. 23 (2011) 1235–1243, https://doi.org/10.1016/j.cellsig.2011.03.002.
[389] F. Wu, Y. Zhang, B. Sun, A.P. McMahon, Y. Wang, Hedgehog Signaling: From Basic Biology to Cancer Therapy, Cell, Chem. Biol. 24 (2017) 252–280, https://doi.org/10.1016/j.chembiol.2017.02.010.
[390] A. Agyeman, B.K. Jha, T. Mazumdar, J.A. Houghton, Mode and specificity of binding of the small molecule GANT61 to GLI determines inhibition of GLI-DNA binding, Oncotarget. 5 (2014) 4492–4503, https://doi.org/10.18632/oncotarget.2046.
[391] F. Faião-Flores, D.K. Alves-Fernandes, P.C. Pennacchi, S. Sandri, A.L.S.A. Vicente, C. Scapulatempo-Neto, V.L. Vazquez, R.M. Reis, J. Chauhan, C.R. Goding, K.S. Smalley, S.S. Maria-Engler, Targeting the hedgehog transcription factors GLI1 and GLI2 restores sensitivity to vemurafenib-resistant human melanoma cells, Oncogene 36 (2017) 1849–1861, https://doi.org/10.1038/onc.2016.348.
[392] M. Lauth, A. Bergstrom, T. Shimokawa, R. Toftgard, Inhibition of GLI-mediated transcription and tumor cell growth by small-molecule antagonists, Proc. Natl. Acad. Sci. 104 (2007) 8455–8460, https://doi.org/10.1073/pnas.0609699104.
[393] A. Calcaterra, V. Iovine, B. Botta, D. Quaglio, I. D'Acquarica, A. Ciogli, A. Iazzetti, R. Alfonsi, L. Lospinoso Severini, P. Infante, L. Di Marcotullio, M. Mori, F. Ghirga, Chemical, computational and functional insights into the chemical stability of the Hedgehog pathway inhibitor GANT61, J. Enzyme Inhib. Med. Chem. 33 (2018) 349–358, https://doi.org/10.1080/14756366.2017.1419221.
[394] A.L. Ryan, M.C. Fitzgerald, A. Ozsváth, B. Twamley, P. Buglyó, B.M. Murphy, D. M. Griffith, Ni(II), Pd(II), and Pt(II) Complexes of the Hedgehog Pathway Inhibitor GANT61-D, Inorg. Chem. 58 (2019) 16075–16086, https://doi.org/10.1021/acs.inorgchem.9b02632.
[395] R.R. Hurtado, A.S. Harney, M.C. Heffern, R.J. Holbrook, R.A. Holmgren, T.J. Meade, Specific Inhibition of the Transcription Factor Ci by a Cobalt(III) Schiff Base–DNA Conjugate, Mol. Pharm. 9 (2012) 325–333, https://doi.org/10.1021/mp2005577.
[396] C. Doglioni, S. Piccinin, S. Demontis, M.G. Cangi, L. Pecciarini, C. Chiarelli, M. Armellin, T. Vukosavljevic, M. Boiocchi, R. Maestro, Alterations of β-Catenin Pathway in Non-Melanoma Skin Tumors, Am. J. Pathol. 163 (2003) 2277–2287, https://doi.org/10.1016/S0002-9440(10)63585-7.
[397] R. Uka, C. Britschgi, A. Krättli, C. Matter, D. Mihic, M.J. Okoniewski, M. Gualandi, R. Stupp, P. Cinelli, R. Dummer, M.P. Levesque, O. Shakhova, Temporal activation of WNT/β-catenin signaling is sufficient to inhibit SOX10 expression and block melanoma growth, Oncogene 39 (2020) 4132–4154, https://doi.org/10.1038/s41388-020-1267-7.
[398] K.-H.-M. Chow, R.-W.-Y. Sun, J.B.B. Lam, C.-K.-L. Li, A. Xu, D.-L. Ma, R. Abagyan, Y. Wang, C.-M. Che, A Gold(III) porphyrin complex with antitumor properties Targets the Wnt/ -catenin pathway, Cancer Res. 70 (2010) 329–337, https://doi.org/10.1158/0008-5472.CAN-09-3324.
[399] H.A. Khan, B. Mutus, Protein disulfide isomerase a multifunctional protein with multiple physiological roles, Front. Chem. 2 (2014), https://doi.org/10.3389/fchem.2014.00070.
[400] S. Hager, K. Korbula, B. Bielec, M. Grusch, C. Pirker, M. Schosserer, L. Liendl, M. Lang, J. Grillari, K. Nowikovsky, V.F.S. Pape, T. Mohr, G. Szakács, B.K. Keppler,

W. Berger, C.R. Kowol, P. Heffeter, The thiosemicarbazone Me2NNMe2 induces paraptosis by disrupting the ER thiol redox homeostasis based on protein disulfide isomerase inhibition, Cell Death Dis. 9 (2018), https://doi.org/10.1038/s41419-018-1102-z.

[401] S. Hager, V.F.S. Pape, V. Pósa, B. Montsch, L. Uhlik, G. Szakács, S. Tóth, N. Jabronka, B.K. Keppler, C.R. Kowol, É.A. Enyedy, P. Heffeter, High Copper Complex Stability and Slow Reduction Kinetics as Key Parameters for Improved Activity, Paraptosis Induction, and Impact on Drug-Resistant Cells of Anticancer Thiosemicarbazones, Antioxid. Redox Signal. 33 (2020) 395–414, https://doi.org/10.1089/ars.2019.7854.

[402] J.L. Morgado-Pascual, S. Rayego-Mateos, L. Tejedor, B. Suarez-Alvarez, M. Ruiz-Ortega, Bromodomain and extraterminal proteins as novel epigenetic targets for renal diseases, Front. Pharmacol. 10 (2019) 1315, https://doi.org/10.3389/fphar.2019.01315.

[403] Y. Taniguchi, The bromodomain and extra-terminal domain (BET) family: Functional anatomy of BET paralogous proteins, Int. J. Mol. Sci. 17 (11) (2016) 1849.

[404] A. Trivedi, A. Mehrotra, C.E. Baum, B. Lewis, T. Basuroy, T. Blomquist, R. Trumbly, F.V. Filipp, V. Setaluri, I.L. De La Serna, Bromodomain and extra-terminal domain (BET) proteins regulate melanocyte differentiation, Epigenetics and Chromatin. 13 (2020) 14, https://doi.org/10.1186/s13072-020-00333-z.

[405] M.F. Segura, B. Fontanals-Cirera, A. Gaziel-Sovran, M.V. Guijarro, D. Hanniford, G. Zhang, P. González-Gomez, M. Morante, L. Jubierre, W. Zhang, F. Darvishian, M. Ohlmeyer, I. Osman, M.M. Zhou, E. Hernando, BRD4 sustains melanoma proliferation and represents a new target for epigenetic therapy, Cancer Res. 73 (2013) 6264–6276, https://doi.org/10.1158/0008-5472.CAN-13-0122-T.

[406] T. Xiang, J.-y. Bai, C. She, D.-J. Yu, X.-Z. Zhou, T.-L. Zhao, Bromodomain protein BRD4 promotes cell proliferation in skin squamous cell carcinoma, Cell. Signal. 42 (2018) 106–113.

[407] A. Pettenuzzo, R. Pigot, L. Ronconi, Metal-based glycoconjugates and their potential in targeted anticancer chemotherapy, Metallodrugs. 1 (2016), https://doi.org/10.1515/medr-2015-0002.

[408] L. Szablewski, Expression of glucose transporters in cancers, Biochim. Biophys. Acta - Rev. Cancer. 2013 (1835) 164–169, https://doi.org/10.1016/j.bbcan.2012.12.004.

[409] H.R. Rezvani, N. Ali, L.J. Nissen, G. Harfouche, H. De Verneuil, A. Taïeb, F. Mazurier, HIF-1α in epidermis: Oxygen sensing, cutaneous angiogenesis, cancer, and non-cancer disorders, J, Invest. Dermatol. 131 (2011) 1793–1805, https://doi.org/10.1038/jid.2011.141.

[410] I. Seleit, O.A. Bakry, D.R. Al-Sharaky, R.A.A. Ragab, shimaa A. Al-Shiemy, Evaluation of Hypoxia Inducible Factor-1α and Glucose Transporter-1 Expression in Non Melanoma Skin Cancer: An Immunohistochemical Study, J. Clin. Diagn. Res. 11 (2017) EC09. www.jcdr.net (accessed July 24, 2020).

[411] B. Zbytek, D.L. Peacock, T.N. Seagroves, A. Slominski, Putative role of hif transcriptional activity in melanocytes and melanoma biology, Dermatoendocrinol. 5 (2013) 239–251, https://doi.org/10.4161/derm.22678.

[412] L. Zhou, Y. Wang, M. Zhou, Y. Zhang, P. Wang, X. Li, J. Yang, H. Wang, Z. Ding, HOXA9 inhibits HIF-1α-mediated glycolysis through interacting with CRIP2 to repress cutaneous squamous cell carcinoma development, Nat. Commun. 9 (2018) 1–17, https://doi.org/10.1038/s41467-018-03914-5.

[413] Y.S. Cho, C.H. Kim, J.W. Park, Involvement of HIF-1α in UVB-induced epidermal hyperplasia, Mol. Cells 28 (2009) 537–543, https://doi.org/10.1007/s10059-009-0148-2.

[414] C.A. Elmets, J.L. Viner, A.P. Pentland, W. Cantrell, H. Lin, H. Bailey, S. Kang, K.G. Linden, M. Heffernan, M. Duvic, E. Richmond, B.E. Elewski, A. Umar, W. Bell, G. B. Gordon, Chemoprevention of Nonmelanoma Skin Cancer With Celecoxib: A Randomized, Double-Blind, Placebo-Controlled Trial, JNCI J. Natl. Cancer Inst. 102 (2010) 1835–1844, https://doi.org/10.1093/jnci/djq442.

[415] V.M. Voiculescu, C.V. Lisievici, M. Lupu, C. Vajaitu, C.C. Draghici, A.V. Popa, I. Solomon, T.I. Sebe, M.M. Constantin, C. Caruntu, Mediators of inflammation in topical therapy of skin cancers, Mediators Inflamm. 2019 (2019) 1–15.

[416] L.F. Fecker, E. Stockfleth, I. Nindl, C. Ulrich, T. Forschner, J. Eberle, The role of apoptosis in therapy and prophylaxis of epithelial tumours by nonsteroidal anti-inflammatory drugs (NSAIDs), Br. J. Dermatol. 156 (2007) 25–33, https://doi.org/10.1111/j.1365-2133.2007.07856.x.

[417] D. Wang, R.N. Dubois, Prostaglandins and cancer, Gut 55 (2006) 115–122, https://doi.org/10.1136/gut.2004.047100.

[418] S. Thangamani, H. Mohammad, M.F.N. Abushahba, T.J.P. Sobreira, M.N. Seleem, Repurposing auranofin for the treatment of cutaneous staphylococcal infections, Int. J. Antimicrob. Agents 47 (2016) 195–201, https://doi.org/10.1016/j.ijantimicag.2015.12.016.

[419] S. Medici, M. Peana, G. Crisponi, V.M. Nurchi, J.I. Lachowicz, M. Remelli, M. Antonietta, Silver coordination compounds : A new horizon in medicine, Coord. Chem. Rev. 327–328 (1940) 349–359, https://doi.org/10.1016/j.ccr.2016.05.015.

[420] S. Medici, M. Peana, V.M. Nurchi, M.A. Zoroddu, Medical Uses of Silver: History, Myths, and Scientific Evidence, J. Med. Chem. 62 (2019) 5923–5943, https://doi.org/10.1021/acs.jmedchem.8b01439.

[421] M. Popova, O. Isayev, A. Tropsha, Deep reinforcement learning for de novo drug design, Sci. Adv. 4 (2018) eaap7885, https://doi.org/10.1126/sciadv.aap7885.

[422] A. Lavecchia, Deep learning in drug discovery: opportunities, challenges and future prospects, Drug Discov. Today. 24 (2019) 2017–2032, https://doi.org/10.1016/j.drudis.2019.07.006.

[423] F.R. de Gruijl, C.P. Tensen, Pathogenesis of Skin Carcinomas and a Stem Cell as Focal Origin, Front. Med. 5 (2018) 165, https://doi.org/10.3389/fmed.2018.00165.

[424] F. Adhami, M. Safavi, M. Ehsani, S.K. Ardestani, F. Emmerling, F. Simyari, Synthesis, crystal structure, and cytotoxic activity of novel cyclic systems in [1,2,4]thiadiazolo[2,3-a]pyridine benzamide derivatives and their copper[ii] complexes, Dalton Trans. 43 (2014) 7945–7957, https://doi.org/10.1039/C3DT52905C.